CZECH TECHNICAL UNIVERSITY
IN PRAGUE

Faculty of Nuclear Sciences and Physical
Engineering

Department of Physics

Research work

Event shape analysis in ultrarelativistic nuclear collisions

Renata Kopečná

Supervisor: doc. Mgr. Boris Tomášik, Ph.D.

Prague, 2015

ČESKÉ VYSOKÉ UČENÍ TECHNICKÉ
V PRAZE
Fakulta Jaderná a Fyzikálně Inženýrská
Katedra Fyziky

Výzkumný úkol

Analýza tvaru události v ultrarelativistických jaderných srážkách

Renata Kopečná

Supervisor: doc. Mgr. Boris Tomášik, Ph.D.

Praha, 2015

Prohlášení:

Prohlašuji, že jsem svůj výzkumný úkol vypracovala samostatně a použila jsem pouze podklady (literaturu, projekty, software, atd.) uvedené v přiloženém seznamu.

Nemám závažný důvod proti užití tohoto školního díla ve smyslu § 60 Zákona č. 121/2000 Sb., o právu autorském, o právech souvisejících s právem autorským a o změně některých zákonů (autorský zákon).

V Praze dne

Renata Kopečná

Title:

Event shape analysis in ultrarelativistic nuclear collisions

Author: Renata Kopečná

Specialization: Experimental nuclear and particle physics

Sort of project: Research work

Supervisor: doc. Mgr. Boris Tomášik, Ph.D.

Abstract:

Quark-gluon plasma (QGP) is newly-discovered very dense state of matter expected to be present few microseconds after the Big Bang. Nowadays, it is present in the first fm/c during high-energy heavy-ion collisions. Small drop of QGP, called fireball, can be created in high-energy nuclear collisions, observed in facilities such as Relativistic Heavy Ion-Collider (RHIC) or Large Hadron Collider (LHC). However, it is not possible to study this state of matter directly, we are able to study hadrons that escaped the system after it disintegrates. We focus on studying the QGP properties via azimuthal angle distribution and its anisotropies. These anisotropies are generated mainly in the early stage of the collision. Therefore, they are a good probe for initial conditions.

One way of studying the event shape, called *event-shape engineering*, was introduced in [1]. The main idea is to compare all kinds of collisions and separate those with similar initial conditions. It compares events using their *flow vector*. This vector gives us the idea of where in which azimuthal direction most of the particle are emitted. Assuming negligible nonflow, flow vector distribution provides information about flow fluctuations.

Our work studies the angular distribution via the algorithm, proposed in [2] and [3]. This algorithm was initially used for distinguishing good scientific authors from bad authors using their citation record. In this case, we sort events according to their angular record. The algorithm compares and sorts different azimuthal angle histograms according to their similarity. It uses the Bayesian concept of probability. The algorithm allows us to determine a good measure of events. It's simplicity allows many different ways of event analysis. Moreover, it provides a multiplicity-independent insight.

The aim of this thesis is to study angular record of the events via the algorithm. We study several different measures of events. The algorithm is implemented in a code

entitled ESSTER and we present its functionality on simple examples. Some of the processed events are generated with the event generator DRAGON [4]. We discuss the advantages and disadvantages of this approach.
Key words: Quark-Gluon plasma, heavy-ion collisions, transverse flow, event shape engineering

Název práce:

Analýza tvaru události v ultrarelativistických jaderných srážkách

Zaměření: Experimentální jaderná a částicová fyzika

Druh práce: Výzkumný úkol

Autor: Renata Kopečná

Abstrakt:
Kvark-gluonová plazma (QGP) je nově objevený velmi hustý stav hmoty. Předpokládá se, že byla přítomna prvních několik mikrosekund po Velkém Třesku. Dnes vzniká při těžko-iontových srážkách, realizovaných ve vědeckých zařízeních jako je relativistický těžko-iontový collider RHIC nebo velký hadronový urychlovač LHC. Tuto hmotu ovšem nelze pozorovat přímo, studujeme ji pouze protřednictvím produkovaných hadronů, které pocházejí z malé kapky QGP - *fireballu*. Ve středu našeho zájmu jsou distribuce azimutálního úhlu vylétávajících částic a jejich anizotropie. Tyto anizotropie vznikají v raném stádiu vývoje srážky, proto je výhodné je studovat.

Jedním ze způsobů studie tvaru události je takzvaný *event-shape engineering* [1]. Hlavní myšlenkou je porovnávání různých srážek a vytřídit z nich takové srážky, které vycházejí z podobných počátečních podmínek. Event-shape engineering porovnává srážky pomocí tzv. *vektoru toku*, který říká, ve kterém směru bylo emitováno nejvíe částic. Pokud zanedbáme efekty nesouvisející s tokem, vektor toku nám podává informaci o fluktuacích toku.

Tato práce pojendává o studii úhlové distribuce pomocí algoritmu posaného v [2] a [3]. Původně byl tento algoritmus použit na odlišení dobrých vědců od špatných na základě záznamů o počtu citací jejich článků. V našem případě odlišujeme srážky. Algoritmus porovnvá a třídí jednotlivé histogramy azimutálního úhlu podle podobnosti jejich tvaru. Využívá při tom Bayesovský koncept pravděpodobnosti. Navíc tento algoritmus umožňuje nalezení veličiny, podle které lze eventy takto třídit. Jeho jednodchost umožňuje zkoumat více přístupů ke studiu tvaru událostí. Jednou z jeho hlavních výhod je nezávislost na multiplicitě.

Cílem této práce je tedy studovat tvar události pomocí výše zmíněného algoritmu. Zaměřili jsme se na několik veličin, podle kterých lze srážk třídit. Představujeme program ESSTER a výsledky pomocí něj získané, diskutujeme výhody a nevýhody tohoto přístupu. Nakonec jsme využili pokročilý Monte Carlo model DRAGON [4].
Klíčová slova: Kvark-gluonové plazma, těžko-iontové srážky, příčný tok, event shape engineering

Acknowledgement

I would like to express my special appreciation to my supervisor, doc. Tomášik. Without his patience, encouragement, questioning my statements and constant help both with physics and programming this thesis would not have been possible. I am also very grateful for his language check.

I would also like to thank all the academic staff at the department of physics for their enthusiasm and willingness to help anytime. Besides the academic staff, my sincere thanks goes to my friends from the department of physics for the stimulating discussions, for their encouragement and personal support. Last but not least, special thanks goes to my friends and family.

Contents

Introduction

High-energy heavy ion collisions provide a unique tool to investigate many topics of present physics. We can study the equation of state of nuclear matter, properties of quark-gluon plasma or its transition back to hadrons. We speak about ultrarelativistic particles, meaning their speed is almost the speed of light, leaving their Lorentz factor $\gamma \gg 1$. This means the velocity bigger than $0.95c$. Heavy ions are nuclei much heavier than proton or neutron.

Every collision has different initial conditions. Event shape analysis can help us sort events according to their initial conditions. This means that we are able to select events where similar physics processes evolve. This can lead to better understanding of quark-gluon plasma properties.

In this work, we present a study of azimuthal anisotropies via Bayesian statistics proposed in [2].

First chapter describes basic properties of QGP and introduces the motivation for our study. Second chapter briefly describes *Event Shape Engineering* method and its relation to our study. Next chapter characterizes the used algorithm, discusses its advantages, disadvantages and limitations. Our toy model and the program used for the analysis is described in the fourth chapter. Last chapter reports our results.

1 Motivation

Recent experiments at facilities such as Relativistic Heavy Ion-Collider (RHIC) or Large Hadron Collider (LHC) suggest the existence of so-called *quark-gluon plasma* (QGP). This state of matter may provide us with information about the early stages of our universe, the behavior of compact stars and much more. We are not able to study QGP directly. We study all its properties via analyzing produced hadrons, mainly at experiments STAR and PHENIX at RHIC and at ALICE at the LHC, using computer simulations or using mathematical models and simplifications.

1.1 Quark-gluon plasma

Quark-gluon plasma is very dense state of matter expected to be present few microseconds after the Big Bang. Nowadays, it is present in the first fm/c during high-energy heavy-ion collisions. Small drop of QGP, called *fireball* can be created. Due to the analogy with the expansion of hot universe, these collisions are called *Little Bangs*. It can be described as an ultra-dense matter, where quarks and gluons are free to move over distances larger than size of a hadron (we say they are *deconfined*).

The name *plasma* comes from the analogy with classic plasma. Neutral atoms, forming the matter as we know it, are dissolved into ions and free electrons. In QGP, instead of atoms, there are hadrons dissolved into deconfined colored degrees of freedom: quarks and gluons.

Formation of QGP is a process requiring very high energy density. Hadrons have to be very close to each other. Temperature needed for this process is called *critical temperature* T_c. The temperature depends on baryon chemical potential, denoted as μ_B. The value of critical temperature T_c for $\mu_B = 0$ is nowadays estimated at 140 - 175 MeV.

Despite previous expectations, it turns out that QGP behaves as an almost perfect fluid. The lower limit for its shear viscosity η/s is $\hbar/4\pi$, established using AdS/CFT theory. We focus at the ratio η/s because it is a dimensionless quantity.

The existence of QGP was first suggested in the 1970's. The idea of studying QGP via heavy-ion collisions appeared in the 1980's. First suggestions of the possible existence of the QGP appeared

at the Super Proton Synchrotron in CERN in the 1990's, first results talking about the possible creation of QGP were published in 2000's. Hence, this topic is very present and requires a lot of future studies.

1.2 Studying quark-gluon plasma

As mentioned before, the only experimental way to study QGP is to study hadrons originating from the fireball. Illustrative parallel is studying properties of a drop of water using only the vaporized steam. The transformation from QGP to hadronic gas is called *hadronization*. We mainly study production of different hadrons, their spatial distribution and their transverse momentum distribution. There are also several interesting ratios of these quantities, such as *nuclear modification factor* R_{AA}. It is defined as a ratio of produced particles in ion-ion collision and the yield of proton-proton collision normalized by a number of collisions.

Our work is focused on the spatial distribution of particles, more precisely on azimuthal angle distribution, collective flow and on azimuthal angle anisotropies, described in the following section. Flow is mainly generated by pressure gradients inside the fireball, the energy density is very high as well as the pressure. Since the fireball is placed in vacuum, there is a big difference in the pressure. The flow anisotropies are developed mainly during the initial moments of the collision. Hence, they are a good initial-state probe.

2 Event Shape Engineering

Event shape engineering was proposed in 2012 by Jurgen Schukraft, Anthony Timmins and Sergei A. Voloshin [1]. The main idea is to compare all kinds of collisions and separate those with similar initial conditions. Initial conditions in heavy-ion collisions fluctuate from event to event. The anisotropies in the collective flow are developed mainly in the early stage of the collision. Therefore, they can provide us with information about the initial conditions.

2.1 Anisotropic flow

Initial conditions can be studied via *collective flow anisotropies*. Since QGP is behaving as an expanding viscous fluid with, simply said, hotter and colder places, anisotropies in the flow are present. These anisotropies are studied using Fourier expansion of the azimuthal angle distribution:

$$\frac{dN}{dyd^2p_T} = \frac{dN}{2\pi p_T dy dp_T}\left[1 + \sum_{n=1}^{\infty} 2v_n \cos(n(\Phi - \Phi_n))\right] . \tag{1}$$

Notation is usual: N is the number of particles, p_T indicates transverse momentum, y rapidity, Φ is particle's azimuthal angle relative to the reaction plane, Φ_n is n^{th} reaction plane azimuthal angle. The reaction plane is theoretically defined as a plane made up by the beam axis and the impact parameter [5]. The v_n coefficients are n^{th} *differential flows*. The average over p_T and y gives us *integrated flow*. There are experimental results confirming the existence of differential flows up to hexagonal flow v_6 [6].

Event shape engineering is performed using two subevents: one (subevent 'a') is used for the event selection, the other (subevent 'b') is used for physical analysis. Subevents are selected at random or in a given momentum region. This measure reduces nonphysical biases, such as nonflow effects [1]. On the other hand, there is an information loss.

Main idea of event shape engineering is selecting events according to the *magnitude of reduced flow vector* q_n. Simplified description of this vector is that this vector determines the direction,

where most particles are emitted. *Flow vectors* are defined as

$$\vec{Q}_n = \left(\sum_{i=1}^{M} \cos(n\phi_i) \, , \sum_{i=1}^{M} \sin(n\phi_i) \right) \tag{2}$$

and their magnitudes

$$q_n = Q_n / \sqrt{M} \, , \tag{3}$$

where M denotes multiplicity of the subevent, ϕ_i is particle azimuthal angle in given subevent. The magnitude of flow vector can be also obtained from the data via particle correlation as

$$q_n^2 = 1 + (M-1) \left\langle \cos[n(\phi_i - \phi_j)] \right\rangle_{i \neq j} \, , \tag{4}$$

where angular brackets denote average over all particles in the given subevent.

Assuming there is negligible nonflow, q_n distribution provides information about flow fluctuations. If there are nonflow effects, especially when there are correlations even between both subevents, it is practical to use two subevents separated by a significant pseudorapidity gap [1].

3 The event sorting method

This thesis works with the Bayesian concept of probability. In this interpretation, probability is measure of the belief whether the data are true or not. For example, if we are sure that an ordinary die is legitimate, the probability of rolling six is 1/6. However, if we know the die is loaded, the probability would be higher or smaller (depending on the way how the die is manipulated).

This may seem very subjective. Nonetheless even scientist are not truly objective when evaluating the data. Nice example can be found in [7]: ask a biologist, whether a particular gene is one of the genes that determines left-handedness. From his experience, he has partial knowledge whether it is one of the 'left-handed' genes or not. Mathematically, there are only two possibilities, yes or no. Bayesian probability says that there is for example 33% chance (belief) the gene is left-handed. The Bayesian probability can be also described as a plausibility of proposition.

The main relation used in this thesis is the *Bayes' theorem*. It allows us to rewrite conditional probability of event A given event B, denoted as $P(A|B)$, using the probability of event B given event A $P(B|A)$. Mathematically, denoting probability of event A and B as $P(A)$ and $P(B)$

$$P(A|B) = \frac{P(B|A)P(A)}{P(B)}\,. \tag{5}$$

Moreover, it is possible to rewrite probability of event B via a set of different events $\{\mathrm{A}_1, \ldots, \mathrm{A}_n\}$ meeting the condition $\sum_1^n P(A_i) = 1$:

$$P(B) = \sum_1^n P(B|A_i)P(A_i)\,. \tag{6}$$

Worth mentioning is the difference between $P(A|B)$ and $P(B|A)$. The following simple example shows the difference: let A denote it is raining. Let B denote it is cloudy. Probability that there are clouds given it is raining (which can be denoted as $P(B|A)$) is almost one. On the other hand, the probability that it is raining given there are clouds (denoted as $P(A|B)$) is not even close to one, not all cloudy days are rainy days.

3.1 Algorithm description

Since we are interested in azimuthal angle distribution, first we make an azimuthal angle histogram. We denote the angle bins using Roman letters, meaning we have n bins denoted as $1, \ldots, i, \ldots, n$. Any event is described by a set of numbers of particles in its angle histogram's bins $\{n_1, \ldots, n_i, \ldots, n_n\}$. An example of such an event can be seen in figure 1. This event is described by a record {70, 67, 78, 72, 59, 44, 58, 72, 62, 80, 61, 68, 58, 72, 68, 75, 85, 91, 89, 59, 63, 52, 37, 49, 48, 54, 60, 67, 70, 74}. The multiplicity of this event is 1962.

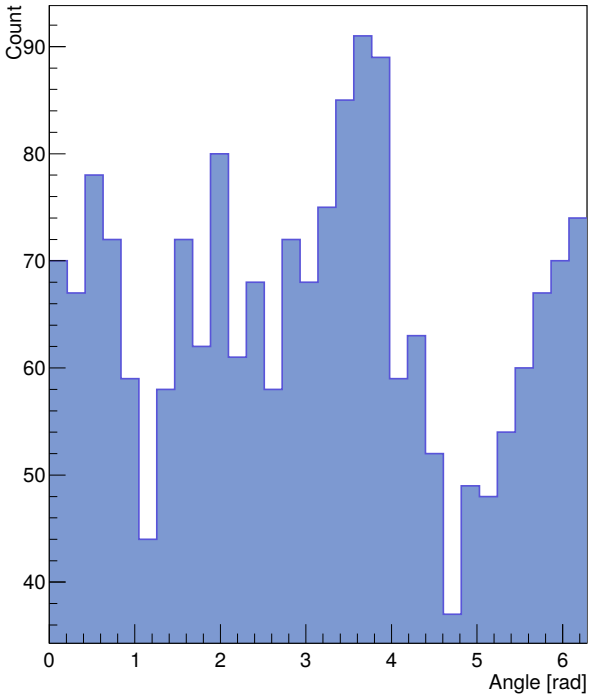

Figure 1: Azimuthal angle histogram example.

Then, we make an event histogram according to some good measure: we started with q_2, defined in previous section, and binned them into deciles: meaning we have 10 bins with the same number of events. We will denote these event bins using Greek letters: we have ω event bins $1, \ldots, \mu, \ldots, \omega$. Also, we denote the probability that an event lies in a bin μ as $P(\mu)$.

Now, we will perform a bayesian analysis of this data. We want to obtain the probability that the event with record $\{n_i\}$ belongs to an event bin μ, mathematically denoted as $P(\mu|\{n_i\})$. Using Bayes' theorem (5) and eq. (6), we can rewrite $P(\mu|\{n_i\})$ using the probability $P(\{n_i\}|\mu)$ that an event in the bin μ has an angle record $\{n_i\}$:

$$P(\mu|\{n_i\}) = \frac{P(\{n_i\}|\mu)P(\mu)}{P(\{n_i\})} = \frac{P(\{n_i\}|\mu)P(\mu)}{\sum_{\mu'} P(\{n_i\}|\mu')P(\mu')} \,. \tag{7}$$

The probability $P(\{n_i\}|\mu)$ can be calculated as

$$P(\{n_i\}|\mu) = N! \prod_i \frac{P(i|\mu)^{n_i}}{n_i!} \,, \tag{8}$$

where we used the probability $P(i|\mu)$ that particle is in the i^{th} bin given the event is in the event bin μ and where N denotes total number of particles (multiplicity). This formula represents all the possible permutations of particles among their angle bins. As can be seen, substituting for $P(\{n_i\}|\mu)$ in eq. (7) leads to canceling all factorials. This makes the computation much easier.

The probability $P(i|\mu)$ can be simply calculated as the number of particles in ith bin for all events in μ divided by the number of all particles in all events in μ.

Now, let us go back to the eq. (7) and rewrite it in the terms of $P(i|\mu)$:

$$P(\mu|\{n_i\}) = \frac{\prod_i P(i|\mu)^{n_i} P(\mu)}{\sum_{\mu'} \prod_i P(i|\mu')^{n_i} P(\mu')} \,. \tag{9}$$

Worth noticing is the fact, that this fraction uses *all* the available data. Hence, if there are rare events, their statistical influence is highly suppressed.

Now, we know the probability that an event with the record $\{n_i\}$ belongs to the event bin μ. From this information, one can easily obtain the mean event bin number

$$\hat{\mu} = \sum_{\mu} \mu P(\mu|\{n_i\}) \tag{10}$$

and we can sort the events according to their $\hat{\mu}$. We obtain new μ bins, we do the bayesian analysis again, obtain new $\hat{\mu}$. We repeat this until the event bins μ remain unchanged.

For readers comfort, we add simple bullet overview of the algorithm with fig. 2 depicting the structure of the algorithm.

1. For every event make azimuthal angle $\frac{dN}{d\phi}$ histogram.

2. Order events according to *something* (q_2) into deciles.

3. For each angle bin i and event bin μ calculate the probability that particle is in the i^{th} bin given the event is in the event-bin μ:

$$P(i|\mu) = \frac{\text{\# of particles in i}^{th}\text{ bin for all events in } \mu}{\text{\# of all particles in all events in } \mu} \,.$$

4. Calculate the probability that an event in bin μ is described by a set of numbers $\{n_i\}$ denoting n_i particles belong to i^{th} bin, reducing the factorials in eq. 8

$$P(\{n_i\}|\mu) = \prod_i P(i|\mu)^{n_i} .$$

5. For each event with record $\{n_i\}$ calculate the probability that it belongs to the bin μ

$$P(\mu|\{n_i\}) = \frac{P(\{n_i\}|\mu)\, p(\mu)}{P(\{n_i\})} = \frac{P(\{n_i\}|\mu)\, p(\mu)}{\sum_{\mu'} P(\{n_i\}|\mu')\, p(\mu')} .$$

6. For every event calculate 'average bin number'

$$\hat{\mu} = \sum_{\mu} \mu P(\mu|\{n_i\}) .$$

7. Sort according to $\hat{\mu}$.

8. Repeat from the third step until the μ bins remains unchanged.

There are several assumption we made through the process. We assume the events are strongly correlated. Since the shapes of the event varies only by the magnitude of flows, events are correlated. This means we can also neglect transient correlations.

3.2 Errors

One of the advantages of this method is the possibility of calculating the error of original bin assignment. In the terms of probability, we are able to calculate the probability $P(\alpha|\beta)$ that an event originally assigned to bin β ('*before*') ends up in bin α ('*after*') after applying the sorting algorithm. We will calculate this probability as an average of the probability $P(\alpha|\{n_i\})$ for all events $\{n_i\}$ in bin β:

$$P(\alpha|\beta) = \frac{1}{N_\beta} \sum_{\{n_i\}\in\beta} P(\alpha|\{n_i\}) \tag{11}$$

If the original sorting variable was good, we expect the values of $P(\alpha|\beta)$ to be approximately one around diagonal, and approximately zero elsewhere.

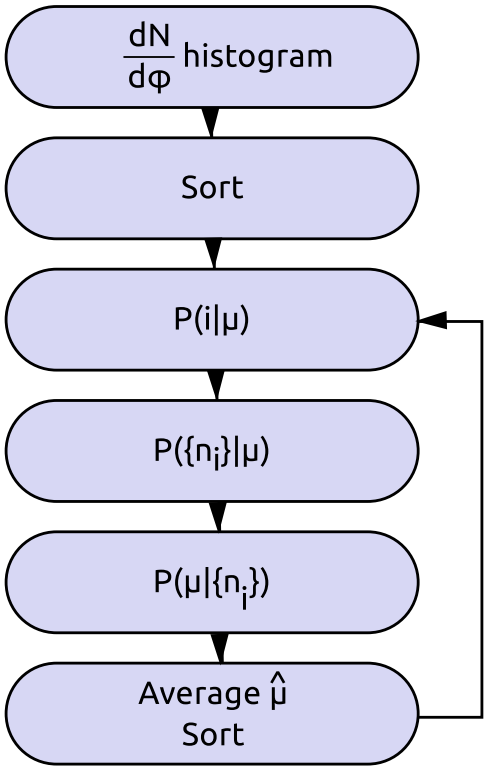

Figure 2: Algorithm description.

3.3 Kullback - Leibler divergence

Kullback - Leibler divergence (sometimes also referred as *relative entropy*) is used as a measure for two probability distributions p and q. It is often used as a measure of the information gain in moving from a prior distribution to a posterior distribution. The KL divergence is defined as

$$KL[p,q] = \sum_i p_i \ln\left(\frac{p_i}{q_i}\right) . \tag{12}$$

Of course, in the case of continuous distribution, one replaces the sum with an integral. It is not a metric since $KL[p,q] \neq KL[q,p]$. However, for p very similar to q clearly $KL[p,q] \simeq KL[q,p]$.

This measure is good for comparing adjacent event bins α and $\alpha + 1$. We can calculate

$KL[P(\alpha), P(\alpha+1)]$ as

$$KL[P(\alpha), P(\alpha+1)] = \sum_{\{n_i\}} P(\{n_i\}|\alpha) \ln \left(\frac{P(\{n_i\}|\alpha)}{P(\{n_i\}|\alpha+1)} \right) .$$

The probability of $P(\alpha|\alpha+1)$ is clearly exponentially sensitive to the KL divergence. The initial measure discriminates best if the KL divergence is largest, since the difference in adjacent bins is large. There could occur problems during the computation in case there were empty bins. In this case, the difference between $KL[P(\alpha), P(\alpha+1)]$ and $KL[P(\alpha+1), P(\alpha)]$ is large. However, the particle multiplicity is high enough to fill all the angle bins (and there is no point in making angle bins so narrow they would be empty) and we divided the events into quantiles. Therefore, there are no empty bins.

4 Program 'ESSTER' documentation

For the purpose of generating, analyzing and sorting events, we made a simple program called ESSTER. It stands for **E**vent-**S**hape **S**or**TER**.

4.1 Toy Model

For generating events, we used a simple toy model. As a default random number generator, we use the generator proposed in [8]. We use equation

$$\frac{dN}{d\phi} \propto 1 + \sum_{n=1}^{\infty} 2v_n \cos(n(\phi - \Psi_n)) \tag{13}$$

for generating azimuthal angles ϕ. We set the v_n parameters for each event randomly, depending quadratically on multiplicity M: $v_n = aM^2 + bM + c$ and smeared according to Gaussian, where a, b and c are coefficients obtained from [9] and [10]. The setting of the corresponding v_n parameters is in the appendix A. These coefficients were fit to the ATLAS measurements of v_n in the p_T bin 2-3 MeV and from [10]. The result of the fit is in the fig. 3. Also, the event plane angle Ψ_n is set randomly for every event and is independent for every n. Moreover, for every particle we independently generate p_T according to equation

$$\frac{dN}{dp_T} = Cp_T e^{-\frac{p_T}{T}}\,, \tag{14}$$

where we set the parameter T as 400 MeV. This is motivated by the LHC data.

4.2 General description

The model is written in C++. It was written using Linux operating system. It consists of nine source files: several simple complementary methods are defined in `additional.cpp`. The generator of random numbers is defined in `generator.cpp`. Toy model generator of azimuthal angle and transverse momentum is stored in `toymodel.cpp`. Analysis takes place in `analyze.cpp`, in

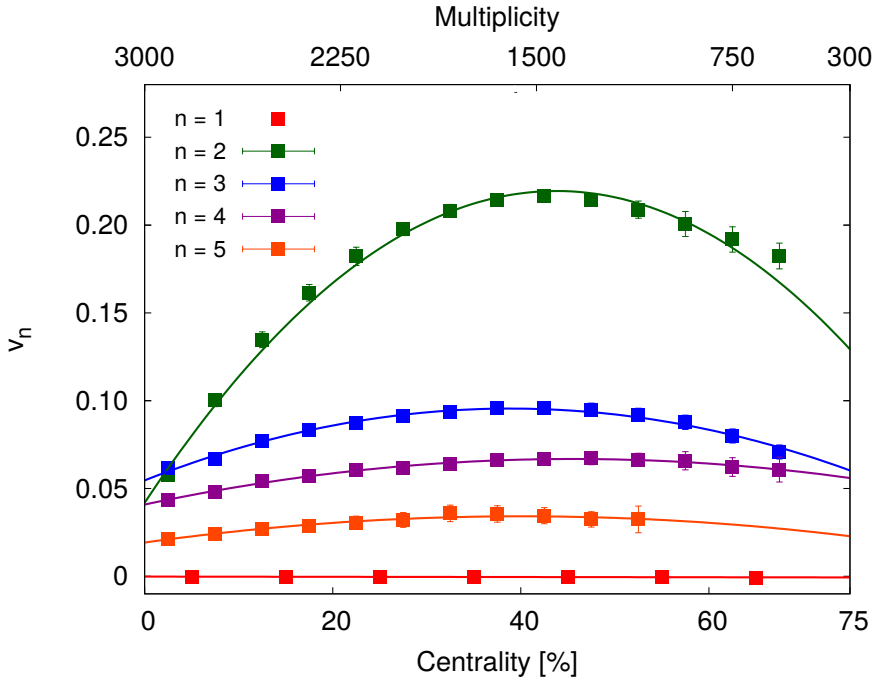

Figure 3: Flow dependence on centrality and multiplicity. Data points are obtained from [9] and [10]. The data points are fitted with a quadratic function, fit coefficients are in the tab. 2.

`list.cpp` we defined one-way linked list and its basic operations used for this purpose. The algorithm, described in 3.1, is implemented in `bins.cpp`. The main source is `main.cpp`. Moreover, there are is a source file used for ROOT analysis [11] `my_root.cpp`. For correlation matrices and eigenvalues calculation, a few methods are implemented in `eigenvalues.cpp`, where we used LAPACK (Linear Algebra PACKAge) [12]. LAPACK was written in Fortran 90 and includes routines used for solving problems from linear algebra, like systems of linear equations or eigenvalues and eigenvector problem.

We used a header file `nr3`, taken from [8] as a source for the random number generator. Toy model and other parameters can be set in the `parameters.h`. We define the maximum order of Fourier decomposition Fn, applied both for analysis (analyzes all v_n up to Fn) and toy model parts. The reason we did so is for simple constriction/extension of the program. We also set the parameter T in eq. (14), denoted as TT. Furthermore, we define number of generated events ($NoEvents$) and multiplicity range ($multi\_min$, $multi\_max$). The parameters described in the

tab. 2 are defined here as well as the sigma of the Gaussian smearing of differential flows. The parameters used in the sorting algorithm are defined here: the quantile and number of angle bins. In this header file, basic constants like π are set.

We add a `makefile` for simple compilation.

4.3 File organization

We added one header file `additional.h`, where all the file names can be specified and where we defined some special functions used in the program, for example function converting integer into string. The files are saved in a folder tree depicted in fig. 4. The path is defined via `MAIN_PATH` parameter, the name of the main folder is `MAIN_NAME`. There are three subfolders of the main folder: `GEN_FOLDER`, where the generated events are stored; `AN_FOLDER`, where the analysis of the events stored in `GEN_FOLDER` is stored and `BIN_FOLDER`, where the output from our algorithm is stored. The information about histograms from ROOT is stored in `ROOT_FOLDER`. All the folders are made automatically.

There are also sub-folders: their name is made according to the following key: imagine having 20 bins, events rotated according to the Ψ_3, initialy sorted according to q_2, the events are flipped as described later, and there is no normalization, the folder is `bins20_psi3_init2_flip1_norm0`. First part denotes the number of bins, second reflects the rotation, third initial sorting variable, last two are booleans; including flipped events and multiplicity normalization.

4.4 Data analysis

The program is able to analyze data using cumulant method, event plane method and event shape engineering. These methods are described for example in [1] and [5]. For simple constriction/extension of the program, the results are output into files `AN_EPM`, `AN_CUMM` and `AN_ESE`, defined in `additional.h`.

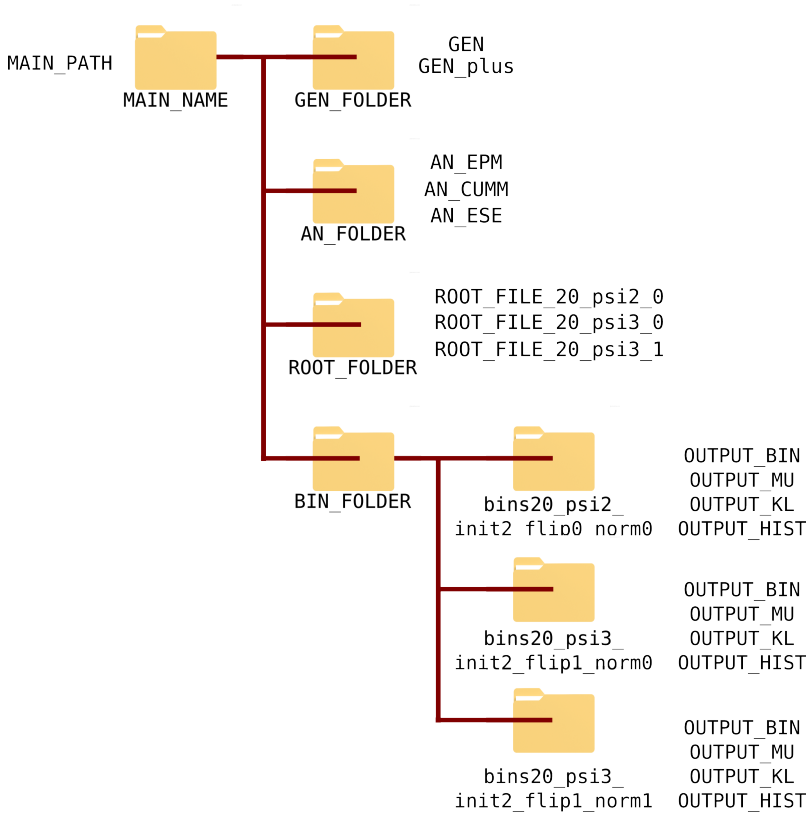

Figure 4: Folder tree description.

4.5 Sorting algorithm implementation

The algorithm is implemented in the source file `bins.cpp`. The classes used for this are defined in its corresponding header `bins.h`. The struct *event_vector* contains all the relevant data about an event. *event_array* stores all the events. Main work is done in the class *index_table*, where all the procedures described in (3.1) are implemented. For initial sorting we used simple quicksort. Later during the iteration, we used insertion method. The reason for this choice is that we assume events are almost sorted. For this case, quicksort shows bad performance.

4.6 Correlation matrices

For the analysis of our results, we need covariance and correlation matrices as well as their eigenvalues. For that purpose, we define class `my_matrix`, where we define basic methods for work with

matrices, as well as methods for obtaining their eigenvalues and eigenvectors using LAPACK [12].

4.7 ROOT analysis

In order to make azimuthal angle histograms, one needs to run a simple ROOT analysis. The functions are stored in `my_root.cpp` Since not every running of the algorithm requires running of this analysis, we made it a separate procedure. Moreover, it is a useful tool for figure productions, corresponding drawing procedures are also stored here.

4.8 Program running

When running the program, additional commands are needed. If there are none, program will write out help report. The commands are listed in the tab. 1. The commands `-bin`, `-fig` and `-eig` needs the information about initial sorting and about the initial rotation of the events, optionally the information about the normalization and flipping of the events. In case of a missing parameter, ESSTER outputs an information about the missing parameter and writes out help report.

-gen	Generates $NoEvents$ events.
-cml	Analyses generated events via cumulant method.
-epm	Analyses generated events via event plane method.
-epm+	Analyses generated events via event plane method (with p_T weighing).
-ESE	Analyses generated events via event shape engineering.
-psi_0	Rotate events according to maximum.
-psi_n	Rotate events according to the n^{th} event plane.
-mul	Normalizes events according to multiplicity.
-bin	Starts the sorting algorithm.
-q0	Initially sorts the events randomly.
-qn	Initially sorts the events according to q_n.
-flip	Flips half of the events after sorting and sorts them once more.
-fig	Draws histogram figures.
-eig	Outputs correlation and covariance matrices into corresponding folder.
-help	Writes out help report.
-exit	Does nothing.
-test	Testing mode used for development.

Table 1: Program ESSTER commands.

5 Results

In general, we generated 5000 events as described in 4.1. The azimuthal angle histograms consist of 20 bins, the total width is 2π. We divided events into deciles. This means there are 10 'packs' of the events, each consisting of 500 events. The prior, used in 3.1, is then 1/10.

As an example and for later reference, we present two cases: first we tested the algorithm. The events were generated with elliptic flow only, $v_2 \in (0, 0.1)$, multiplicity was uniform. We initially rotated each event according to the second reaction plane and sorted it them according to v_2. The algorithm converged immediately. The dependence of the final mean bin number $\hat{\mu}$ on the elliptic flow v_2 can be found in the fig. 5a. As expected, the error matrix (meaning the probability $P(\alpha|\beta)$ as calculated in the sec. 3.2), is rather diagonal (fig. 5b). The corners are darker (the probability $P(0|0)$ and $P(9|9)$ is higher) because we have finite number of bins.

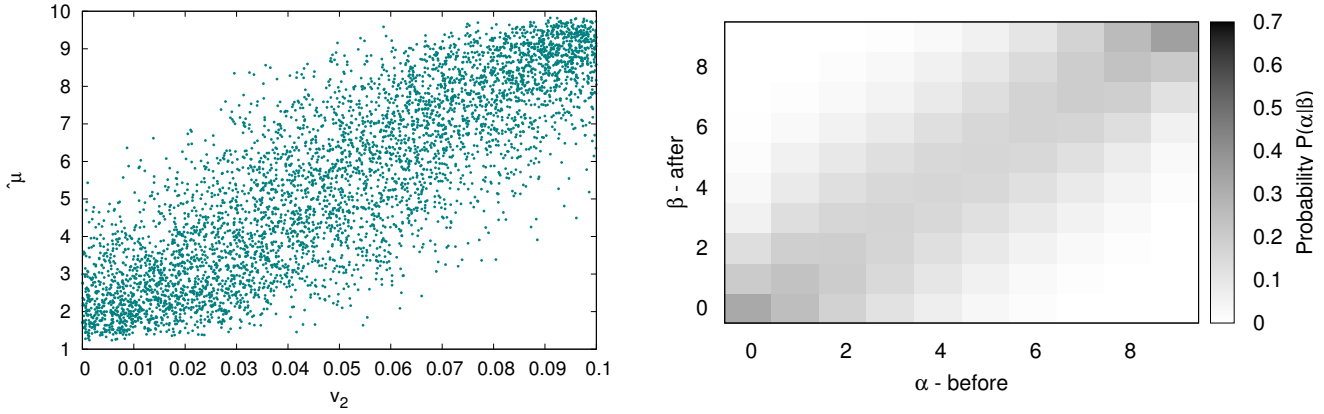

(a) (b)

Figure 5: Algorithm testing results for events with elliptic flow only, $v_2 \in (0, 0.1)$, v_2 distribution is uniform. Events were initially arranged according to v_2. (a) Average bin number $\hat{\mu}$ dependence on v_2. Rather linear shape suggest v_2 is a good measure. (b) Error matrix. Probability of initial bin assignment given the final bin assignment $P(\alpha|\beta)$ as described in 3.2.

The second example presents events generated with linearly multiplicity-dependent v_2, $M \in (300, 3000)$. Once again, initial rotation is according to Ψ_2. In this case, we originally sorted events according to a random number $\in (0, 1)$. This means we initially assigned every event a random

number from zero to one and sorted it according to this number, then we applied the algorithm. It took 108 steps to converge. This is a good reference for initial sorting variable; if the number of steps is higher, it means the events were initially sorted wrongly or inversely proportionally. On the other hand, this number is just a rough estimate, for any conclusion, higher statistics is required. The results are in the fig. 6. The lines that appear around numbers 1, 2, 3, 8, 9 and 10 suggest the algorithm best discriminates the events in the bins on the edge and that the events in the central bins 4 - 7 are very similar to each other.

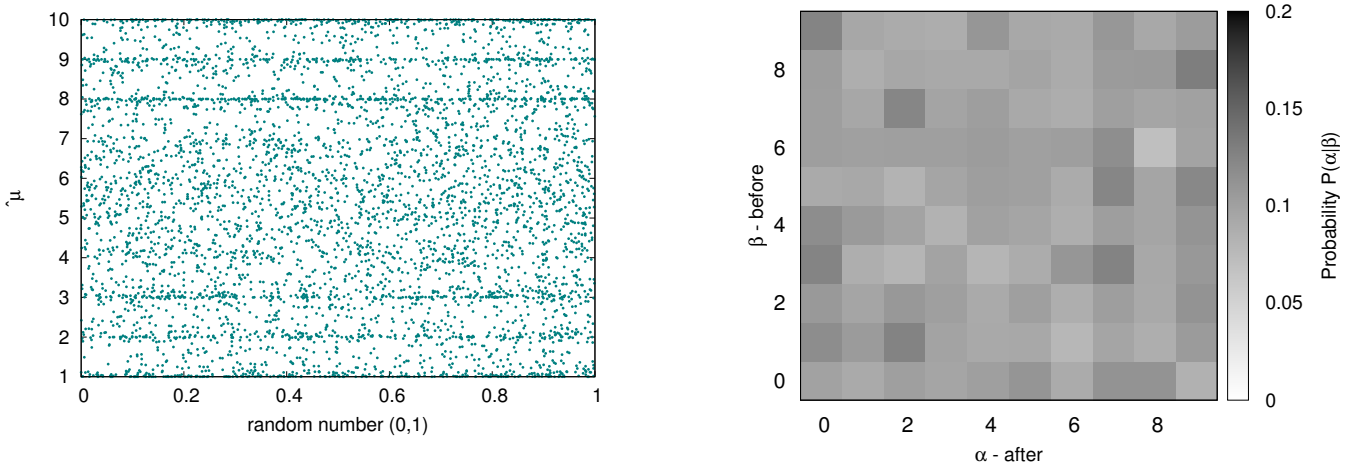

(a) (b)

Figure 6: Algorithm testing results for events with elliptic flow only, $v_2 \sim M$. Events were initially arranged randomly. (a) Average bin number $\hat{\mu}$ dependence on random number. The datapoints make noise, meaning the initial measure was random. (b) Error matrix. Probability of initial bin assignment given the final bin assignment $P(\alpha|\beta)$ as described in 3.2.

5.1 Elliptic flow

Next step was generating events with directed and elliptic flow as described in the section 4.1. We are interested in azimuthal angle histograms. This leads to the question how to initially rotate the events. Since directed flow v_1 is much smaller than v_2, we assume the events are rather elliptic, and the second reaction plane is the only significant plane. Hence, we rotated the events initially in such a way so that Ψ_2 is zero.

5.1.1 Random initial arrangement

First, we initially sorted the events according to a random number, as well as we did in the previous example. The algorithm converged after 65 steps. First, in the fig. 7a, we present the final $\hat{\mu}$ dependence on the initial sorting variable, in this case a random number $\in (0, 1)$. It is clear that the this dependence looks like a noise with sharp line around the bin number nine. This is again caused by a big difference in the last few bins. This discrimination between bins can be also seen in the fig. 7b and fig. 7c. The figures depict the $\hat{\mu} = \hat{\mu}(v_2)$ dependence for both methods we used for event analysis, meaning cumulant and event plane method. Figure 7d shows the error matrix described in 3.2. The matrix is almost uniform, with darker and lighter places, caused again by the finite number of events and bins.

For the illustration of the sorting power of this algorithm, we include in the appendix fig. 75. In these figures, we present average event angle distribution for each one of the ten event bins μ before the algorithm was applied and after the algorithm was used. The fig. 75a confirms that random arrangement results in the same average azimuthal angle histograms. The elliptic shape of the event is visible. The fig. 75b shows that the events are organized from the most 'round' ones (with the lowest v_2) to the most elliptic ones (with the highest v_2).

To confirm the results in the fig. 7, we calculated the correlation coefficient between the final bin number μ number and the elliptic flow, the value is -0.960. Apparently, those two variables are inversely proportional.

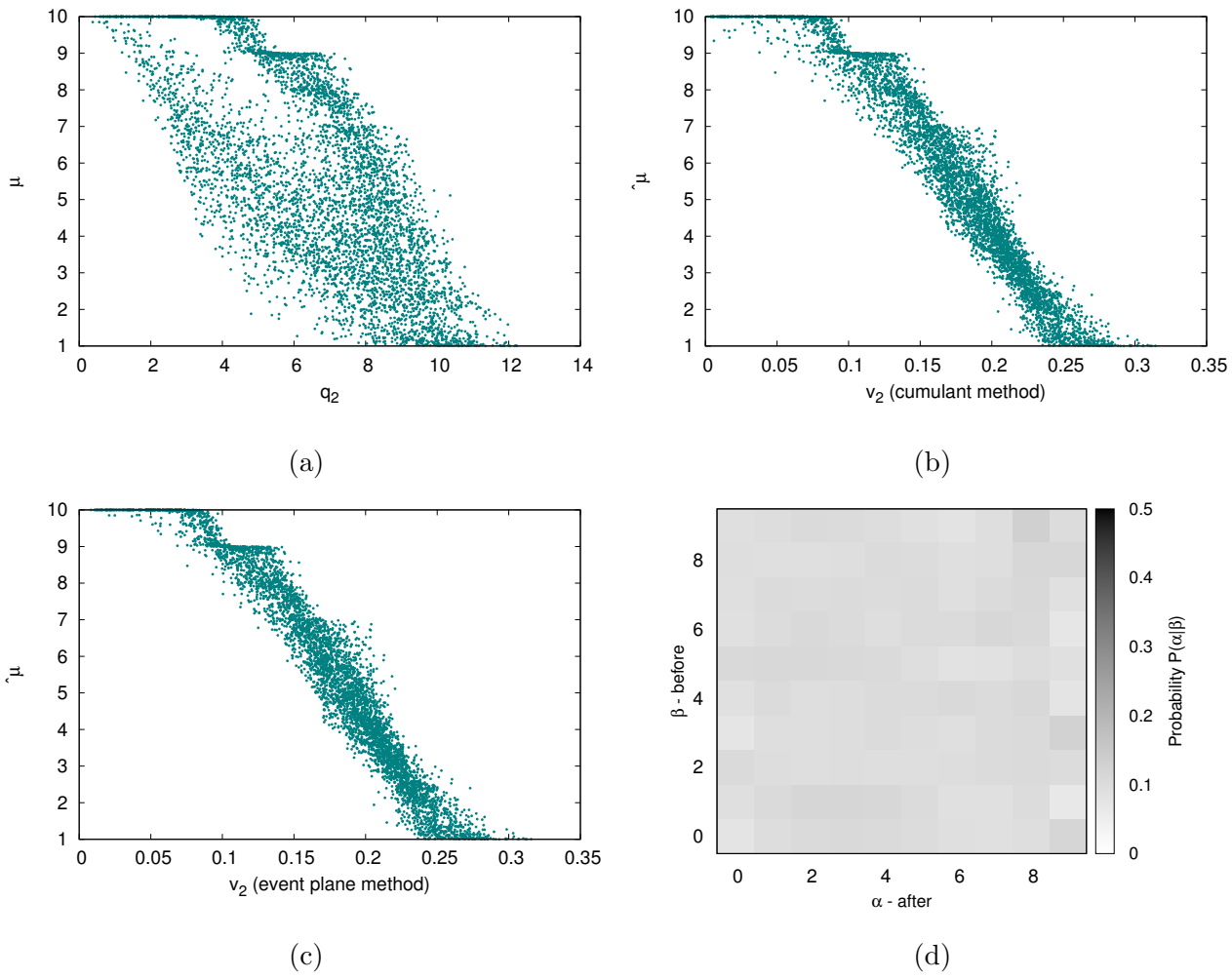

Figure 7: Algorithm results for initially random arrangement. (a) Average bin number $\hat{\mu}$ dependence on q_2. (b) Average bin number $\hat{\mu}$ dependence on v_2. v_2 was obtained via cumulant method. (c) Average bin number $\hat{\mu}$ dependence on v_2. v_2 was obtained via event plane method. (d) Error matrix. Probability of initial bin assignment given the final bin assignment $P(\alpha|\beta)$.

Normalized histograms

Since we were interested in the properties of the algorithm, we also normalized the histograms with respect to the multiplicity and bin width. The results are rather surprising. It took only 8 steps for the algorithm to converge. The results are in the fig. 8. This time, the final $\hat{\mu}$ are very close to 5. This fact suggest that the algorithm does not discriminate very well. On the other hands, the results for the $\hat{\mu} = \hat{\mu}(v_2)$ dependence is clearly linear. The error matrix is rather uniform. The vertical stripes suggest the measure is very poor [2].

For visual comparison of the event bins, we include fig. 76a and fig. 76b. Once again, we present average event angle distribution for every bin μ before the algorithm was applied and after the algorithm was used. Figure 76a confirms that random arrangement results in the same average azimuthal angle histograms. The elliptic shape of the event is visible. Figure 76b shows that the events are organized from the most 'round' ones (with the lowest v_2) to the most elliptic ones (with the highest v_2). This is consistent with the fig. 8b and the fig. 8c. In this case, the correlation coefficient between the final bin number μ number and the elliptic flow is 0.996.

The comparison between fig. 8, fig. 76 and fig. 7, fig. 75 illustrates the power of the algorithm. Despite the random arrangement of the events, the algorithm converged and arranged the events according to their shape; in the first case, the algorithm sorted the event from the biggest v_2 to smallest. In the second case, the events are arranged from smallest to highest v_2.

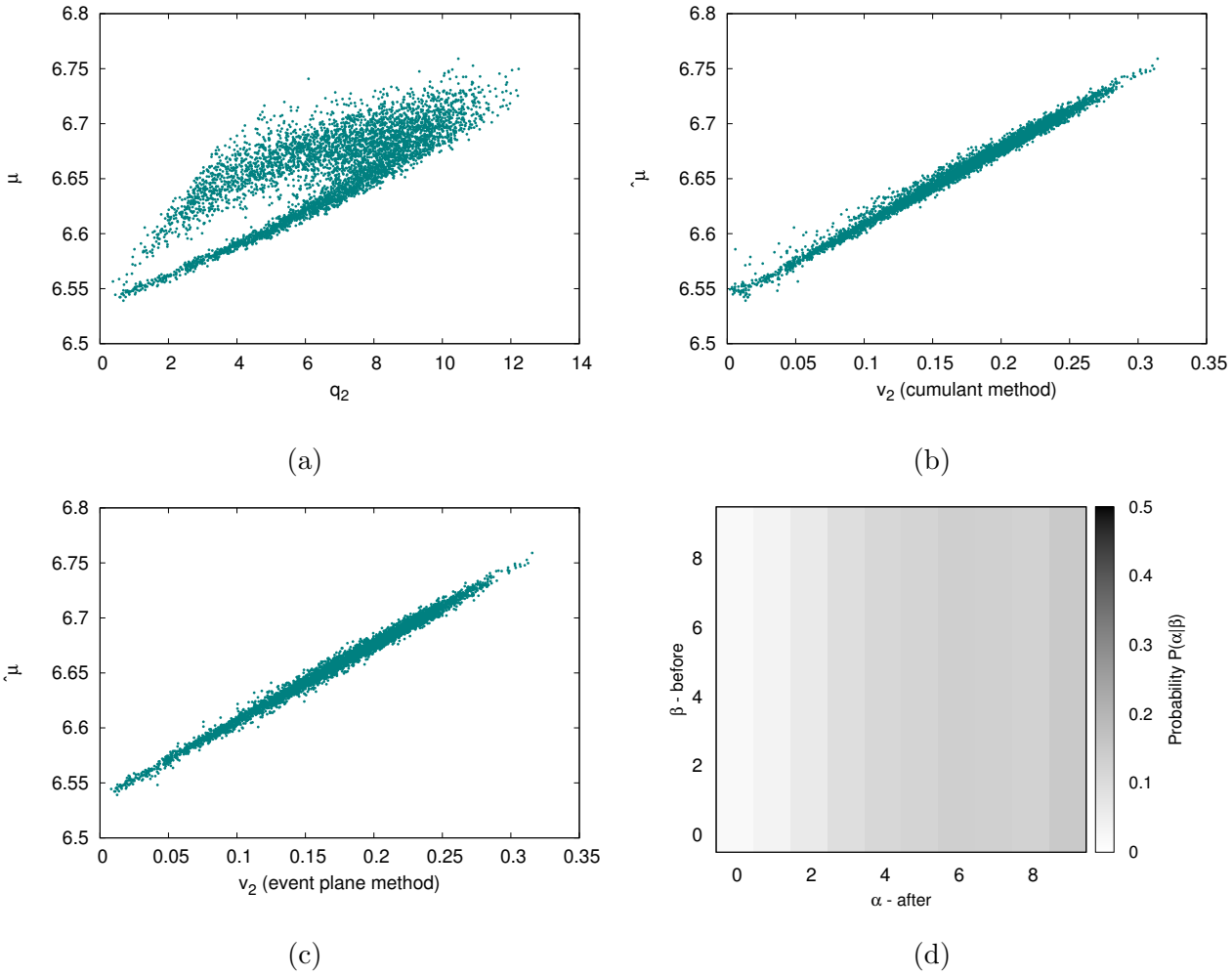

Figure 8: Algorithm results for initially random arrangement and normalized histograms. (a) Average bin number $\hat{\mu}$ dependence on q_2. (b) Average bin number $\hat{\mu}$ dependence on v_2. v_2 was obtained via cumulant method. (c) Average bin number $\hat{\mu}$ dependence on v_2. v_2 was obtained via event plane method. (d) Error matrix. Probability of initial bin assignment given the final bin assignment $P(\alpha|\beta)$.

5.1.2 Initial arrangement according to q_2

Next step was to initially arrange events according to q_2. According to [1], this should lead to distinguishing the events according to their shape.

The algorithm converged after 26 steps. This is significantly smaller number than in the previous example, indicating q_2 is a good measure of the event shape. The results can be seen in the fig. 9. First, in the fig. 9a, we present the final average event bin number $\hat{\mu} = \hat{\mu}(q_2)$ dependence. This dependence evinces some pattern, however, not a significant one. The sharp lines around the number one is once again caused by the difference between bins. This discrimination between bins can be also seen in the fig. 9b and fig. 9c, where we present the $\hat{\mu} = \hat{\mu}(v_2)$ dependence for both methods we used for event analysis. Compared to the fig. 7, the final dependence is 'flipped'. This just means that when the initial arrangement was random, the algorithm sorted the events from the biggest v_2 to smallest. In this case, the events are arranged from smallest to highest v_2. Figure 10 shows the error matrix. The matrix is not as diagonal as it could be in the case q_2 was a perfect measuring variable. The darker corners are caused by the finite number of event bins. Very interesting are these results compared to fig. 5, where we implemented linear dependence of v_2 on multiplicity. This might be caused by the fact that q_2 by definition scales with $1/\sqrt{M}$. The correlation coefficient between the final bin number μ and v_2 is 0.959, which agrees with the value -0.960 in the case of the random initial arrangement.

All these results suggest possible multiplicity dependence. Figure 9d shows the dependence on multiplicity is not straightforward and that the algorithm rather sorts the events according to their overall shape, not only bin height.

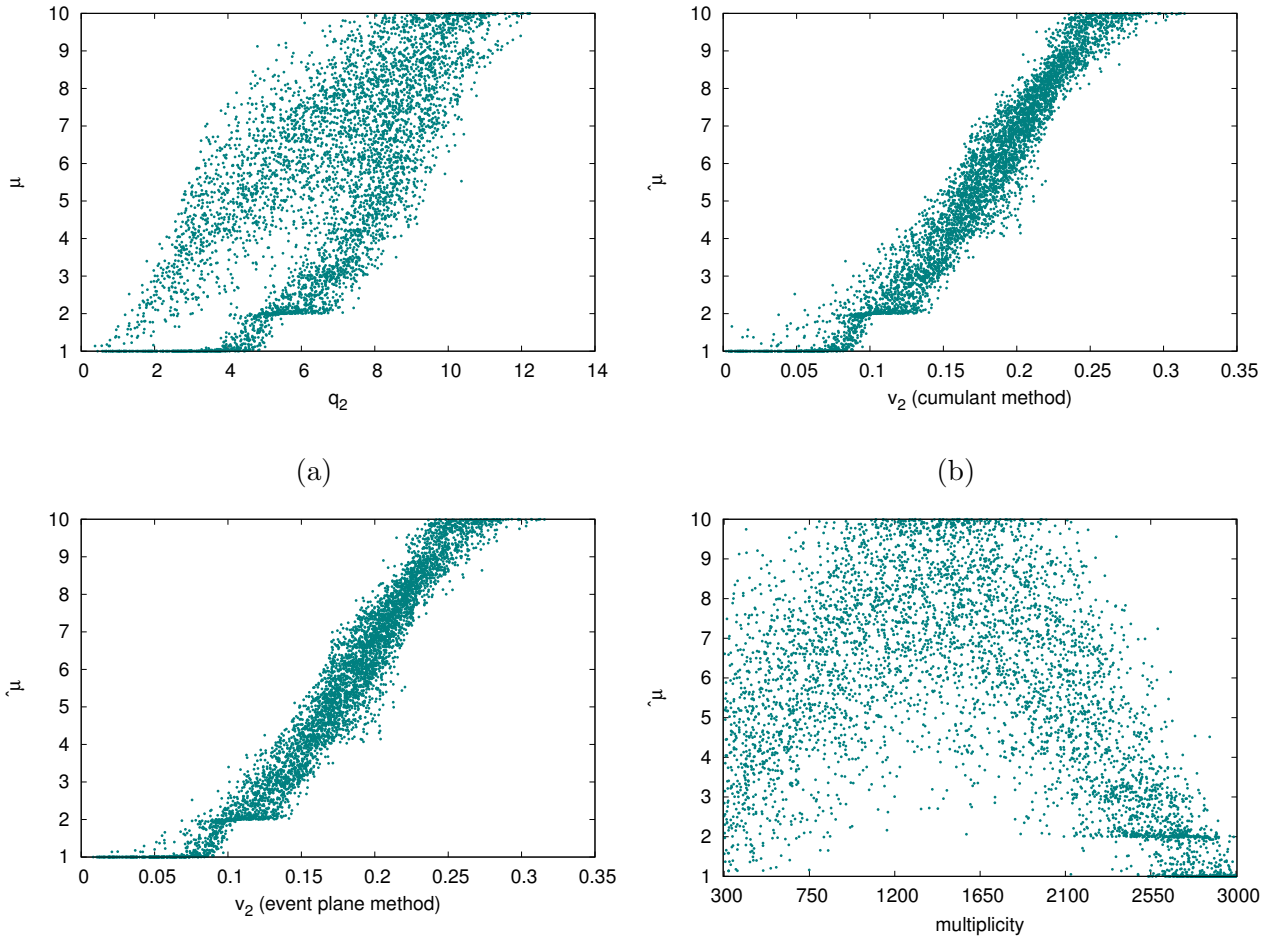

Figure 9: Algorithm results for initial arrangement according to q_2. (a) Average bin number $\hat{\mu}$ dependence on q_2. (b) Average bin number $\hat{\mu}$ dependence on v_2. v_2 was obtained via cumulant method. (c) Average bin number $\hat{\mu}$ dependence on v_2. v_2 was obtained via event plane method. (d) Average bin number $\hat{\mu}$ dependence on multiplicity.

As well as in the previous case, we present figures of average bins before and after the algorithm was applied in the fig. 77. Both figures confirms that the events are organized from the most 'round' ones (with the lowest v_2) to the most elliptic ones (with the highest v_2). However, there is a visible shift in the multiplicity dependence.

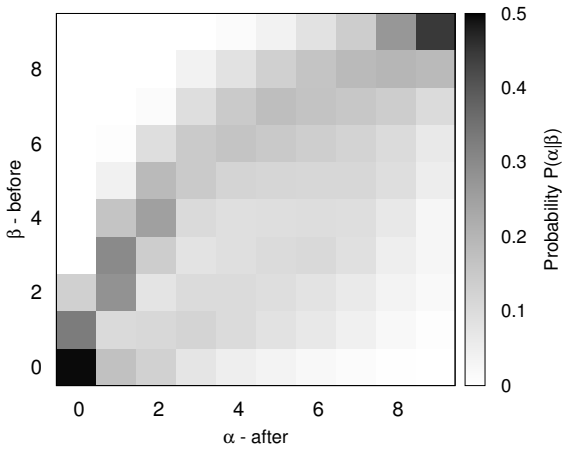

Figure 10: Error matrix. Probability of initial bin assignment given the final bin assignment $P(\alpha|\beta)$.

Normalized histograms

As well as in the case of initial random arrangement, we normalized the histograms with respect to multiplicity and bin width. Even in the case of normalized histograms, the initial sorting according to q_2 leads to sooner convergence, it took only 6 steps to converge. Results are in the fig. 11. The $\hat{\mu} = \hat{\mu}(q_2)$ dependence (fig. 11a) evinces similar shape as in the fig. 9a. The final $\hat{\mu}$ are very close to 5, there are vertical stripes in the error matrix fig. 11c. This leads to the conclusion that the algorithm does not measure normalized histograms very well. The correlation coefficient between the final bin number μ and v_2 is 0.996, which agrees with the initial random arrangement. In this case we does not include the results from cumulant method, since they agree with the event plane method results.

As well as in the previous case, we present figures of average bins before and after the algorithm was applied in the fig. 78.

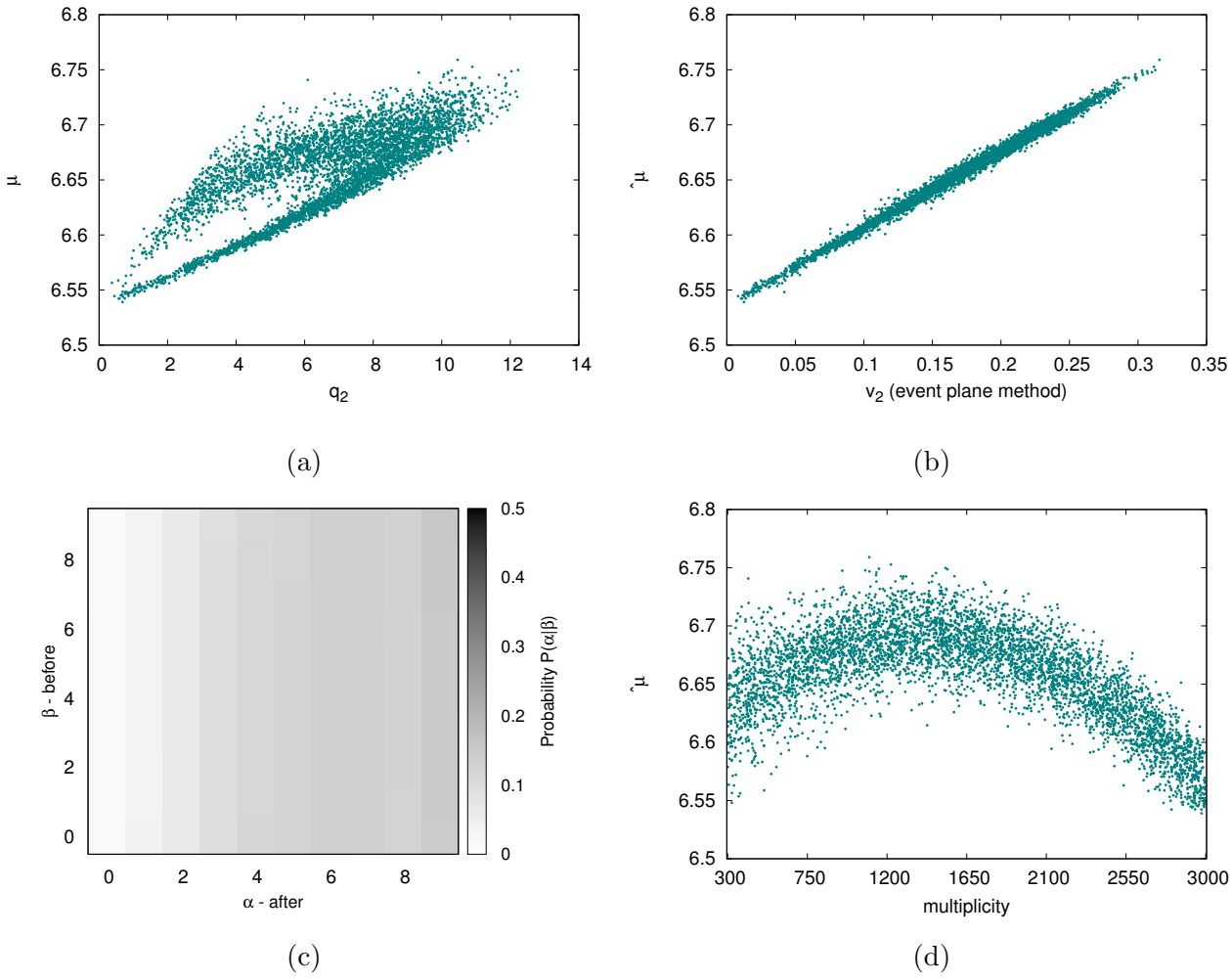

Figure 11: Algorithm results for initial arrangement and normalized histograms according to q_2. (a) Average bin number $\hat{\mu}$ dependence on q_2. (b) Average bin number $\hat{\mu}$ dependence on v_2. v_2 was obtained via event plane method. (c) Error matrix. Probability of initial bin assignment given the final bin assignment $P(\alpha|\beta)$. (d) Average bin number $\hat{\mu}$ dependence on multiplicity.

5.2 Triangular flow

As well as in the previous section, we face the question how to initially rotate the events. Hence, this section is divided into subsections according to the initial rotation of the events.

5.2.1 Initial rotation according to Ψ_2

First, we rotated the events once again according to Ψ_2. This originates from the fact that v_2 contribution to the flow is the highest.

Random arrangement

As a reference, we initially arranged the events randomly. The algorithm converged after 336 steps. This number is five times higher than in the case of events without the triangular flow contribution. This reflects the fact that the events are more unlike and therefore their sorting is more complicated.

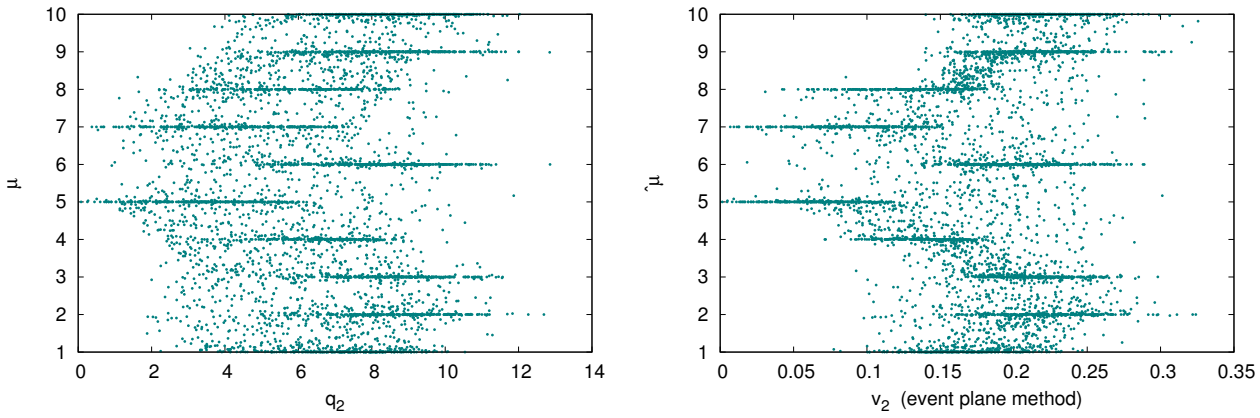

(a) (b)

Figure 12: Algorithm results for initially random arrangement. Events are generated with flow up to triangular flow, initial rotation is according Ψ_2. (a) Average bin number $\hat{\mu}$ dependence on q_2. (b) Average bin number $\hat{\mu}$ dependence on v_2. v_2 was obtained via event plane method.

The results are shown in fig. 12 and fig. 13. In fig. 12a, we present the final $\hat{\mu}$ dependence on the initial sorting variable, in this case a random number $\in (0, 1)$. The sharp lines, mentioned in the previous section, are even more visible. This means the finally arranged bins are very different from

each other. This discrimination between bins can be also seen in the fig. 12b,fig. 13a,fig. 13b and fig. 13c. The figure 13c suggests that the multiplicity and the final bin number μ are not correlated at all. Figure 13d shows the error matrix. The matrix is almost uniform, which is consistent with initial random arrangement. There is no visible correlation between any of the flow coefficients neither. The correlation between μ and v_2 is 0.015, in the case of v_3 it is even less, 0.010.

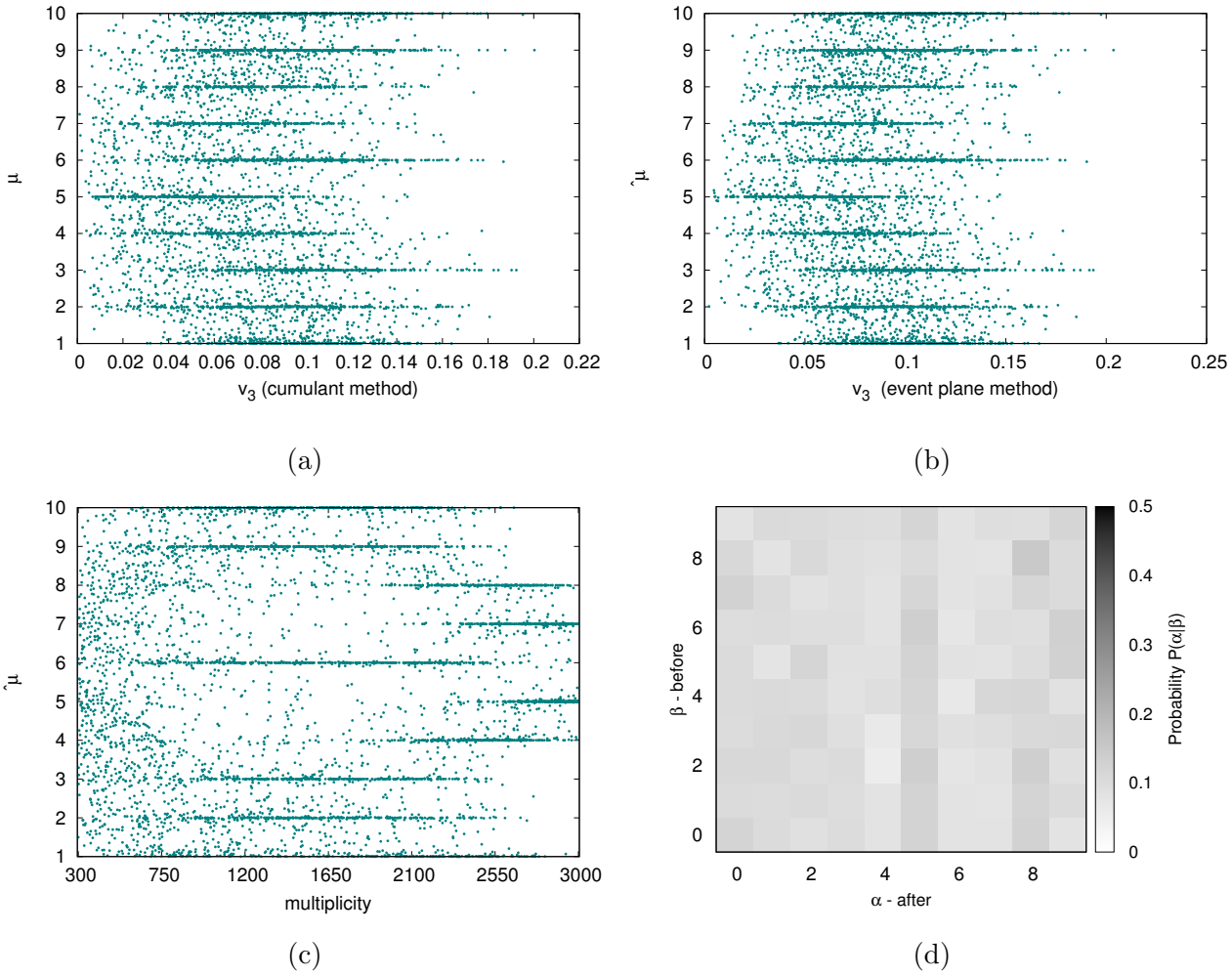

Figure 13: Algorithm results for initially random arrangement. Events are generated with flow up to triangular flow, initial rotation is according Ψ_2. (a) Average bin number $\hat{\mu}$ dependence on v_3. v_3 was obtained via cumulant method. (b) Average bin number $\hat{\mu}$ dependence on v_3. v_3 was obtained via event plane method. (c) Average bin number $\hat{\mu}$ dependence on multiplicity. (d) Error matrix. Probability of initial bin assignment given the final bin assignment $P(\alpha|\beta)$.

The average histograms for each one of the 10 event bins μ before the algorithm was applied and after the algorithm was used are in the appendix in the fig. 79. The fig. 79a confirms that random arrangement results in the same average azimuthal angle histograms. Only elliptic flow is visible, because of the initial rotation. The fig. 79b shows that the events are organized somehow randomly. However, there is a strong contribution from the v_3. This suggest that in order to eliminate the bias originating from the initial rotation, one has to include Ψ_3.

Normalized histograms

We also normalized the histograms with respect to the bin width and multiplicity. The ESSTER took 132 steps to converge. This is a high number, compared to 8 steps that it took in the case of presence of v_1 and v_2 only. The results are in fig. 14. Since the results from event plane method and cumulant method are consistent, we provide only the results from event plane method. Once again, fig. 14d suggests the measure is rather bad and that it does not discriminate very well. There is a visible triangular shape in the fig. 14c. However, if we consider the average angle histograms in the fig. 80, even though the contribution form v_3 is significant, elliptic flow plays even bigger role.

Arrangement according to q_2

Once again, next step was to initially arrange events according to q_2. As mentioned before, according to [1], this should lead to distinguishing the events according to their shape.

The algorithm converged after 268 steps. This is comparable number to the initial random arrangement. This suggests q_2 is not a good measure of the event shape. The results are in the fig. 15. There is no visible dependence, even though the error matrix evinces a little 'W' shape.

If we look closer to the average histograms in the fig. 81, there are bins that looks very alike, just like a mirror image of each other, for instance bins 0 and 4 or 7 and 9. This suggest that the arrangement of both Ψ_2 and Ψ_3 plays a role.

There is no correlation between the final bin number and v_2 or v_3. In the first case, the correlation coefficient is 0.081, in the other case 0.015.

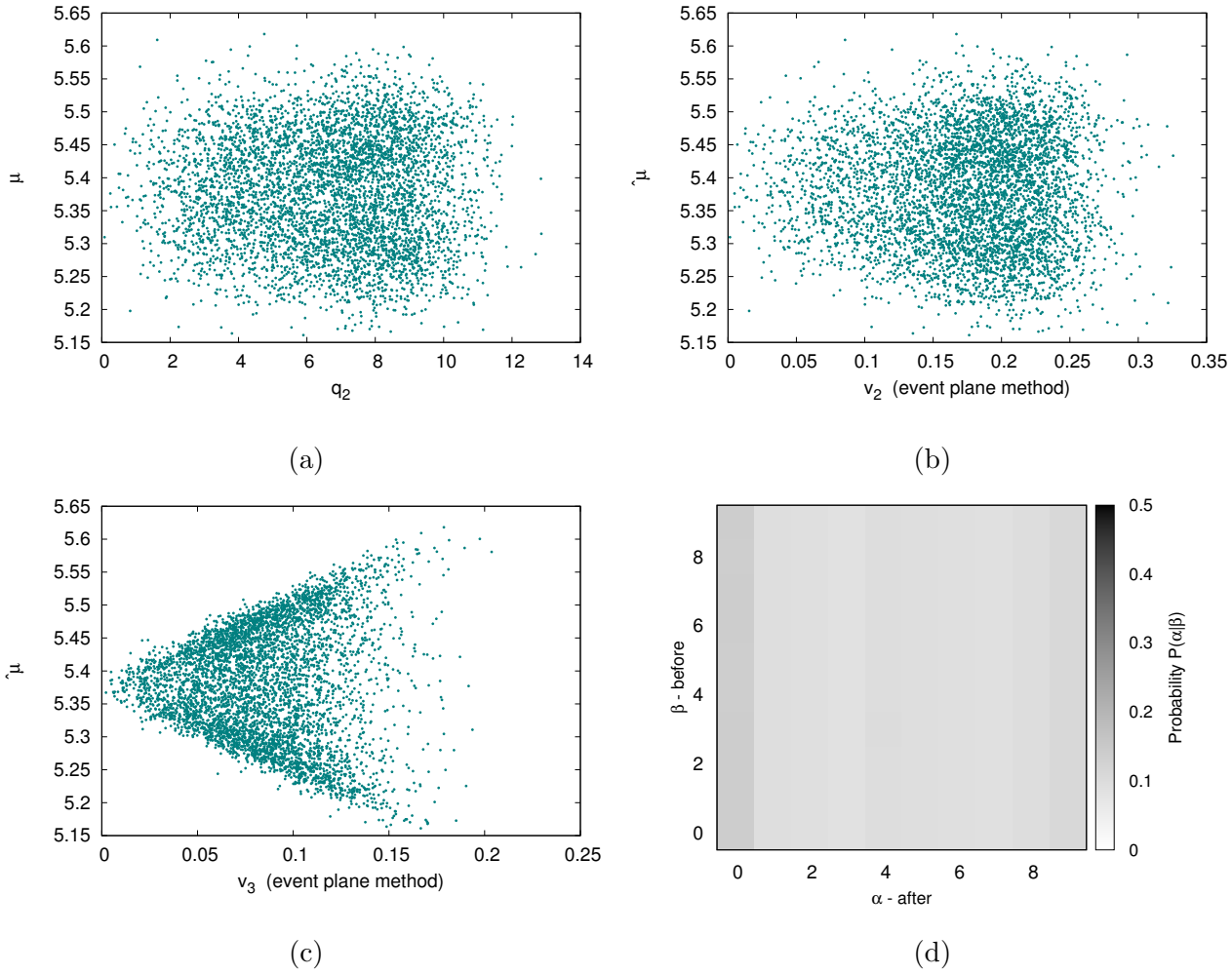

Figure 14: Algorithm results for initially random arrangement and normalized histograms. Events are generated with flow up to triangular flow, initial rotation is according Ψ_2. (a) Average bin number $\hat{\mu}$ dependence on q_2. (b) Average bin number $\hat{\mu}$ dependence on v_2. v_2 was obtained via event plane method. (c) Average bin number $\hat{\mu}$ dependence on v_3. v_3 was obtained via event plane method. (d) Error matrix. Probability of initial bin assignment given the final bin assignment $P(\alpha|\beta)$.

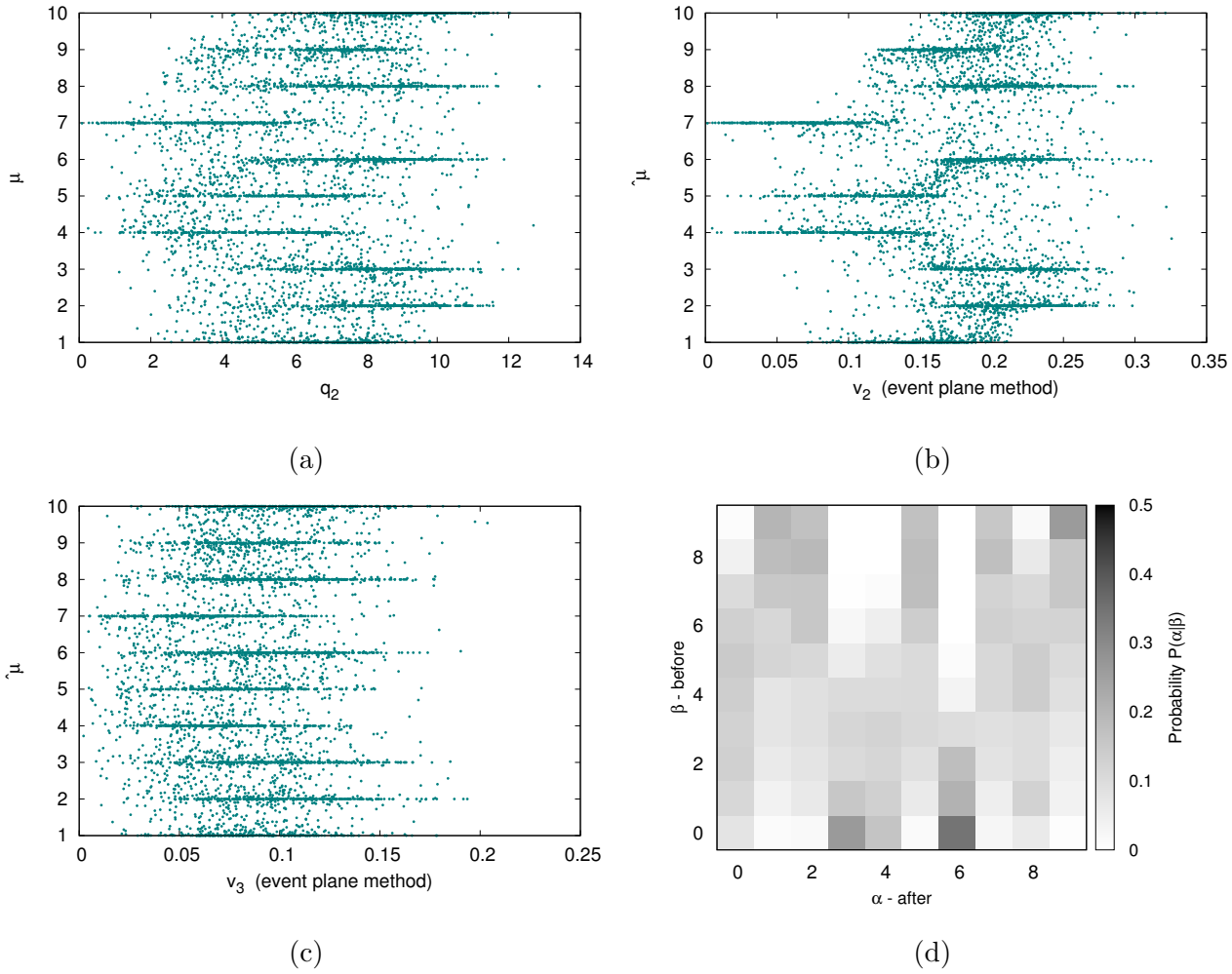

Figure 15: Algorithm results for initial arrangement according to q_2. Events are generated with flow up to triangular flow, initial rotation is according to Ψ_2. (a) Average bin number $\hat{\mu}$ dependence on q_2. (b) Average bin number $\hat{\mu}$ dependence on v_2. v_2 was obtained via event plane method. (c) Average bin number $\hat{\mu}$ dependence on v_3. v_3 was obtained via event plane method. (d) Error matrix. Probability of initial bin assignment given the final bin assignment $P(\alpha|\beta)$.

Normalized histograms

The algorithm converged after 131 steps. This is comparable number to the initial random arrangement for normalized histograms. The results are in the fig. 16. They suggest this is not a good measure at all. Once again note that the final mean bin number $\hat{\mu}$ ranges from 5.45 to 5.95. There is no correlation between the final bin number μ and v_2 is 0.115 and between μ and v_3 is

0.039. As well in the case of not normalized histograms, the average histograms in the fig. 82, there are bins that looks very alike, just like a mirror image of each other, suggesting the importance of interplay of both Ψ_2 and Ψ_3.

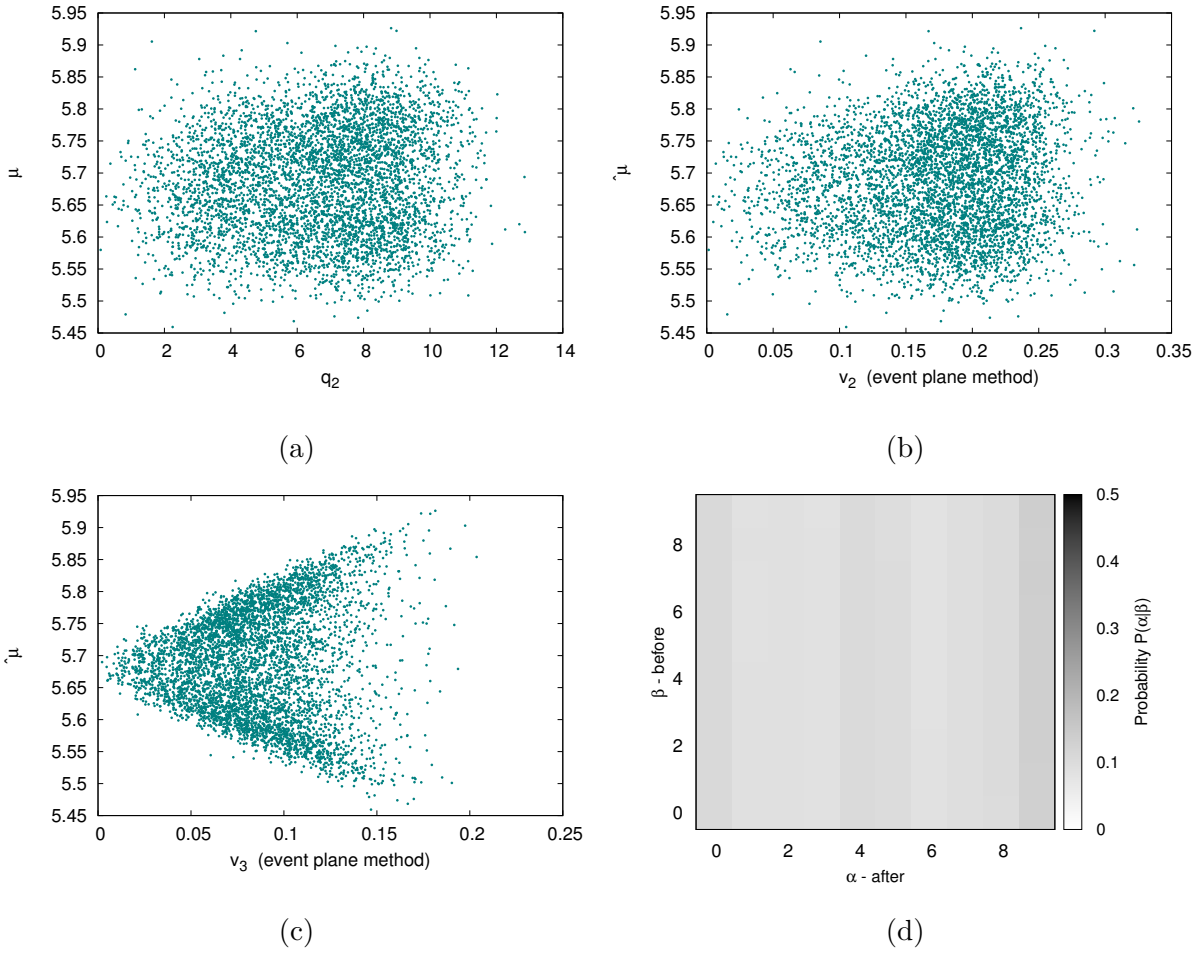

Figure 16: Algorithm results for initial arrangement according to q_2. Events are generated with flow up to triangular flow, histograms were normalized, initial rotation is according to Ψ_2. (a) Average bin number $\hat{\mu}$ dependence on q_2. (b) Average bin number $\hat{\mu}$ dependence on v_2. v_2 was obtained via event plane method. (c) Average bin number $\hat{\mu}$ dependence on v_3. v_3 was obtained via event plane method. (d) Error matrix. Probability of initial bin assignment given the final bin assignment $P(\alpha|\beta)$.

5.2.2 Initial rotation according to Ψ_3

As argued before, the initial rotation provides a bias. Therefore, we tried to rotate the events according to Ψ_3. The technique was the same as in the case of Ψ_2, we rotated the events in a such way that Ψ_3 is zero.

Random arrangement

The algorithm converged after 96 steps. This seems faster than in the case of rotation according to Ψ_2, however, when we run the algorithm again, the number of steps varies in the order of hundreds. The results are in the fig. 17 and in the fig. 18. The results suggest that the discrimination in the bins is very strong, however, there is no relation between v_2 or v_3 and the final bin number μ. The correlation between v_2 and μ is -0.065 and the correlation between v_3 and μ is -0.035. The results from event plane method and cumulant method are consistent, therefore, from now on we include only results from event plane method.

The average histograms are in the fig. 83. The fig. 83a confirms that random arrangement results in the same average azimuthal angle histograms, this time the triangular flow is nicely visible and dominant. In the fig. 83b, elliptic flow seems to be dominant, even though there is an interplay between elliptic and triangular flow.

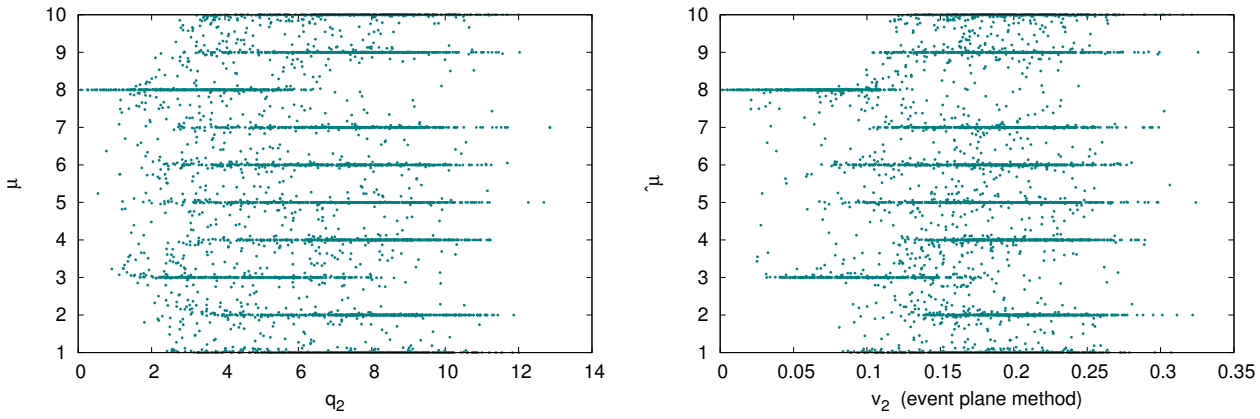

(a) (b)

Figure 17: Algorithm results for initially random arrangement. Events are generated with flow up to triangular flow, initial rotation is according to Ψ_3. (a) Average bin number $\hat{\mu}$ dependence on q_2. (b) Average bin number $\hat{\mu}$ dependence on v_2, v_2 was obtained via event plane method.

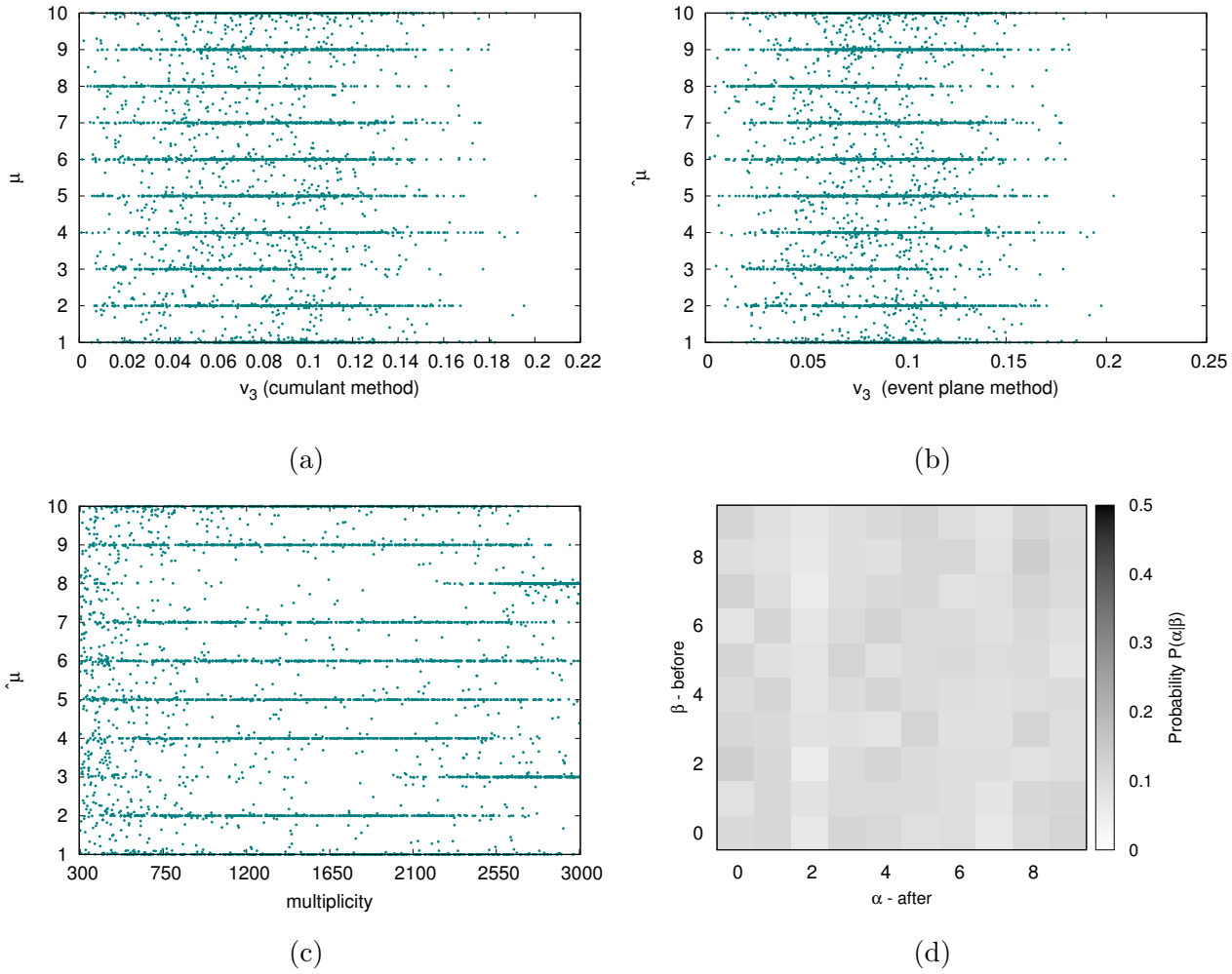

Figure 18: Algorithm results for initially random arrangement. Events are generated with flow up to triangular flow, initial rotation is according to Ψ_3. (a) Average bin number $\hat{\mu}$ dependence on v_3. v_3 was obtained via cumulant method. (b) Average bin number $\hat{\mu}$ dependence on v_3. v_3 was obtained via event plane method. (c) Average bin number $\hat{\mu}$ dependence on multiplicity. (d) Error matrix. Probability of initial bin assignment given the final bin assignment $P(\alpha|\beta)$.

Normalized histograms

The ESSTER converged after 96 steps. Surprisingly, this is the same number as in the case of non-normalized histograms. The results are in the fig. 19 and in the fig. 20. Unfortunately, fig. 20d suggest the measure is rather bad. There is a visible v_2 dependence on final average bin number $\hat{\mu}$. Figures 20a and 20b suggest the triangular flow is not a good measure. The multiplicity dependence in fig. 20c evinces signs of some symmetry, one can see two mirror arcs. The correlation between v_2 and μ is 0.015 and the correlation between v_3 and μ is 0.016, meaning there is no apparent correlation.

The average histograms are in the fig. 84. Figure 84b confirms that elliptic flow is dominant and that triangular flow contribution is not negligible.

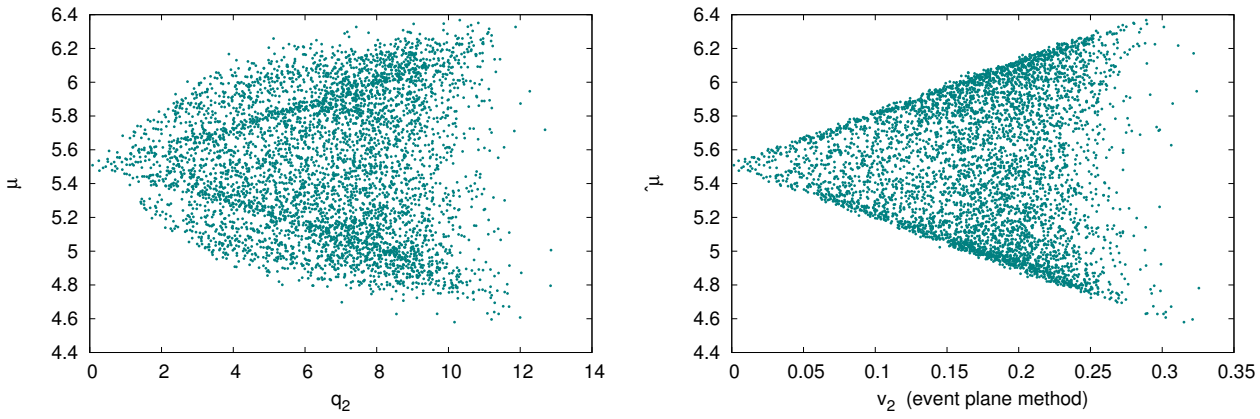

(a) (b)

Figure 19: Algorithm results for initially random arrangement. Events are generated with flow up to triangular flow, histograms normalized, initial rotation is according to Ψ_3. (a) Average bin number $\hat{\mu}$ dependence on q_2. (b) Average bin number $\hat{\mu}$ dependence on v_2. v_2 was obtained via event plane method.

Arrangement according to q_2

The algorithm failed to converge. We stopped the process after 5000 steps. This means the event shape somehow depends on q_2. However the relation is not obvious. The result are in the fig. 21. There is a significant difference between bins 4,5 and the rest of the bins (see fig. 21d). Question is, whether it s caused by the relation between the shape of the event and q_2 or simply by the

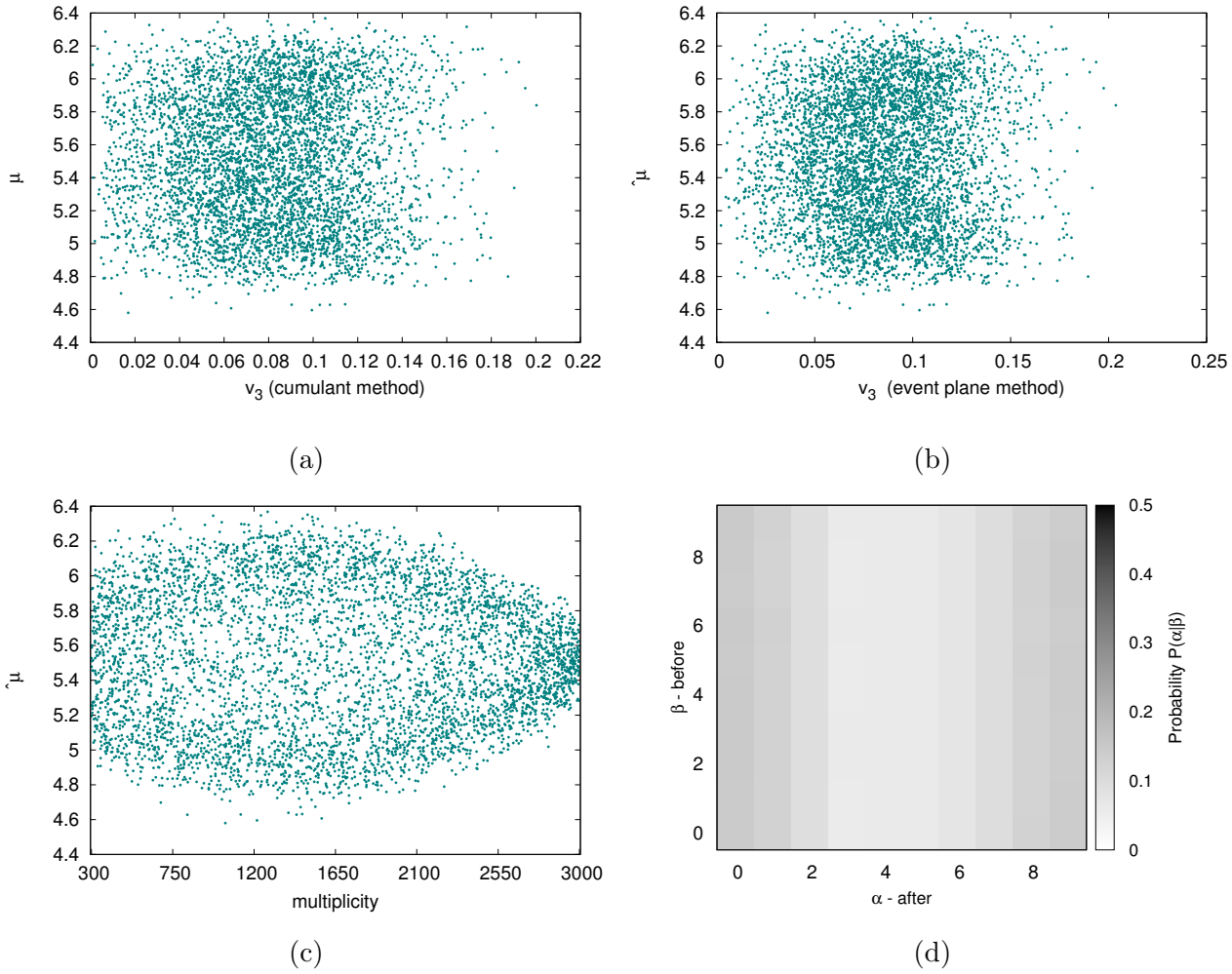

Figure 20: Algorithm results for initially random arrangement. Events are generated with flow up to triangular flow, histograms normalized, initial rotation is according to Ψ_3. (a) Average bin number $\hat{\mu}$ dependence on v_3. v_3 was obtained via cumulant method. (b) Average bin number $\hat{\mu}$ dependence on v_3. v_3 was obtained via event plane method. (c) Average bin number $\hat{\mu}$ dependence on multiplicity. (d) Error matrix. Probability of initial bin assignment given the final bin assignment $P(\alpha|\beta)$.

ESSTER not converging. The correlation between final bin number μ and v_2 is 0.005, μ and v_3 is slightly higher, 0.02. The average histograms are in the fig. 85. Compared to the fig. 83, the initial random sorting leaves the events organizes somehow differently, meaning the starter and end point are shifted. This once again leads to the need of somehow flipping the events.

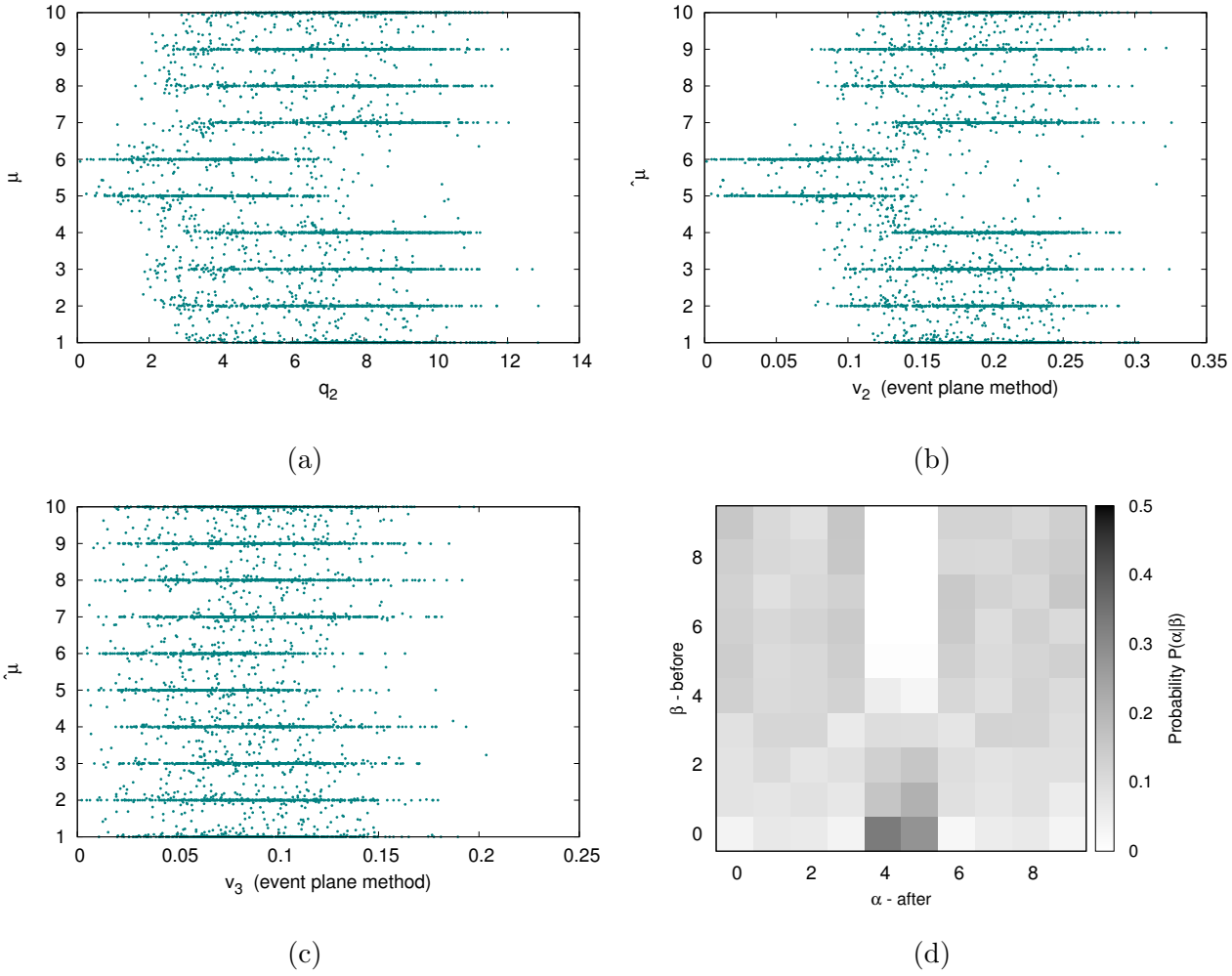

Figure 21: Algorithm results for initial arrangement according to q_2. Events are generated with flow up to triangular flow, initial rotation is according to Ψ_3. (a) Average bin number $\hat{\mu}$ dependence on initially assigned random number. (b) Average bin number $\hat{\mu}$ dependence on v_2. v_2 was obtained via event plane method. (c) Average bin number $\hat{\mu}$ dependence on v_3. v_3 was obtained via event plane method. (d) Error matrix. Probability of initial bin assignment given the final bin assignment $P(\alpha|\beta)$

Normalized histograms

In this case, the algorithm converged after 91 steps. This is comparable to the number of steps the program took to sort the events rotated according to Ψ_2. But the results (fig. 22 and fig. 23) are very different. The triangular shape of the dependence of final mean bin number $\hat{\mu}$ on v_2 and q_2 is visible in fig. 22a as well as in fig. 22b. It seems that v_3 is not important, see fig. 23a. Even though the error matrix (fig. 23c) suggest the measure is rather bad, this results lead to the idea of including mirror images of the events. Looking at the fig. 86b, the results agree with the fig. 85b.

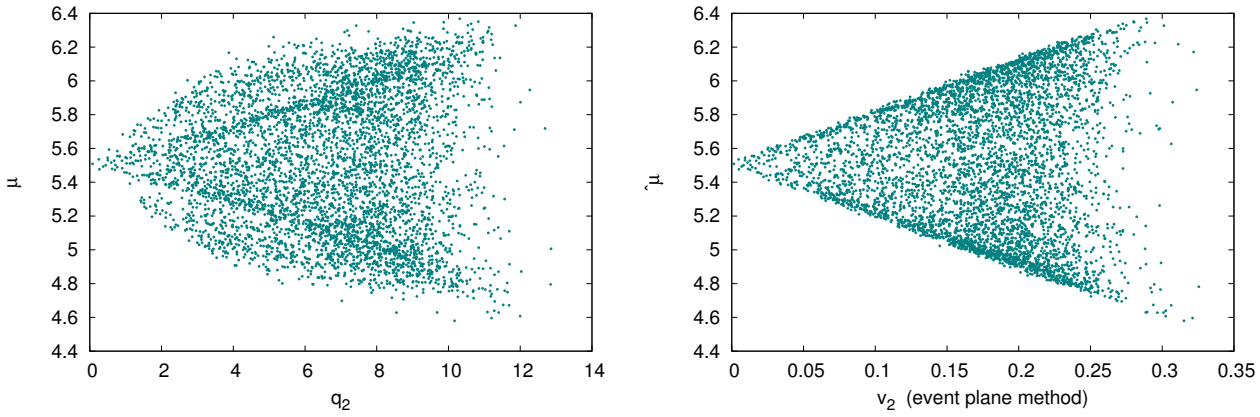

(a) (b)

Figure 22: Algorithm results for initial arrangement according to q_2. Events are generated with flow up to triangular flow, histograms normalized, initial rotation is according to Ψ_3. (a) Average bin number $\hat{\mu}$ dependence on q_2. (b) Average bin number $\hat{\mu}$ dependence on v_2. v_2 was obtained via event plane method.

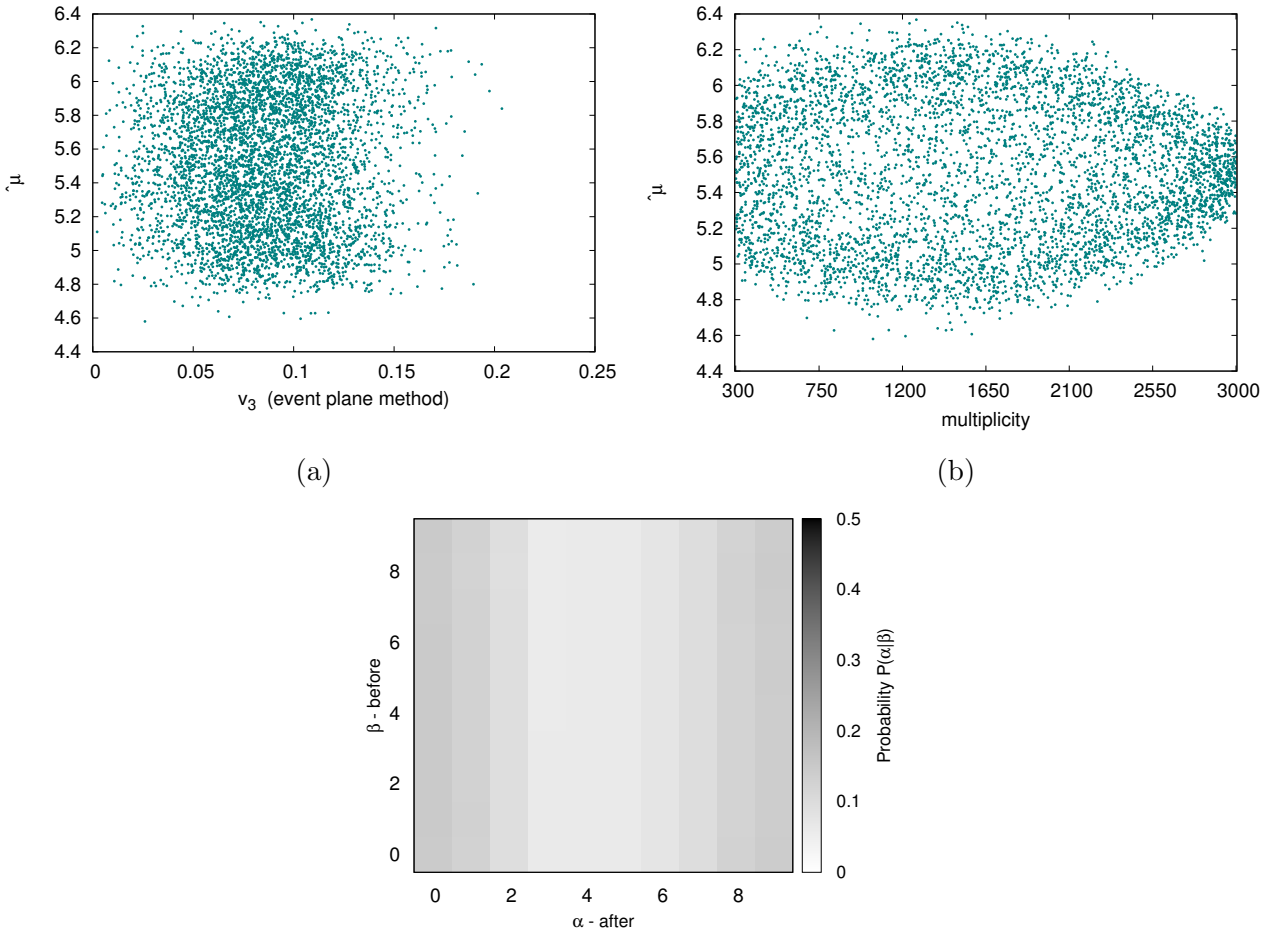

(a) (b)

(c)

Figure 23: Algorithm results for initial arrangement according to q_2. Events are generated with flow up to triangular flow, histograms normalized, initial rotation is according to Ψ_3. (a) Average bin number $\hat{\mu}$ dependence on v_3. v_3 was obtained via event plane method. (b) Average bin number $\hat{\mu}$ dependence on multiplicity. (c) Error matrix. Probability of initial bin assignment given the final bin assignment $P(\alpha|\beta)$.

5.2.3 Initial rotation according to Ψ_2 and Ψ_3

Considering the previous results, we tried to initially rotate the events with respect to both Ψ_2 and Ψ_3. We found the angle between Ψ_2 and Ψ_3. If $\Psi_2 < \Psi_3$, we made a mirror image of the whole event. This might solve the problem with the similarity between the events mentioned in the case of rotation according to Ψ_2 and Ψ_3.

Random arrangement

It took 46 steps for the algorithm to converge, which is even better result than in the case of rotation according to Ψ_3. The results are in the fig. 24. The results suggest that the discrimination in the bins is very strong. However, there is no visible dependence on q_2, v_2 or v_3. The correlation between the final bin number μ is -0.002 in the case of elliptic flow, for triangular flow it is -0.009. The average histograms are in the fig. 87. The results suggest that v_2 is more significant than v_3. It is obvious that there is no need for the events to be flipped, the average histograms does not evince any similarity.

Normalized histograms

It took 18 steps for the ESSTER to converge, which is even better result than in the case of rotation according to Ψ_3. The results are in the fig. 25. The results suggest that the discrimination in the bins is very low (fig. 25d), note that the mean bin number $\hat{\mu}$ is between 4.2 and 6.4. Once again, the triangular shape of dependence $\hat{\mu} = \hat{\mu}(v_2)$ (fig. 25b) is apparent. The correlation between the final bin number μ and v_3 is -0.102, between μ and v_3 it is -0.032.

If we look closer to the average histograms in the fig. 88, the bins looks sorted rather well. There are no bins that looks shifted to other bins or bins that look like a mirror image of each other. This together with the fig. 87, this suggest that the choice of rotating the events according to both Ψ_2 and Ψ_3 is a good choice.

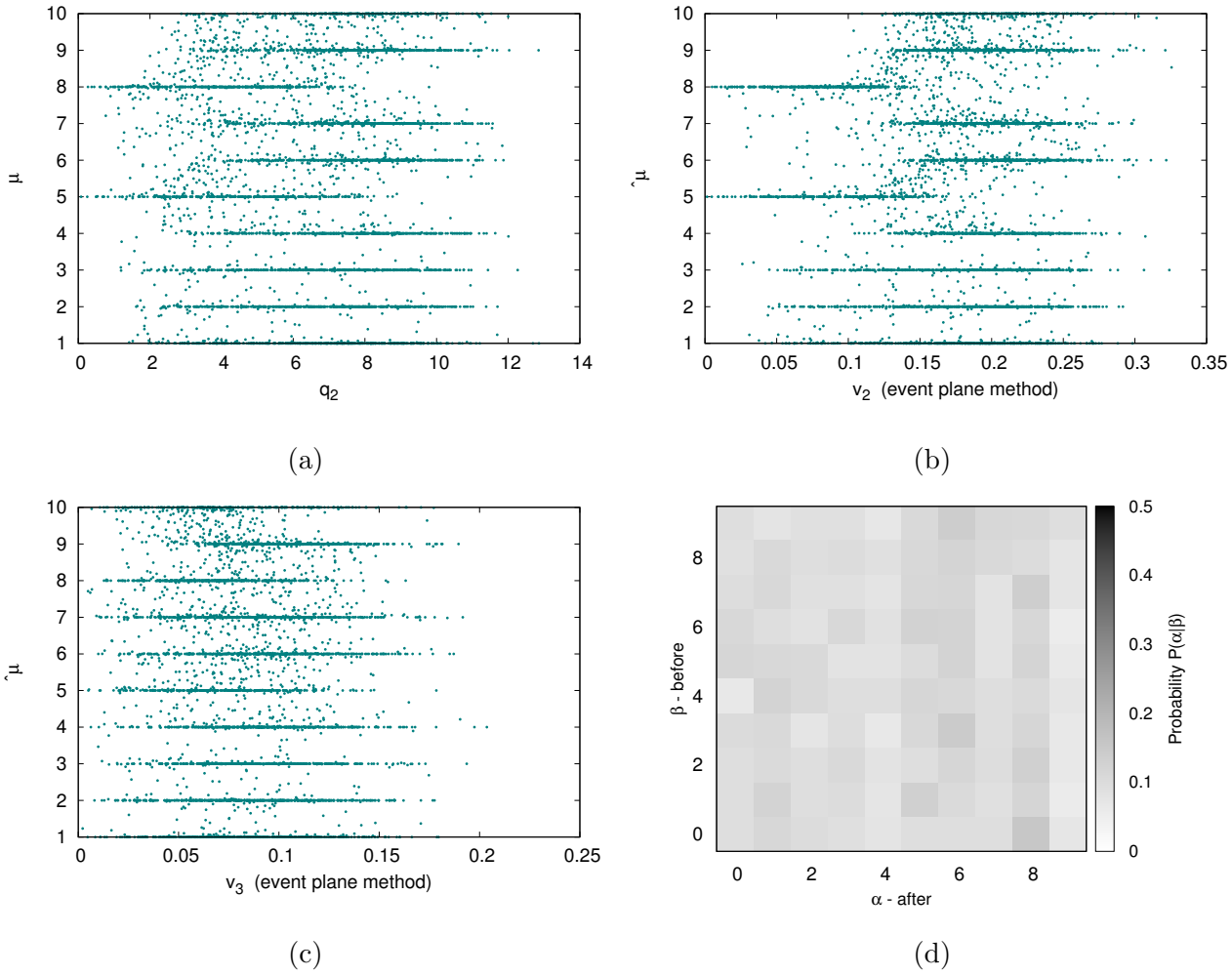

Figure 24: Algorithm results for initially random arrangement. Events are generated with flow up to triangular flow, initial rotation is according to Ψ_2 and Ψ_3. (a) Average bin number $\hat{\mu}$ dependence on q_2. (b) Average bin number $\hat{\mu}$ dependence on v_2. v_2 was obtained via event plane method. (c) Average bin number $\hat{\mu}$ dependence on v_3. v_3 was obtained via event plane method. (d) Error matrix. Probability of initial bin assignment given the final bin assignment $P(\alpha|\beta)$.

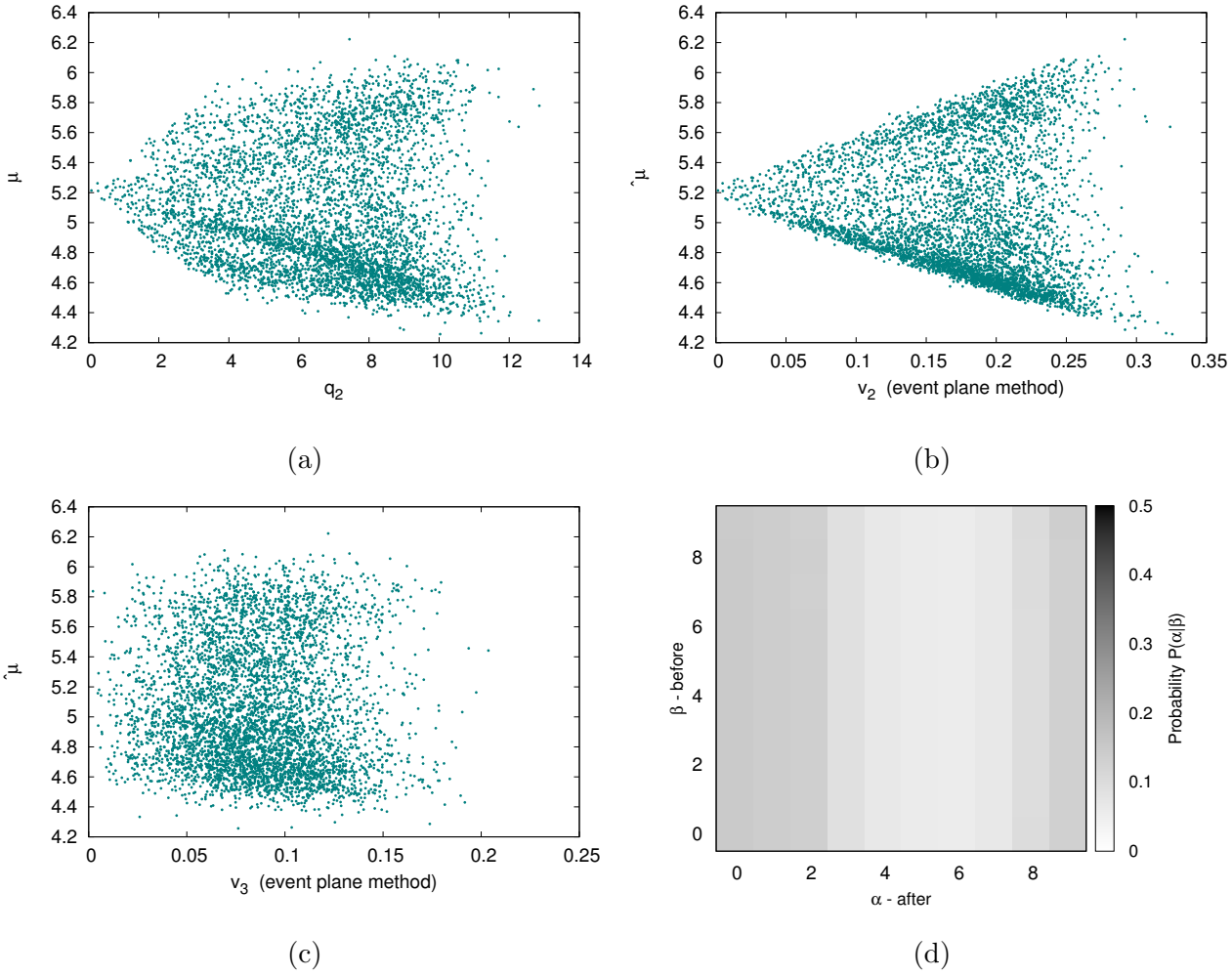

Figure 25: Algorithm results for initially random arrangement. Events are generated with flow up to triangular flow, histograms were normalized and rotated according to Ψ_2 and Ψ_3. (a) Average bin number $\hat{\mu}$ dependence on q_2. (b) Average bin number $\hat{\mu}$ dependence on v_2. v_2 was obtained via event plane method. (c) Average bin number $\hat{\mu}$ dependence on v_3. v_3 was obtained via event plane method. (d) Error matrix. Probability of initial bin assignment given the final bin assignment $P(\alpha|\beta)$.

Arrangement according to q_2

Once again, the algorithm failed to converge. We stopped the program at 5000 steps. The results are in the fig. 26. The error matrix in the fig. 26d evinces two significantly different stripes in the bins 5 and 7, supported by the fig. 26a and 26b, where one can see that lines around $\hat{\mu}$ are shifted to the left compared to the other lines. The correlation between v_2 and μ is -0.025 and the correlation between v_3 and μ is -0.014, meaning there are inversely proportional to μ. This results is rather surprising, but consistent with the failure of convergence; it took so many steps because the algorithm had to reverse the initial arrangement. On the other hand, this coefficients are so small that negative correlation can be just a fluctuation.

Comparing the average histograms in the fig. 89 to the histograms in the fig. 87, we see that the results are exactly the same, the bins are separate from each other and there is no other possibility of 'starting' and 'end' bins. This confirms that the choice of rotating the events according to both Ψ_2 and Ψ_3 is a better than the Ψ_2 and Ψ_3 rotations. Furthermore, it means that the program almost converged and that there is some relation between q_2 and μ, however it is not a straightforward relation.

Normalized histograms

The ESSTER converged after 22 steps. The results are in the fig. 27. As expected, fig. 27d suggest the measure is rather bad. There is a visible triangular q_2 and v_2 dependence on final average bin number $\hat{\mu}$, the v_2 dependence is sharper. Figure 25c confirms that the triangular flow is not a good measure. The correlation between v_2 and μ is 0.102 and the correlation between v_3 and μ is 0.032, meaning there is no apparent correlation.

The average histograms are in the fig. 90. Figure 90b confirms that elliptic flow is dominant and that triangular flow contribution is not negligible. There are no similar of mirror bins.

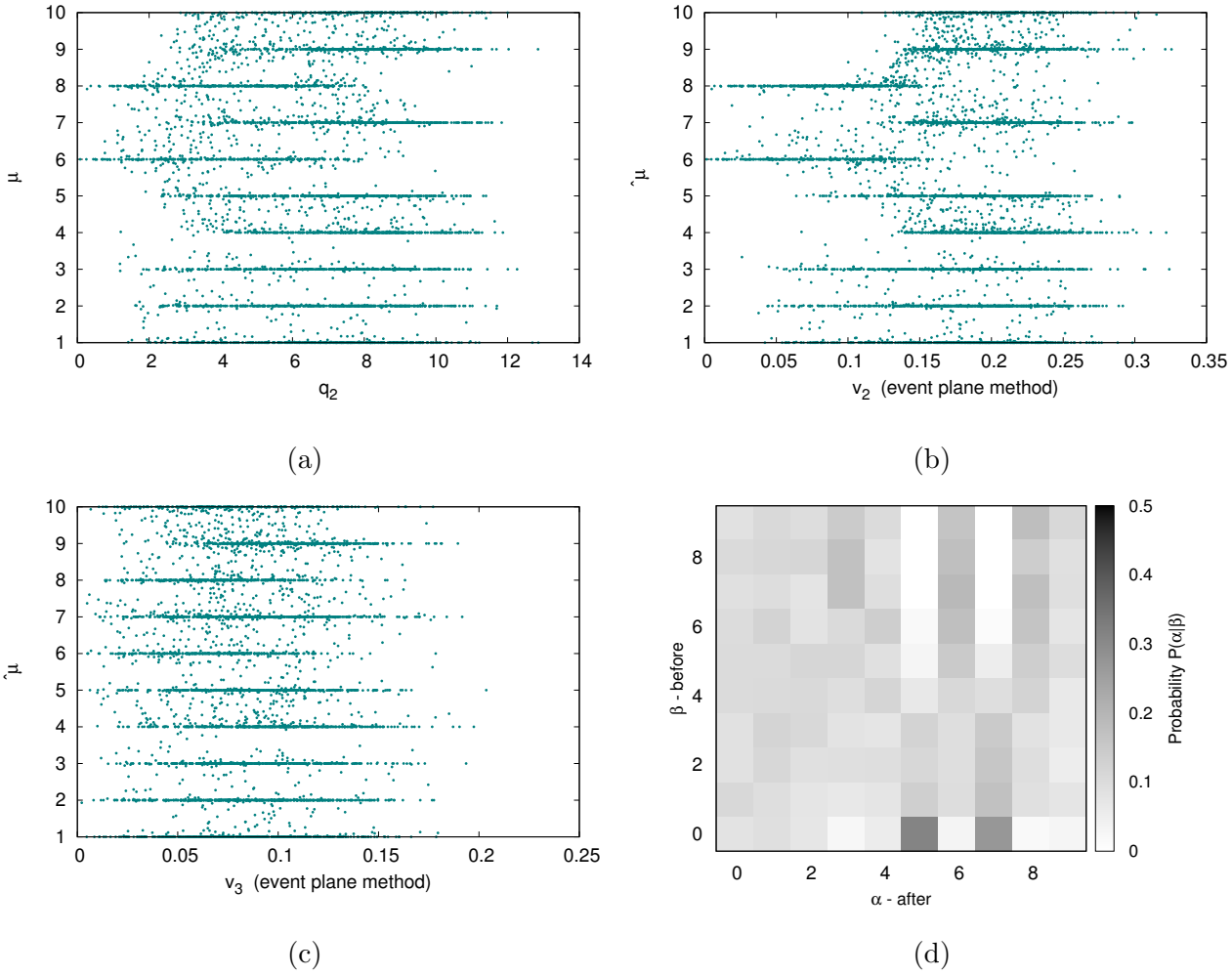

Figure 26: Algorithm results for initial arrangement according to q_2. Events are generated with flow up to triangular flow, histograms were normalized and rotated according to Ψ_2 and Ψ_3. (a) Average bin number $\hat{\mu}$ dependence on q_2. (b) Average bin number $\hat{\mu}$ dependence on v_2. v_2 was obtained via event plane method. (c) Average bin number $\hat{\mu}$ dependence onv_3. v_3 was obtained via event plane method (d) Error matrix. Probability of initial bin assignment given the final bin assignment $P(\alpha|\beta)$.

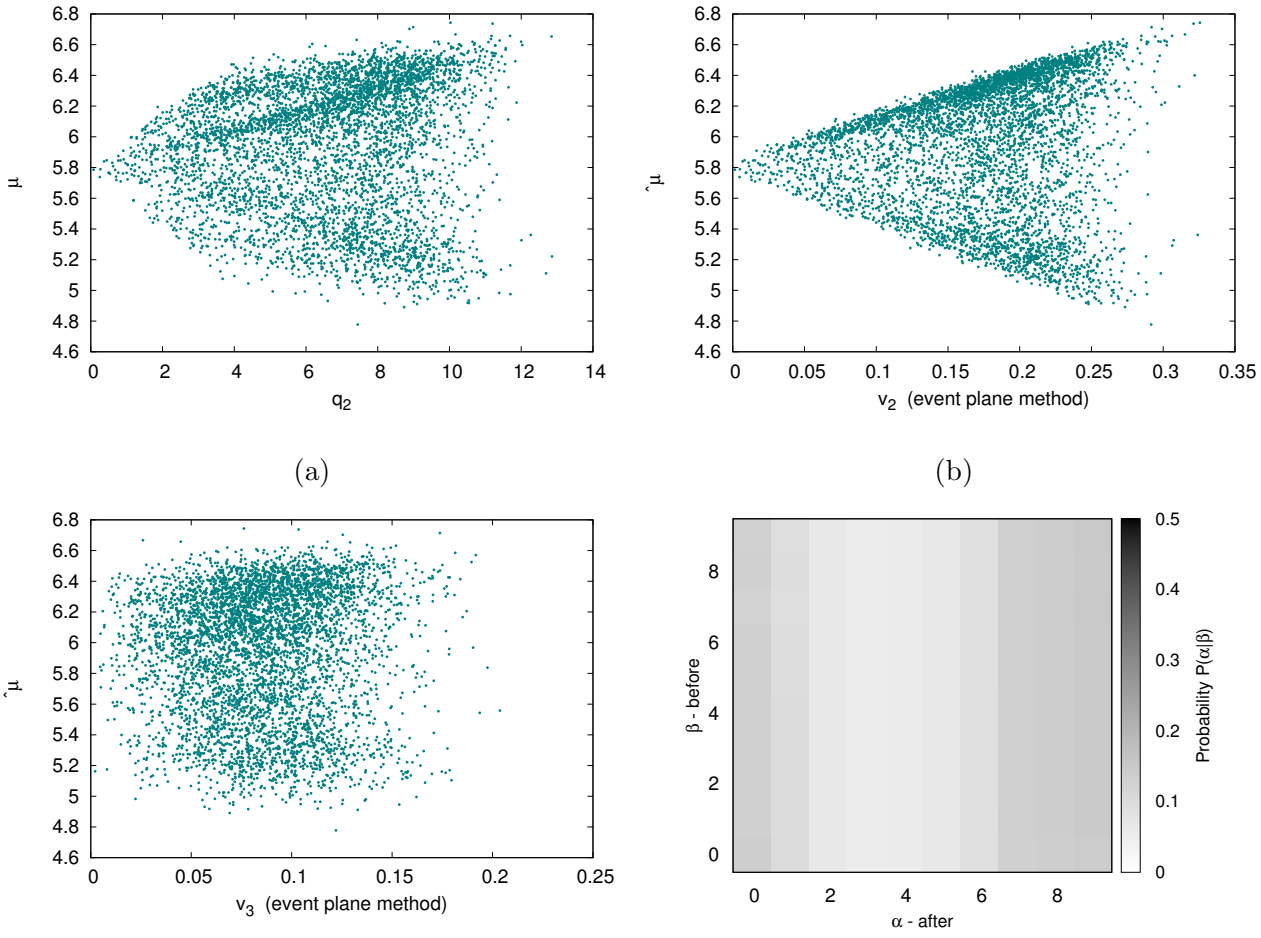

Figure 27: Algorithm results for initial arrangement according to q_2, normalized histograms were initially rotated according to Ψ_2 and Ψ_3. (a) Average bin number $\hat{\mu}$ dependence on q_2. (b) Average bin number $\hat{\mu}$ dependence on v_2. v_2 was obtained via event plane method. (c) Average bin number $\hat{\mu}$ dependence on multiplicity. (d) Error matrix. Probability of initial bin assignment given the final bin assignment $P(\alpha|\beta)$.

5.3 Higher harmonics flow

We were interested in the effect of higher harmonics. We generated events with flow coefficients up to pentagonal flow v_5.

5.3.1 Initial rotation according to Ψ_2

Random arrangement

The results are in the fig. 28, fig. 29 and 30. It took 95 steps to converge. There are very sharp lines around the integers, so this measure discriminates quite well. We present the final bin number μ dependence on v_2, v_3, v_4, and v_5. The only quantity that differs from completely random distribution is v_2 with a slight shift in the central bins. The correlations between the final bin number μ and flow coefficients v_2, v_3, v_4 and v_5 are rather high, compared to the previous results: the highest coefficient is in the case of v_2: 0.299, in the case of v_3 is 0.112, v_4 0.041 and v_5 0.031.

The average bins are in the fig. 91. There are several bins that look alike. It is obvious, if compared to the fig. 79 or fig. 81 that v_4 and v_5 plays a minimum role.

Normalized histograms

The results are in the fig. 31, fig. 32 and fig. 33. There are no sharp lines around the integers, taking into account fig. 33d, this measure discriminates quite bad. The difference between flow obtained from different methods are negligible. The only quantity that differs from completely random distribution is v_3, where one can see the triangular shape, which is rather surprising. The correlations between the final bin number μ and flow coefficients v_2, v_3, v_4 and v_5 are rather almost zero for all cases. The average bins are in the fig. 92. It is clear that the upper row is a mirror image of the lower row. Therefore, we present results for the flipped events in the next paragraph.

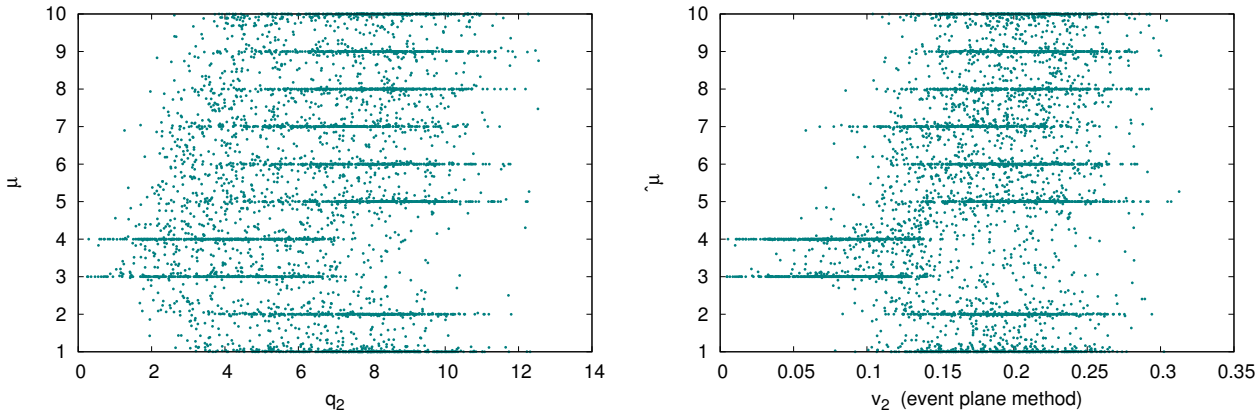

Figure 28: Algorithm results for initially random arrangement. Events are generated with flow up to pentagonal flow, initial rotation is according Ψ_2. (a) Average bin number $\hat{\mu}$ dependence on q_2. (b) Average bin number $\hat{\mu}$ dependence on v_2. v_2 was obtained via event plane method. (c) Average bin number $\hat{\mu}$ dependence on v_3. v_3 was obtained via cumulant method. (d) Average bin number $\hat{\mu}$ dependence on v_3. v_3 was obtained via event plane method.

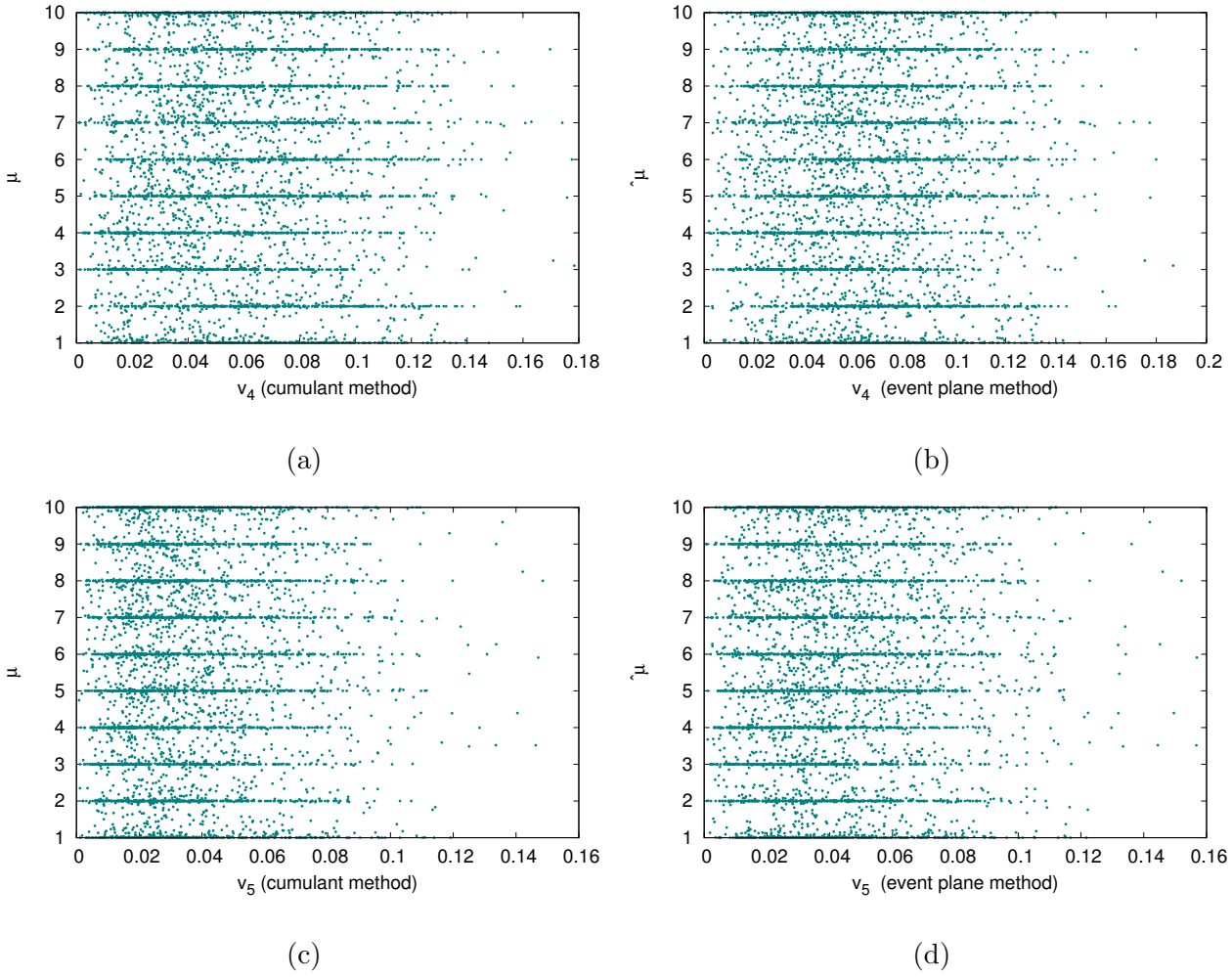

(a) (b)

(c) (d)

Figure 29: Algorithm results for initially random arrangement. Events are generated with flow up to pentagonal flow, initial rotation is according Ψ_2. (a) Average bin number $\hat{\mu}$ dependence on v_4. v_4 was obtained via cumulant method. (b) Average bin number $\hat{\mu}$ dependence on v_4. v_4 was obtained via event plane method. (c) Average bin number $\hat{\mu}$ dependence on v_5. v_5 was obtained via cumulant method. (d) Average bin number $\hat{\mu}$ dependence on v_5. v_5 was obtained via event plane method.

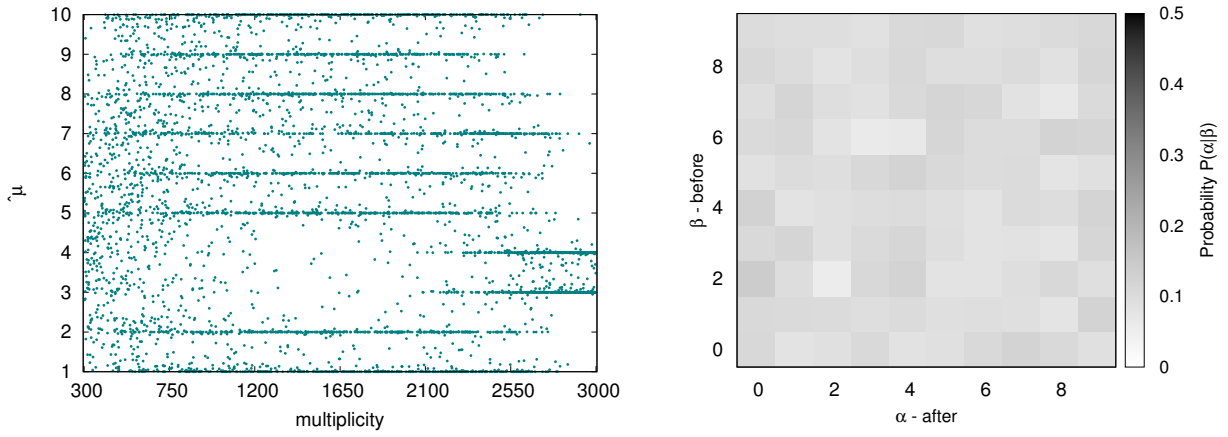

(a) (b)

Figure 30: Algorithm results for initially random arrangement. Events are generated with flow up to pentagonal flow, initial rotation is according Ψ_2.(a) Average bin number $\hat{\mu}$ dependence on multiplicity. (b) Error matrix. Probability of initial bin assignment given the final bin assignment $P(\alpha|\beta)$.

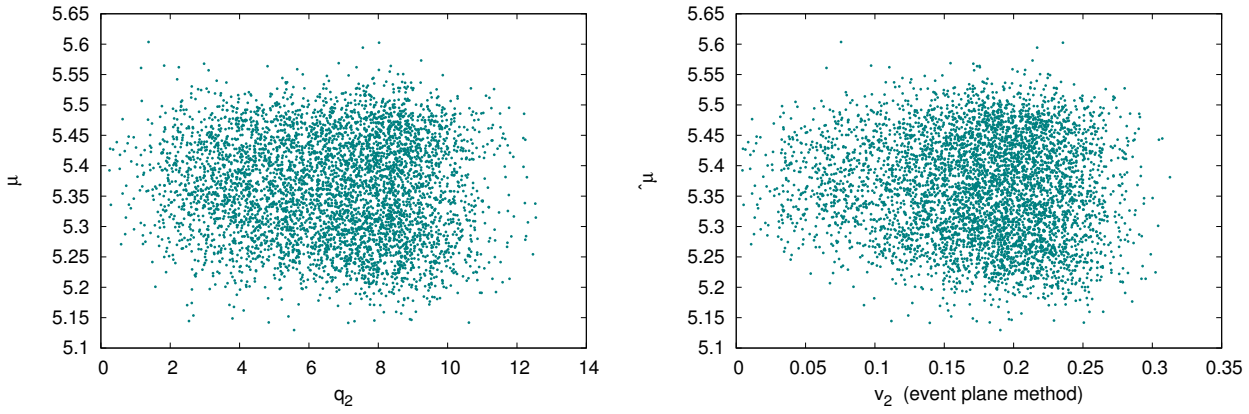

(a) (b)

Figure 31: Algorithm results for initially random arrangement. Events are generated with flow up to pentagonal flow, initial rotation is according Ψ_2, histograms are normalized. (a) Average bin number $\hat{\mu}$ dependence on q_2. (b) Average bin number $\hat{\mu}$ dependence on v_2. v_2 was obtained via event plane method.

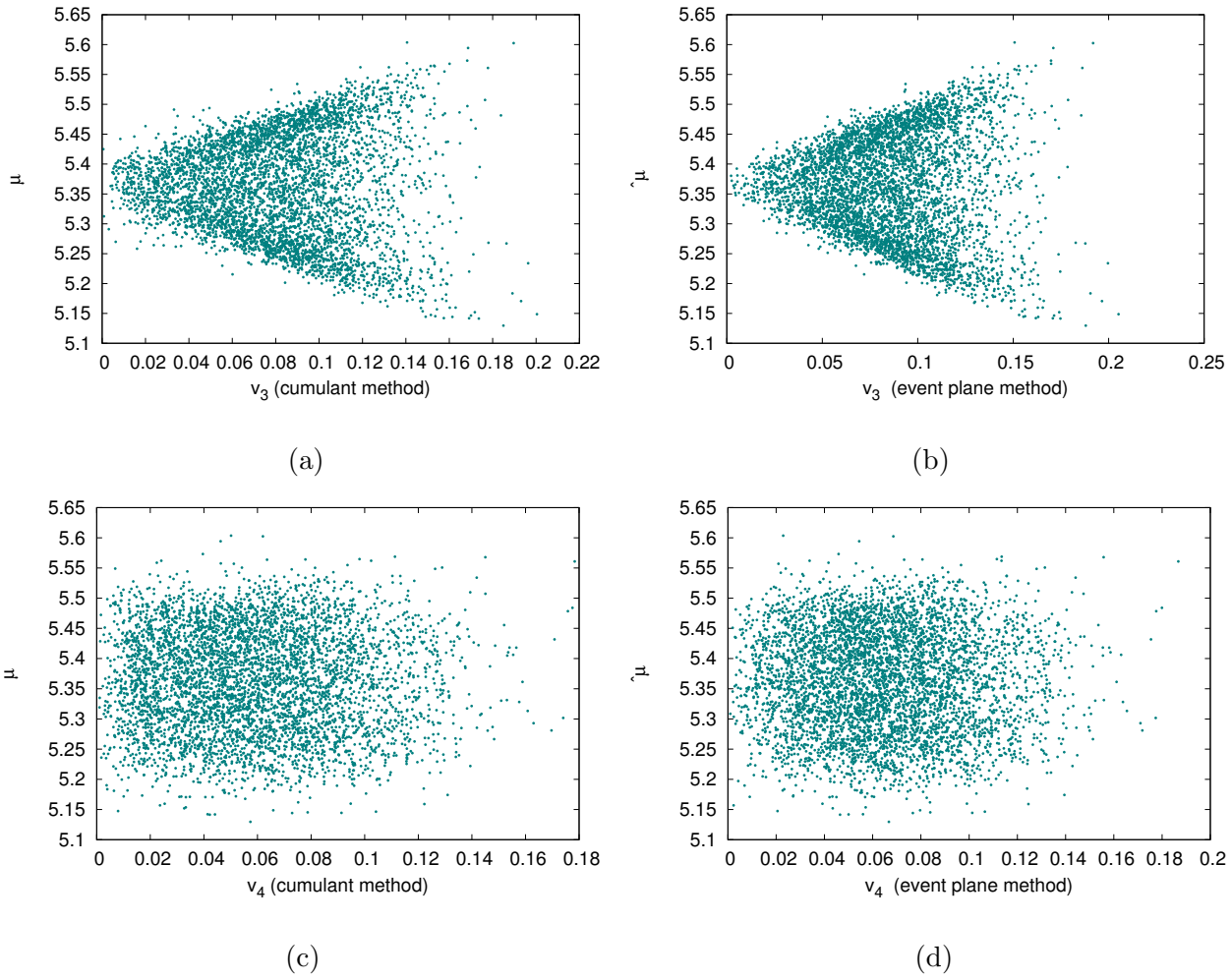

(a) (b)

(c) (d)

Figure 32: Algorithm results for initially random arrangement. Events are generated with flow up to pentagonal flow, initial rotation is according Ψ_2, histograms are normalized. (a) Average bin number $\hat{\mu}$ dependence on v_3. v_3 was obtained via cumulant method. (b) Average bin number $\hat{\mu}$ dependence on v_3. v_3 was obtained via event plane method. (c) Average bin number $\hat{\mu}$ dependence on v_4. v_4 was obtained via cumulant method. (d) Average bin number $\hat{\mu}$ dependence on v_4. v_4 was obtained via event plane method.

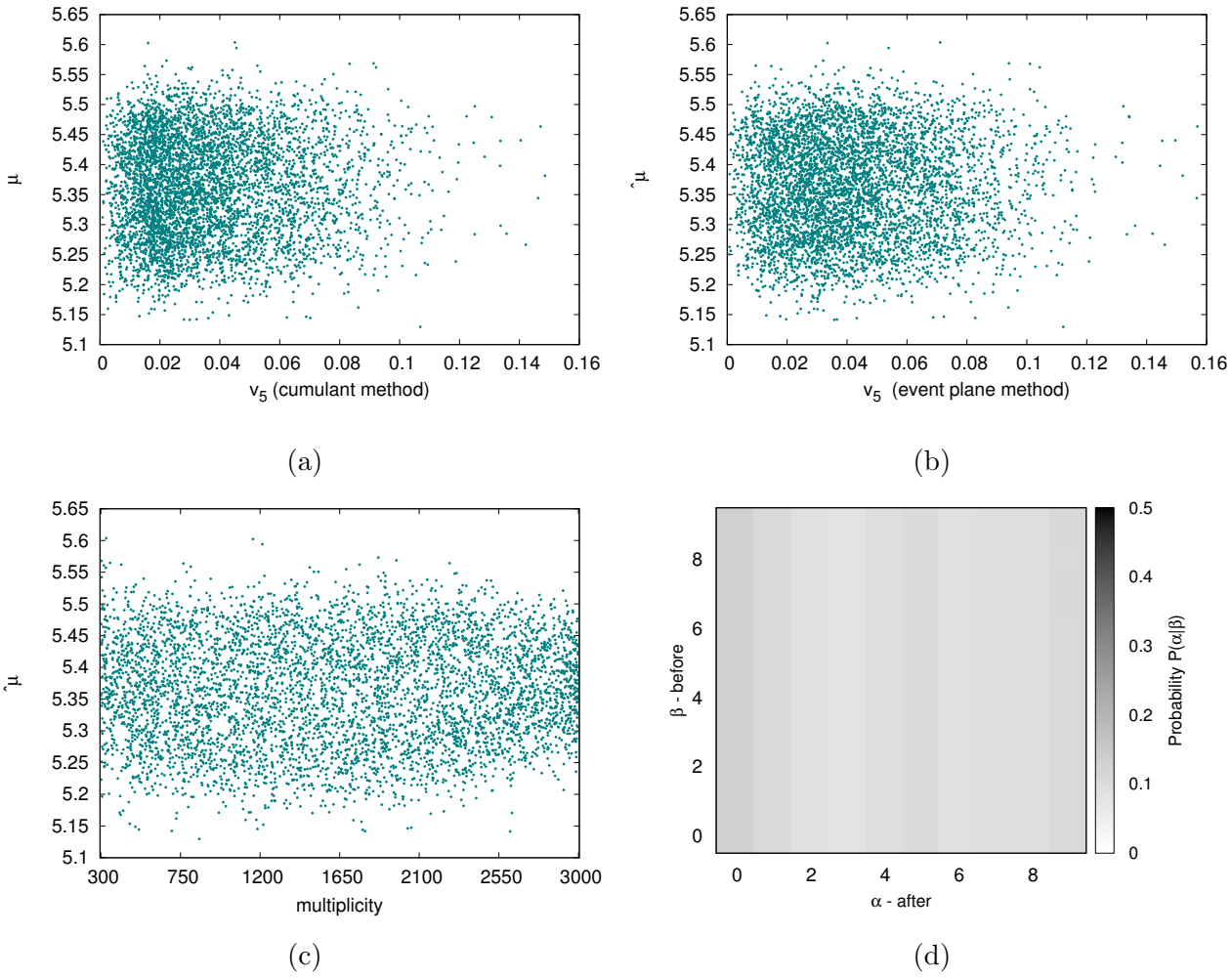

Figure 33: Algorithm results for initially random arrangement. Events are generated with flow up to pentagonal flow, initial rotation is according Ψ_2, histograms are normalized. (a) Average bin number $\hat{\mu}$ dependence on v_5. v_5 was obtained via cumulant method. (b) Average bin number $\hat{\mu}$ dependence on v_5. v_5 was obtained via event plane method. (c) Average bin number $\hat{\mu}$ dependence on multiplicity. (d) Error matrix. Probability of initial bin assignment given the final bin assignment $P(\alpha|\beta)$.

Flipped events

We run the normalized histograms through the algorithm. After convergence, we took the first half of the sorted events and flipped them over, i.e. transformed them as $\phi \to -\phi$. In total, it took 166 steps. The results are in the fig. 34 and fig. 35. There is no significant difference compared to the fig. 28, fig. 29 and fig. 30. The only visible change is that the error matrix is more uniform (fig. 35b). However, there is a big difference in the average bins in the fig. 93. The results are rather different to the previous one.

Arrangement according to q_2

The results are in the fig. 36 and fig. 37. The ESSTER once again failed to converge. The average bins are in the fig. 94. The results are rather different to the converged case of initially random arrangement, therefore we cannot make any conclusions here.

Normalized histograms

The results are in the fig. 38 and the fig. 39, it took 138 steps for the algorithm to converge. The results are consistent with the results from initially random arrangement. It is obvious that the measure does not discriminate very well. The correlation coefficients are almost zero in all the cases of v_2, v_3, v_4, and v_5. The average bins are in the fig. 95. The histograms are the same as in the fig. 92. We already did the 'flipping' in this case, therefore we are not including the case of initial q_2 arrangement.

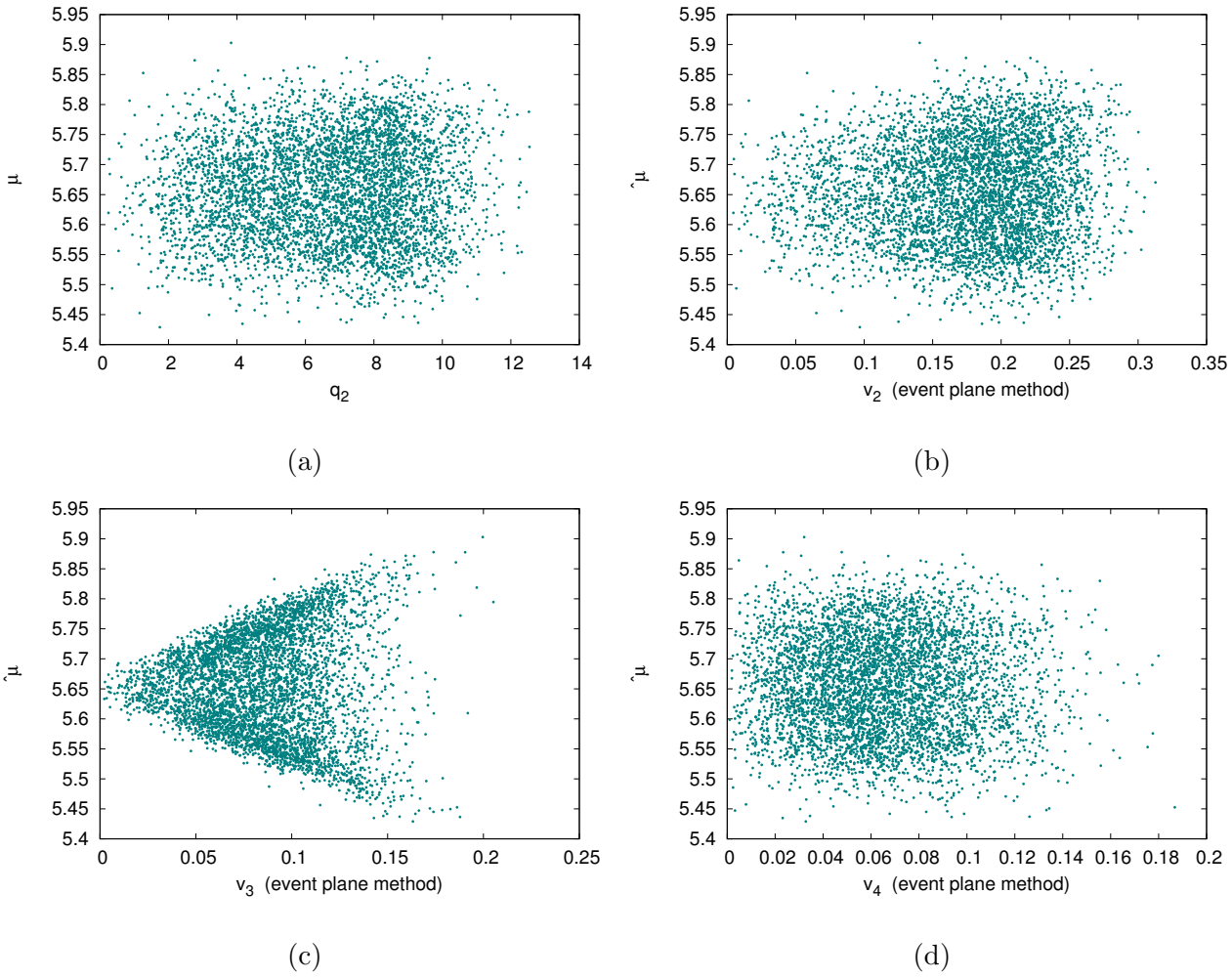

Figure 34: Algorithm results for initially random arrangement. Events are generated with flow up to pentagonal flow, initial rotation is according Ψ_2, histograms are normalized, events are flipped. (a) Average bin number $\hat{\mu}$ dependence on q_2. (b) Average bin number $\hat{\mu}$ dependence on v_2. v_2 was obtained via event plane method. (c) Average bin number $\hat{\mu}$ dependence on v_3. v_3 was obtained via event plane method. (d) Average bin number $\hat{\mu}$ dependence on v_4. v_4 was obtained via event plane method.

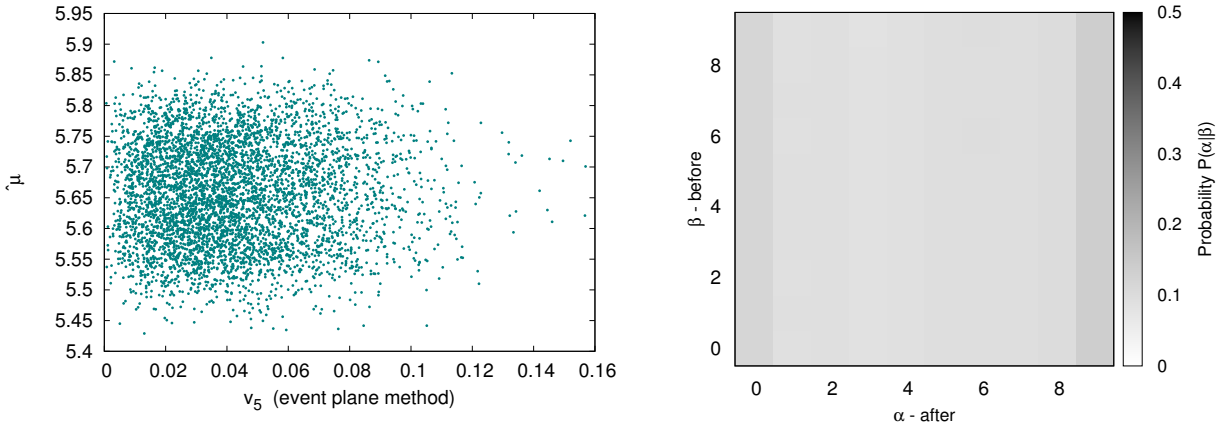

(a) (b)

Figure 35: Algorithm results for initially random arrangement. Events are generated with flow up to pentagonal flow, initial rotation is according Ψ_2, events are flipped, histograms are normalized. (a) Average bin number $\hat{\mu}$ dependence on v_5. v_5 was obtained via event plane method. (b) Error matrix. Probability of initial bin assignment given the final bin assignment $P(\alpha|\beta)$.

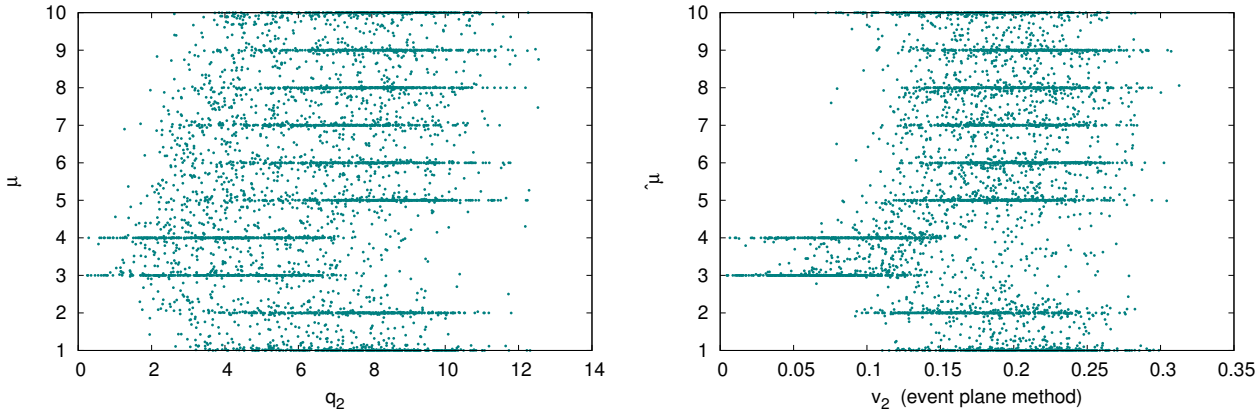

(a) (b)

Figure 36: Algorithm results for initial arrangement according to q_2. Events are generated with flow up to pentagonal flow, initial rotation is according Ψ_2. (a) Average bin number $\hat{\mu}$ dependence on q_2. (b) Average bin number $\hat{\mu}$ dependence on v_2. v_2 was obtained via event plane method.

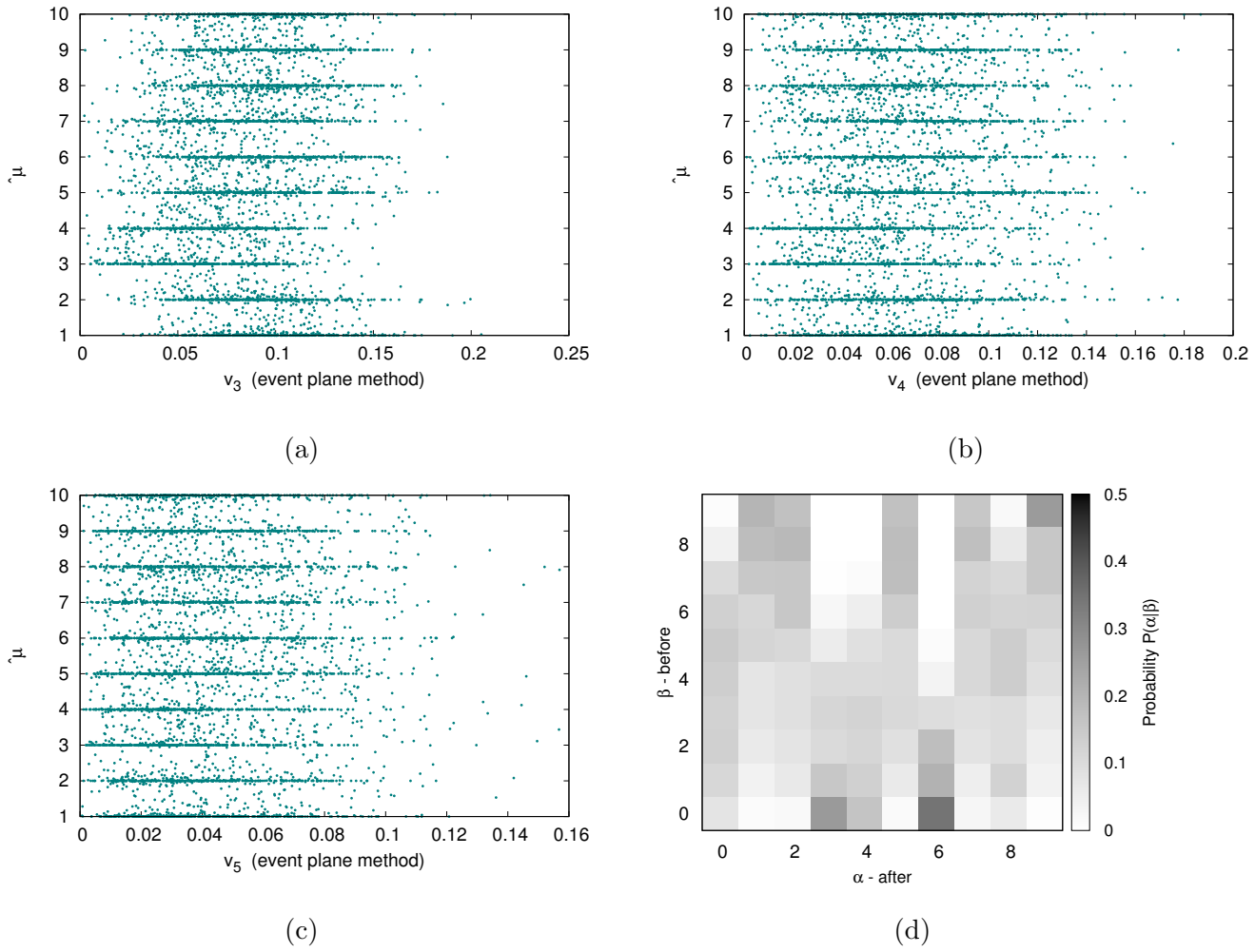

Figure 37: Algorithm results for initial arrangement according to q_2. Events are generated with flow up to pentagonal flow, initial rotation is according Ψ_2. (a) Average bin number $\hat{\mu}$ dependence on v_3. v_3 was obtained via event plane method. (b) Average bin number $\hat{\mu}$ dependence on v_4. v_4 was obtained via event plane method. (c) Average bin number $\hat{\mu}$ dependence on v_5. v_5 was obtained via event plane method. (d) Error matrix. Probability of initial bin assignment given the final bin assignment $P(\alpha|\beta)$.

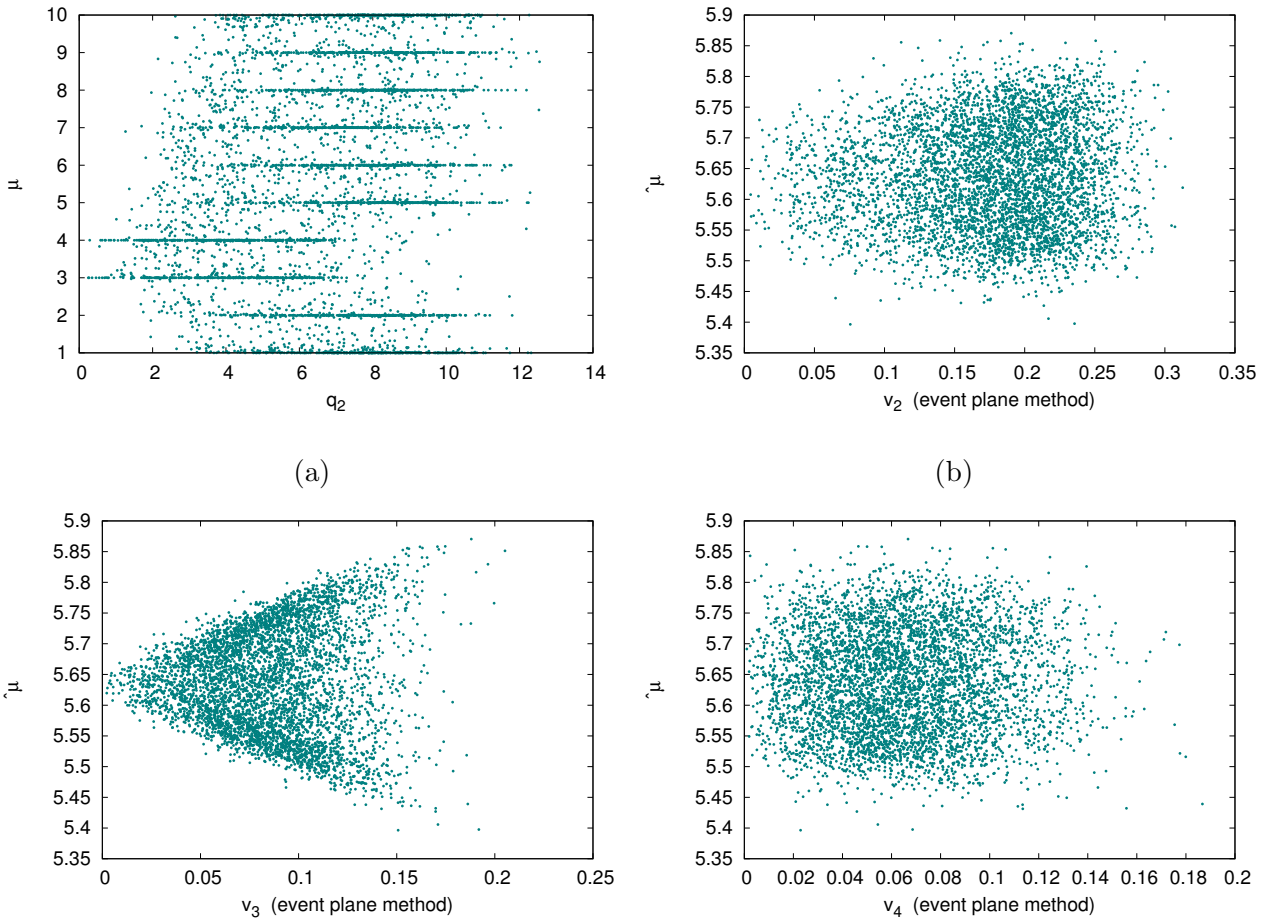

Figure 38: Algorithm results for initial arrangement according to q_2. Events are generated with flow up to pentagonal flow, initial rotation is according Ψ_2, histograms are normalized. (a) Average bin number $\hat{\mu}$ dependence on q_2. (b) Average bin number $\hat{\mu}$ dependence on v_2. (c) Average bin number $\hat{\mu}$ dependence on v_3. (d) Average bin number $\hat{\mu}$ dependence on v_4.

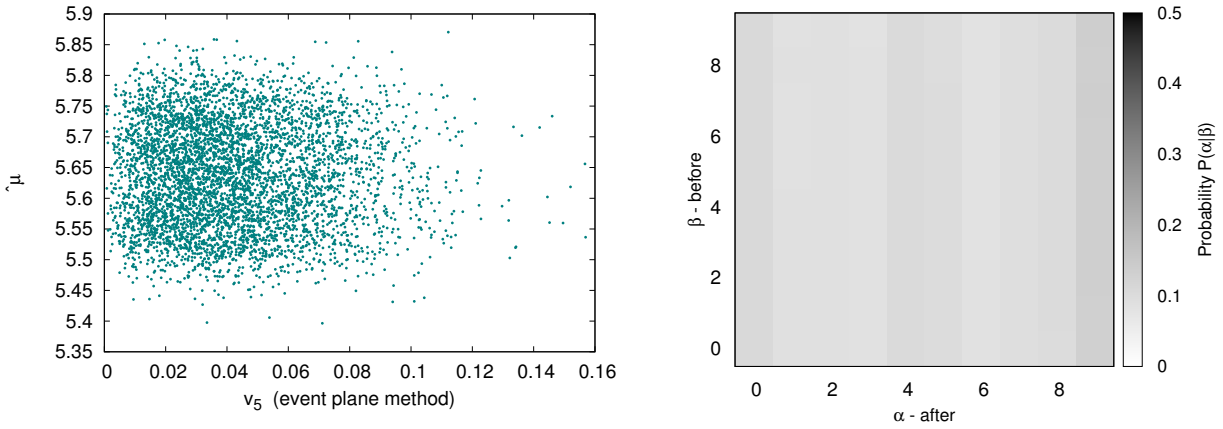

(a) (b)

Figure 39: Algorithm results for initial arrangement according to q_2. Events are generated with flow up to pentagonal flow, initial rotation is according Ψ_2, histograms are normalized. (a) Average bin number $\hat{\mu}$ dependence on v_5. (b) Error matrix. Probability of initial bin assignment given the final bin assignment $P(\alpha|\beta)$.

5.3.2 Initial rotation according to Ψ_3

Random arrangement

The results are in the fig. 40, fig. 41, and fig. 42,. It took 189 steps to converge. There are very sharp lines around the integers, so this measure discriminates quite well. Once again we present the final bin number μ dependence on v_2, v_3, v_4, and v_5. The correlations between the final bin number μ and flow coefficients v_2, v_3, v_4 and v_5 are even smaller than in the case of rotation according to Ψ_2: in the case of v_2 0.019, in the case of v_3 it is 0.012, v_4 0.002 and v_5 0.001.

The average bins are in the fig. 96. The results are very similar to the fig. 83 or fig. 85, i.e. indeed v_4 and v_5 plays a minimum role.

Normalized histograms

The results are in the fig. 43, fig. 44 and fig. 45. There are no sharp lines around the integers, taking into account fig. 45d, this measure discriminates quite bad. The difference of the results from different method are negligible. Interesting is the fact that instead of v_3 having triangular shape, this time v_2 does. The correlations between the final bin number μ and flow coefficients v_2, v_3, v_4 and v_5 are consistent with zero. The average bins are in the fig. 97. It is clear that the upper row is a mirror image of the lower row. Hence, present results for the flipped events in the next paragraph.

Flipped events

We run the normalized histograms through the algorithm. After convergence, we took the first half of the sorted events and flipped them over. In total, it took ESSTER 81 steps to converge. The results are in the fig. 46 and the fig. 47.. There is no significant difference compared to the fig. 43, fig. 44 and fig. 45. However, there is a big difference in the average bins in the fig. 98 compared to the fig. 97. The results are rather different to the previous one.

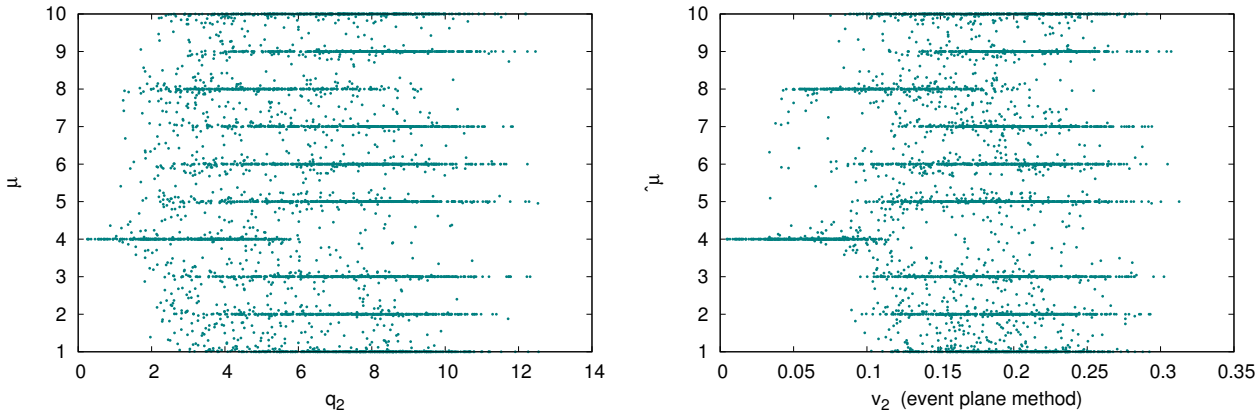

Figure 40: Algorithm results for initially random arrangement. Events are generated with flow up to pentagonal flow, initial rotation is according Ψ_3. (a) Average bin number $\hat{\mu}$ dependence on q_2. (b) Average bin number $\hat{\mu}$ dependence on v_2. v_2 was obtained via event plane method. (c) Average bin number $\hat{\mu}$ dependence on v_3. v_3 was obtained via cumulant method. (d) Average bin number $\hat{\mu}$ dependence on v_3. v_3 was obtained via event plane method.

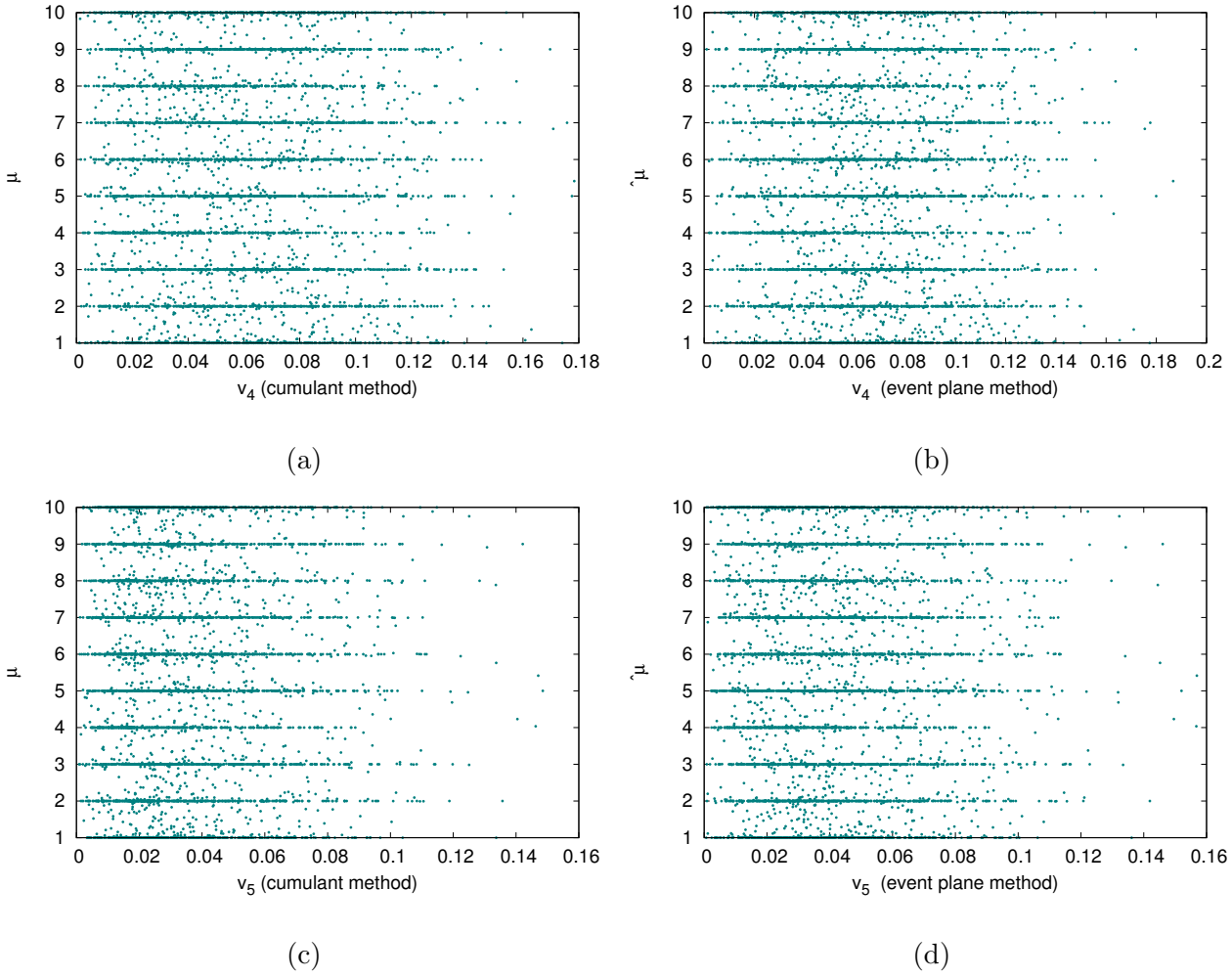

Figure 41: Algorithm results for initially random arrangement. Events are generated with flow up to pentagonal flow, initial rotation is according Ψ_3. (a) Average bin number $\hat{\mu}$ dependence on v_4. v_4 was obtained via cumulant method. (b) Average bin number $\hat{\mu}$ dependence on v_4. v_4 was obtained via event plane method. (c) Average bin number $\hat{\mu}$ dependence on v_5. v_5 was obtained via cumulant method. (d) Average bin number $\hat{\mu}$ dependence on v_5. v_5 was obtained via event plane method.

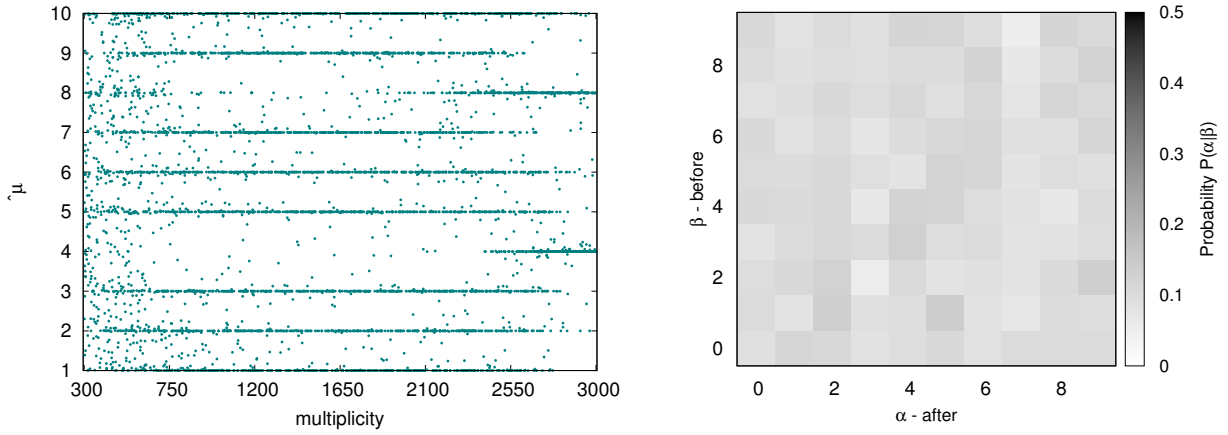

(a) (b)

Figure 42: Algorithm results for initially random arrangement. Events are generated with flow up to pentagonal flow, initial rotation is according Ψ_3. (a) Average bin number $\hat{\mu}$ dependence on multiplicity. (b) Error matrix. Probability of initial bin assignment given the final bin assignment $P(\alpha|\beta)$.

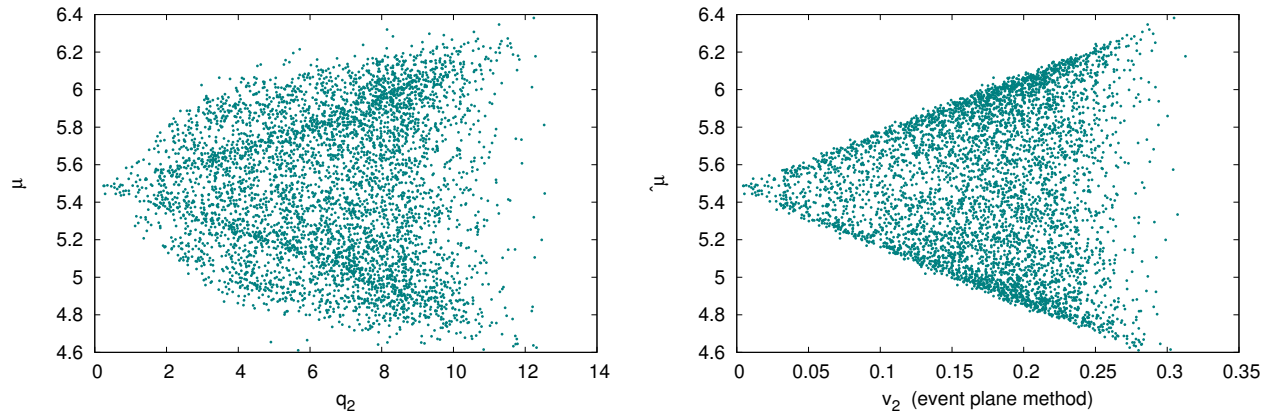

(a) (b)

Figure 43: Algorithm results for initially random arrangement. Events are generated with flow up to pentagonal flow, initial rotation is according Ψ_3, histograms are normalized. (a) Average bin number $\hat{\mu}$ dependence on on q_2. (b) Average bin number $\hat{\mu}$ dependence on v_2. v_2 was obtained via event plane method.

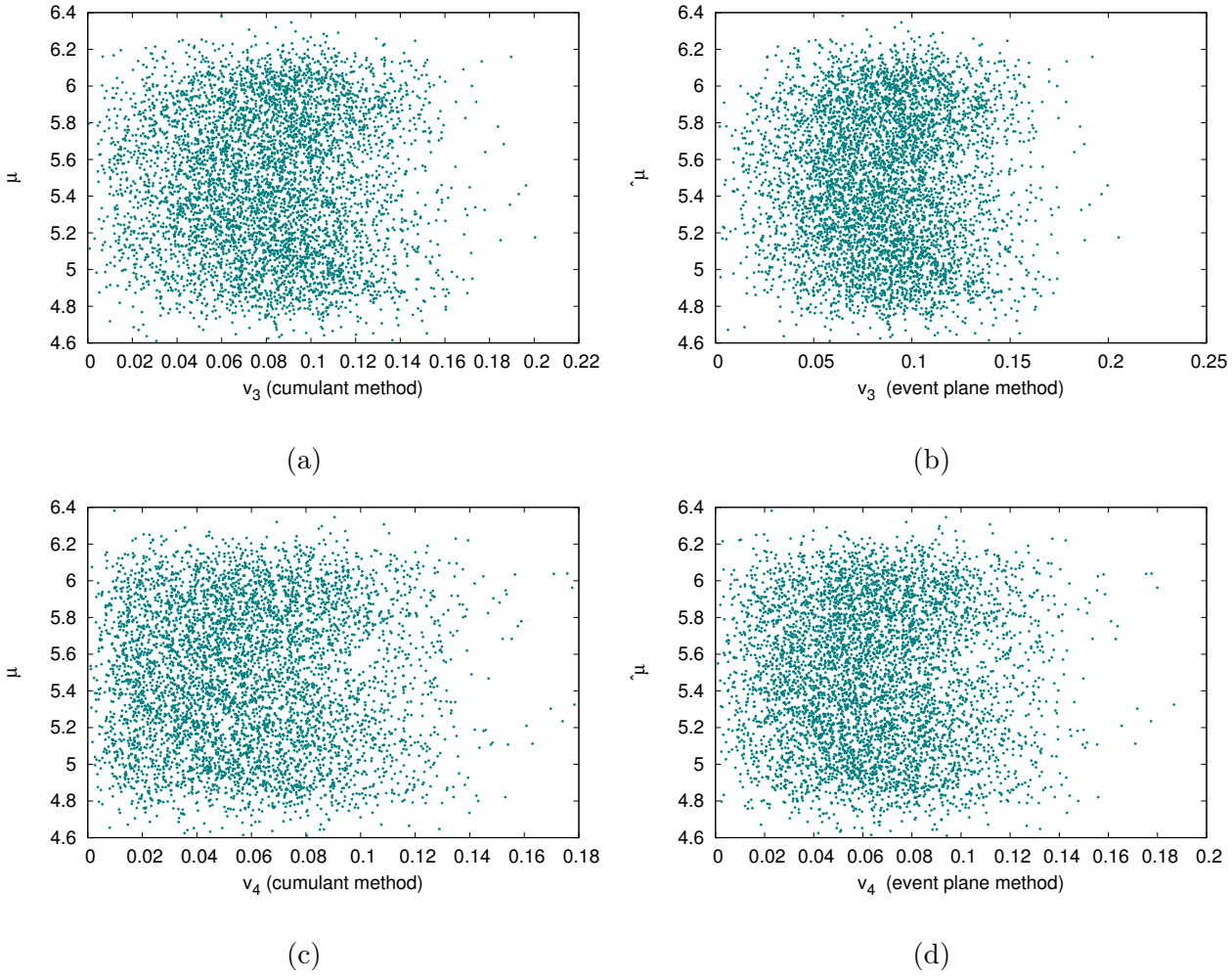

(a) (b)

(c) (d)

Figure 44: Algorithm results for initially random arrangement. Events are generated with flow up to pentagonal flow, initial rotation is according Ψ_3, histograms are normalized. (a) Average bin number $\hat{\mu}$ dependence on v_3. v_3 was obtained via cumulant method. (b) Average bin number $\hat{\mu}$ dependence on v_3. v_3 was obtained via event plane method. (c) Average bin number $\hat{\mu}$ dependence on v_4. v_4 was obtained via cumulant method. (d) Average bin number $\hat{\mu}$ dependence on v_4. v_4 was obtained via event plane method.

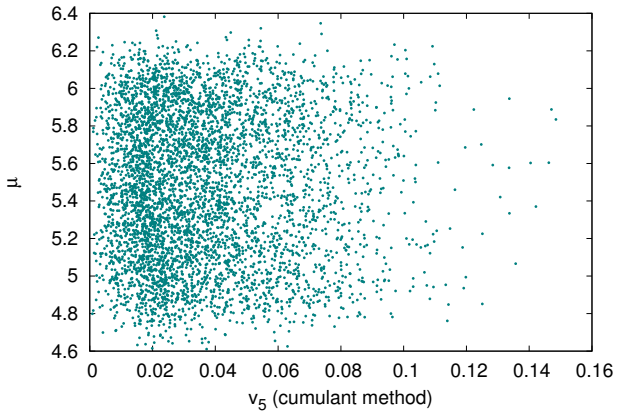

(a)

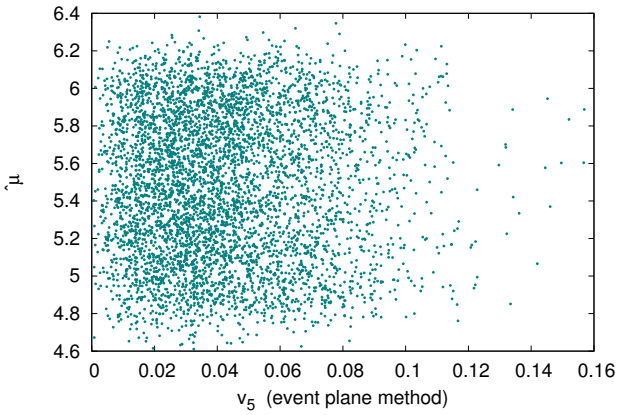

(b)

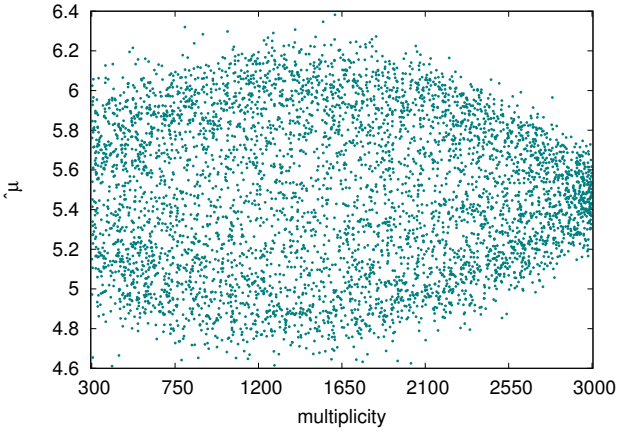

(c) Average bin number $\hat{\mu}$ dependence on multiplicity.

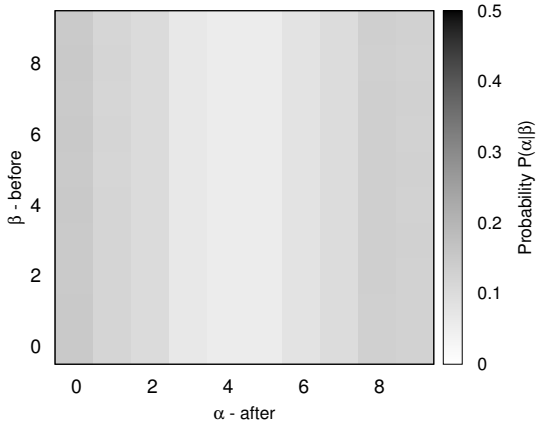

(d)

Figure 45: Algorithm results for initially random arrangement. Events are generated with flow up to pentagonal flow, initial rotation is according Ψ_3, histograms are normalized. (a) Average bin number $\hat{\mu}$ dependence on v_5. v_5 was obtained via cumulant method. (b) Average bin number $\hat{\mu}$ dependence on v_5. v_5 was obtained via event plane method. (c) Average bin number $\hat{\mu}$ dependence on multiplicity. (d) Error matrix. Probability of initial bin assignment given the final bin assignment $P(\alpha|\beta)$.

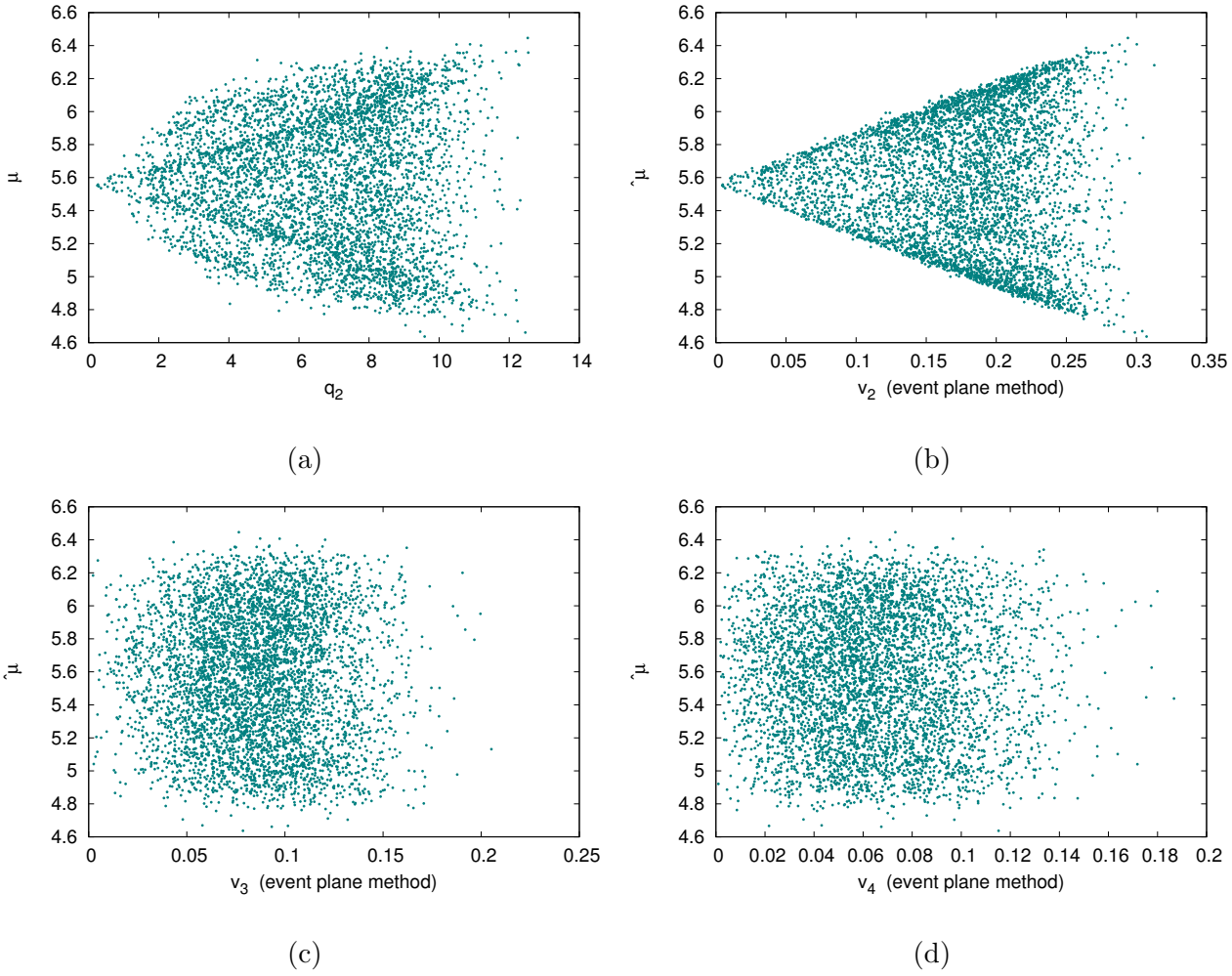

Figure 46: Algorithm results for initially random arrangement. Events are generated with flow up to pentagonal flow, initial rotation is according Ψ_3, events are flipped, histograms are normalized. (a) Average bin number $\hat{\mu}$ dependence on q_2. (b) Average bin number $\hat{\mu}$ dependence on v_2. v_2 was obtained via event plane method. (c) Average bin number $\hat{\mu}$ dependence on v_3. v_3 was obtained via event plane method. (d) Average bin number $\hat{\mu}$ dependence on v_4. v_4 was obtained via event plane method.

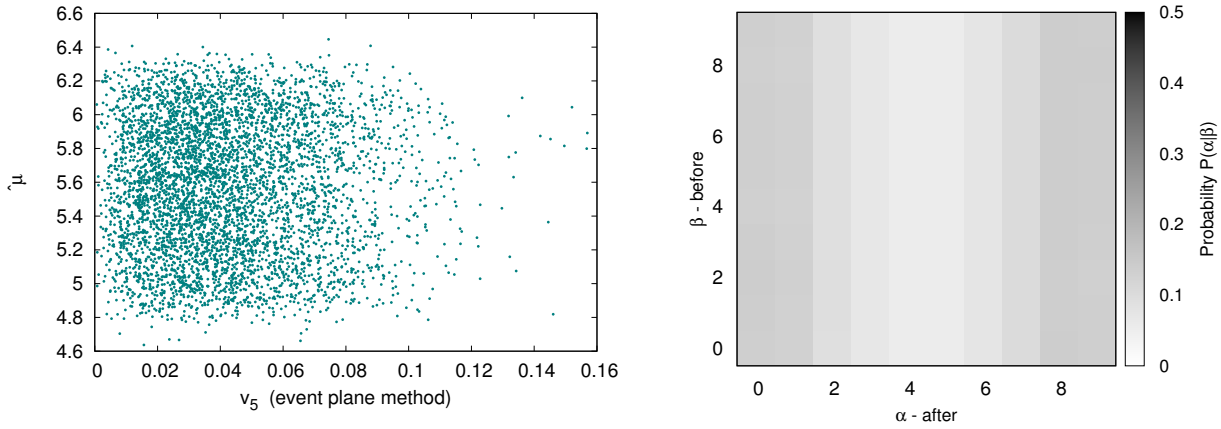

(a) (b)

Figure 47: Algorithm results for initially random arrangement. Events are generated with flow up to pentagonal flow, initial rotation is according Ψ_3, events are flipped, histograms are normalized. (a) Average bin number $\hat{\mu}$ dependence on v_5. v_5 was obtained via event plane method. (b) Error matrix. Probability of initial bin assignment given the final bin assignment $P(\alpha|\beta)$.

Arrangement according to q_2

The results are in the fig. 48 and fig. 49 . It took only 93 steps to converge. It is obvious from fig. 48b and fig. 49b that the two middle bins are very different compared to the rest of them. It is apparent also in the average bins fig. 99.

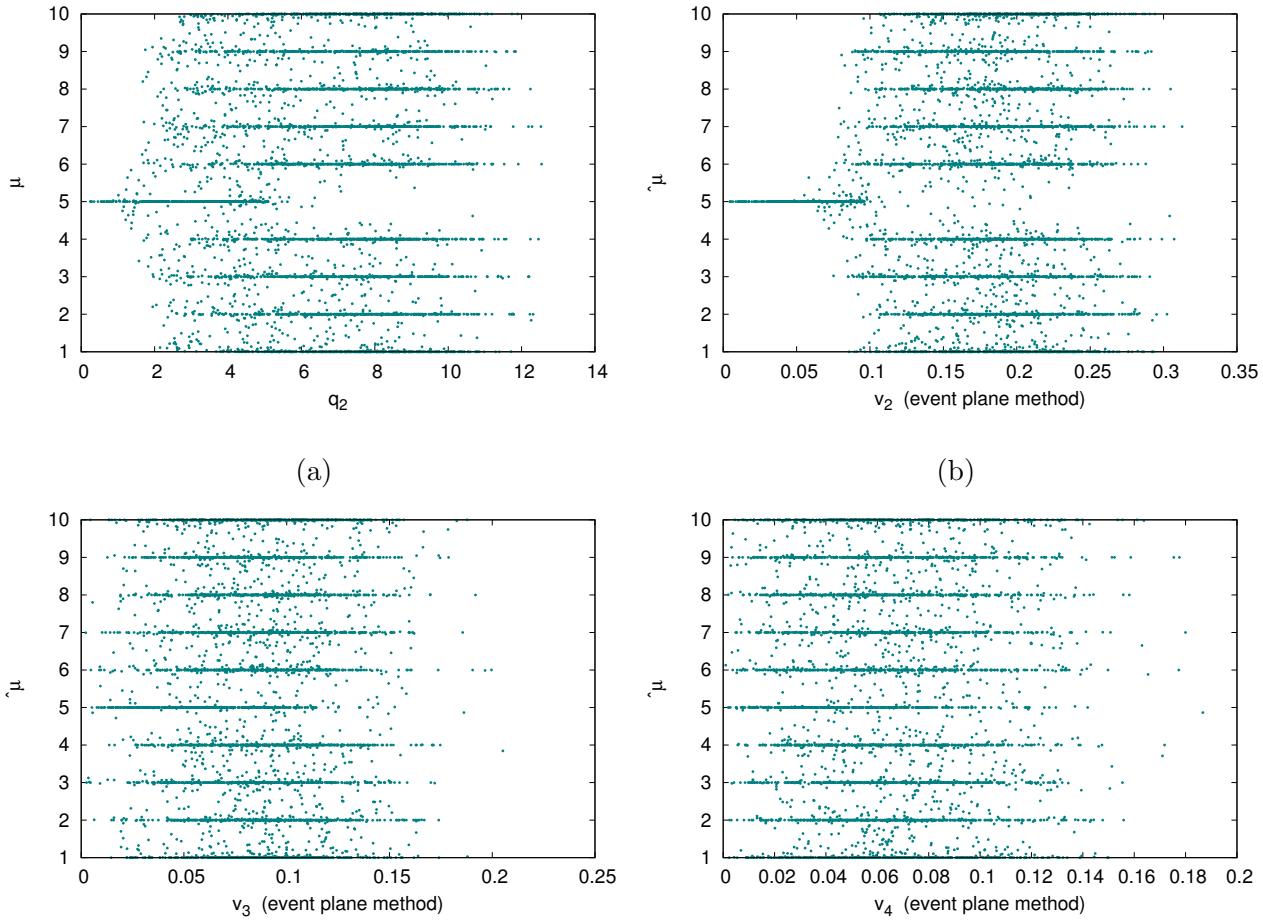

Figure 48: Algorithm results for initial arrangement according to q_2. Events are generated with flow up to pentagonal flow, initial rotation is according Ψ_3. (a) Average bin number $\hat{\mu}$ dependence on q_2. (b) Average bin number $\hat{\mu}$ dependence on v_2. v_2 was obtained via event plane method. (c) Average bin number $\hat{\mu}$ dependence on v_3. v_3 was obtained via event plane method. (d) Average bin number $\hat{\mu}$ dependence on v_4. v_4 was obtained via event plane method.

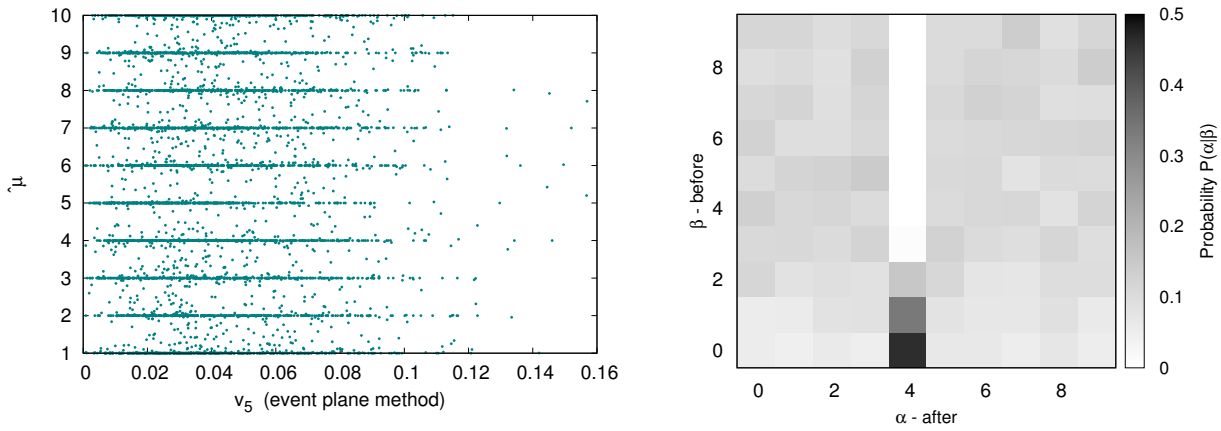

(a) (b)

Figure 49: Algorithm results for initial arrangement according to q_2. Events are generated with flow up to pentagonal flow, initial rotation is according Ψ_3. (a) Average bin number $\hat{\mu}$ dependence on v_5. v_5 was obtained via event plane method. (b) Error matrix. Probability of initial bin assignment given the final bin assignment $P(\alpha|\beta)$.

Normalized histograms

The results are in the fig. 50 and the fig. 51, it took only 12 steps for the algorithm to converge. The results are consistent with the results from initially random arrangement. It is obvious that the measure does not discriminate very well. The correlation coefficients are almost zero in all the cases of v_2, v_3, v_4, and v_5. The average bins are in the fig. 100. The histograms are the same as in the fig. 97. We already did the 'flipping' in this case, therefore we are not including the case of q_2 arrangement.

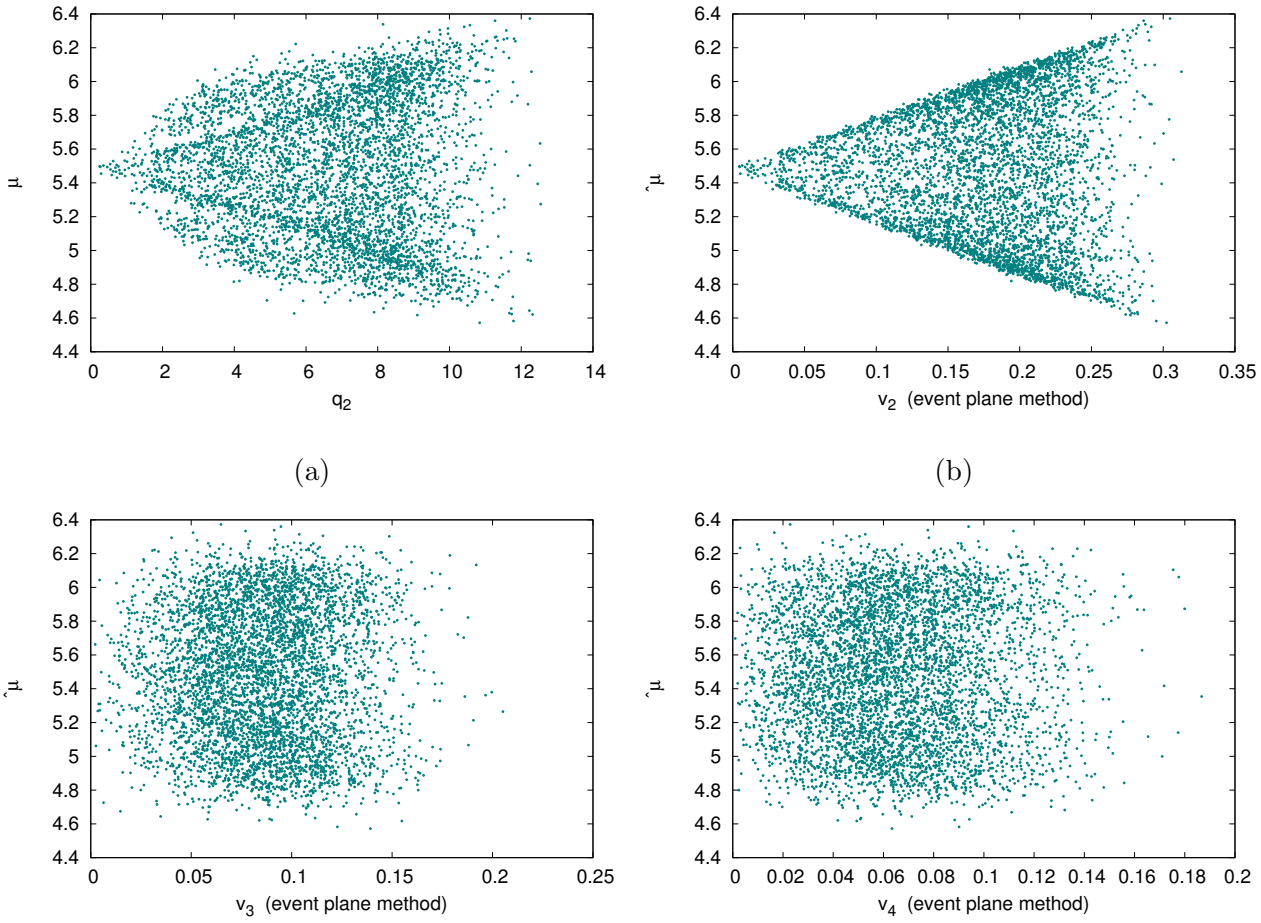

Figure 50: Algorithm results for initial arrangement according to q_2. Events are generated with flow up to pentagonal flow, initial rotation is according Ψ_3, histograms are normalized. (a) Average bin number $\hat{\mu}$ dependence on q_2. (b) Average bin number $\hat{\mu}$ dependence on v_2. v_2 was obtained via event plane method. (c) Average bin number $\hat{\mu}$ dependence on v_3. v_3 was obtained via event plane method. (d) Average bin number $\hat{\mu}$ dependence on v_4. v_4 was obtained via event plane method.

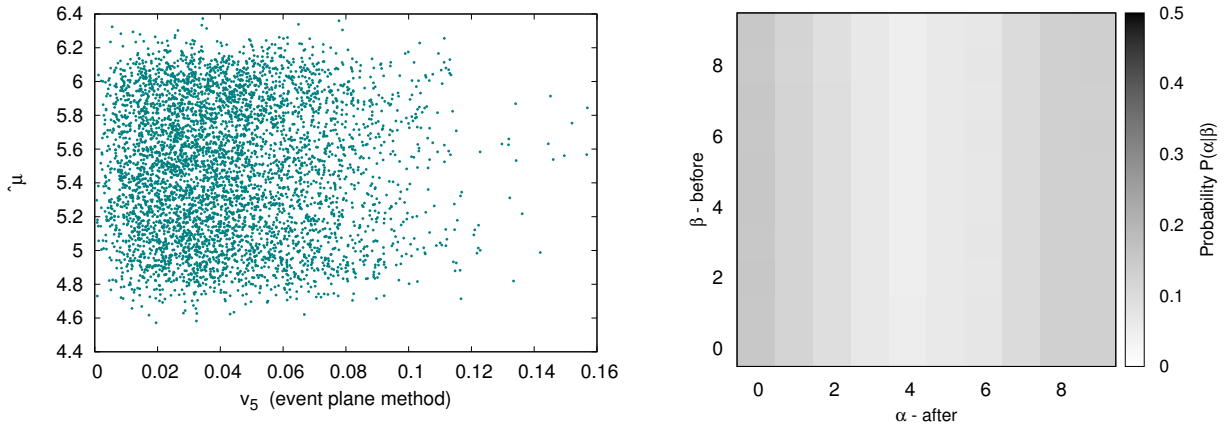

(a) (b)

Figure 51: Algorithm results for initial arrangement according to q_2. Events are generated with flow up to pentagonal flow, initial rotation is according Ψ_3, histograms are normalized. (a) Average bin number $\hat{\mu}$ dependence on v_5. v_5 was obtained via event plane method. (b) Error matrix. Probability of initial bin assignment given the final bin assignment $P(\alpha|\beta)$.

5.3.3 Initial rotation according to Ψ_5

Since we implemented v_4 and v_5 into ESSTER, we tried to initially rotate the events according to Ψ_5. As well as in the previous cases of v_2 and v_3, we rotated the events in such a way that Ψ_5 is zero.

Random arrangement

The results are in the fig. 52, 53 and 53. The program converged after 60 steps. There are very sharp lines around the integers, so this measure discriminates quite well. Once again we present the final bin number μ dependence on v_2, v_3, v_4, and v_5. The correlations between the final bin number μ and flow coefficients v_2, v_3, v_4 and v_5 are in the case of v_2 - 0.006, in the case of v_3 is - 0.002, v_4 0.001 and v_5 - 0.015. Since the vales are close to zero, the negative values might be fluctuations. It is obvious that the importance of v_5 increased.

The average histograms are in the fig. 101. The 5 peaks are nicely visible. Figure 101b shows that v_2 combined with v_3 are the most important, which is consistent with the previous results.

Normalized histograms

The results are in the fig. 55, fig. 56 and fig. 57,. The measure is bad, the only visible dependence is the triangular shape of v_2. Worth emphasizing is the fact that for rotation according to Ψ_2, v_3 has triangular shape. The correlations between the final bin number μ and flow coefficients v_2, v_3, v_4 and v_5 are consistent with zero, highest value is for v_5: 0.025.

The average bins are in the fig. 102. It is clear that this time, there are no mirror images. It is clear that the most significant feature is v_2.

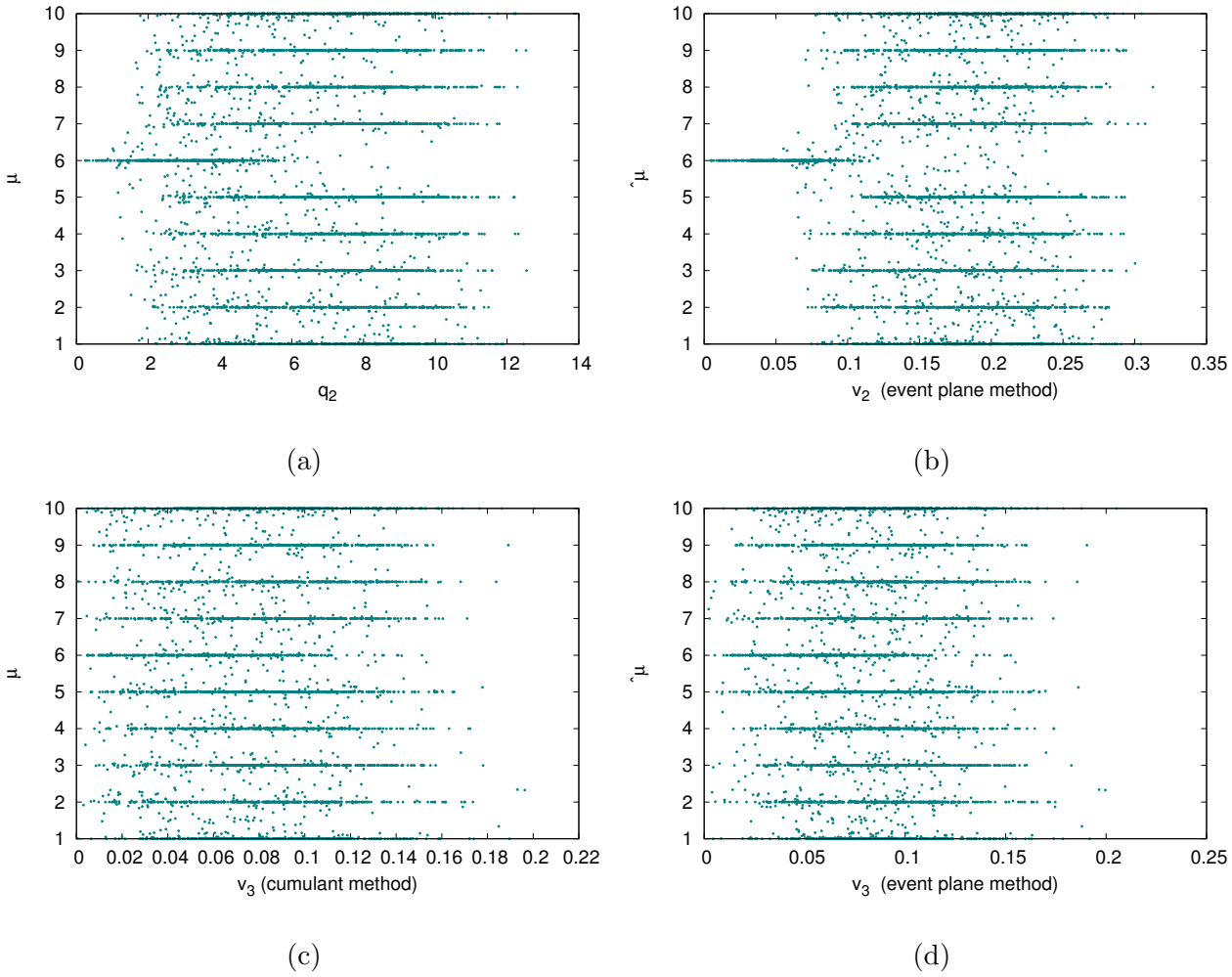

Figure 52: Algorithm results for initially random arrangement. Events are generated with flow up to pentagonal flow, initial rotation is according Ψ_5. (a) Average bin number $\hat{\mu}$ dependence on q_2. (b) Average bin number $\hat{\mu}$ dependence on v_2. v_2 was obtained via event plane method. (c) Average bin number $\hat{\mu}$ dependence on v_3. v_3 was obtained via cumulant method. (d) Average bin number $\hat{\mu}$ dependence on v_3. v_3 was obtained via event plane method.

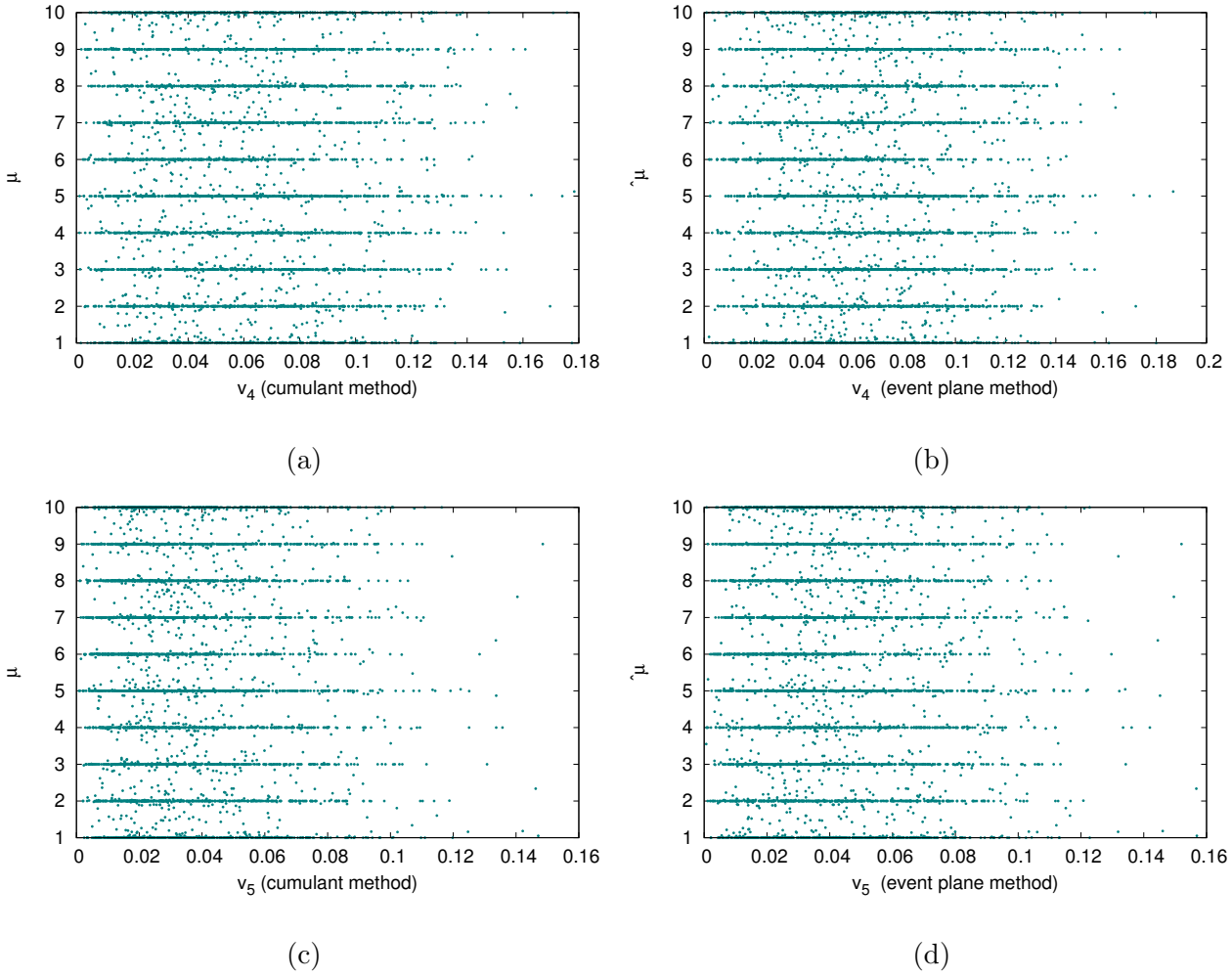

(a) (b)

(c) (d)

Figure 53: Algorithm results for initially random arrangement. Events are generated with flow up to pentagonal flow, initial rotation is according Ψ_5. (a) Average bin number $\hat{\mu}$ dependence on v_4. v_4 was obtained via cumulant method. (b) Average bin number $\hat{\mu}$ dependence on v_4. v_4 was obtained via event plane method. (c) Average bin number $\hat{\mu}$ dependence on v_5. v_5 was obtained via cumulant method. (d) Average bin number $\hat{\mu}$ dependence on v_5. v_5 was obtained via event plane method.

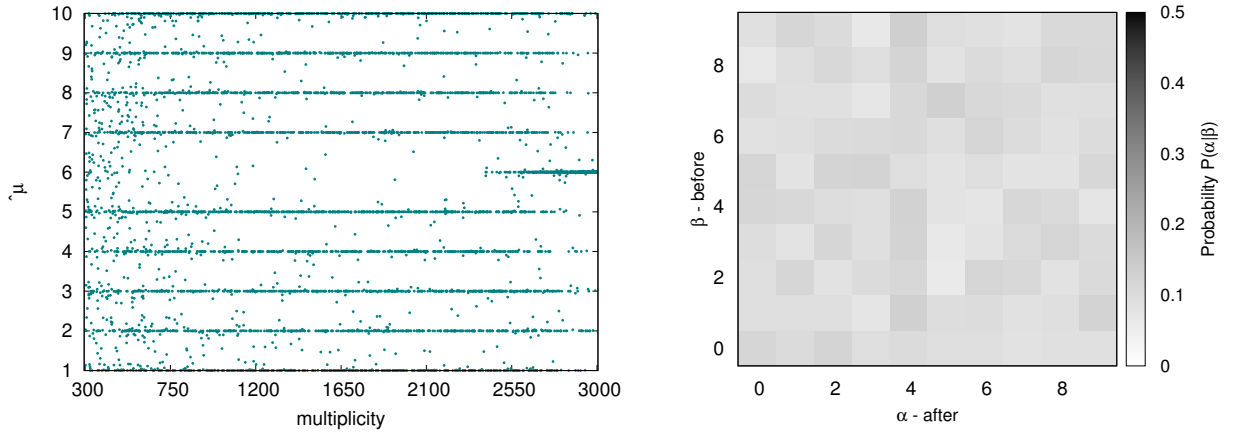

(a) (b)

Figure 54: Algorithm results for initially random arrangement. Events are generated with flow up to pentagonal flow, initial rotation is according Ψ_5. (a) Average bin number $\hat{\mu}$ dependence on multiplicity. (b) Error matrix. Probability of initial bin assignment given the final bin assignment $P(\alpha|\beta)$.

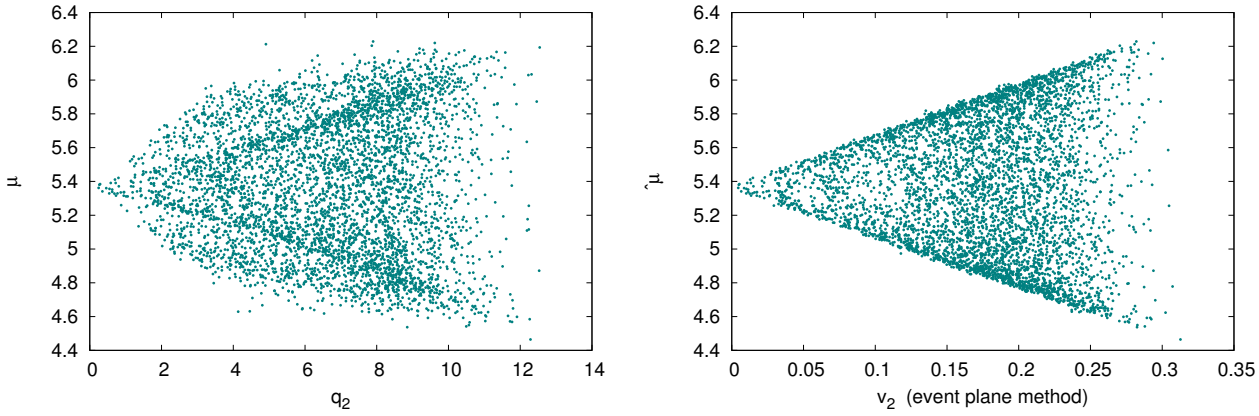

(a) (b)

Figure 55: Algorithm results for initially random arrangement. Events are generated with flow up to pentagonal flow, initial rotation is according Ψ_5, histograms are normalized. (a) Average bin number $\hat{\mu}$ dependence on q_2. (b) Average bin number $\hat{\mu}$ dependence on v_2. v_2 was obtained via event plane method.

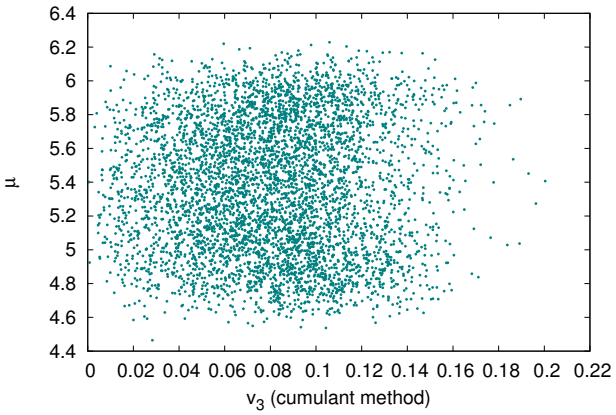

(a)

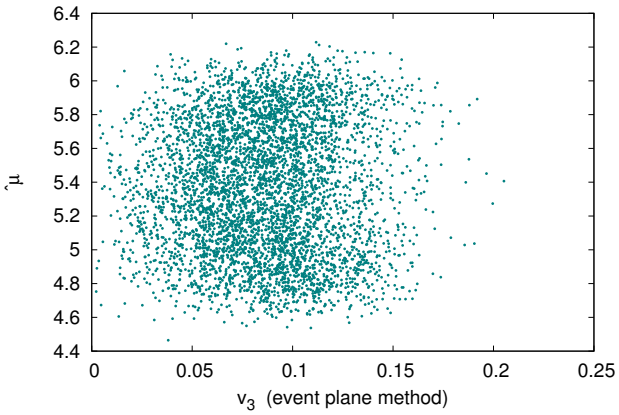

(b)

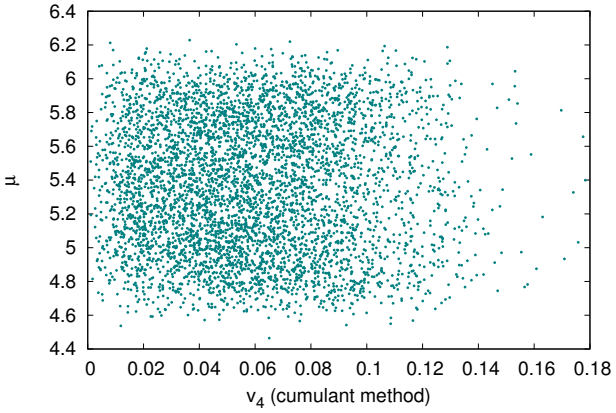

(c) Average bin number $\hat{\mu}$ dependence on v_4. v_4 was obtained via cumulant method.

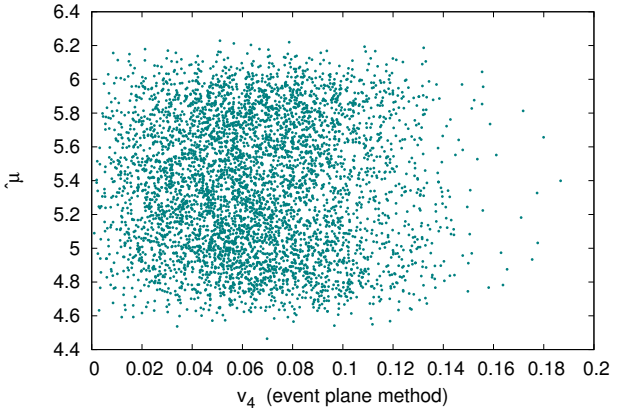

(d)

Figure 56: Algorithm results for initially random arrangement. Events are generated with flow up to pentagonal flow, initial rotation is according Ψ_5, histograms are normalized. (a) Average bin number $\hat{\mu}$ dependence on v_3. v_3 was obtained via cumulant method. (b) Average bin number $\hat{\mu}$ dependence on v_3. v_3 was obtained via event plane method. (c) Average bin number $\hat{\mu}$ dependence on v_4. v_4 was obtained via cumulant method. (d) Average bin number $\hat{\mu}$ dependence on v_4. v_4 was obtained via event plane method.

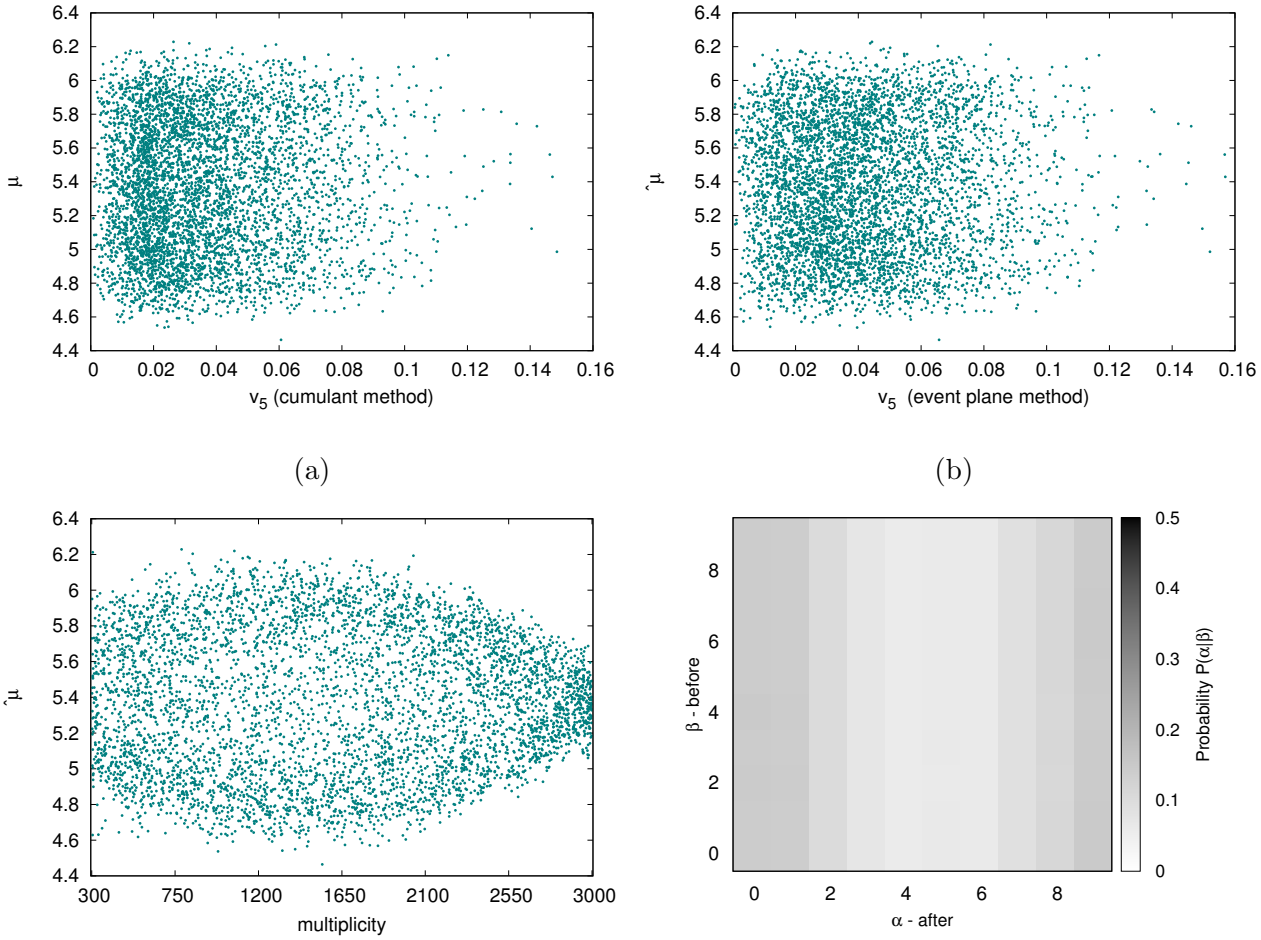

Figure 57: Algorithm results for initially random arrangement. Events are generated with flow up to pentagonal flow, initial rotation is according Ψ_5, histograms are normalized. (a) Average bin number $\hat{\mu}$ dependence on v_5. v_5 was obtained via cumulant method. (b) Average bin number $\hat{\mu}$ dependence on v_5. v_5 was obtained via event plane method. (c) Average bin number $\hat{\mu}$ dependence on multiplicity. (d) Error matrix. Probability of initial bin assignment given the final bin assignment $P(\alpha|\beta)$.

Arrangement according to q_2

The results are in the fig. 58 and fig. 59. It took 699 steps to converge, which is one of the highest numbers presented here. It is obvious from fig. 59b that the bin number 5 is very different compared to the rest of them. This is consistent with fig. 37d and fig. 49b. It is apparent also in the average bins fig. 103. Worth mentioning are the correlation coefficients between v_2, v_3, v_4, v_5 and μ, the values are -0.015, -0.021, -0.017 and 0.031.

Normalized histograms

The results are in the fig. 60 and fig. 61, it took only 55 steps for the algorithm to converge. The results are consistent with the results from initially random arrangement. It is obvious that the measure does not discriminate very well. The correlation coefficients are almost zero in all the cases of v_2, v_3, v_4, and v_5. The average bins are in the fig. 104. The histograms are the same as in the fig. 102.

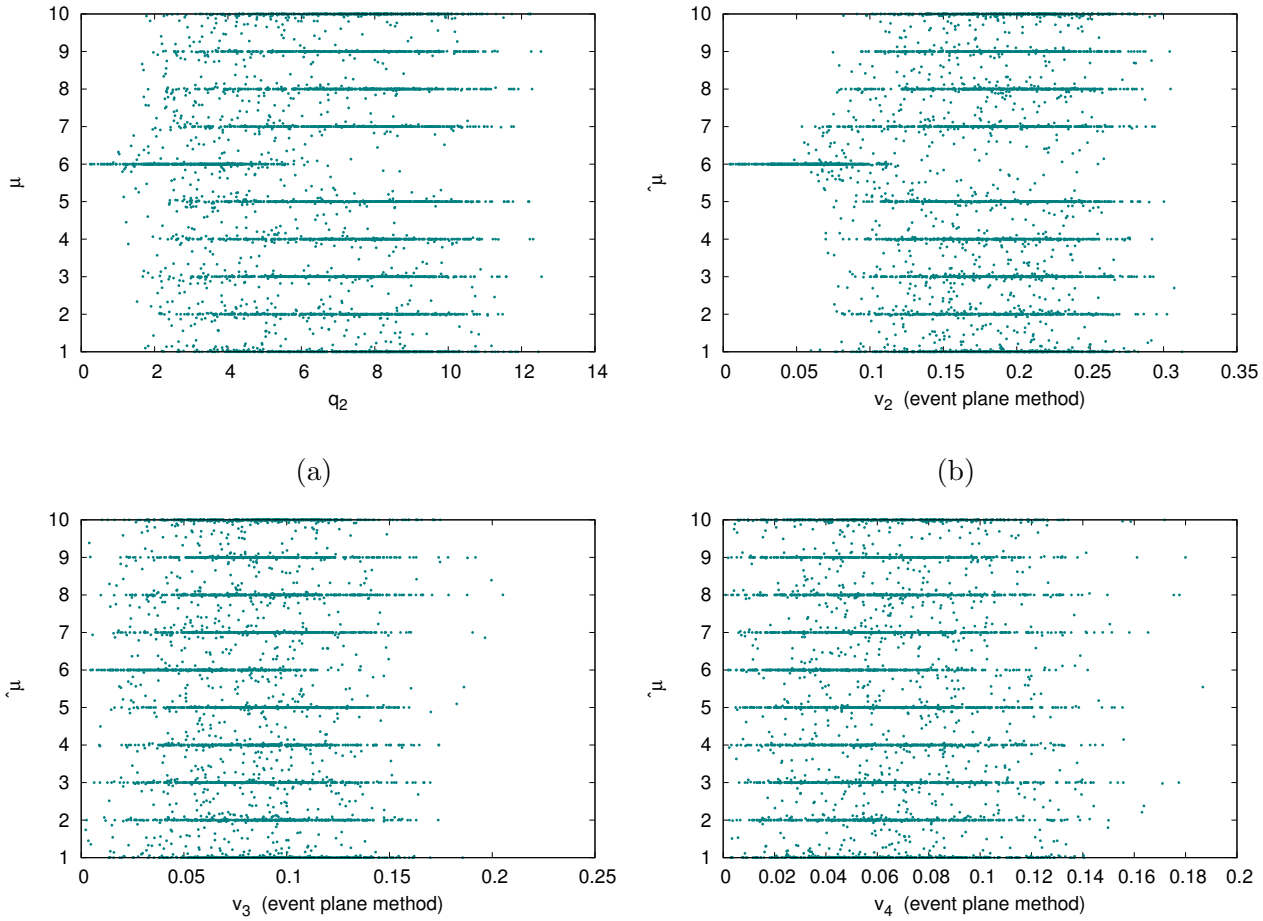

Figure 58: Algorithm results for initial arrangement according to q_2. Events are generated with flow up to pentagonal flow, initial rotation is according Ψ_5. (a) Average bin number $\hat{\mu}$ dependence on q_2. (b) Average bin number $\hat{\mu}$ dependence on v_2. v_2 was obtained via event plane method. (c) Average bin number $\hat{\mu}$ dependence on v_3. v_3 was obtained via event plane method. (d) Average bin number $\hat{\mu}$ dependence on v_4. v_4 was obtained via event plane method.

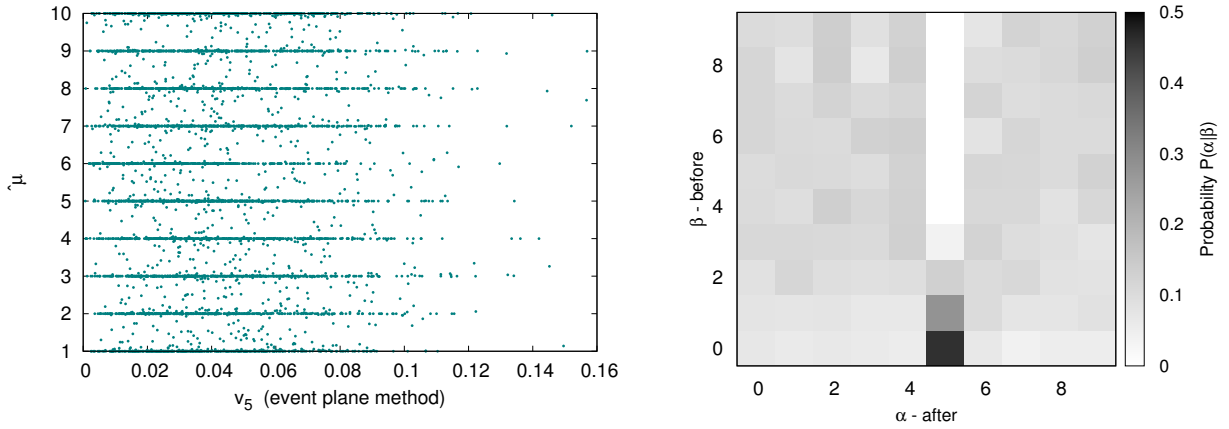

(a) (b)

Figure 59: Algorithm results for initial arrangement according to q_2. Events are generated with flow up to pentagonal flow, initial rotation is according Ψ_5. (a) Average bin number $\hat{\mu}$ dependence on v_5. v_5 was obtained via event plane method. (b) Error matrix. Probability of initial bin assignment given the final bin assignment $P(\alpha|\beta)$.

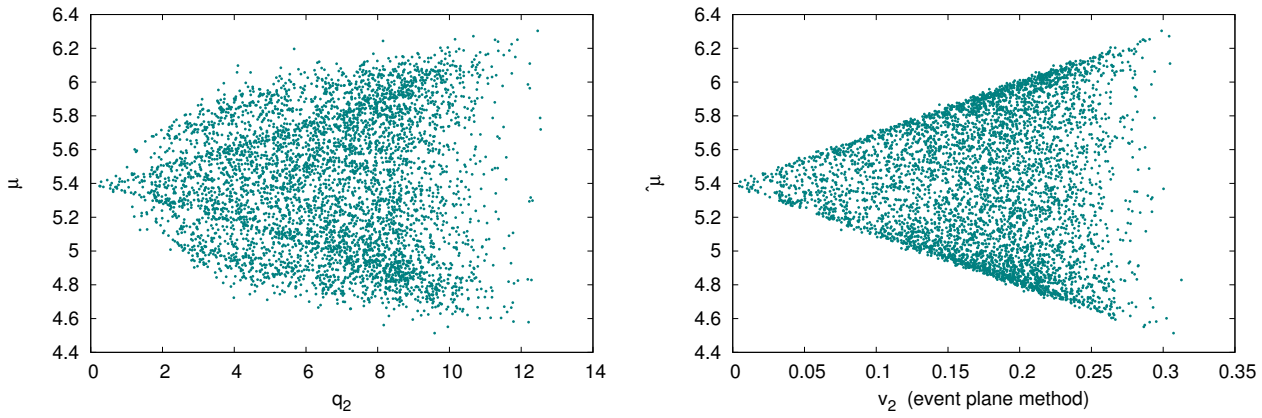

(a) (b)

Figure 60: Algorithm results for initial arrangement according to q_2. Events are generated with flow up to pentagonal flow, initial rotation is according Ψ_5, histograms are normalized. (a) Average bin number $\hat{\mu}$ dependence on q_2. (b) Average bin number $\hat{\mu}$ dependence on v_2. v_2 was obtained via event plane method.

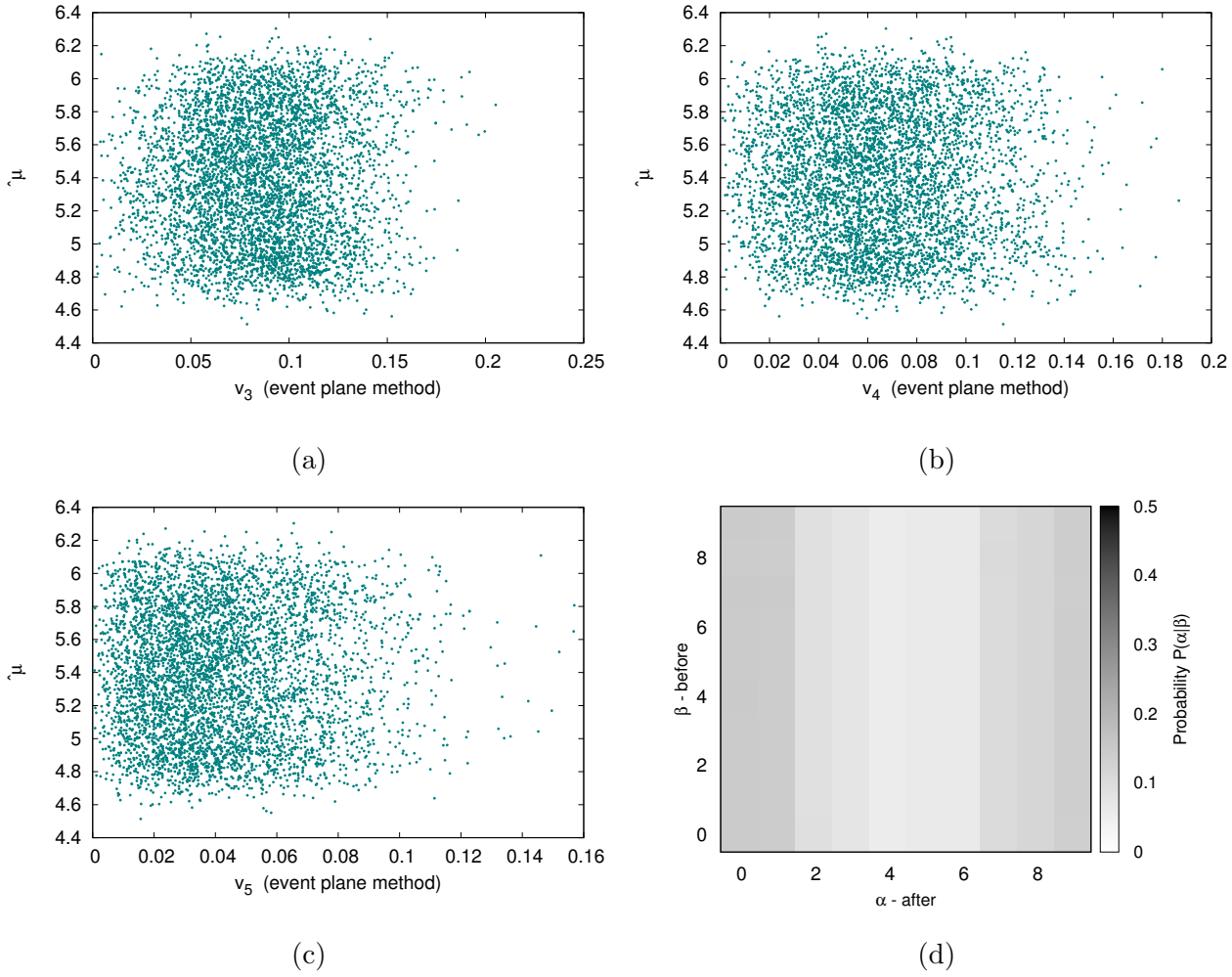

Figure 61: Algorithm results for initial arrangement according to q_2. Events are generated with flow up to pentagonal flow, initial rotation is according Ψ_5, histograms are normalized. (a) Average bin number $\hat{\mu}$ dependence on v_3. v_3 was obtained via event plane method. (b) Average bin number $\hat{\mu}$ dependence on v_4. v_4 was obtained via event plane method. (c) Average bin number $\hat{\mu}$ dependence on v_5. v_5 was obtained via event plane method. (d) Error matrix. Probability of initial bin assignment given the final bin assignment $P(\alpha|\beta)$.

5.3.4 Initial rotation according to Ψ_2 and Ψ_3

As well as in the case of events with flow up to triangular flow, we tried to take into account both Ψ_2 and Ψ_3 and rotated the events in the same way as in 5.2.3. We found the angle between Ψ_2 and Ψ_3. If $\Psi_2 < \Psi_3$, we made a mirror image of the whole event.

Random arrangement

The results are in the fig. 62, fig. 63 and fig. 64. The algorithm took 121 steps to converge. Sharp lines indicate the measure is very discriminating. However, even in this case of rotation there is novisible dependence on any flow coefficient, multiplicity or flow vector magnitude. The correlation coefficients between flow coefficients and final bin number μ are higher than in the previous cases of rotation (v_2 - 0.159, v_3 - 0.054,v_4 -0.057, v_5 -0.016), but they are still very small.

The average bins are in the fig. 105. The results are very similar to the fig. 87, meaning that indeed v_4 and v_5 does not contribute much.

Normalized histograms

The results are in the fig. 65 and fig. 66. The results are almost the same as in the case of events only with flow up to triangular flow. The measure discriminates bad. ESSTER converged after 27 steps. The correlations between the final bin number μ and flow coefficients v_2, v_3, v_4 and v_5 are consistent with zero. The average bins are in the fig. 106. Once again, it is consistent with the fig. 88.

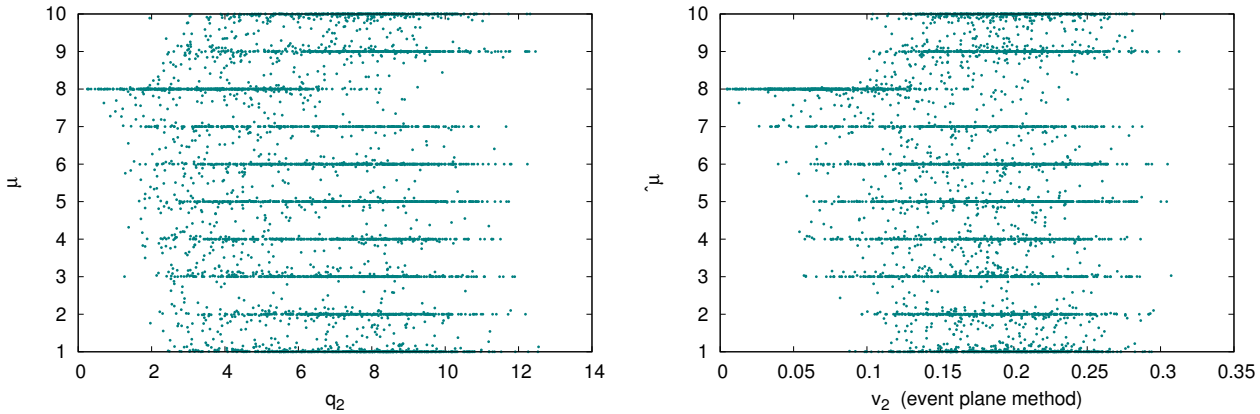

Figure 62: Algorithm results for initially random arrangement. Events are generated with flow up to pentagonal flow, initial rotation is according Ψ_2 and Ψ_3. (a) Average bin number $\hat{\mu}$ dependence on q_2. (b) Average bin number $\hat{\mu}$ dependence on v_2. v_2 was obtained via event plane method. (c) Average bin number $\hat{\mu}$ dependence on v_3. v_3 was obtained via cumulant method. (d) Average bin number $\hat{\mu}$ dependence on v_3. v_3 was obtained via event plane method.

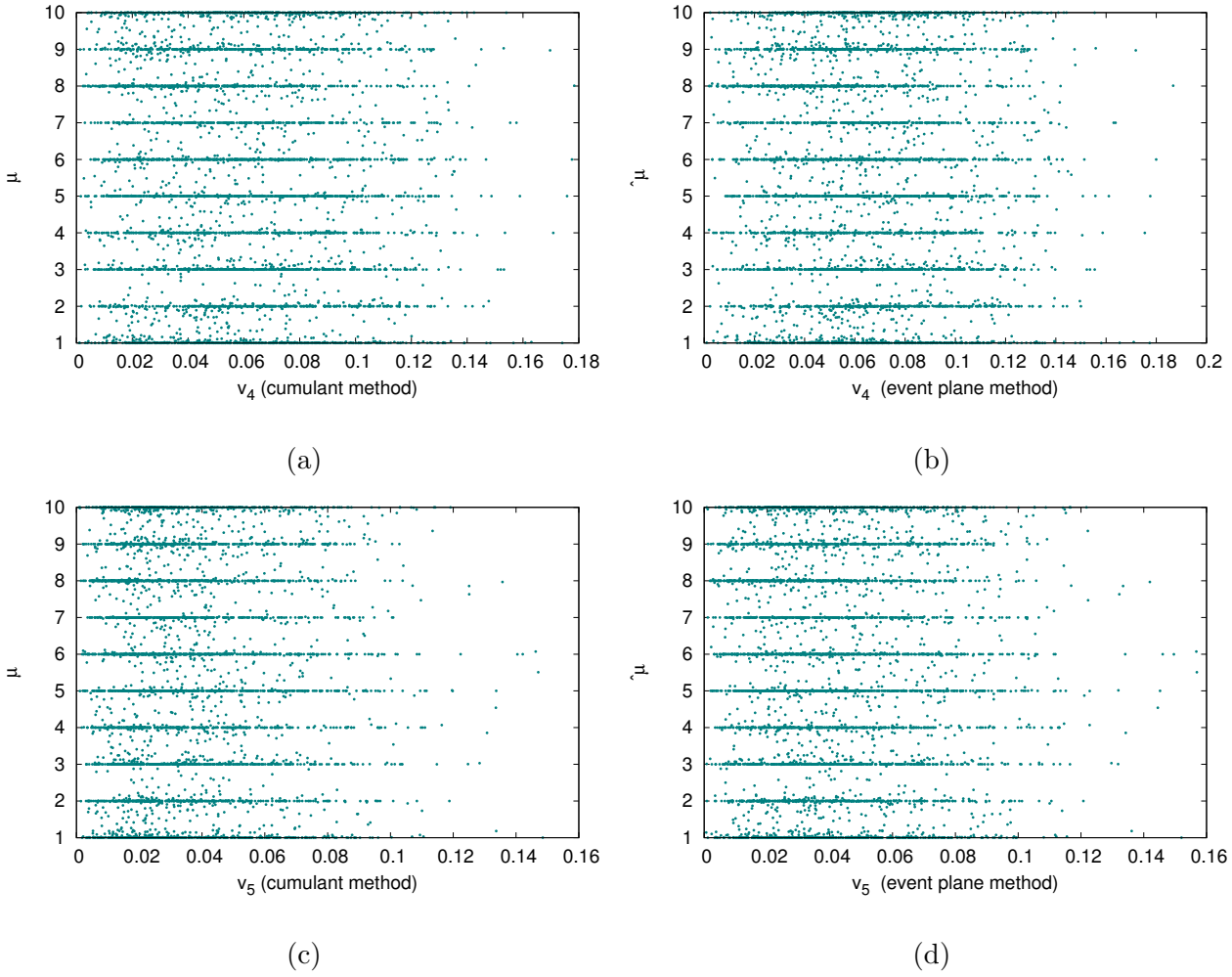

(a) (b)

(c) (d)

Figure 63: Algorithm results for initially random arrangement. Events are generated with flow up to pentagonal flow, initial rotation is according Ψ_2 and Ψ_3. (a) Average bin number $\hat{\mu}$ dependence on v_4. v_4 was obtained via cumulant method. (b) Average bin number $\hat{\mu}$ dependence on v_4. v_4 was obtained via event plane method. (c) Average bin number $\hat{\mu}$ dependence on v_5. v_5 was obtained via cumulant method. (d) Average bin number $\hat{\mu}$ dependence on v_5. v_5 was obtained via event plane method.

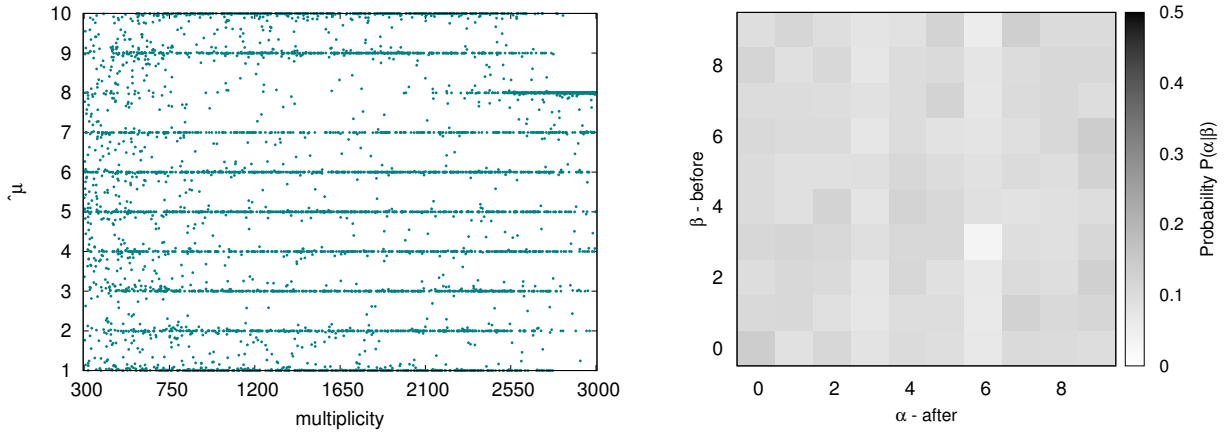

(a) (b)

Figure 64: Algorithm results for initially random arrangement. Events are generated with flow up to pentagonal flow, initial rotation is according Ψ_2 and Ψ_3. (a) Average bin number $\hat{\mu}$ dependence on multiplicity. (b) Error matrix. Probability of initial bin assignment given the final bin assignment $P(\alpha|\beta)$.

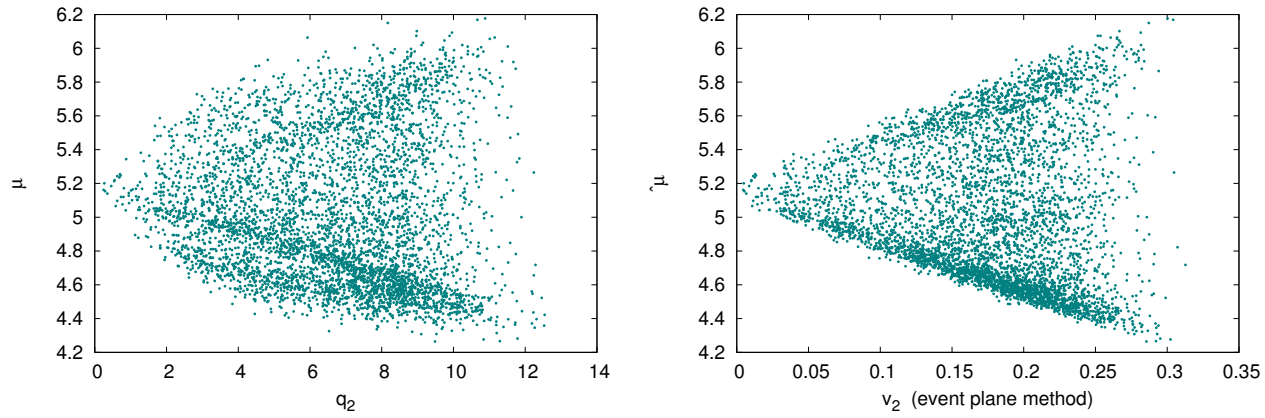

(a) (b)

Figure 65: Algorithm results for initially random arrangement. Events are generated with flow up to pentagonal flow, initial rotation is according Ψ_2 and Ψ_3, histograms are normalized. (a) Average bin number $\hat{\mu}$ dependence on q_2. (b) Average bin number $\hat{\mu}$ dependence on v_2. v_2 was obtained via event plane method.

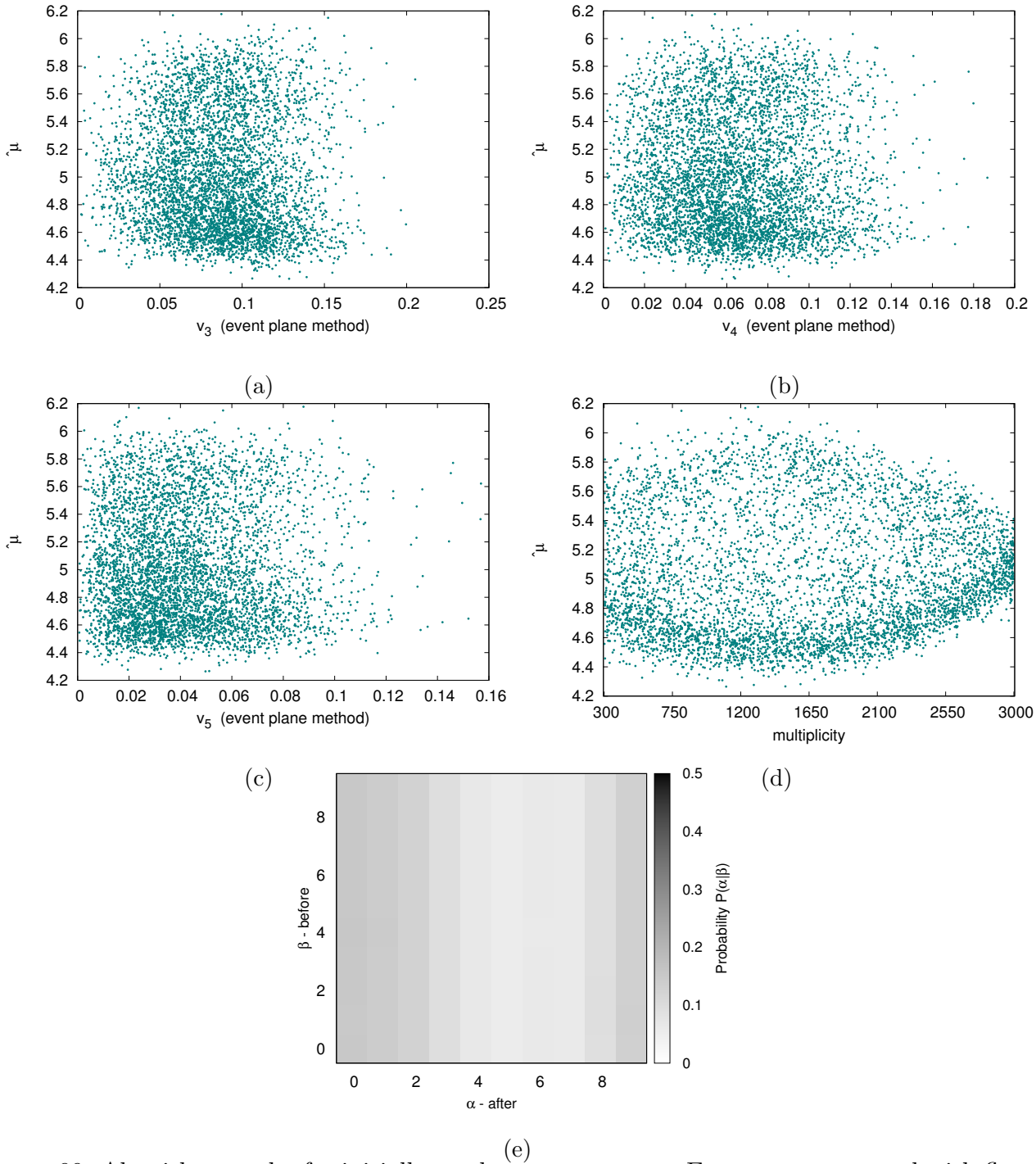

Figure 66: Algorithm results for initially random arrangement. Events are generated with flow up to pentagonal flow, initial rotation is according Ψ_2 and Ψ_3, histograms are normalized. (a) Average bin number $\hat{\mu}$ dependence on v_3. (b) Average bin number $\hat{\mu}$ dependence on v_4. (c) Average bin number $\hat{\mu}$ dependence on v_5.. (d) Average bin number $\hat{\mu}$ dependence on multiplicity. (e) Error matrix. Probability of initial bin assignment given the final bin assignment $P(\alpha|\beta)$.

Arrangement according to q_2

The ESSTER failed to converge. We stopped the algorithm after 5000 steps. The results are in the fig. 67 and 68. It is obvious from fig. 67b and fig. 68b that the bins 2 and 5 are very distinct compared to the rest of them. It is apparent also in the average bins fig. 107. We see that bins 2 and 5 are more 'round' than the rest of them.

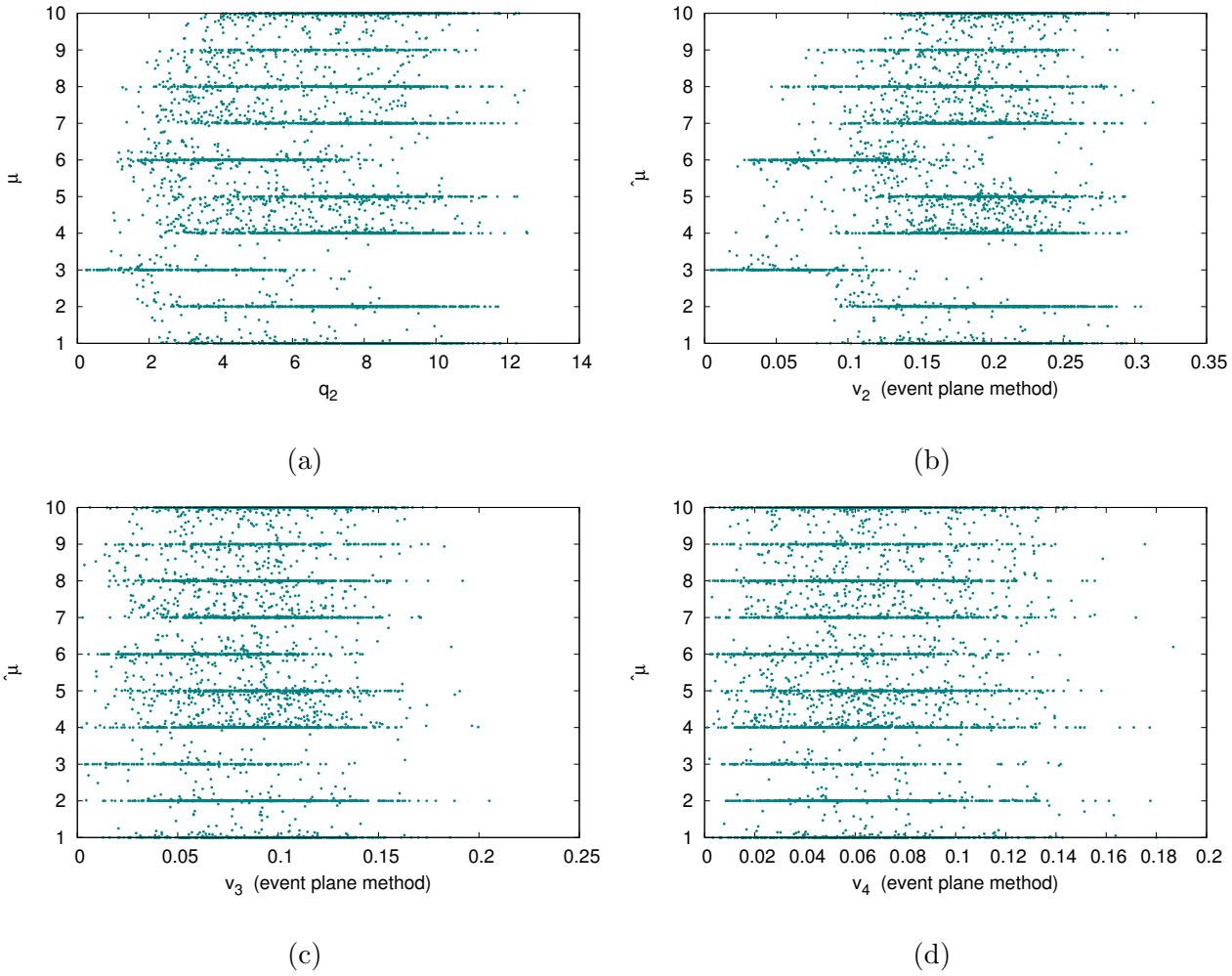

Figure 67: Algorithm results for initial arrangement according to q_2. Events are generated with flow up to pentagonal flow, initial rotation is according Ψ_2 and Ψ_3. (a) Average bin number $\hat{\mu}$ dependence on q_2. (b) Average bin number $\hat{\mu}$ dependence on v_2. v_2 was obtained via event plane method. (c) Average bin number $\hat{\mu}$ dependence on v_3. v_3 was obtained via event plane method. (d) Average bin number $\hat{\mu}$ dependence on v_4. v_4 was obtained via event plane method.

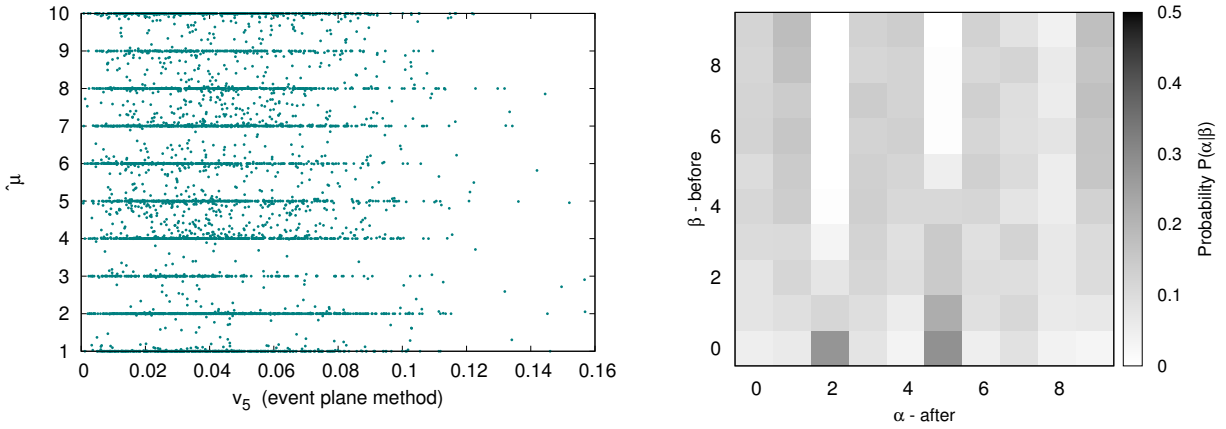

(a) (b)

Figure 68: Algorithm results for initial arrangement according to q_2. Events are generated with flow up to pentagonal flow, initial rotation is according Ψ_2 and Ψ_3. (a) Average bin number $\hat{\mu}$ dependence on v_5. v_5 was obtained via event plane method. (b) Error matrix. Probability of initial bin assignment given the final bin assignment $P(\alpha|\beta)$.

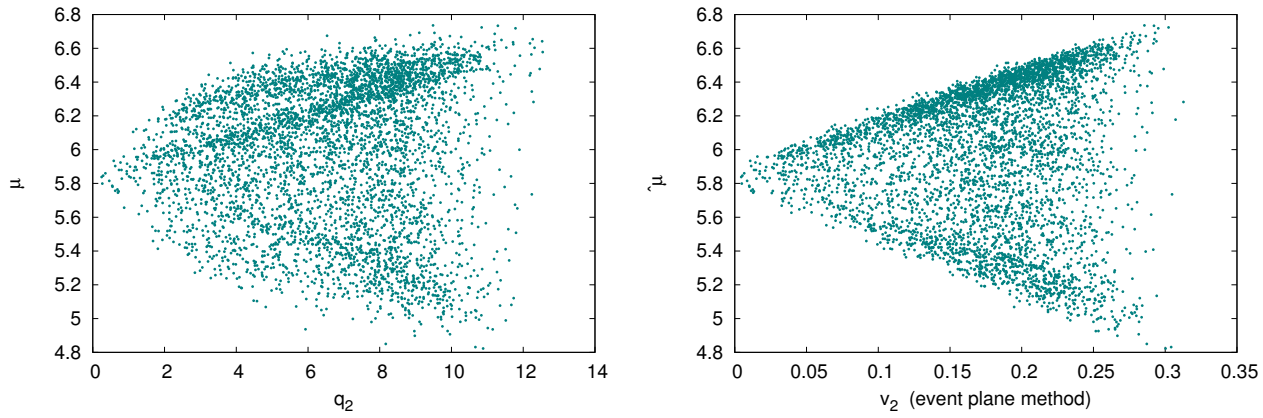

(a) (b)

Figure 69: Algorithm results for initial arrangement according to q_2. Events are generated with flow up to pentagonal flow, initial rotation is according Ψ_2 and Ψ_3, histograms are normalized. (a) Average bin number $\hat{\mu}$ dependence on q_2. (b) Average bin number $\hat{\mu}$ dependence on v_2. v_2 was obtained via event plane method.

Normalized histograms

The results are in the fig. 69 and fig. 70, it took only 21 steps for the algorithm to converge. The results are consistent with the results from initially random arrangement. It is obvious that the measure does not discriminate very well. The correlation coefficients are almost zero in all the cases of v_2, v_3, v_4, and v_5. Note that the mean bin number $\hat{\mu}$ ranges from 4.8 to 4.8. The average bins are in the fig. 108. The histograms are the same as in the fig. 106.

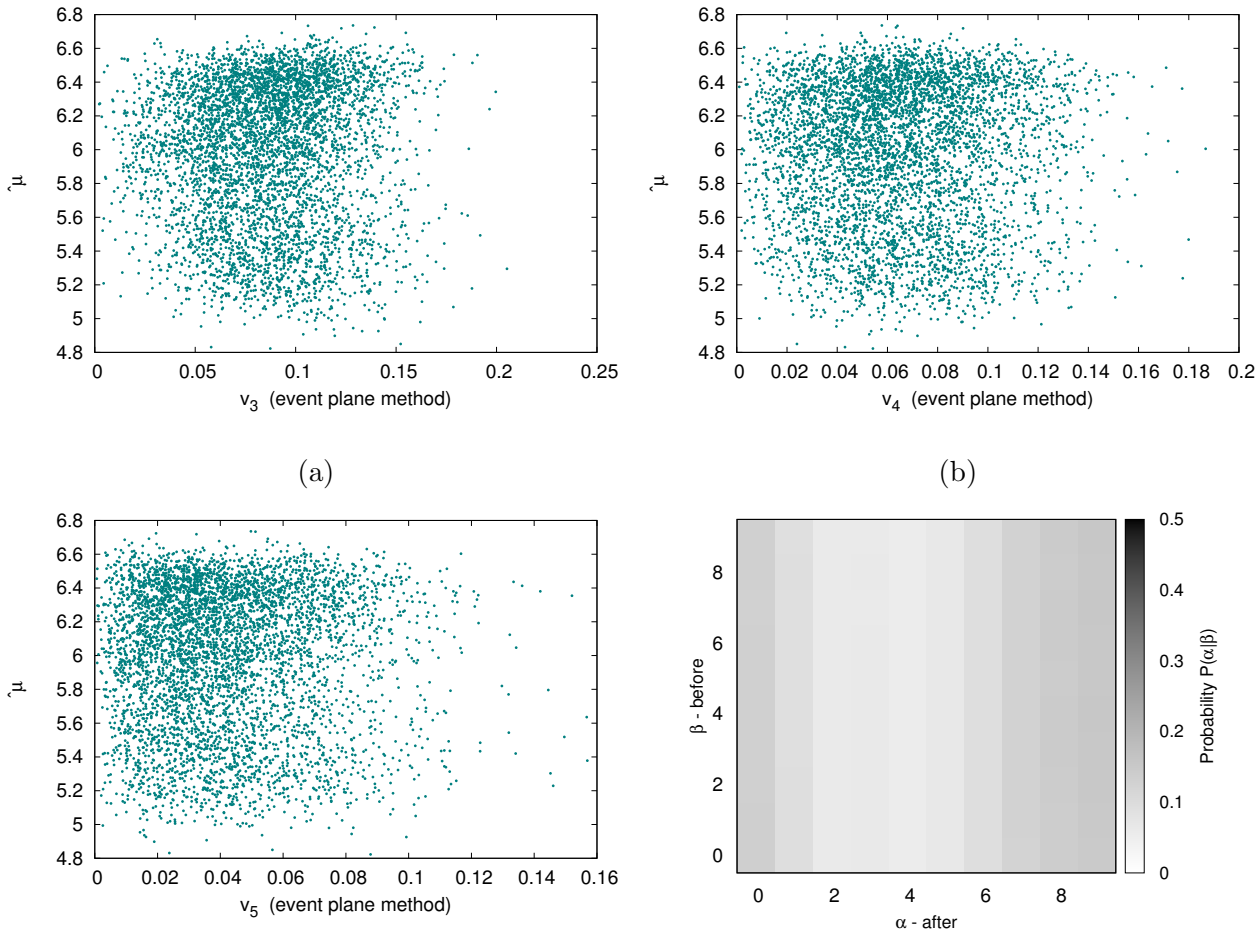

Figure 70: Algorithm results for initial arrangement according to q_2. Events are generated with flow up to pentagonal flow, initial rotation is according Ψ_2 and Ψ_3, histograms are normalized. (a) Average bin number $\hat{\mu}$ dependence on v_3. (b) Average bin number $\hat{\mu}$ dependence on v_4. (c) Average bin number $\hat{\mu}$ dependence on v_5. (d) Error matrix. Probability of initial bin assignment given the final bin assignment $P(\alpha|\beta)$.

5.4 Dragon

Last step was to apply the algorithm on a more advanced model. We used model DRAGON [4] (DRoplet and hAdron GeneratOr for Nuclear collisions). We generated 5000 events, set the kinetic freeze-out temperature to 0.09 GeV, chemical freeze-out temperature to 0.156 GeV. Total dN/dy was set as 1500. We set the flow anisotropy parameter ρ_2 to 0.1 and spatial anisotropy parameter a as 0.95. This parameters are motivated by LHC results for Pb-Pb collisions. In this model, only elliptic flow is present. We run the analysis as described before, for simplicity without p_T weighting, we analyzed charged pions only.

Since there is only elliptic flow present, we initially rotated the events according to Ψ_2.

5.4.1 Random initial arrangement

The algorithm converged after 287 steps. This seems a lot, but since the initial random arrangement varies a lot, this result is not surprising. The results are in the fig. 71. This time, the results from cumulant and event plane method are rather different. Compared to fig. 7, the measure does not discriminate well. There is no correlation between bin number μ and v_2, fig. 71d confirms the measure is not good. This is supported by the average event angle distributions in fig. 109. Even though the events seems to be sorted according to their ellipticity, one can see that the difference between the bins are minimal. The reason is rather simple, all the events have the same v_2, therefore, only the fact that we have finite number of particles and bins makes the difference.

Interesting are the results compared to the toy model (fig. 7c and fig. 71c). The inconsistency with the previous results are simple, the ESSTER toy model is very simple and the methods give the same results only in the limit of ideal shape. In the DRAGON case, the generated particles include decays from resonances, therefore, the results from both methods differs.

This average azimuthal angle histograms are rather surprising (fig. 109b). Once again, the upper row seems to be a mirror image of the bottom row. This suggest the affection of the distribution by resonances.

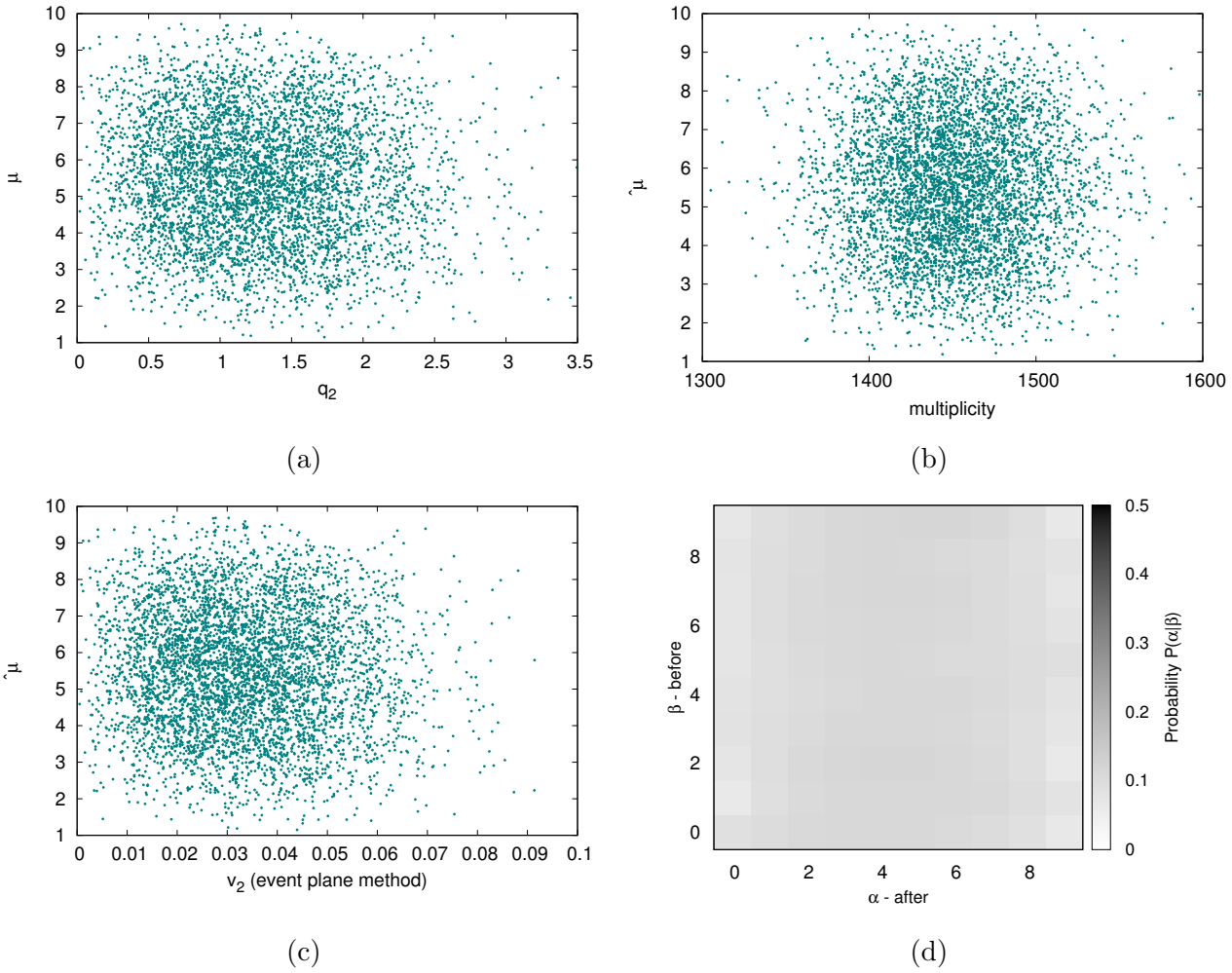

Figure 71: Algorithm results for initially random arrangement. Events were generated via model DRAGON [4]. (a) Average bin number $\hat{\mu}$ dependence on q_2. (b) Average bin number $\hat{\mu}$ dependence on multiplicity M. (c) Average bin number $\hat{\mu}$ dependence on v_2. v_2 was obtained via event plane method. (d) Error matrix. Probability of initial bin assignment given the final bin assignment $P(\alpha|\beta)$.

Normalized histograms

It took 118 steps for the algorithm to converge. The results are in the fig. 72. This time, the final $\hat{\mu}$ are very close to 5, it ranges from 5.47 to 5.53. This means the events are very similar and the the algorithm does not discriminate very well. The error matrix is almost perfectly uniform (fig. 72d). The average histograms in the fig. 110 are consistent with previous result (fig. 109).

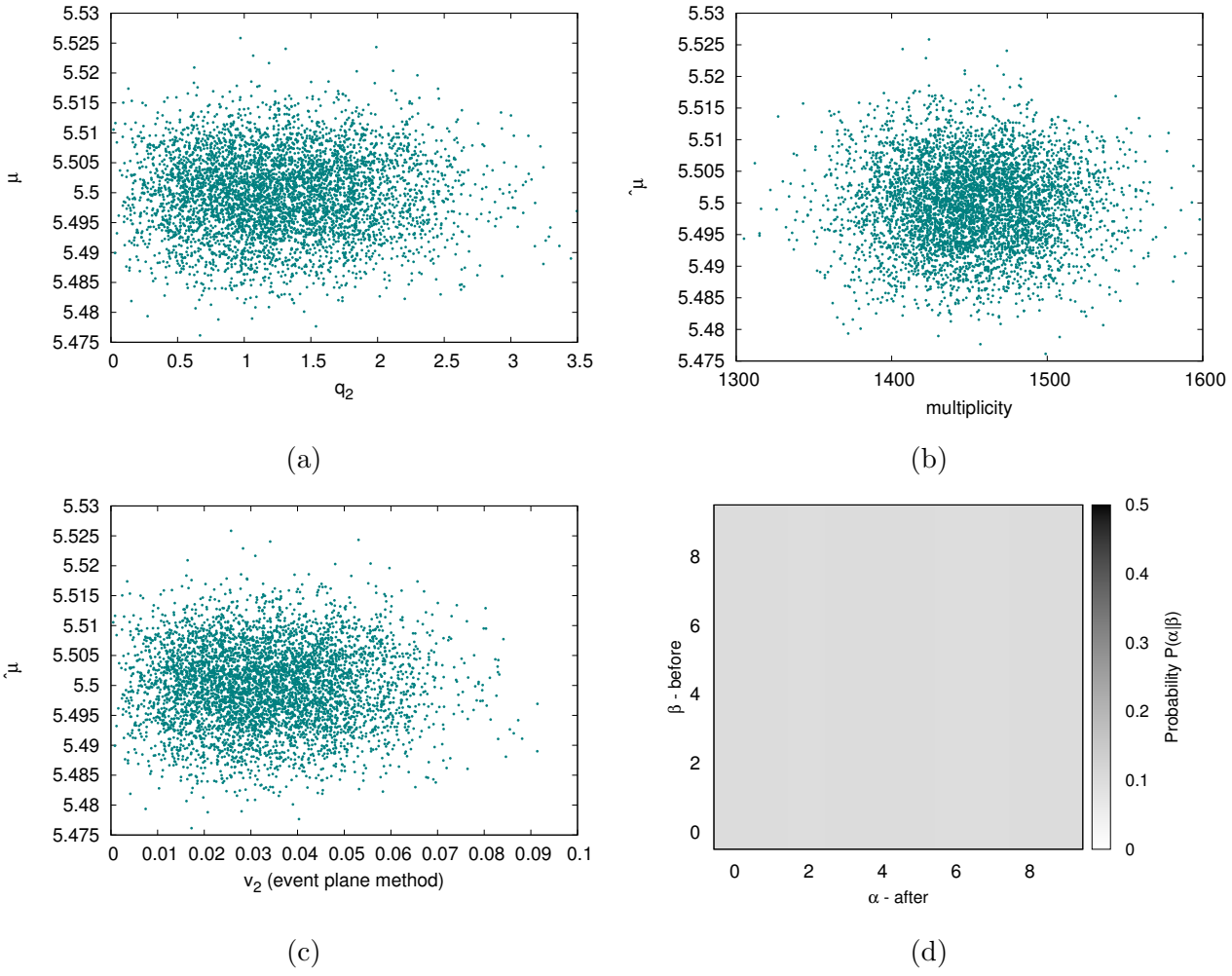

Figure 72: Algorithm results for initially random arrangement and normalized histograms. Events were generated via model DRAGON [4]. (a) Average bin number $\hat{\mu}$ dependence on q_2. (b) Average bin number $\hat{\mu}$ dependence on multiplicity M. (c) Average bin number $\hat{\mu}$ dependence on v_2. v_2 was obtained via event plane method. (d) Error matrix. Probability of initial bin assignment given the final bin assignment $P(\alpha|\beta)$

5.4.2 Initial arrangement according to q_2

The algorithm converged after 1171 steps, which is rather small number, compared to previous cases of failed convergence. However, even in this case (fig. 73) result does not suggest any $\hat{\mu} = \hat{\mu}(v_2)$ or $\hat{\mu} = \hat{\mu}(q_2)$ linear dependence, the correlation between the final bin number μ and v_2 is 0.101.

The average histograms can be found in the fig. 111. In the fig. 111a, one can see the initial arrangement from most 'round' events to the most elliptic ones. However, fig. 111b confirms that the shape of the event is not determined only by v_2.

As well as in the previous case, we present figures of average bins before and after the algorithm was applied in the fig. 111. Both figures confirms that the events are organized from the most 'round' ones (with the lowest v_2) to the most elliptic ones (with the highest v_2). However, there is a visible shift in the multiplicity dependence.

Normalized histograms

It took 120 steps for the algorithm to converge. The results are in the fig. 74. The results are consistent with the random arrangement (fig. 72), as well as average bins before and after the algorithm was applied (fig. 112).

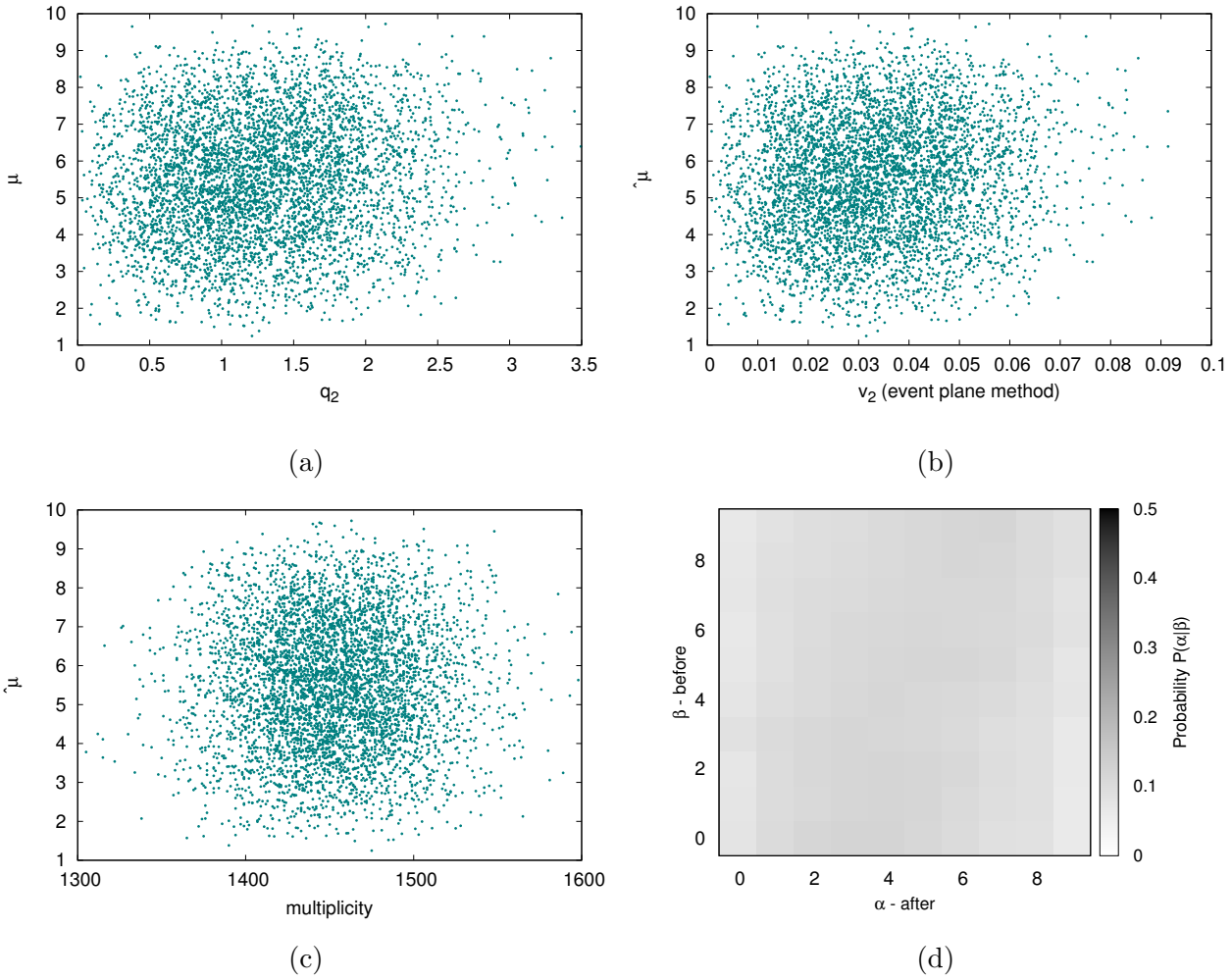

Figure 73: Algorithm results for initial arrangement according to q_2. Events were generated via model DRAGON [4]. (a) Average bin number $\hat{\mu}$ dependence on q_2. (b) Average bin number $\hat{\mu}$ dependence on v_2. v_2 was obtained via event plane method. (c) Average bin number $\hat{\mu}$ dependence on multiplicity. (d) Error matrix. Probability of initial bin assignment given the final bin assignment $P(\alpha|\beta)$.

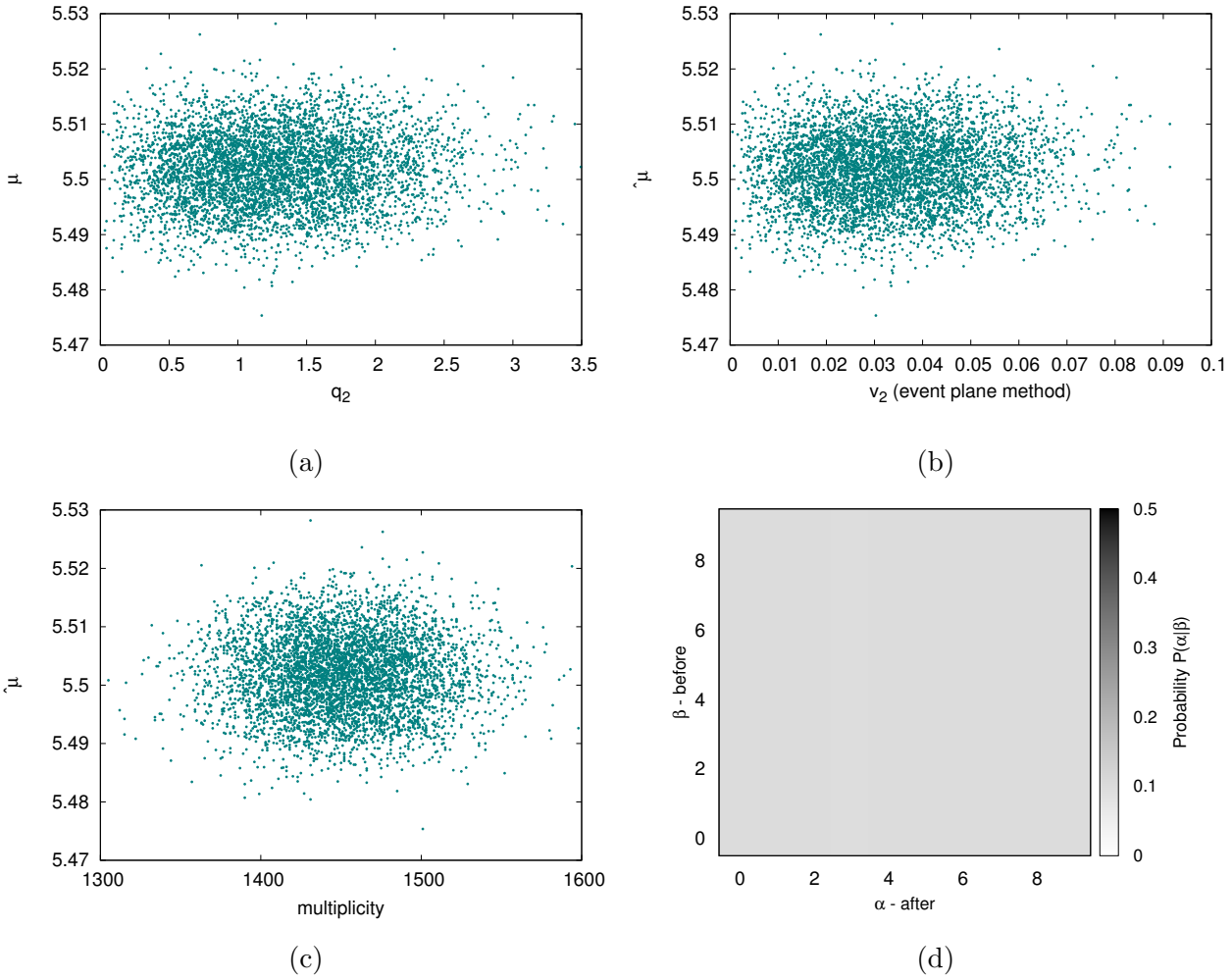

Figure 74: Algorithm results for initial arrangement and normalized histograms according to q_2. Events were generated via model DRAGON [4]. (a) Average bin number $\hat{\mu}$ dependence on q_2. (b) Average bin number $\hat{\mu}$ dependence on v_2. v_2 was obtained via event plane method. (c) Average bin number $\hat{\mu}$ dependence on multiplicity M. (d) Error matrix. Probability of initial bin assignment given the final bin assignment $P(\alpha|\beta)$.

Conclusion

In this research work, we presented a new study of the event shape. We described Event Shape Engineering [1], algorithm used for sorting events and several methods used for further study of the results. We presented our own toy model, analysis tool and event shape sorter ESSTER and the results obtained via this program. The results confirms the importance of elliptic and triangular flow for the event shape analysis and smaller influence of quadrangular and pentagonal flows. We also studied data produced by DRAGON [4], the results indicate the importance of resonances. However, we still have not find the ideal variable for measurement. Moreover, there are many possibilities of initial rotation of the events and possible flipping of the azimuthal angle distribution. It seems that the most significant planes are Ψ_2 and Ψ_3. Results indicate that initial rotation according to the angle between Ψ_2 and Ψ_3 is the rotation causing the smallest bias. Furthermore, since in the case of $\Psi_2 < \Psi_3$ we made a mirror image of the whole event, we minimized the effect of symmetry in the event planes. We suggest further studying of these phenomena in our future work.

A Appendix

n	$a \times 10^{-8}$	$b \times 10^{-5}$	c
1	0	0.016667	- 0.000680
2	- 7.098765	20.06481	0.078744
3	- 2.083333	6.658333	0.042360
4	- 96.38272	2.620769	0.048974
5	- 71.75926	2.236111	0.016730

Table 2: Parameters used for generating multiplicity dependent v_n: $v_n = aM^2 + bM + c$.

B Elliptic flow

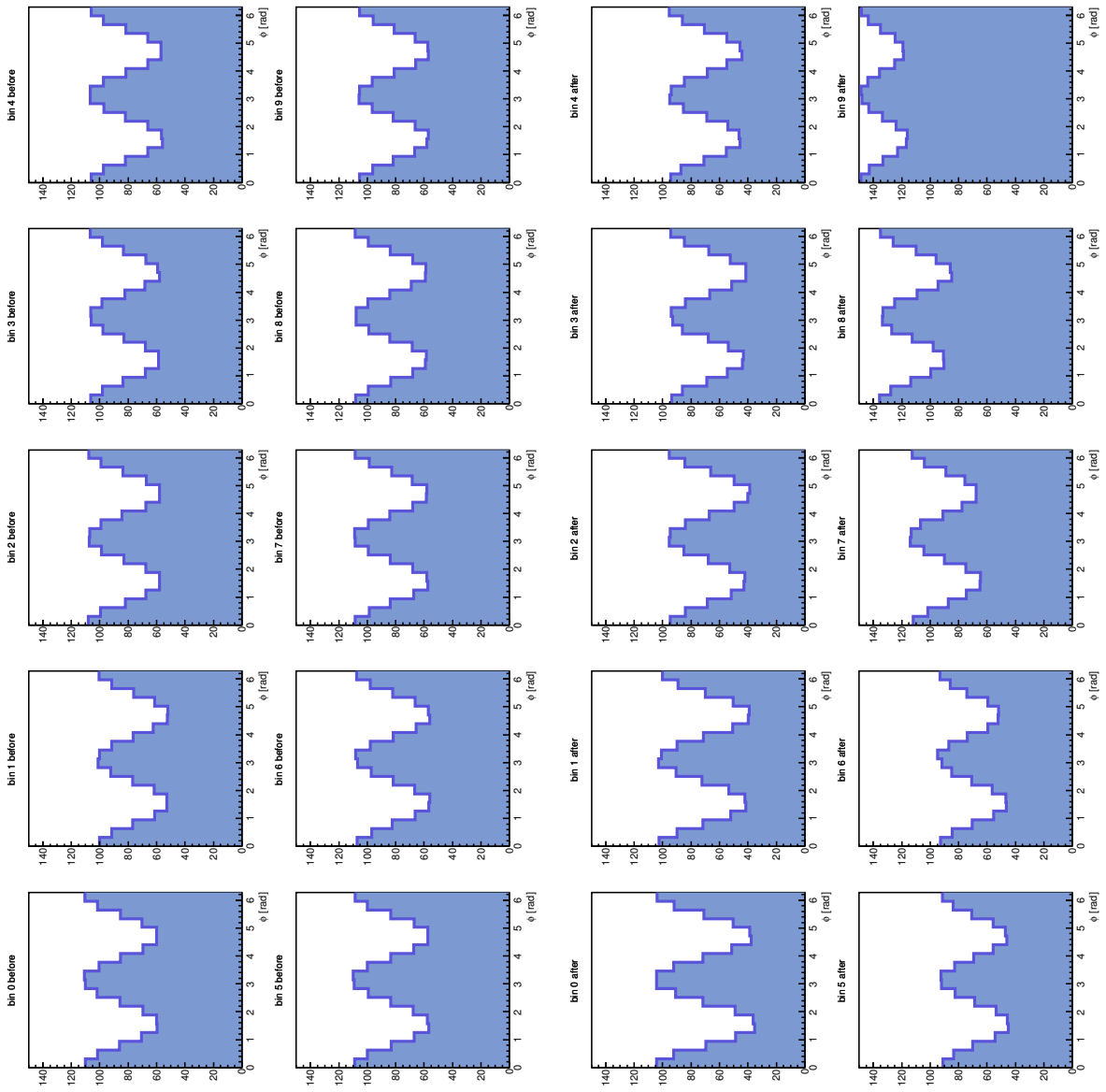

(a) (b)

Figure 75: Average histograms results for initially random arrangement. The y-axis are missing label for the sake of viewers comfort, the y-axis depicts number of particles in the bin. (a) Average angle distribution *before* the algorithm had been used. (b) Average angle distribution *after* the algorithm had been used.

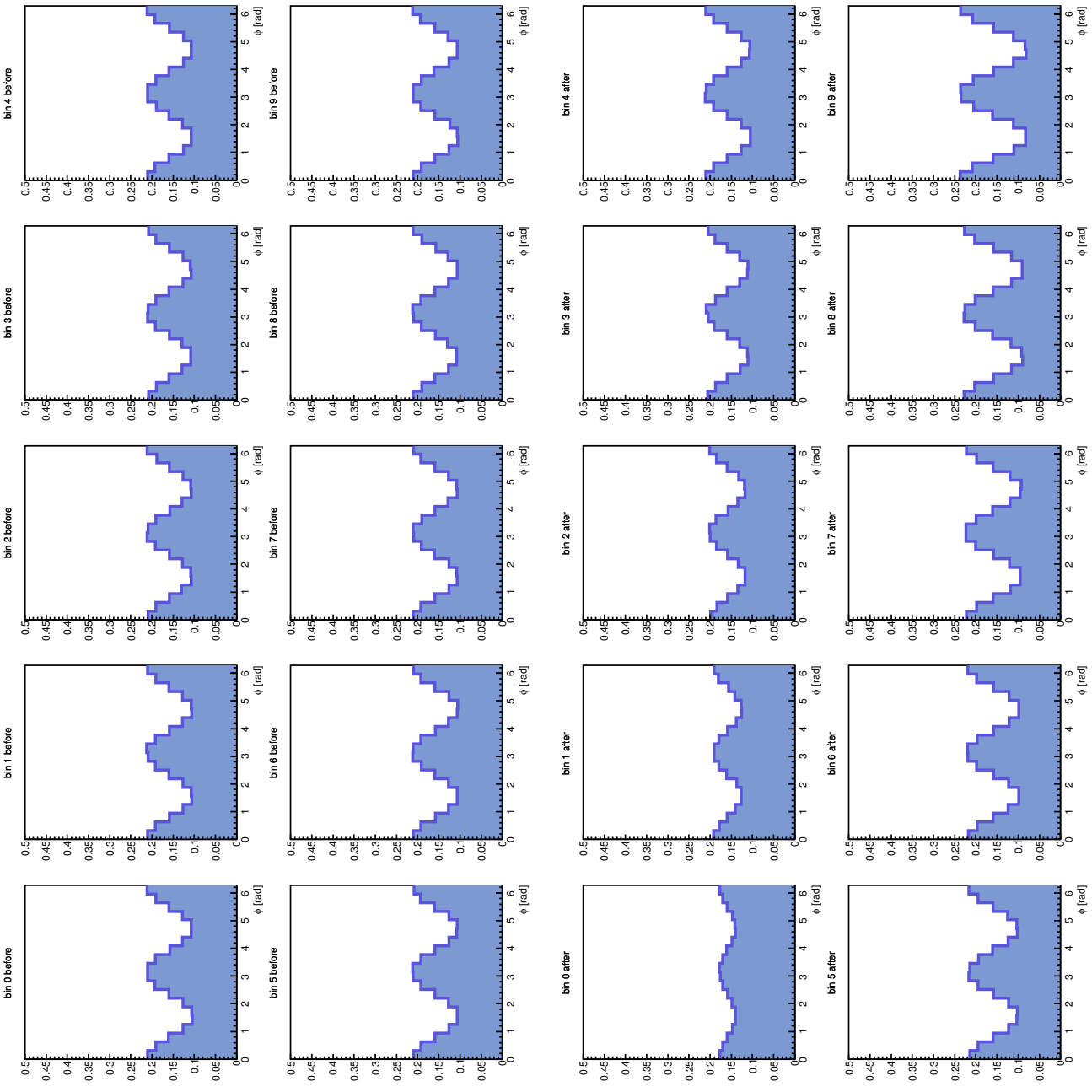

(a) (b)

Figure 76: Average normalized histograms results for initially random arrangement. The y-axis are missing label for the sake of viewers comfort, the y-axis depicts normalized number of particles in the bin. (a) Average angle distribution *before* the algorithm had been used. (b) Average angle distribution *after* the algorithm had been used.

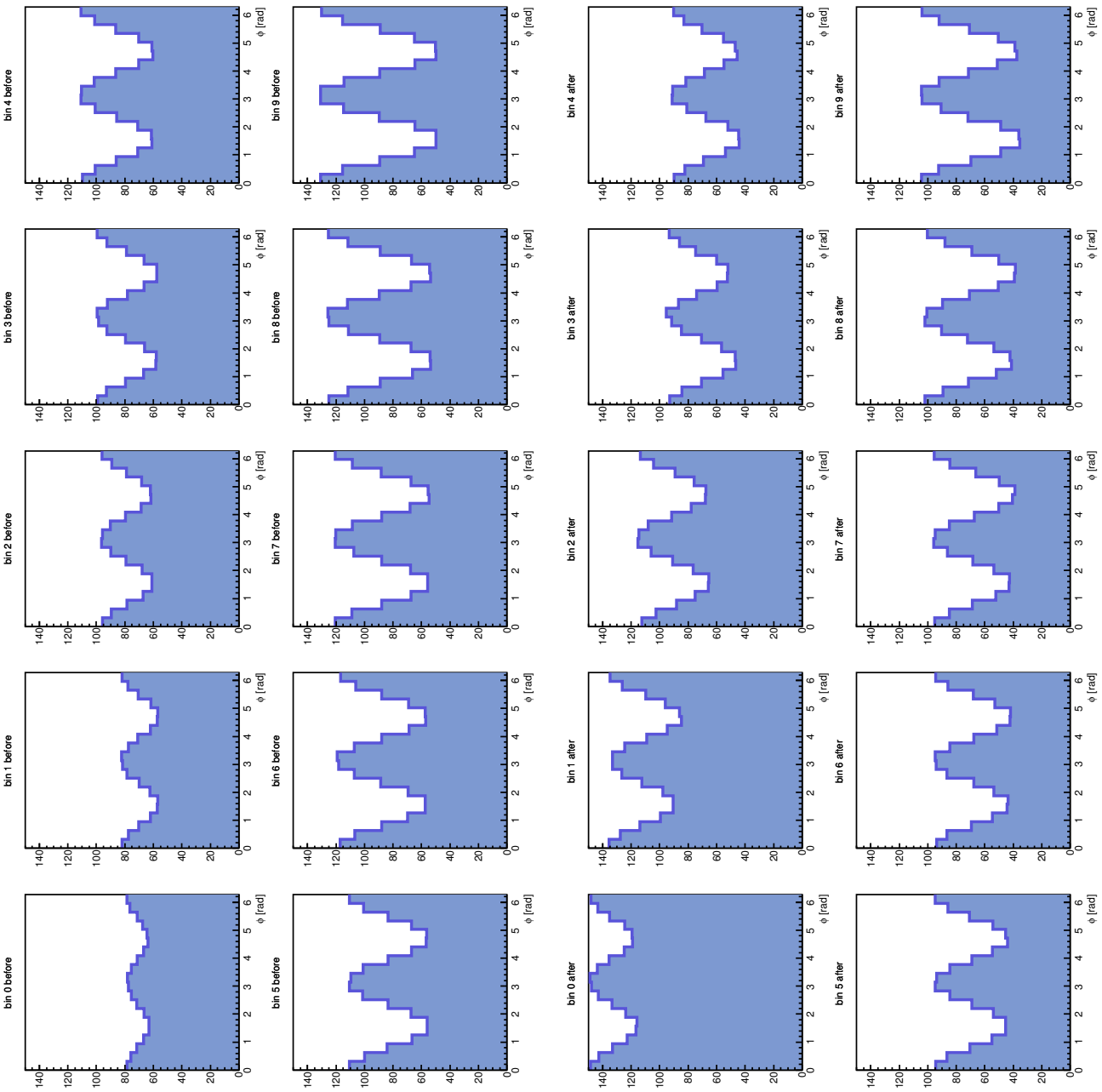

Figure 77: Average histograms results for initial arrangement according to q_2. The y-axis are missing label for the sake of viewers comfort, the y-axis depicts number of particles in the bin. (a) Average angle distribution *before* the algorithm had been used. (b) Average angle distribution *after* the algorithm had been used.

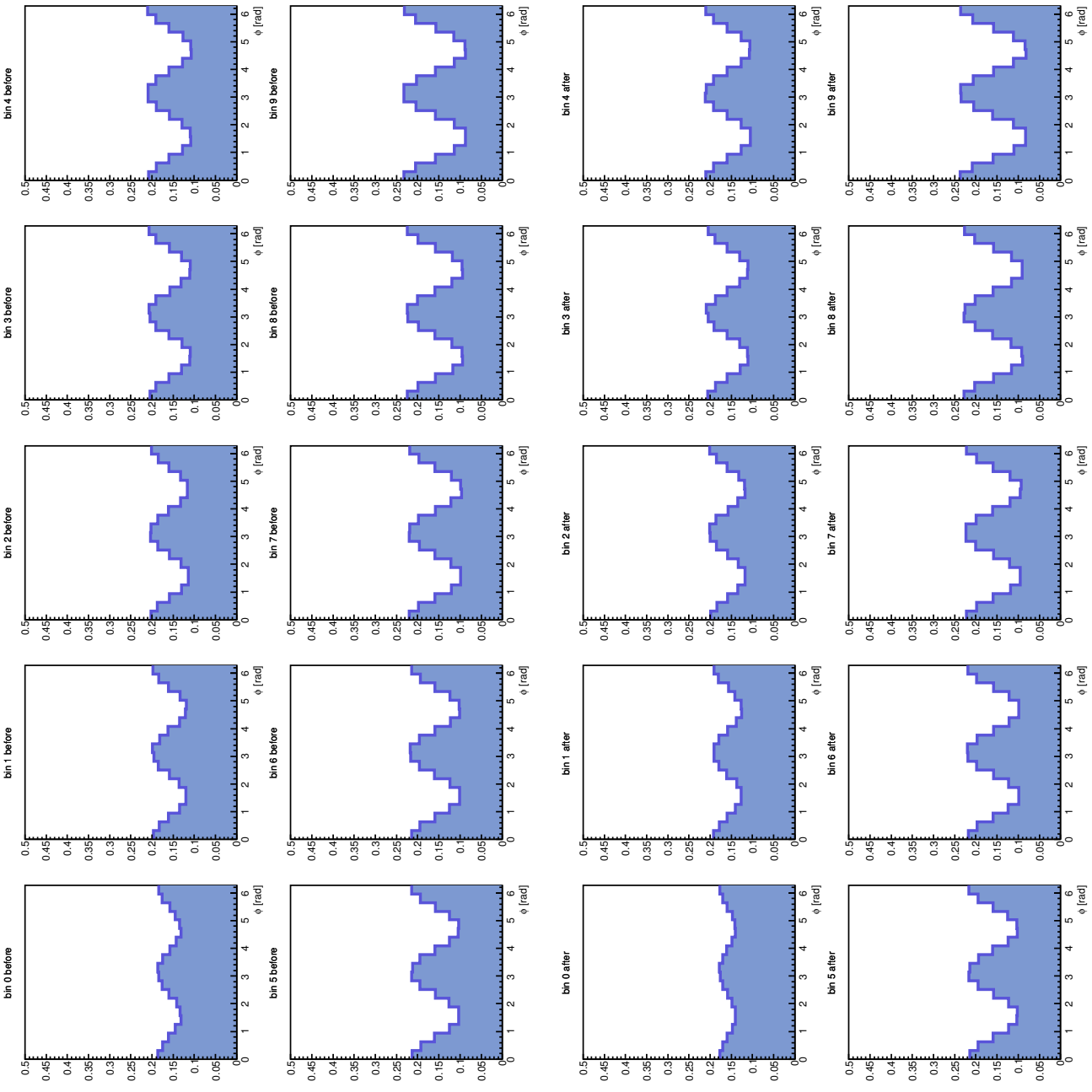

(a) (b)

Figure 78: Average normalized histograms results for initial arrangement according to q_2. The y-axis are missing label for the sake of viewers comfort, the y-axis depicts number of particles in the bin. (a) Average angle distribution *before* the algorithm had been used. (b) Average angle distribution *after* the algorithm had been used.

C Triangular flow

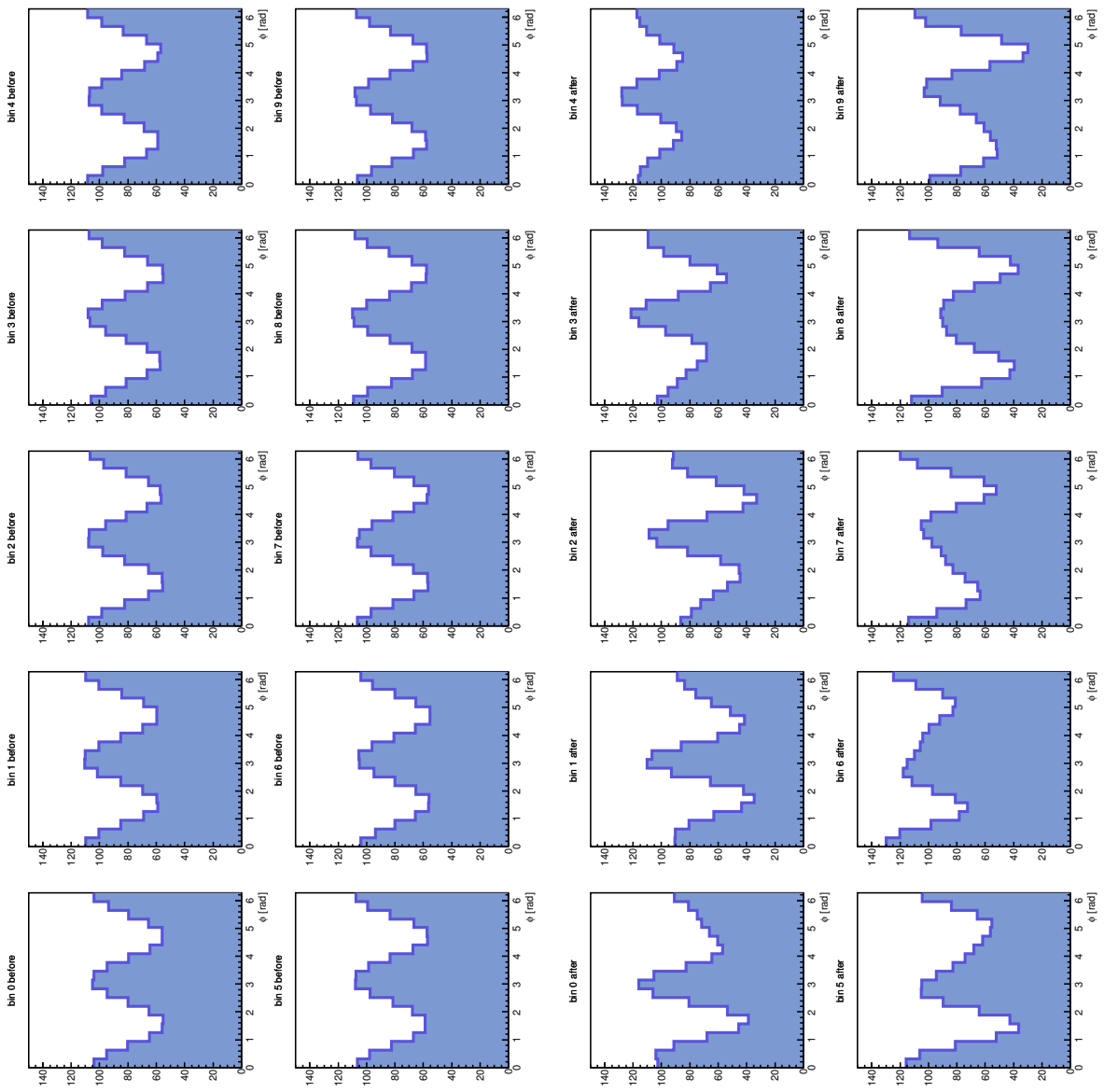

(a) (b)

Figure 79: Average histograms results for initially random arrangement and rotation according to Ψ_2. The y-axis are missing label for the sake of viewers comfort, the y-axis depicts number of particles in the bin. (a) Average angle distribution *before* the algorithm had been used. (b) Average angle distribution *after* the algorithm had been used.

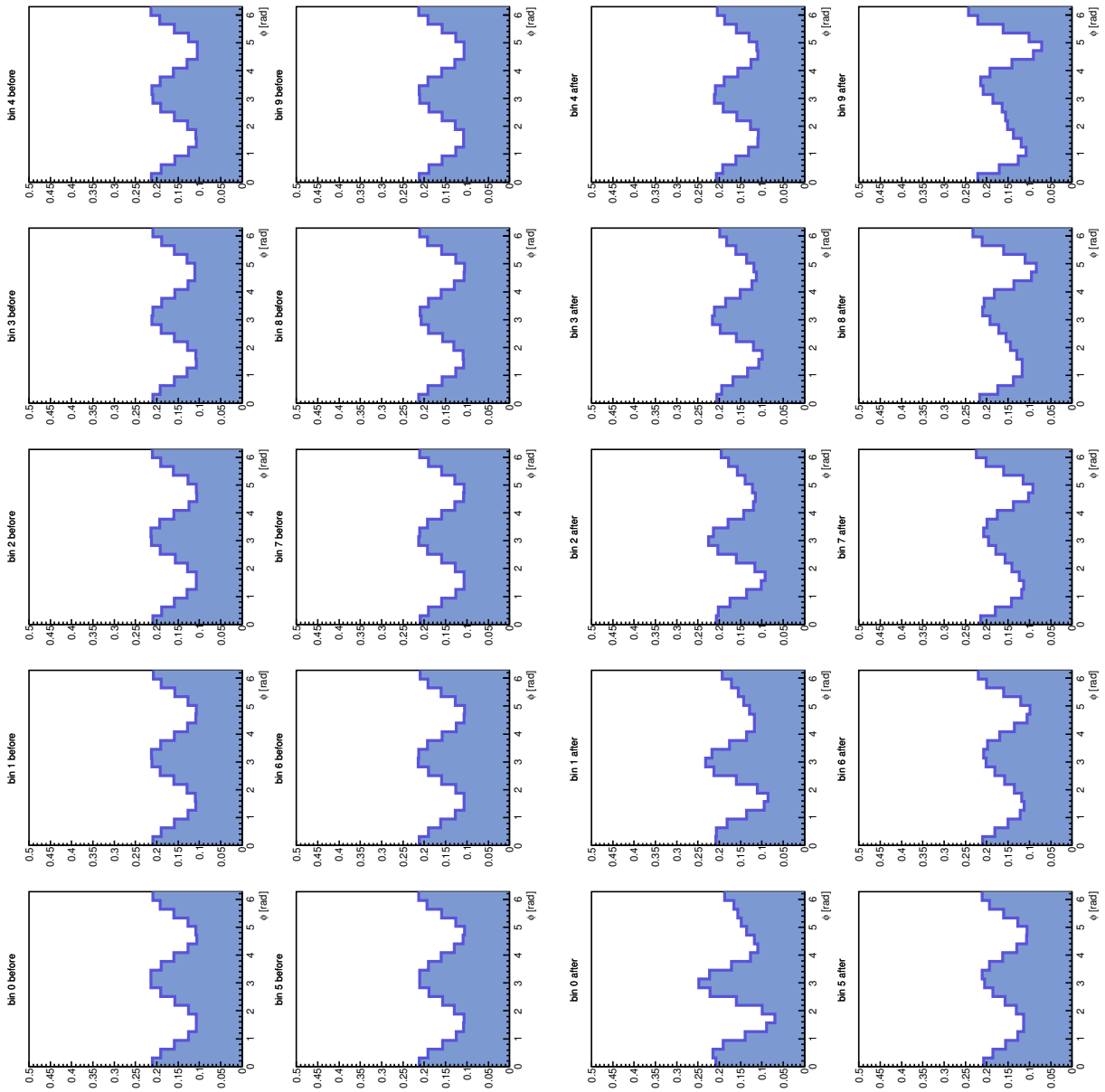

(a) (b)

Figure 80: Average normalized histograms results for initially random arrangement and rotation according to Ψ_2. The y-axis are missing label for the sake of viewers comfort, the y-axis depicts number of particles in the bin. (a) Average angle distribution *before* the algorithm had been used. (b) Average angle distribution *after* the algorithm had been used.

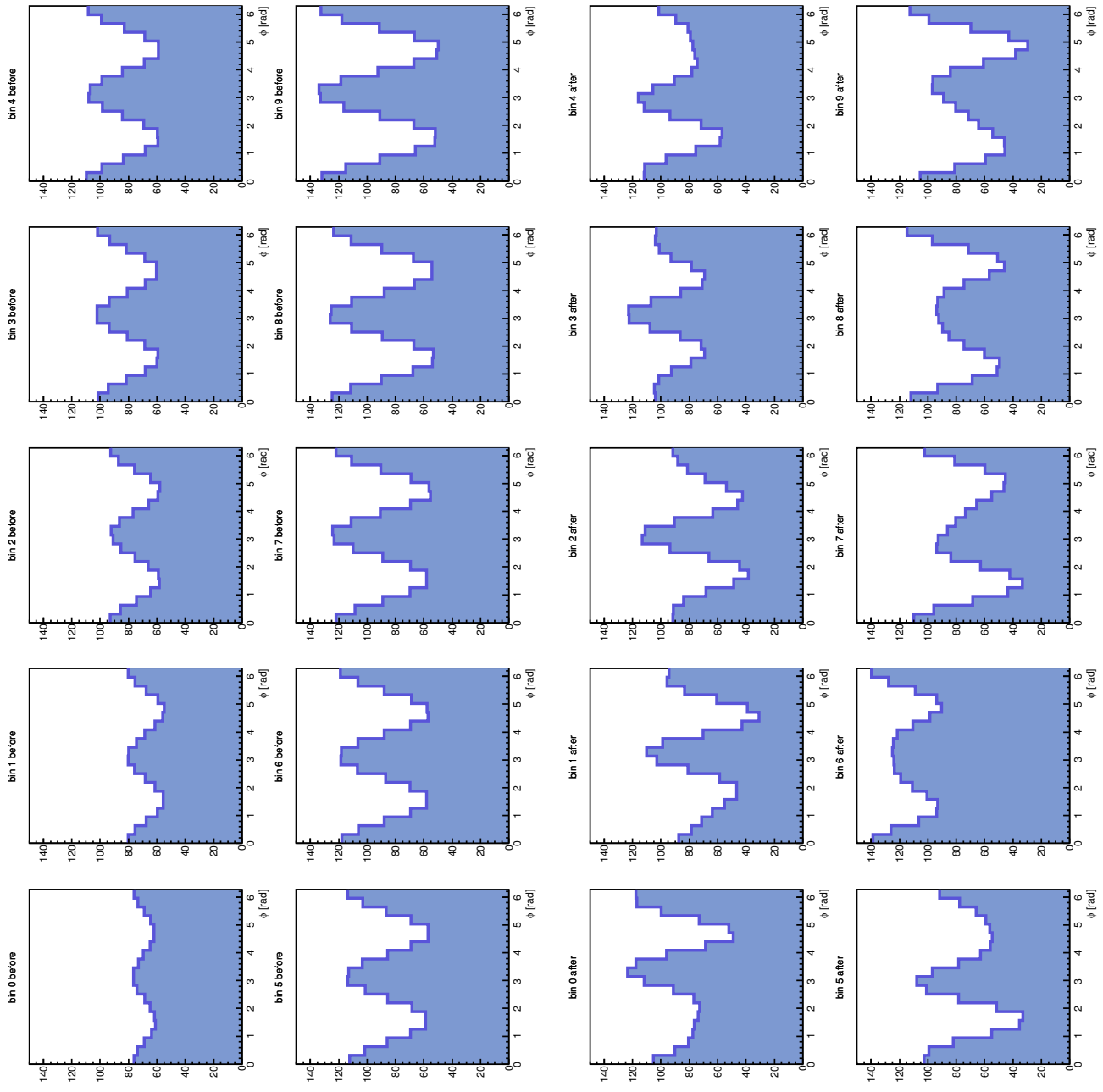

(a) (b)

Figure 81: Average histograms results for initial arrangement according to q_2 and rotation according to Ψ_2. The y-axis are missing label for the sake of viewers comfort, the y-axis depicts number of particles in the bin. (a) Average angle distribution *before* the algorithm had been used. (b) Average angle distribution *after* the algorithm had been used.

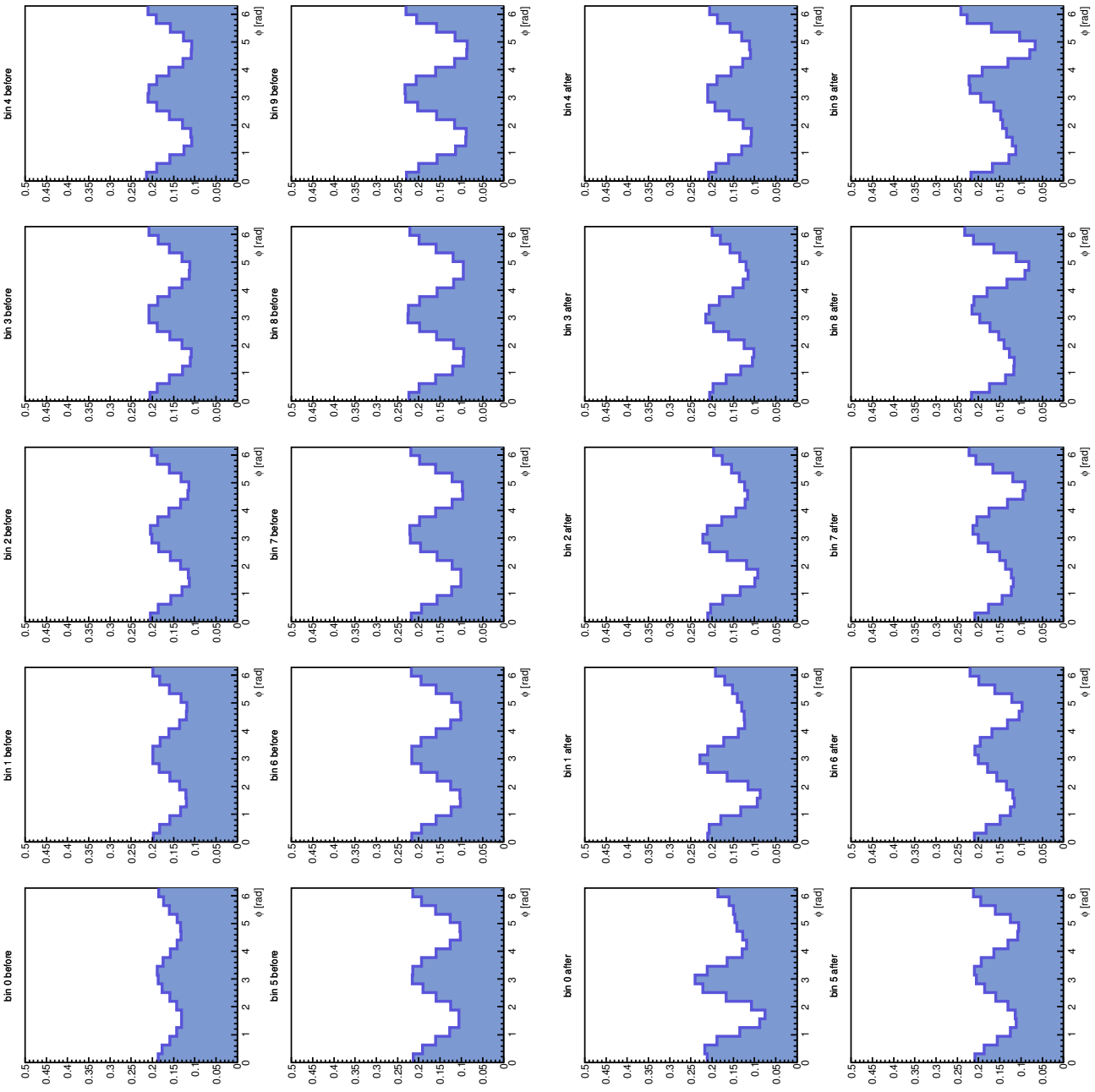

(a) (b)

Figure 82: Average normalized histograms results for initial arrangement according to q_2 and rotation according to Ψ_2. The y-axis are missing label for the sake of viewers comfort, the y-axis depicts number of particles in the bin. (a) Average angle distribution *before* the algorithm had been used. (b) Average angle distribution *after* the algorithm had been used.

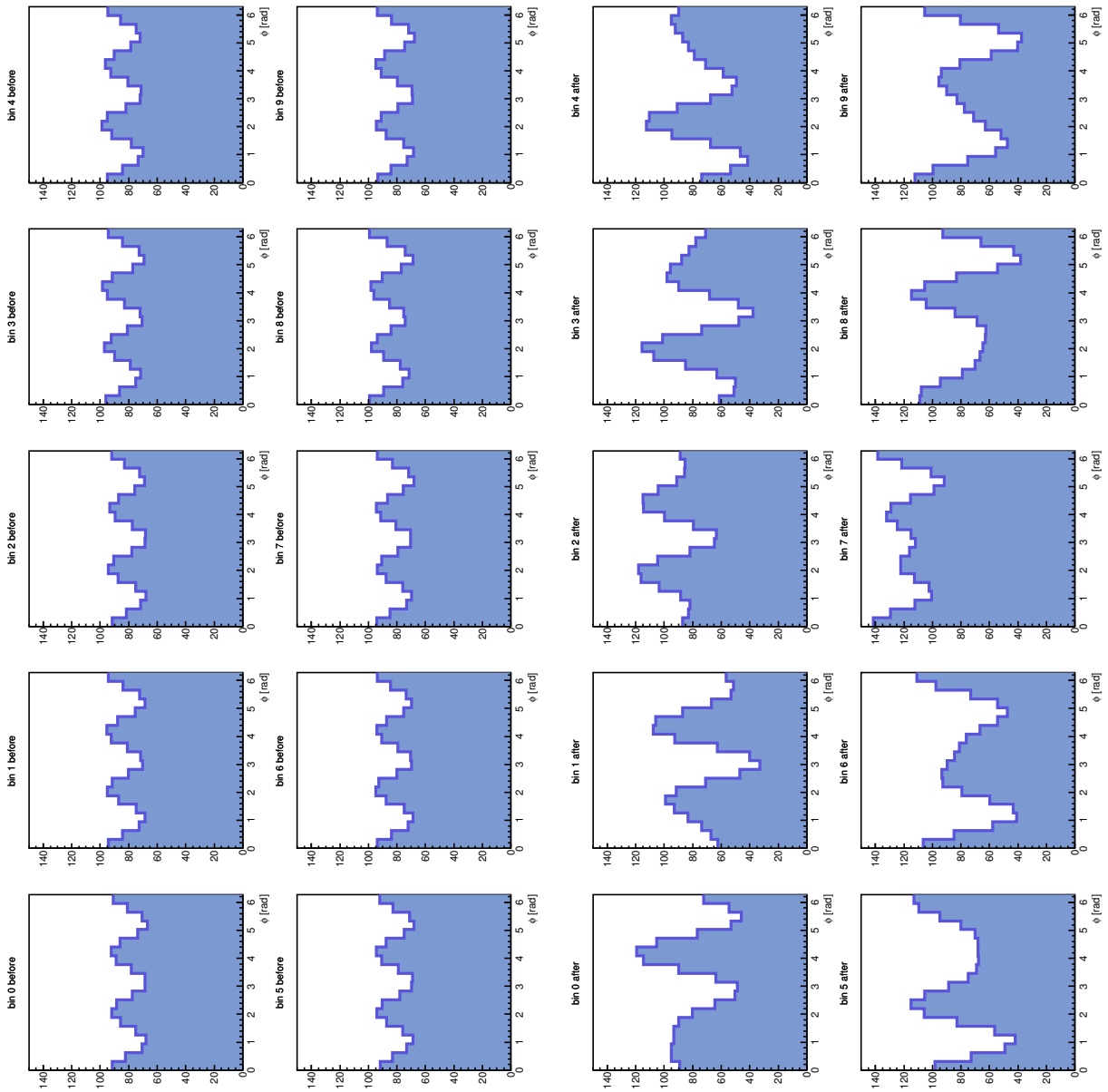

(a) (b)

Figure 83: Average histograms results for initially random arrangement and rotation according to Ψ_3. The y-axis are missing label for the sake of viewers comfort, the y-axis depicts number of particles in the bin. (a) Average angle distribution *before* the algorithm had been used. (b) Average angle distribution *after* the algorithm had been used.

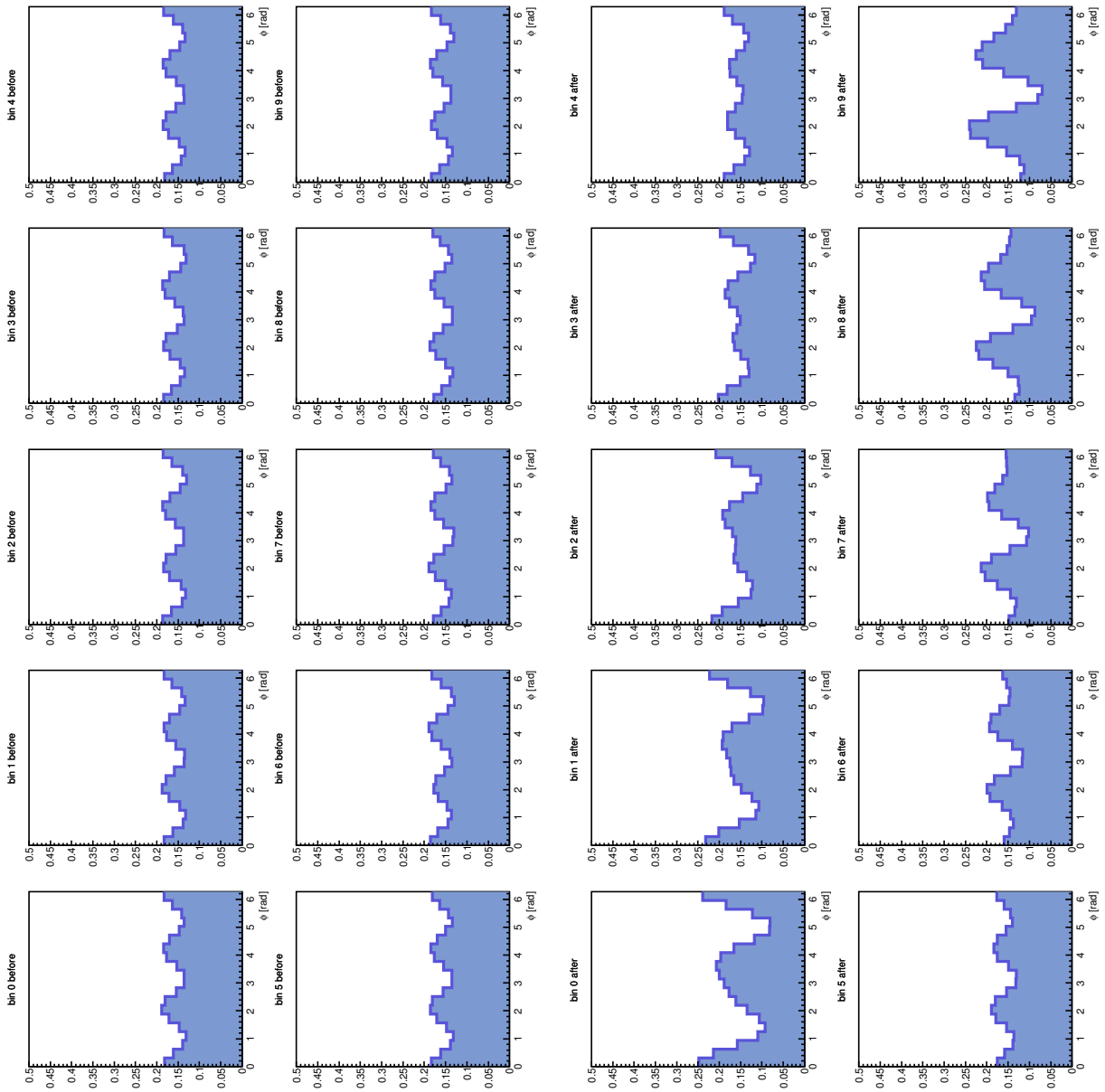

(a) (b)

Figure 84: Average normalized histograms results for initially random arrangement and rotation according to Ψ_3. The y-axis are missing label for the sake of viewers comfort, the y-axis depicts number of particles in the bin. (a) Average angle distribution *before* the algorithm had been used. (b) Average angle distribution *after* the algorithm had been used.

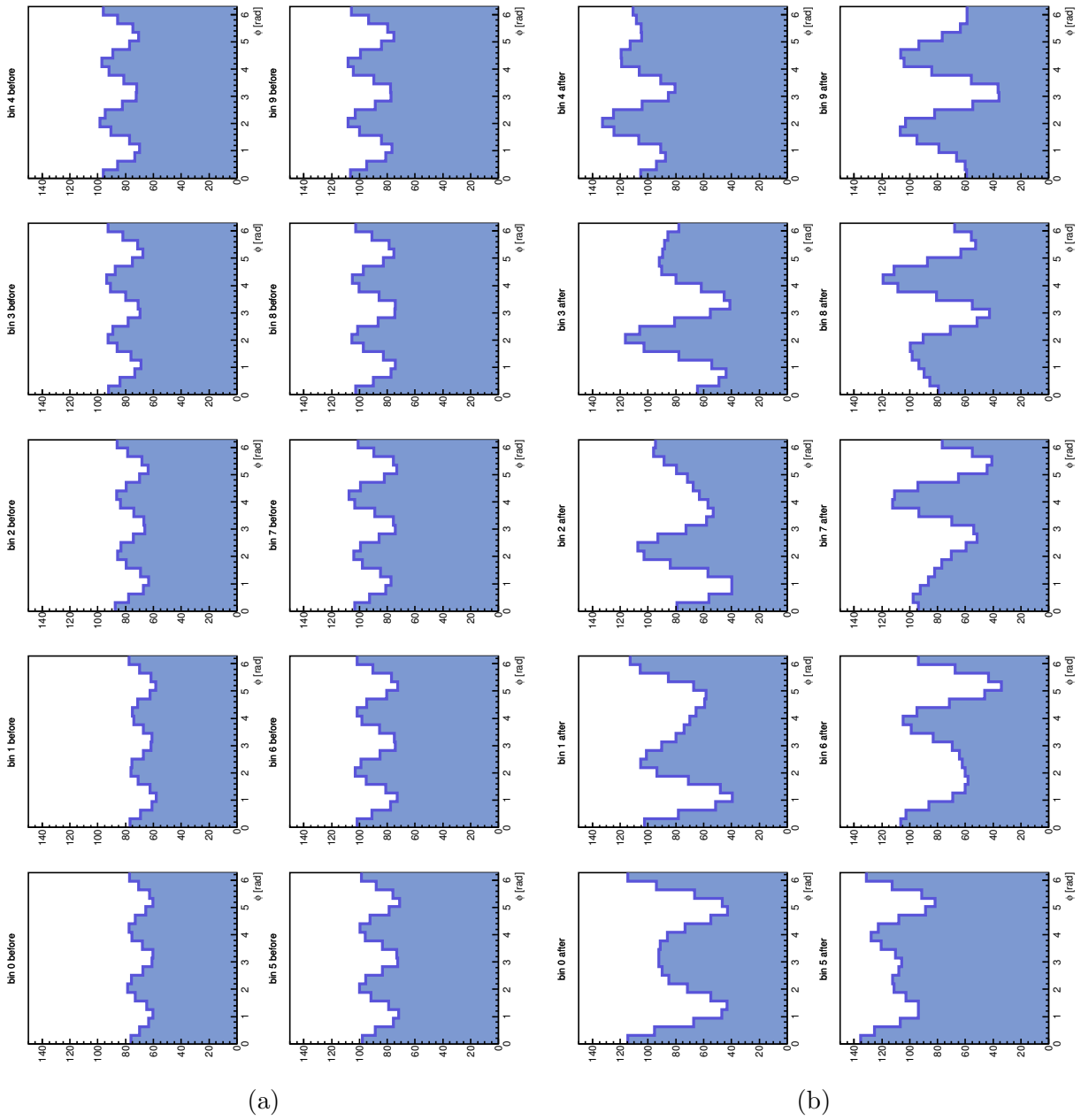

Figure 85: Average histograms results for initial arrangement accoridng to q_2 and rotation according to Ψ_3. The y-axis are missing label for the sake of viewers comfort, the y-axis depicts number of particles in the bin. (a) Average angle distribution *before* the algorithm had been used. (b) Average angle distribution *after* the algorithm had been used.

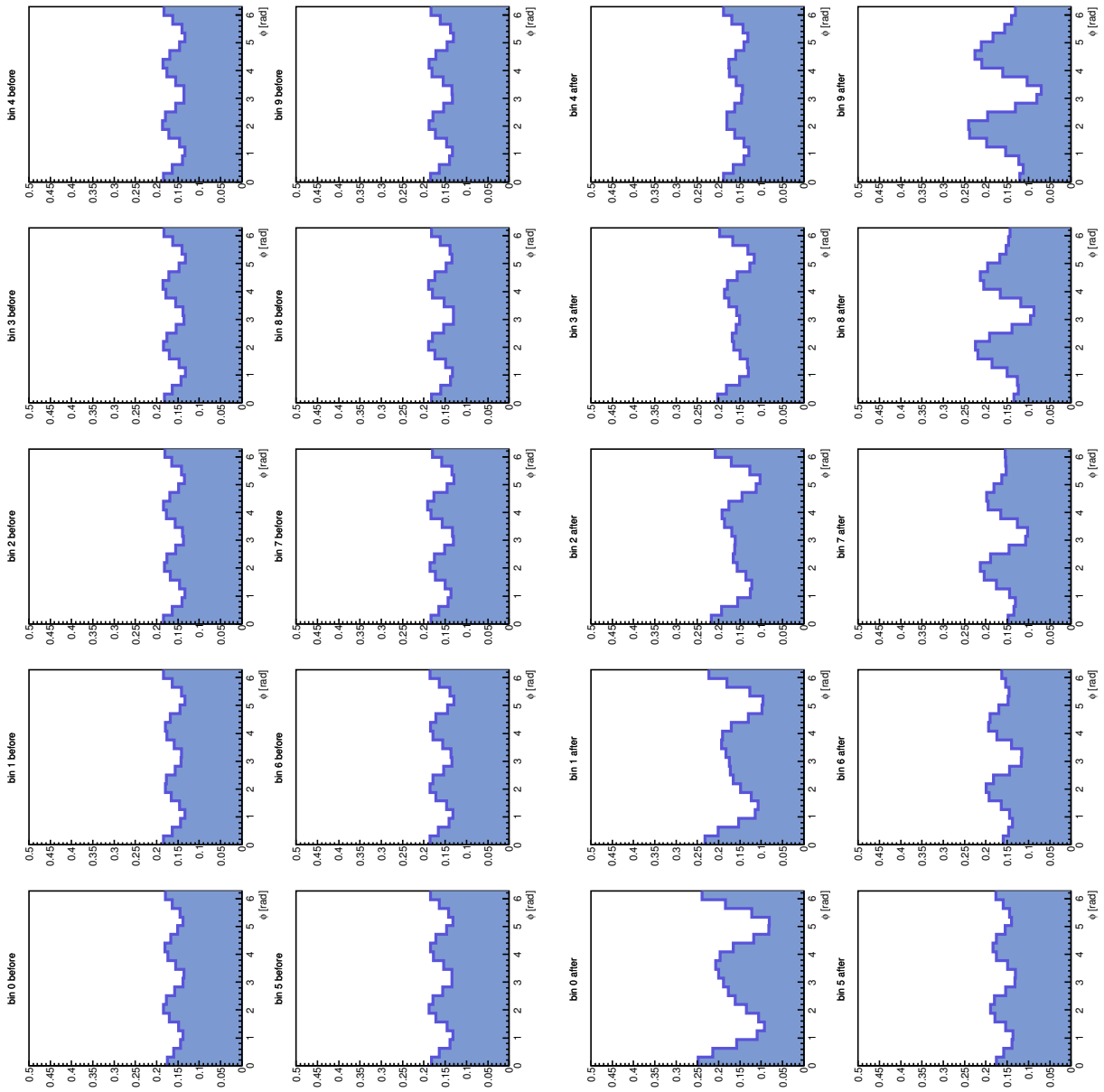

(a) (b)

Figure 86: Average normalized histograms results for initial arrangement accoridng to q_2 and rotation according to Ψ_3. The y-axis are missing label for the sake of viewers comfort, the y-axis depicts number of particles in the bin. (a) Average angle distribution *before* the algorithm had been used. (b) Average angle distribution *after* the algorithm had been used.

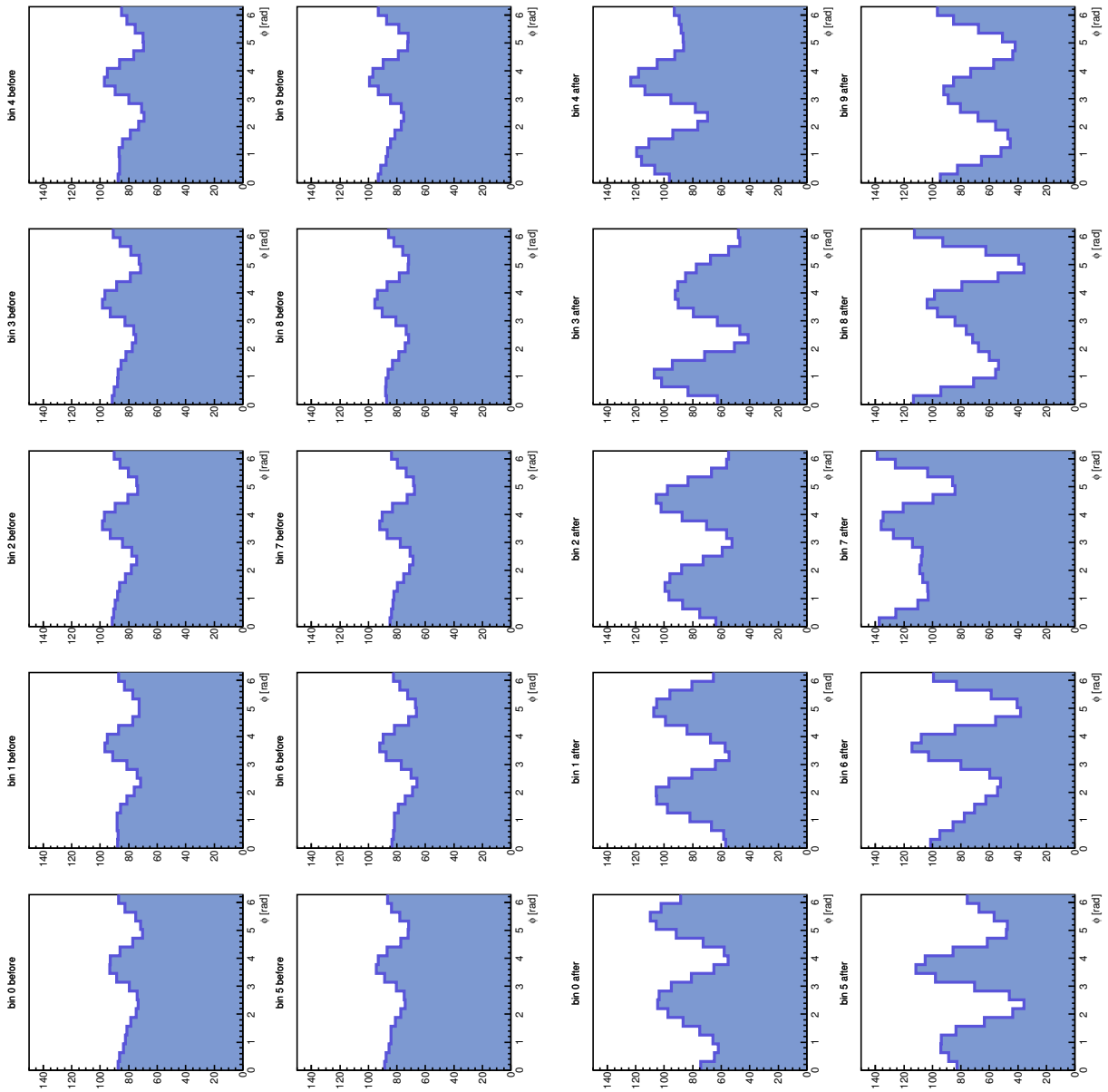

(a) (b)

Figure 87: Average histograms results for initially random arrangement and rotation according to $(\Psi_2 + \Psi_3)/2$. The y-axis are missing label for the sake of viewers comfort, the y-axis depicts number of particles in the bin. (a) Average angle distribution *before* the algorithm had been used. (b) Average angle distribution *after* the algorithm had been used.

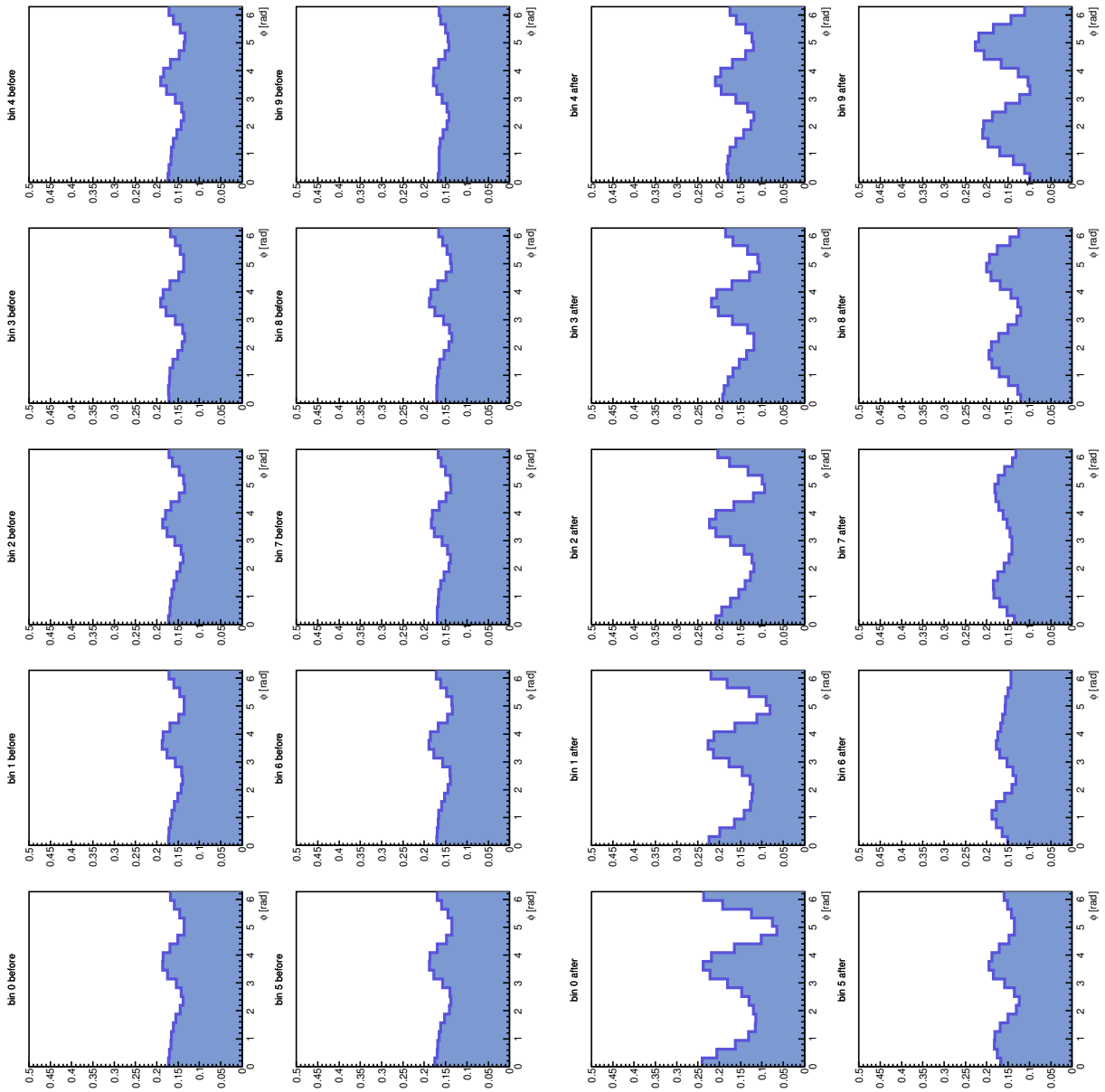

(a) (b)

Figure 88: Average normalized histograms results for initially random arrangement and rotation according to $(\Psi_2 + \Psi_3)/2$. The y-axis are missing label for the sake of viewers comfort, the y-axis depicts number of particles in the bin. (a) Average angle distribution *before* the algorithm had been used. (b) Average angle distribution *after* the algorithm had been used.

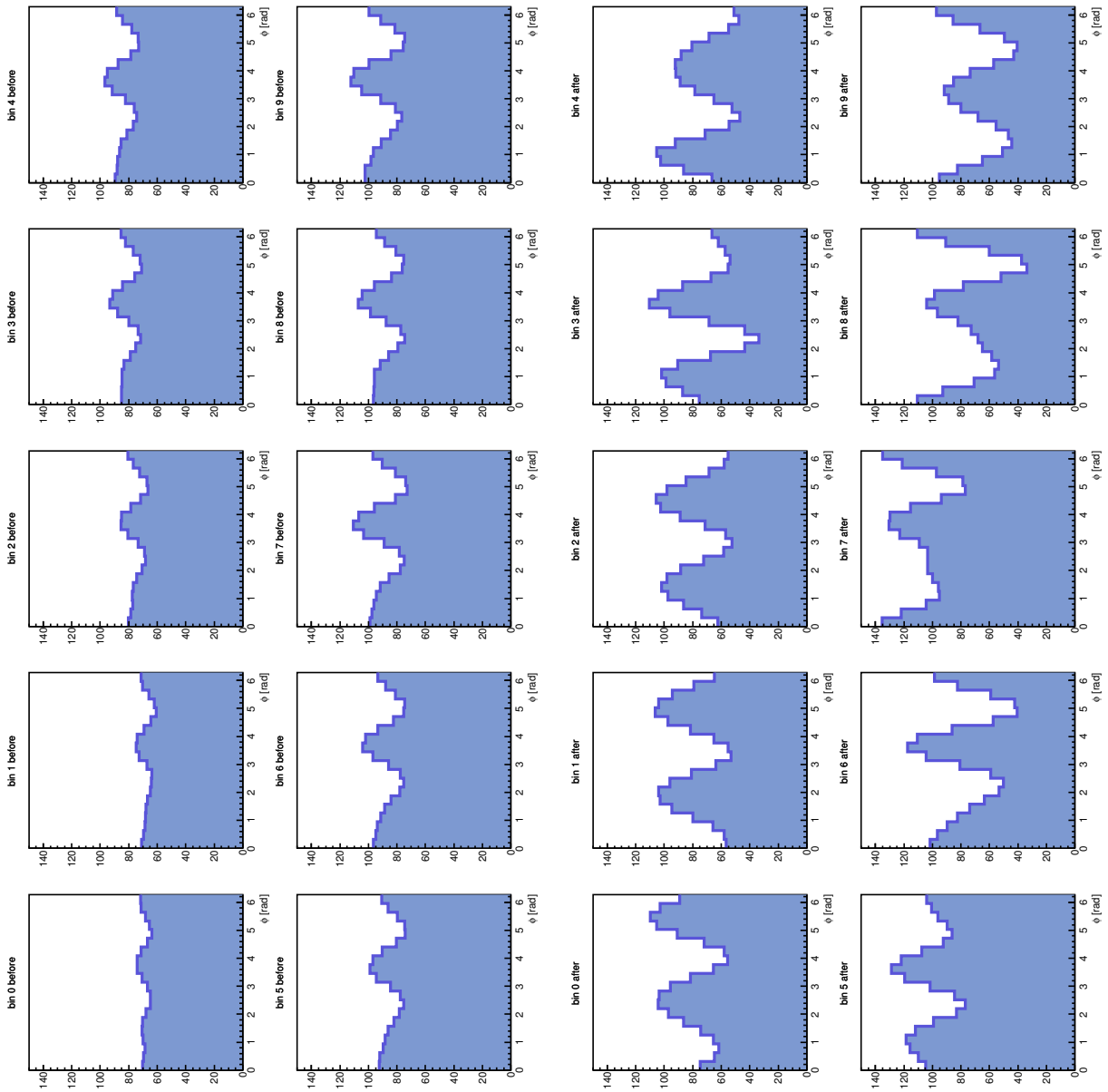

(a) (b)

Figure 89: Average histograms results for initial arrangement according to q_2 and rotation according to $(\Psi_2 + \Psi_3)/2$. The y-axis are missing label for the sake of viewers comfort, the y-axis depicts number of particles in the bin. (a) Average angle distribution *before* the algorithm had been used. (b) Average angle distribution *after* the algorithm had been used.

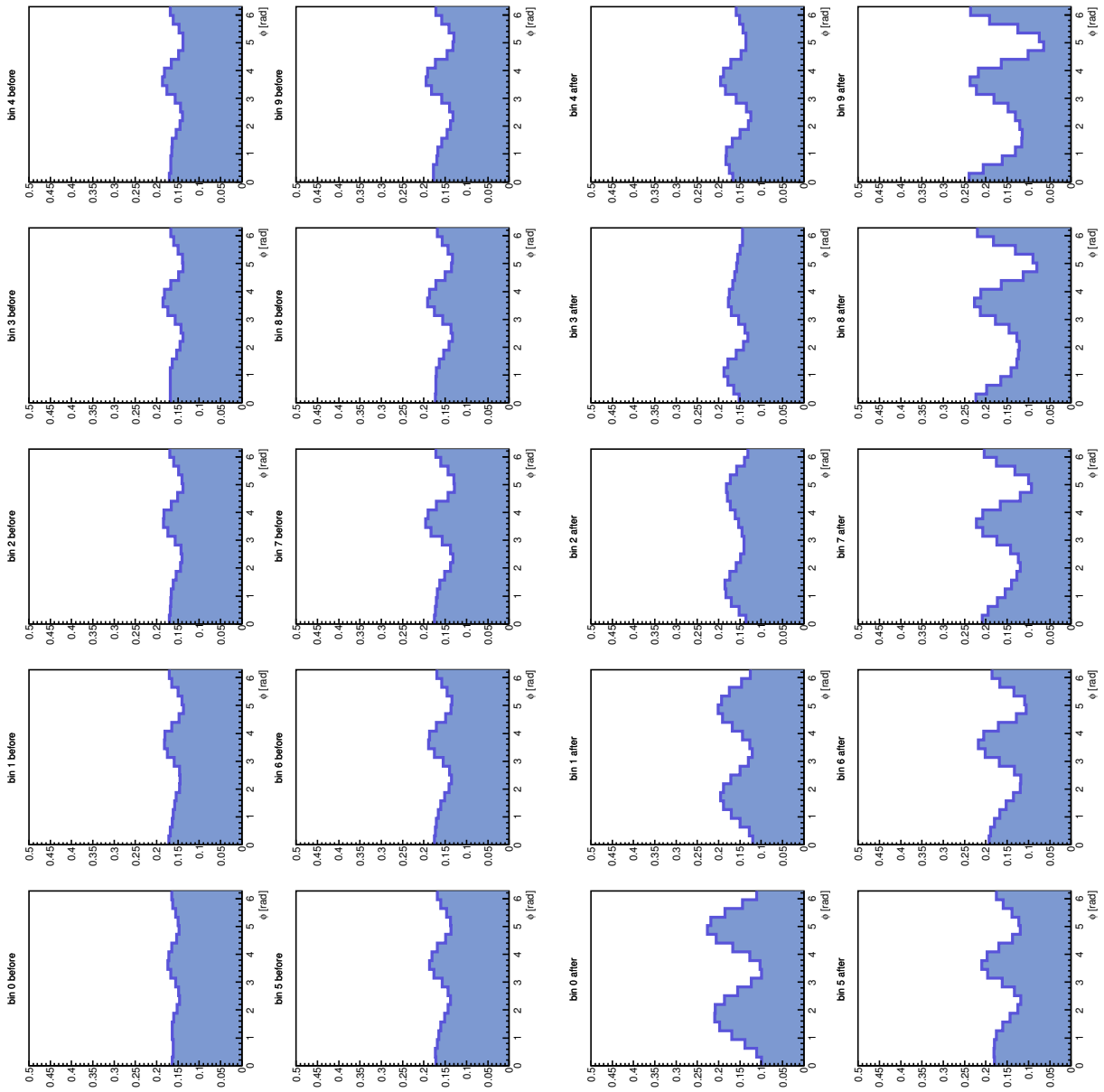

(a) (b)

Figure 90: Average normalized histograms results for initial arrangement according to q_2 and rotation according to $(\Psi_2+\Psi_3)/2$. The y-axis are missing label for the sake of viewers comfort, the y-axis depicts number of particles in the bin. (a) Average angle distribution *before* the algorithm had been used. (b) Average angle distribution *after* the algorithm had been used.

D Pentagonal flow

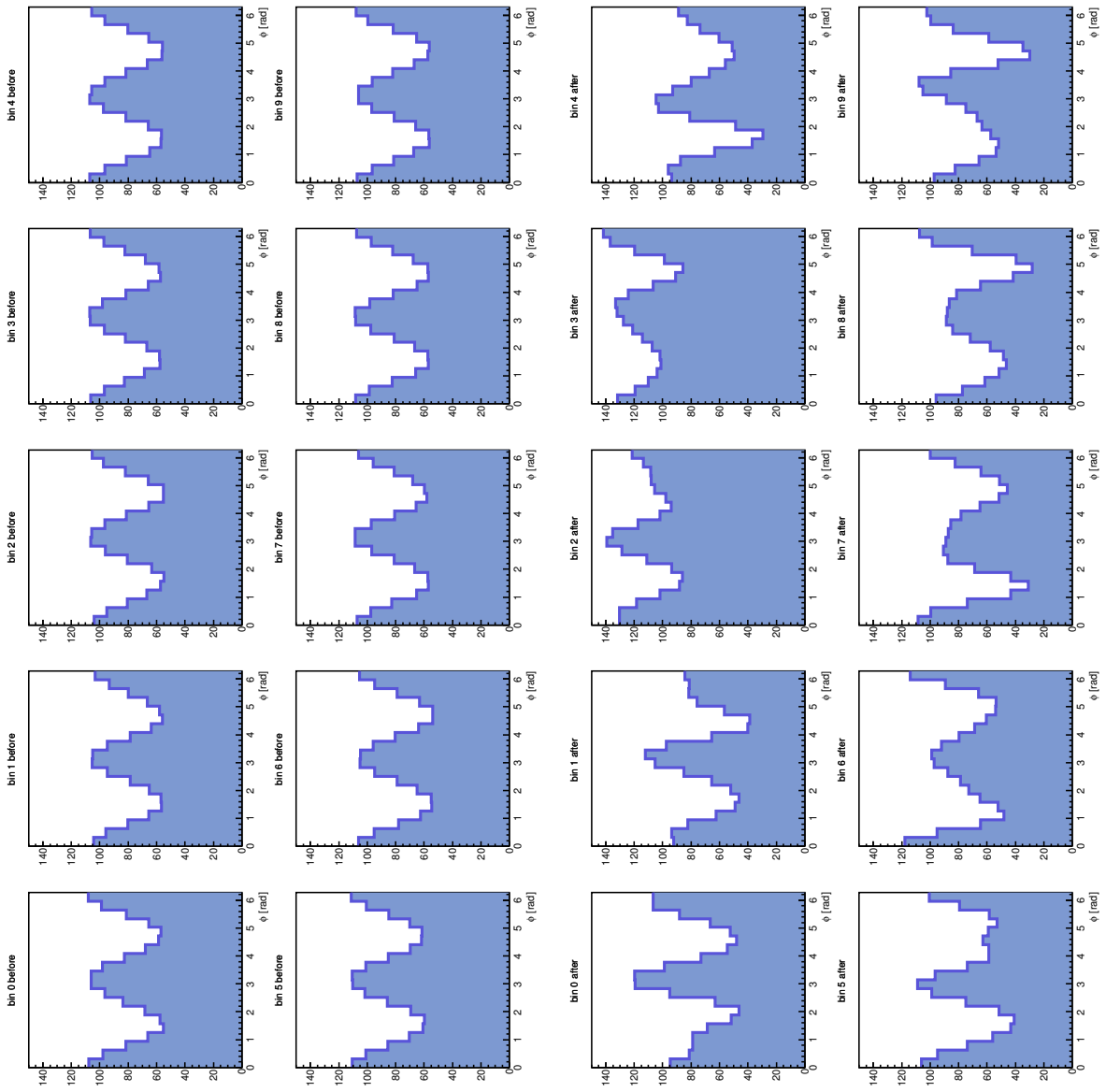

(a) (b)

Figure 91: Average histograms results for initially random arrangement and rotation according to Ψ_2. The y-axis are missing label for the sake of viewers comfort, the y-axis depicts number of particles in the bin. (a) Average angle distribution *before* the algorithm had been used. (b) Average angle distribution *after* the algorithm had been used.

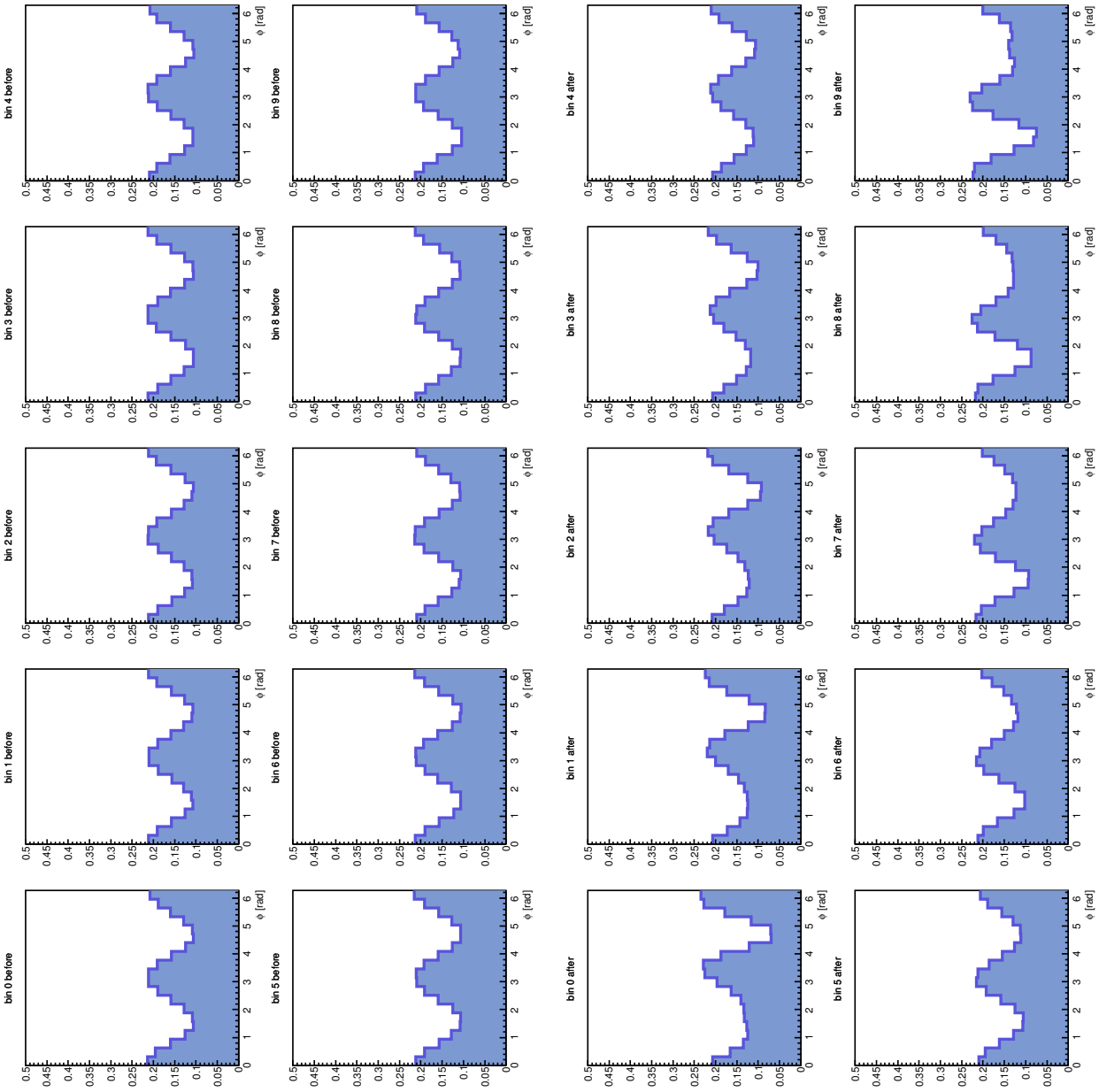

(a) (b)

Figure 92: Average normalized histograms for initially random arrangement and rotation according to Ψ_2. The y-axis are missing label for the sake of viewers comfort, the y-axis depicts number of particles in the bin.(a) Average angle distribution *before* the algorithm had been used. (b) Average angle distribution *after* the algorithm had been used.

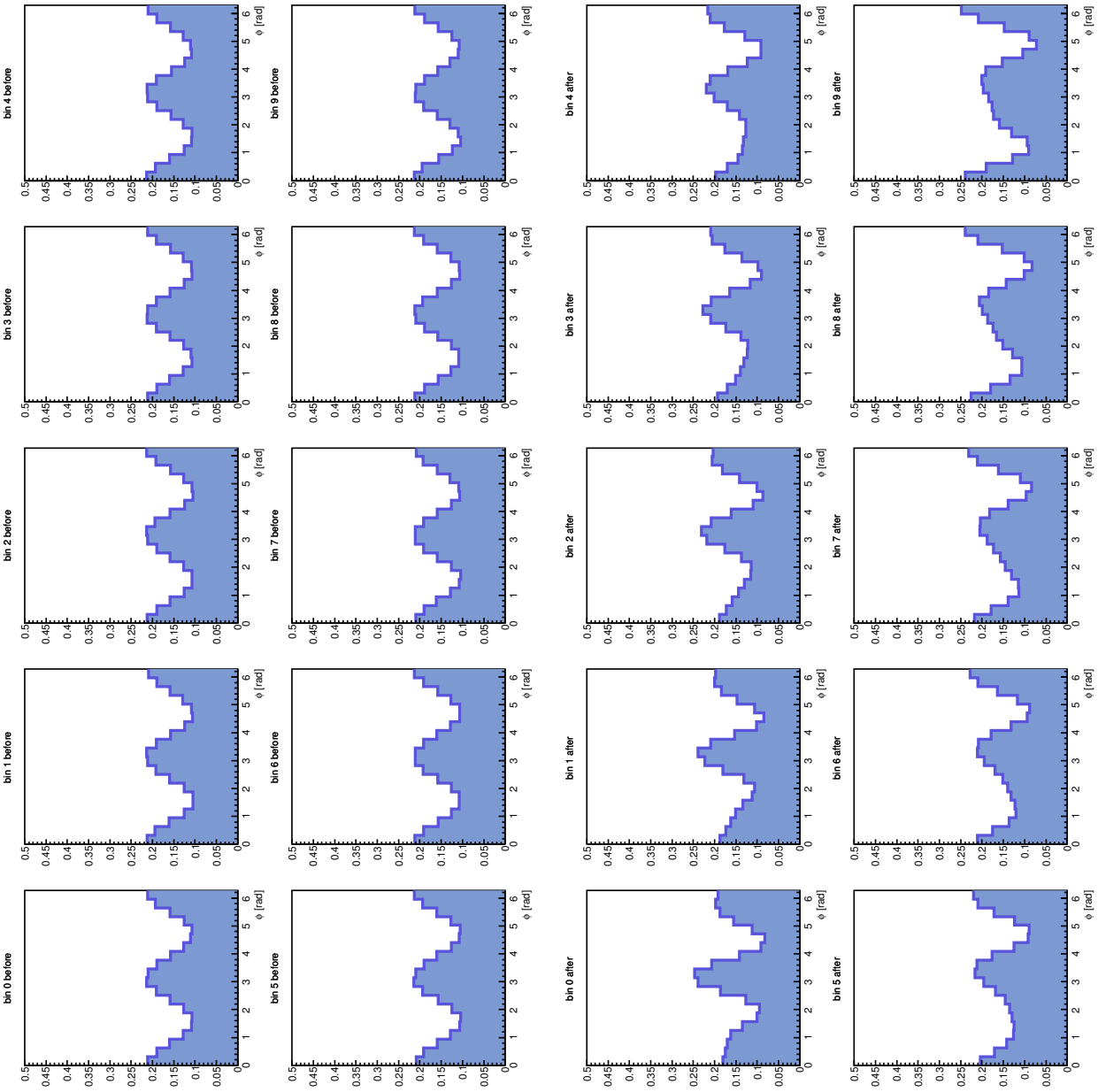

(a) (b)

Figure 93: Average normalized histograms results for flipped events and initially random arrangement and rotation according to Ψ_2. The y-axis are missing label for the sake of viewers comfort, the y-axis depicts number of particles in the bin. (a) Average angle distribution *before* the algorithm had been used. (b) Average angle distribution *after* the algorithm had been used.

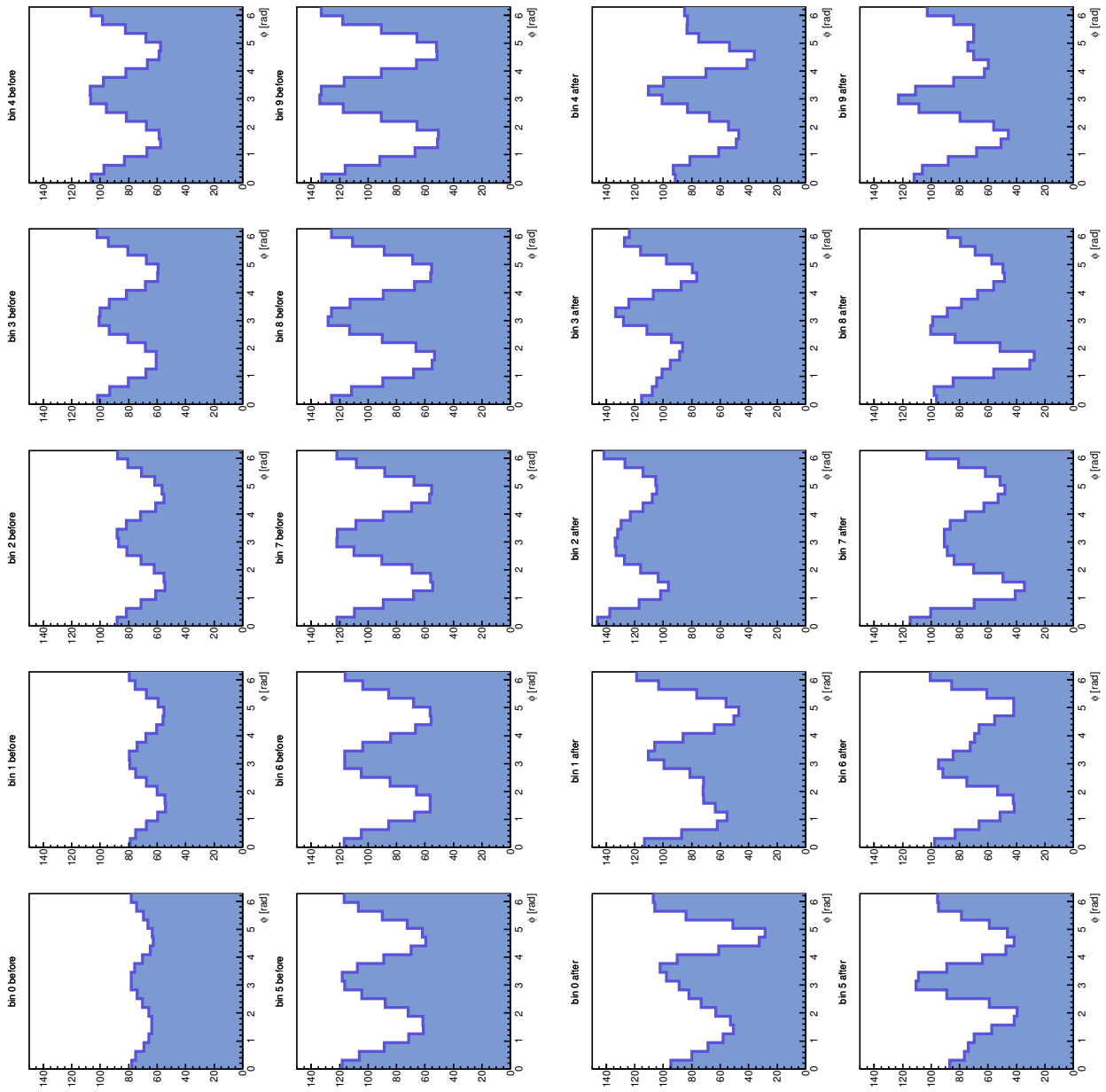

(a) (b)

Figure 94: Average histograms results for initially random arrangement and rotation according to Ψ_2. The y-axis are missing label for the sake of viewers comfort, the y-axis depicts number of particles in the bin. (a) Average angle distribution *before* the algorithm had been used. (b) Average angle distribution *after* the algorithm had been used.

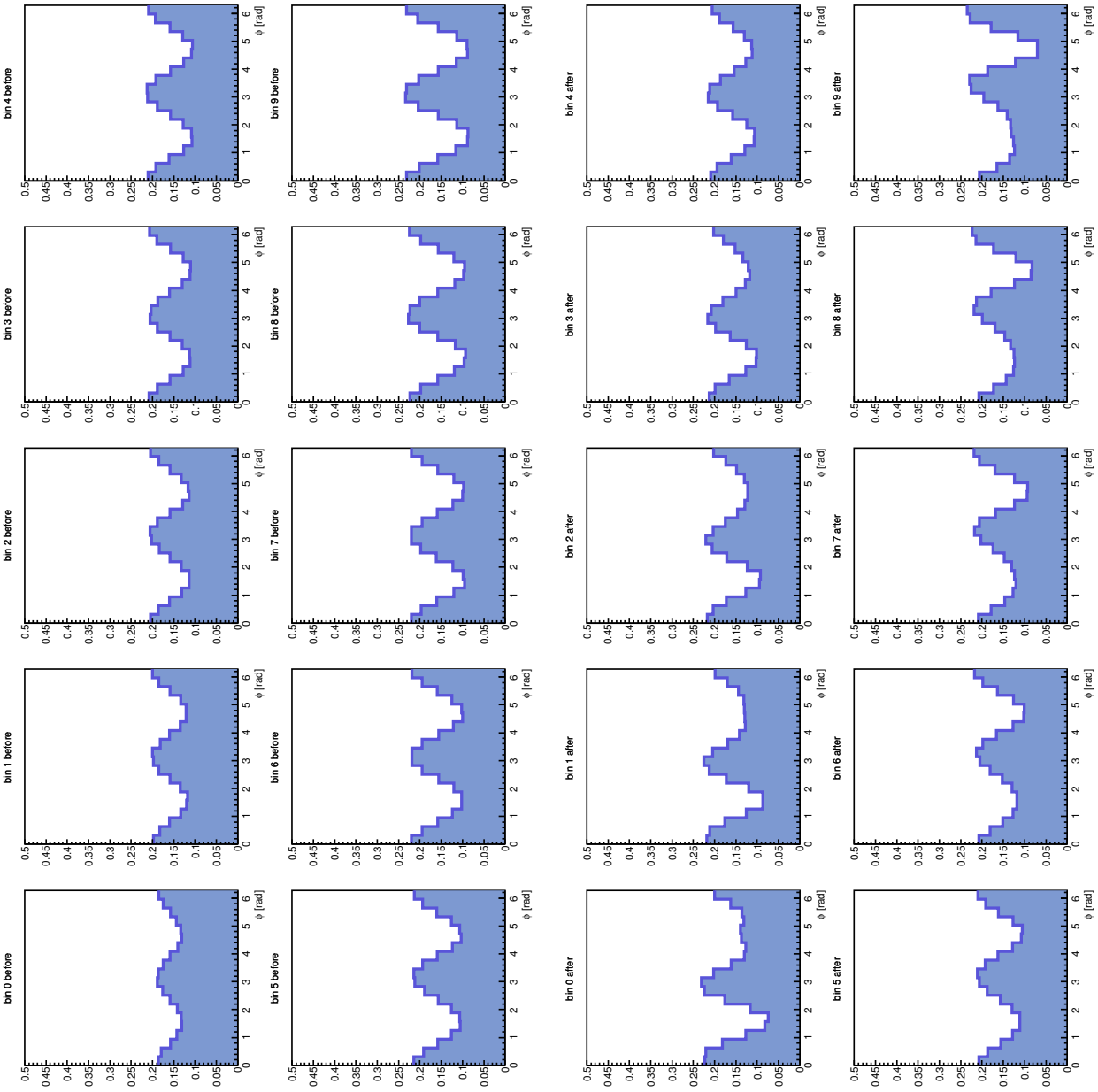

(a) (b)

Figure 95: Average normalized histograms results, initial arrangement according to q_2 and rotation according to Ψ_2. The y-axis are missing label for the sake of viewers comfort, the y-axis depicts number of particles in the bin. (a) Average angle distribution *before* the algorithm had been used. (b) Average angle distribution *after* the algorithm had been used.

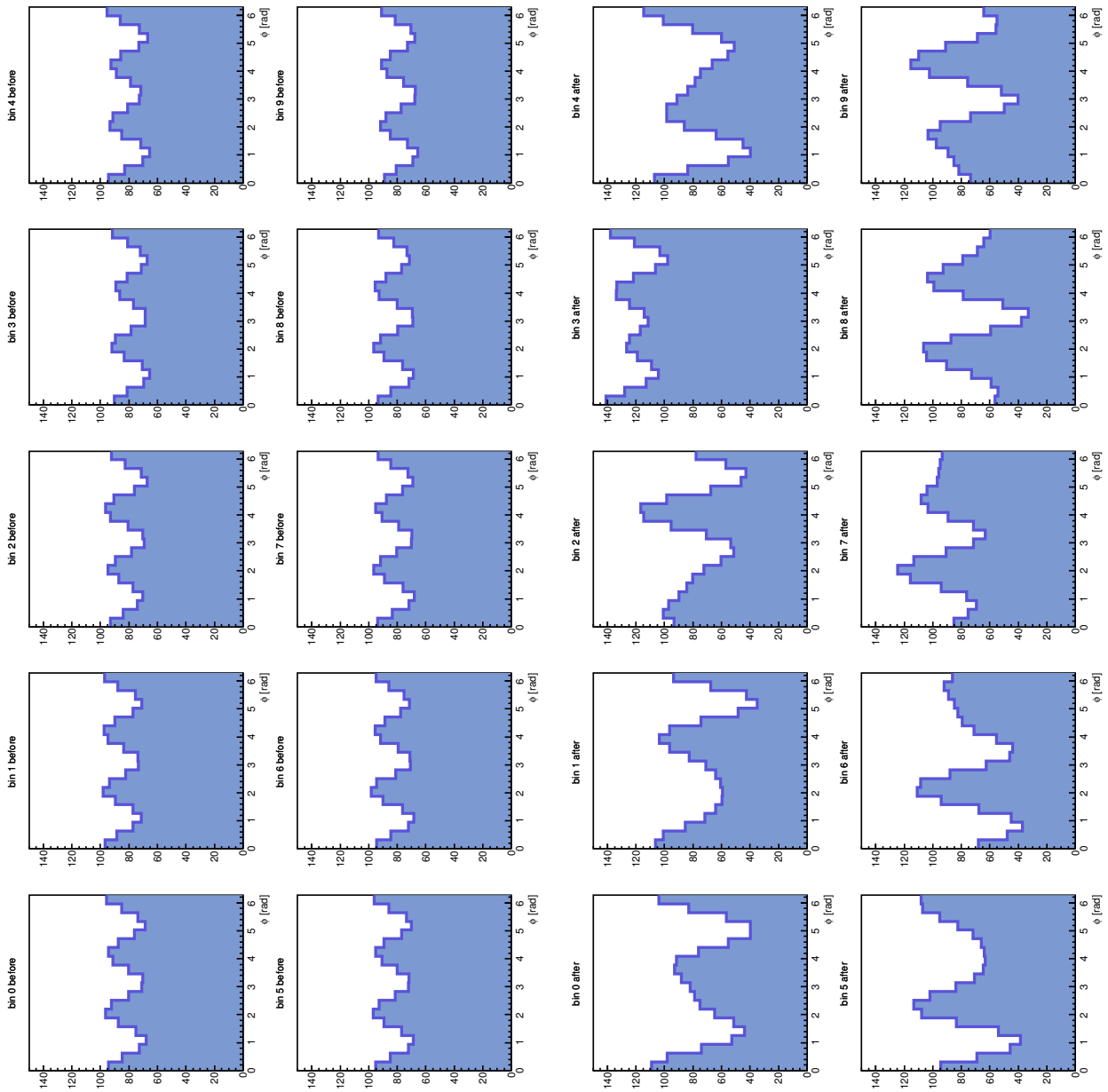

(a) (b)

Figure 96: Average histograms results for initially random arrangement and rotation according to Ψ_3. The y-axis are missing label for the sake of viewers comfort, the y-axis depicts number of particles in the bin. (a) Average angle distribution *before* the algorithm had been used. (b) Average angle distribution *after* the algorithm had been used.

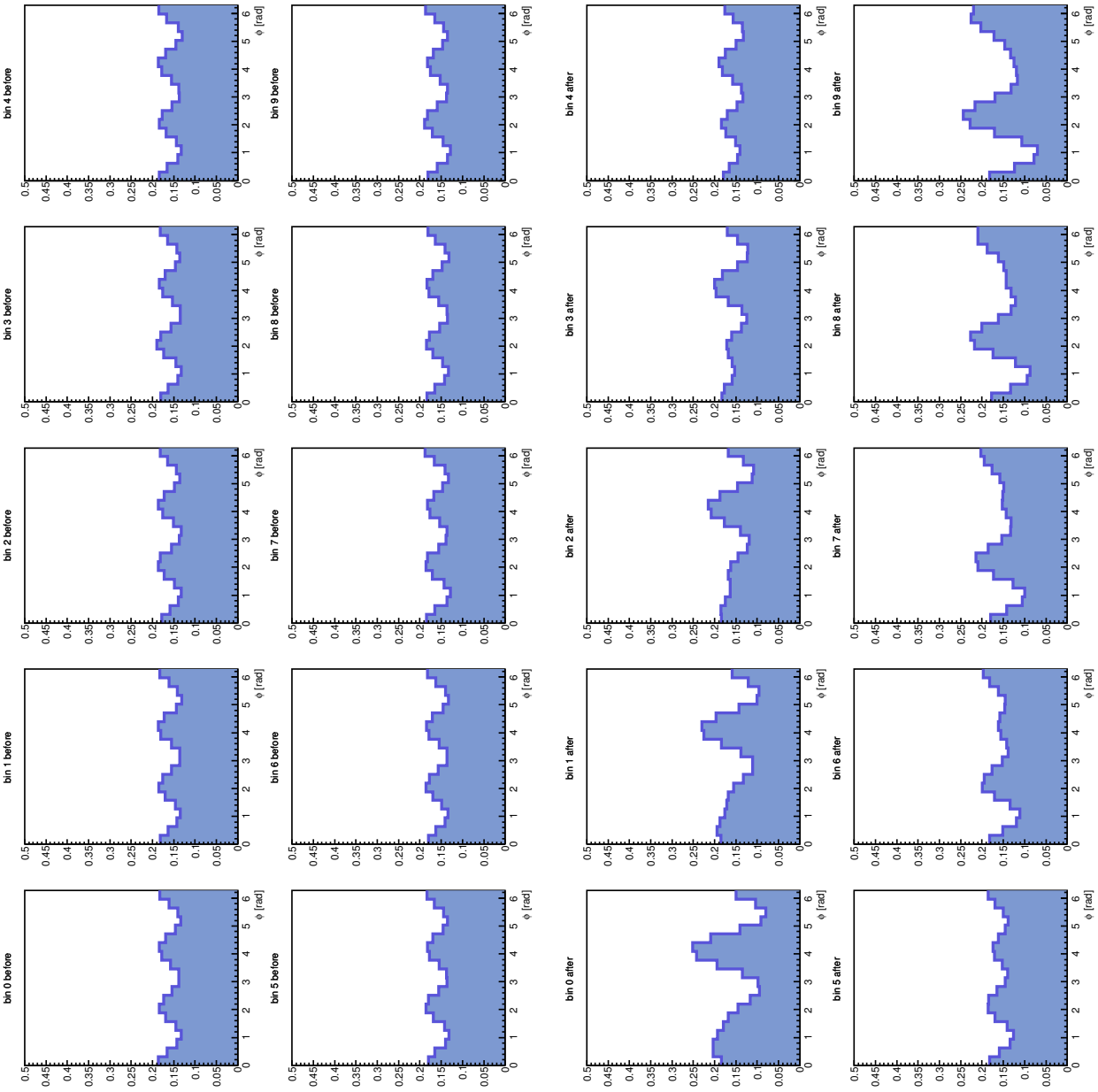

(a) (b)

Figure 97: Average normalized histograms results for initially random arrangement and rotation according to Ψ_3. The y-axis are missing label for the sake of viewers comfort, the y-axis depicts number of particles in the bin. (a) Average angle distribution *before* the algorithm had been used. (b) Average angle distribution *after* the algorithm had been used.

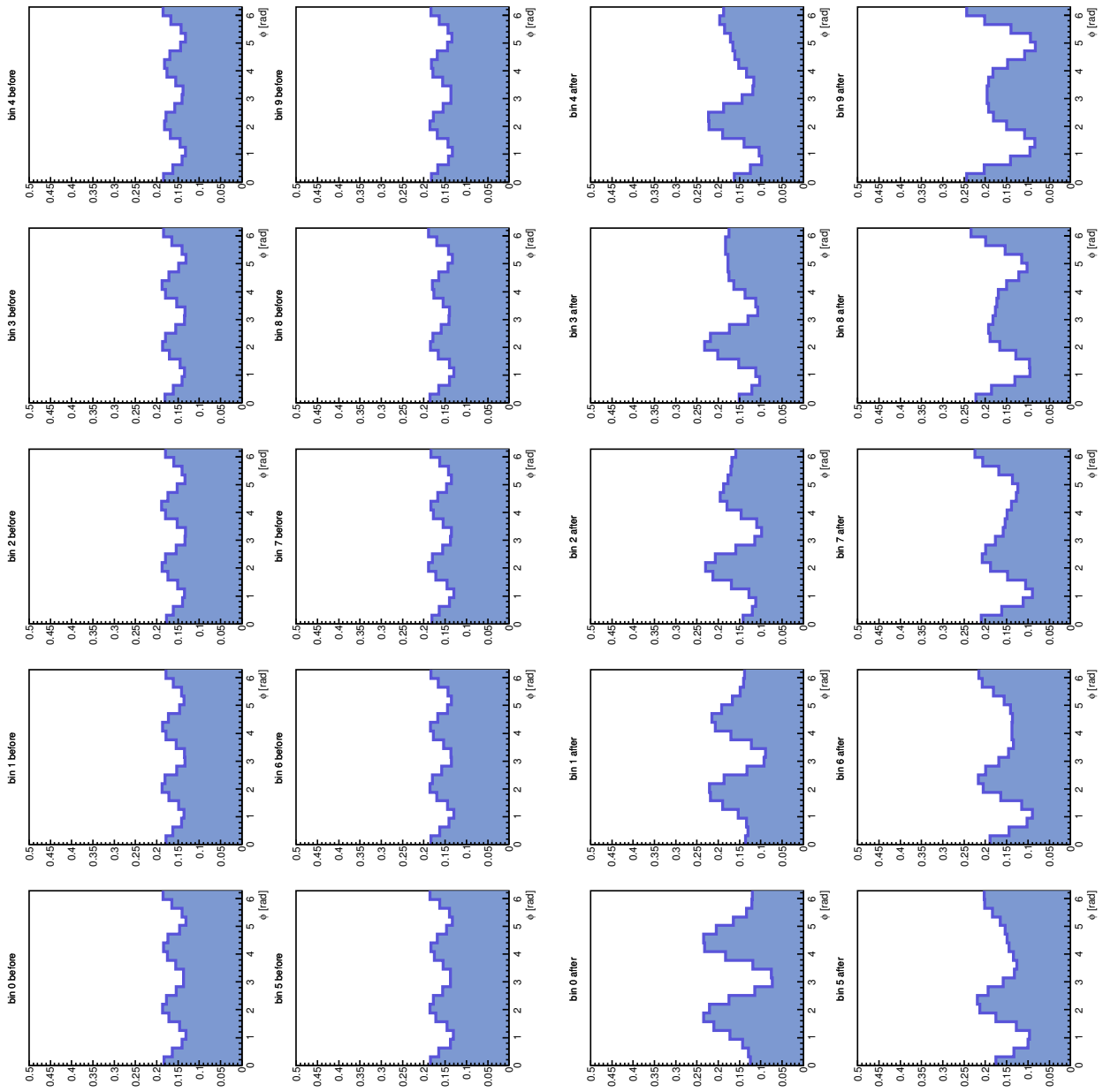

(a) (b)

Figure 98: Average normalized histograms results for flipped events and initially random arrangement and rotation according to Ψ_3. The y-axis are missing label for the sake of viewers comfort, the y-axis depicts number of particles in the bin. (a) Average angle distribution *before* the algorithm had been used. (b) Average angle distribution *after* the algorithm had been used.

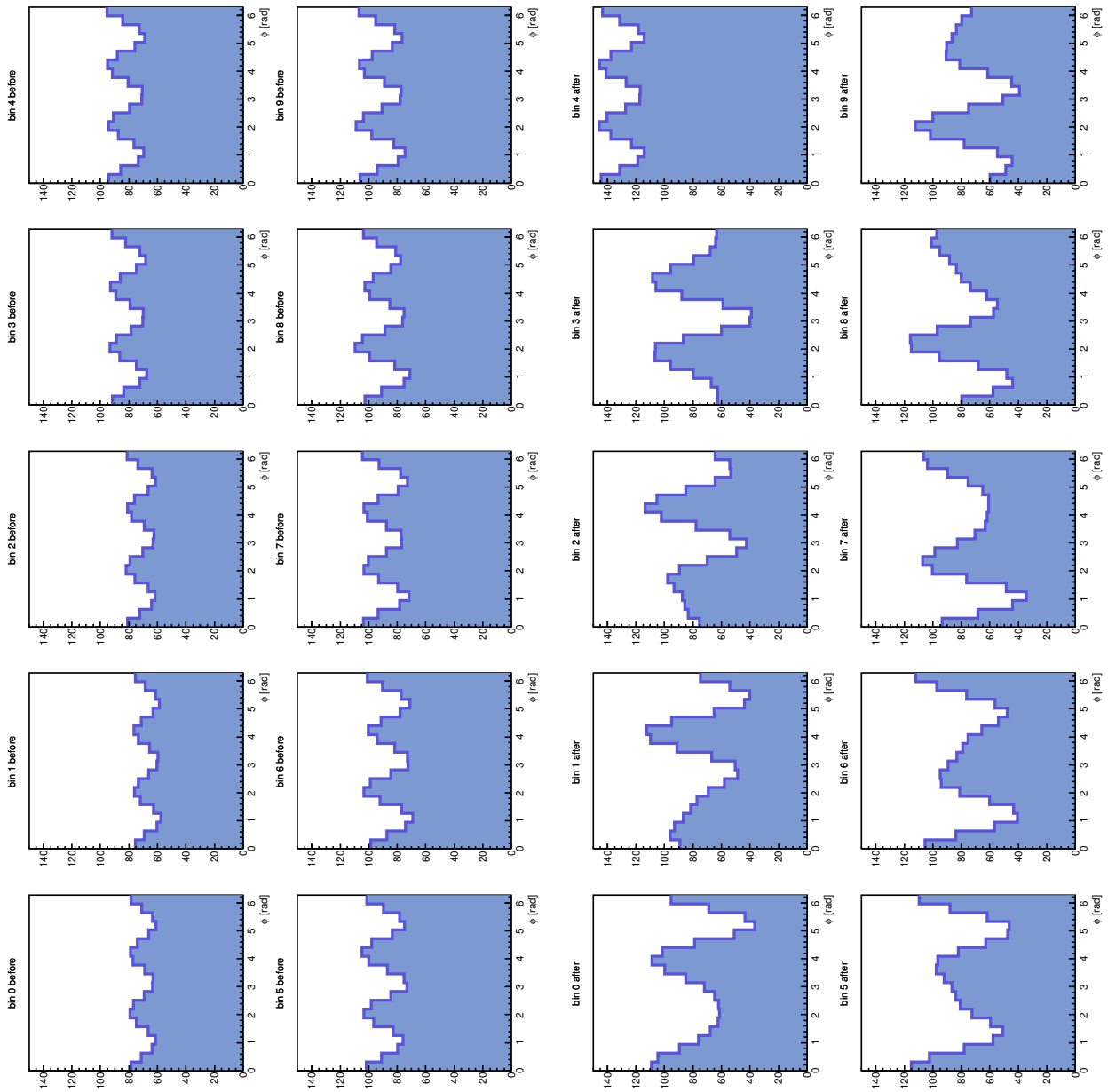

(a) (b)

Figure 99: Average histograms results for initial arrangement according to q_2 and rotation according to Ψ_3. The y-axis are missing label for the sake of viewers comfort, the y-axis depicts number of particles in the bin. (a) Average angle distribution *before* the algorithm had been used. (b) Average angle distribution *after* the algorithm had been used.

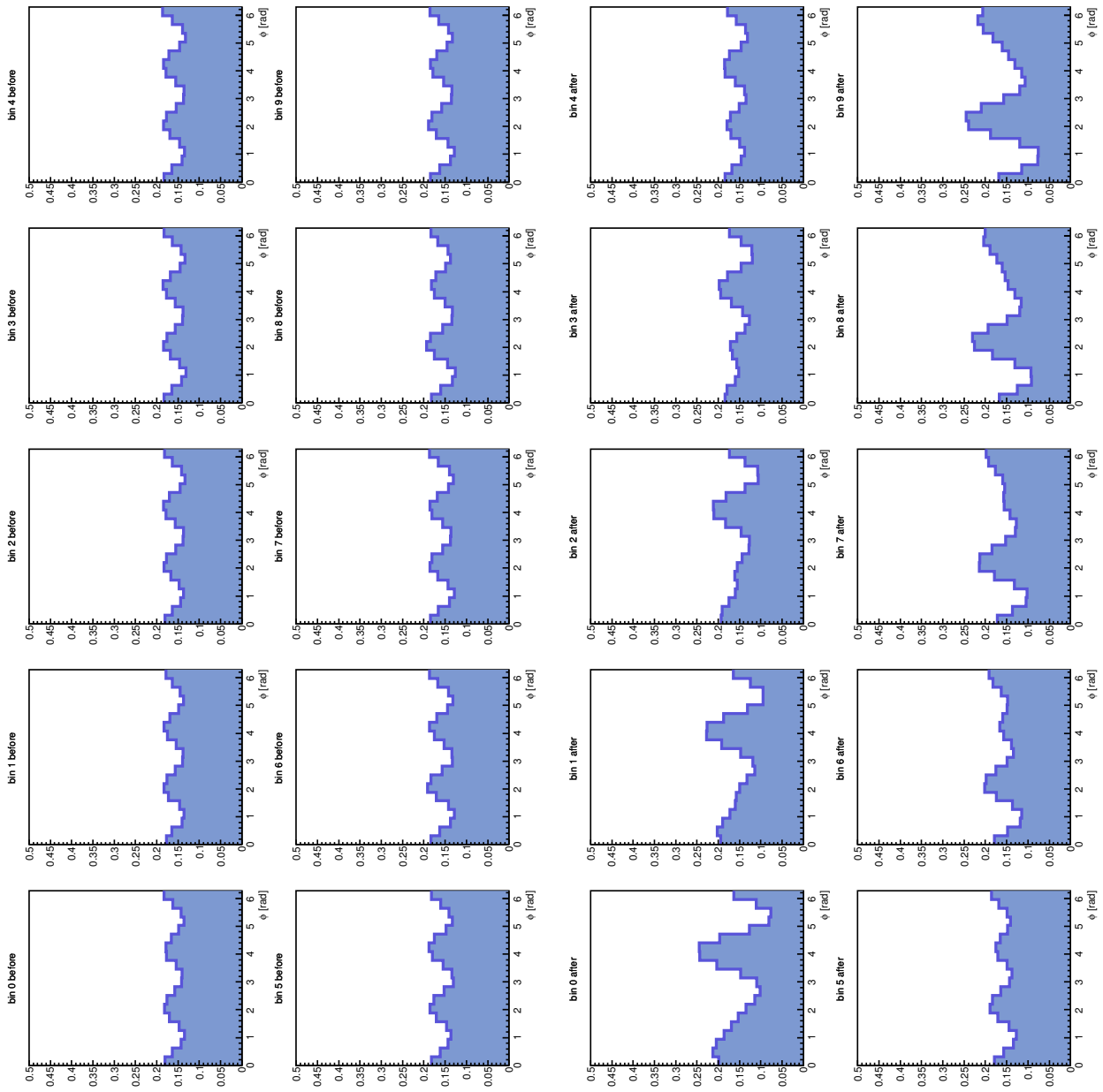

(a) (b)

Figure 100: Average normalized histograms results, initial arrangement according to q_2 and rotation according to Ψ_3. The y-axis are missing label for the sake of viewers comfort, the y-axis depicts number of particles in the bin. (a) Average angle distribution *before* the algorithm had been used. (b) Average angle distribution *after* the algorithm had been used.

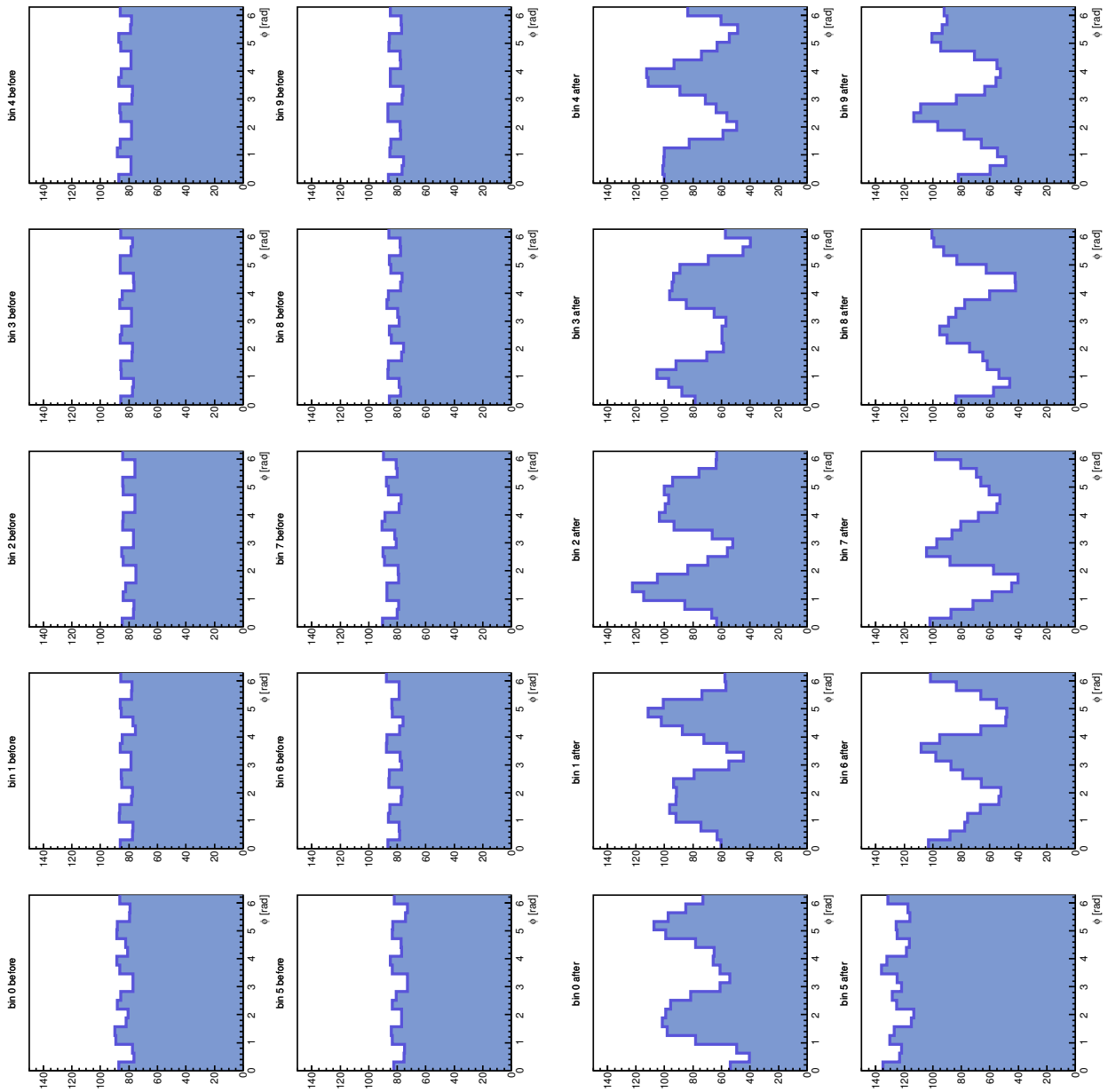

(a) (b)

Figure 101: Average histograms results for initially random arrangement and rotation according to Ψ_5. The y-axis are missing label for the sake of viewers comfort, the y-axis depicts number of particles in the bin. (a) Average angle distribution *before* the algorithm had been used. (b) Average angle distribution *after* the algorithm had been used.

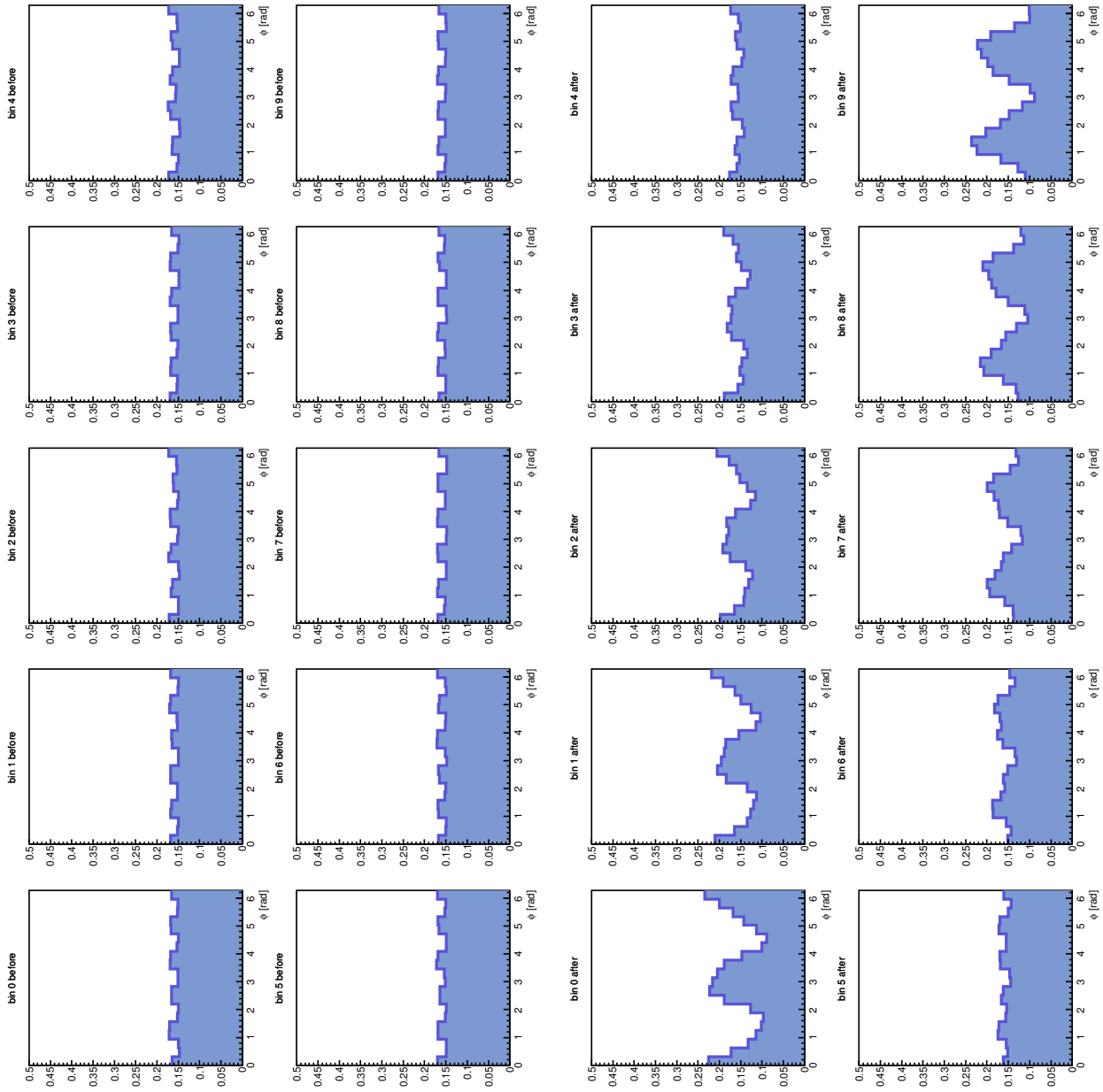

(a) (b)

Figure 102: Average normalized histograms results for initially random arrangement and rotation according to Ψ_5. The y-axis are missing label for the sake of viewers comfort, the y-axis depicts number of particles in the bin. (a) Average angle distribution *before* the algorithm had been used. (b) Average angle distribution *after* the algorithm had been used.

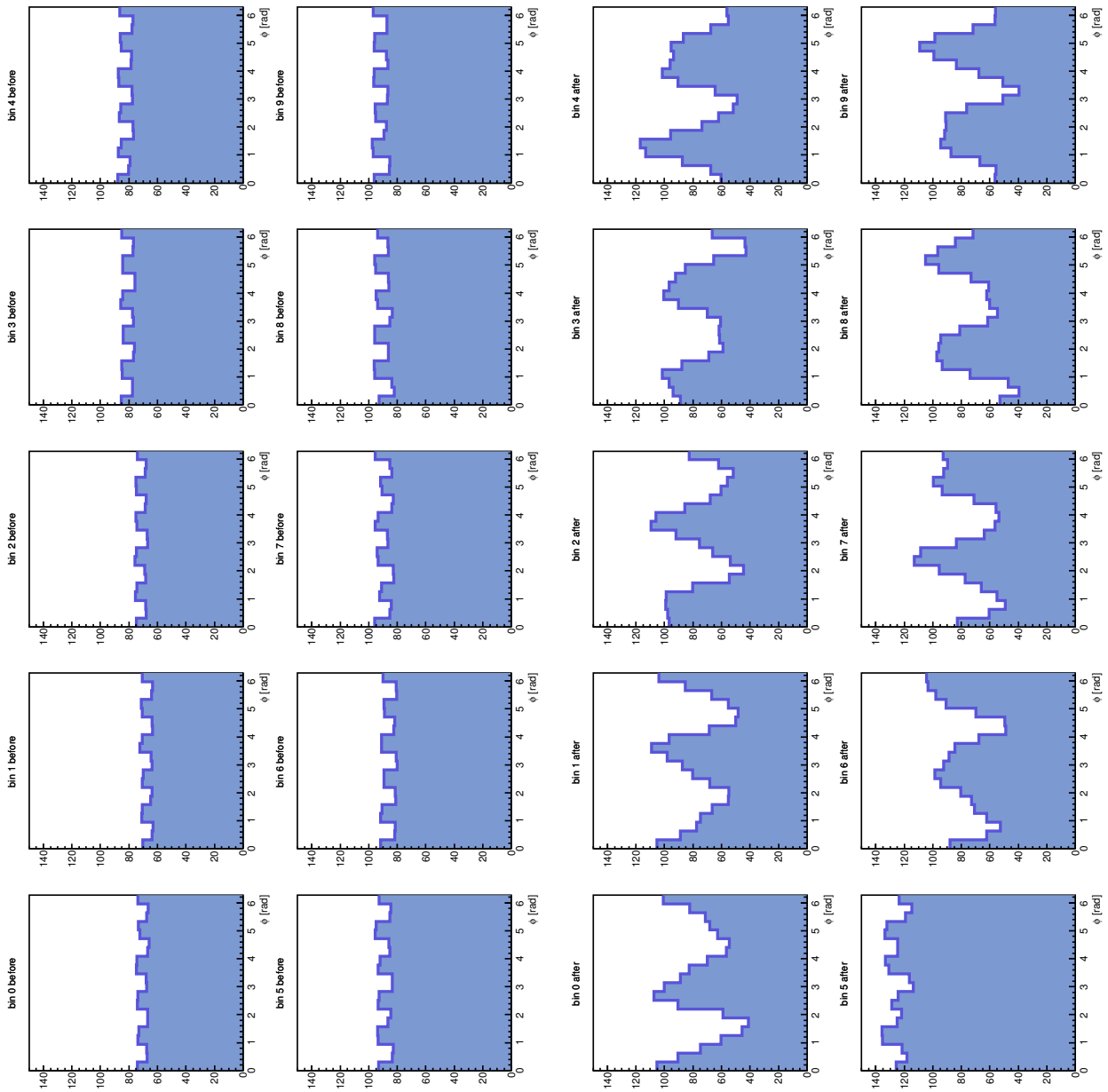

(a) (b)

Figure 103: Average histograms results for initial arrangement according to q_2 and rotation according to Ψ_5. The y-axis are missing label for the sake of viewers comfort, the y-axis depicts number of particles in the bin. (a) Average angle distribution *before* the algorithm had been used. (b) Average angle distribution *after* the algorithm had been used.

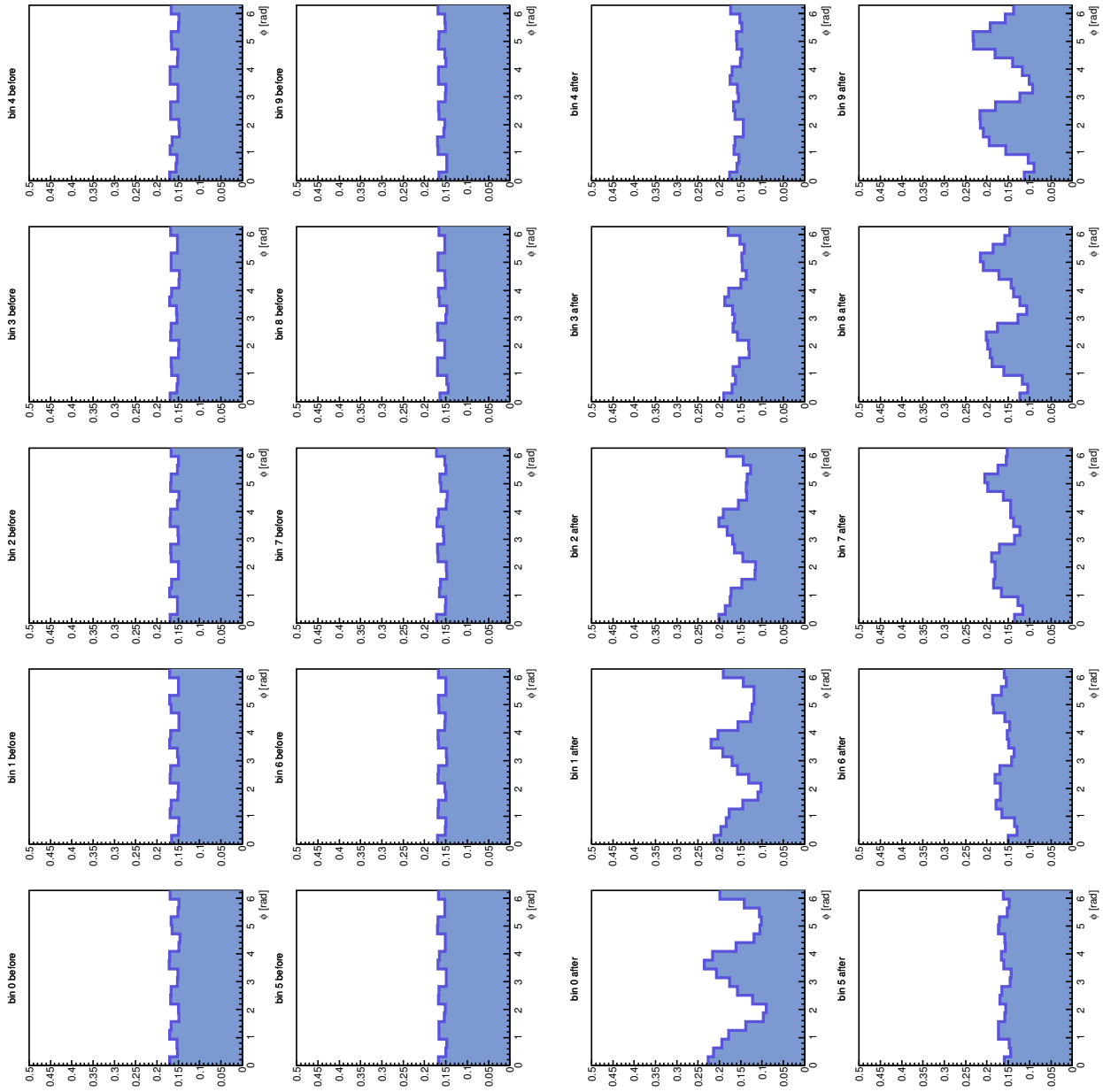

(a) (b)

Figure 104: Average normalized histograms results for initial arrangement according to q_2 and rotation according to Ψ_5. The y-axis are missing label for the sake of viewers comfort, the y-axis depicts number of particles in the bin. (a) Average angle distribution *before* the algorithm had been used. (b) Average angle distribution *after* the algorithm had been used.

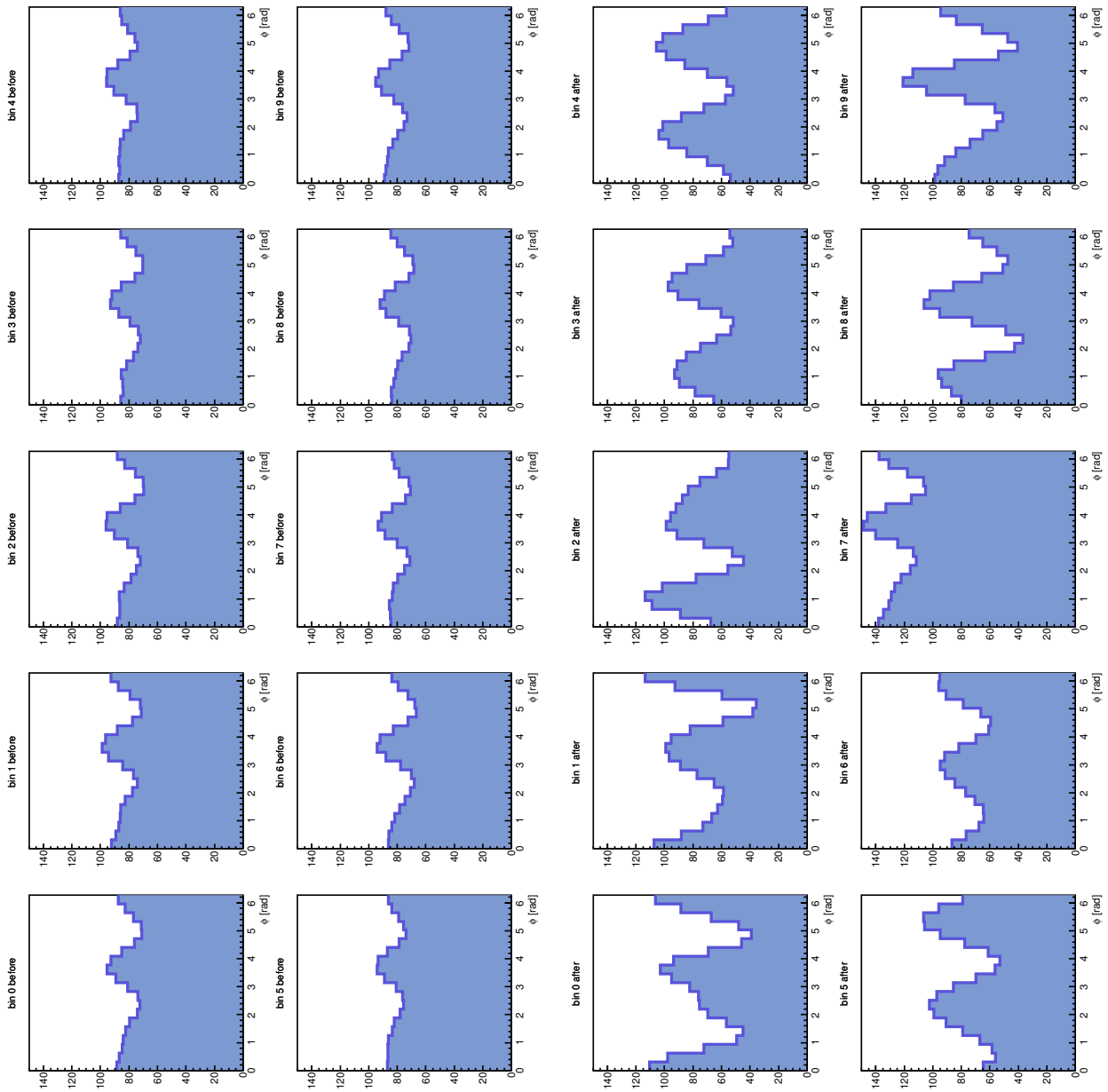

(a) (b)

Figure 105: Average histograms results for initially random arrangement and rotation according to Ψ_2 and Ψ_3. The y-axis are missing label for the sake of viewers comfort, the y-axis depicts number of particles in the bin. (a) Average angle distribution *before* the algorithm had been used. (b) Average angle distribution *after* the algorithm had been used.

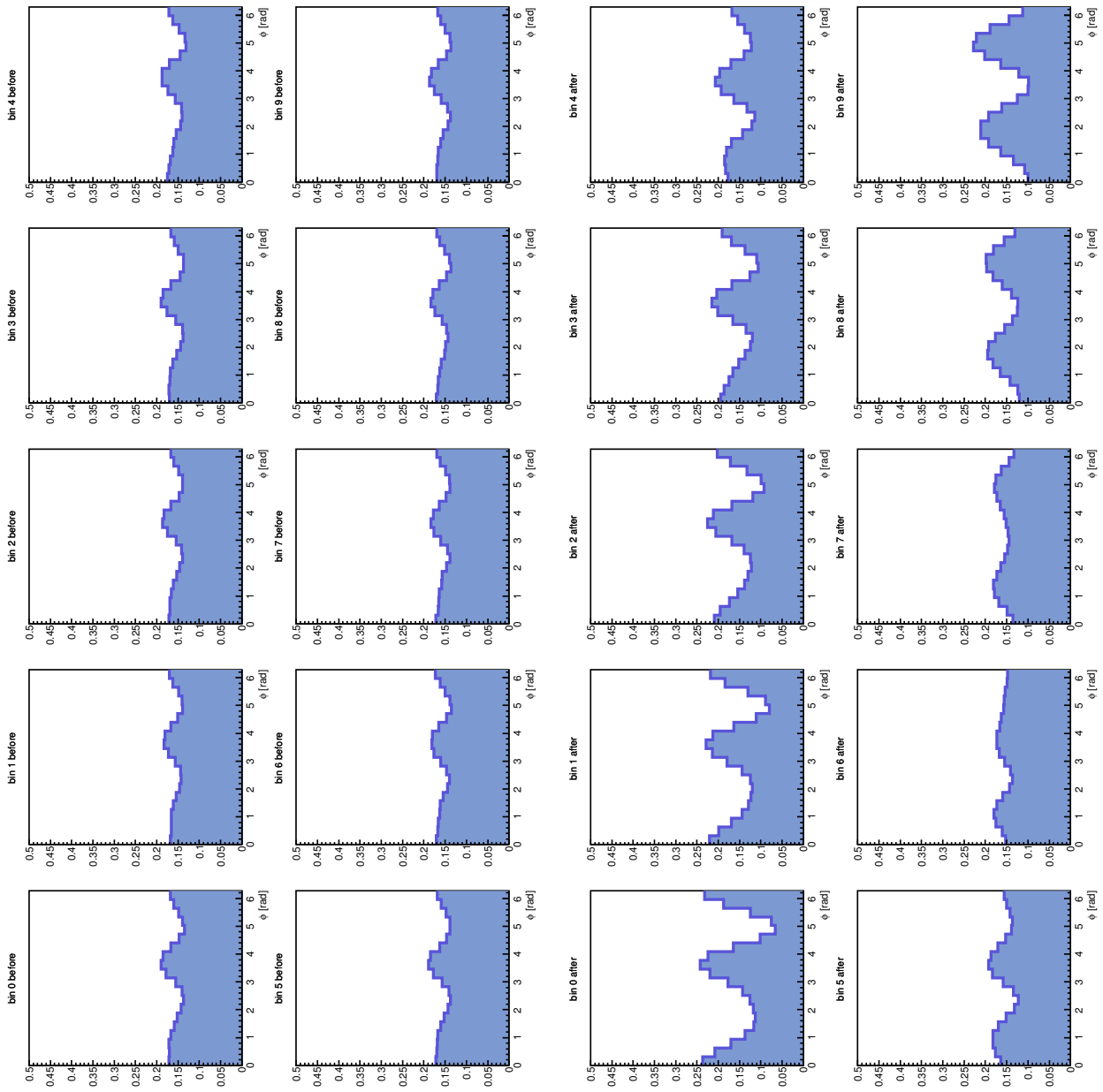

(a) (b)

Figure 106: Average normalized histograms results for initially random arrangement and rotation according to Ψ_2 and Ψ_3. The y-axis are missing label for the sake of viewers comfort, the y-axis depicts number of particles in the bin. (a) Average angle distribution *before* the algorithm had been used. (b) Average angle distribution *after* the algorithm had been used.

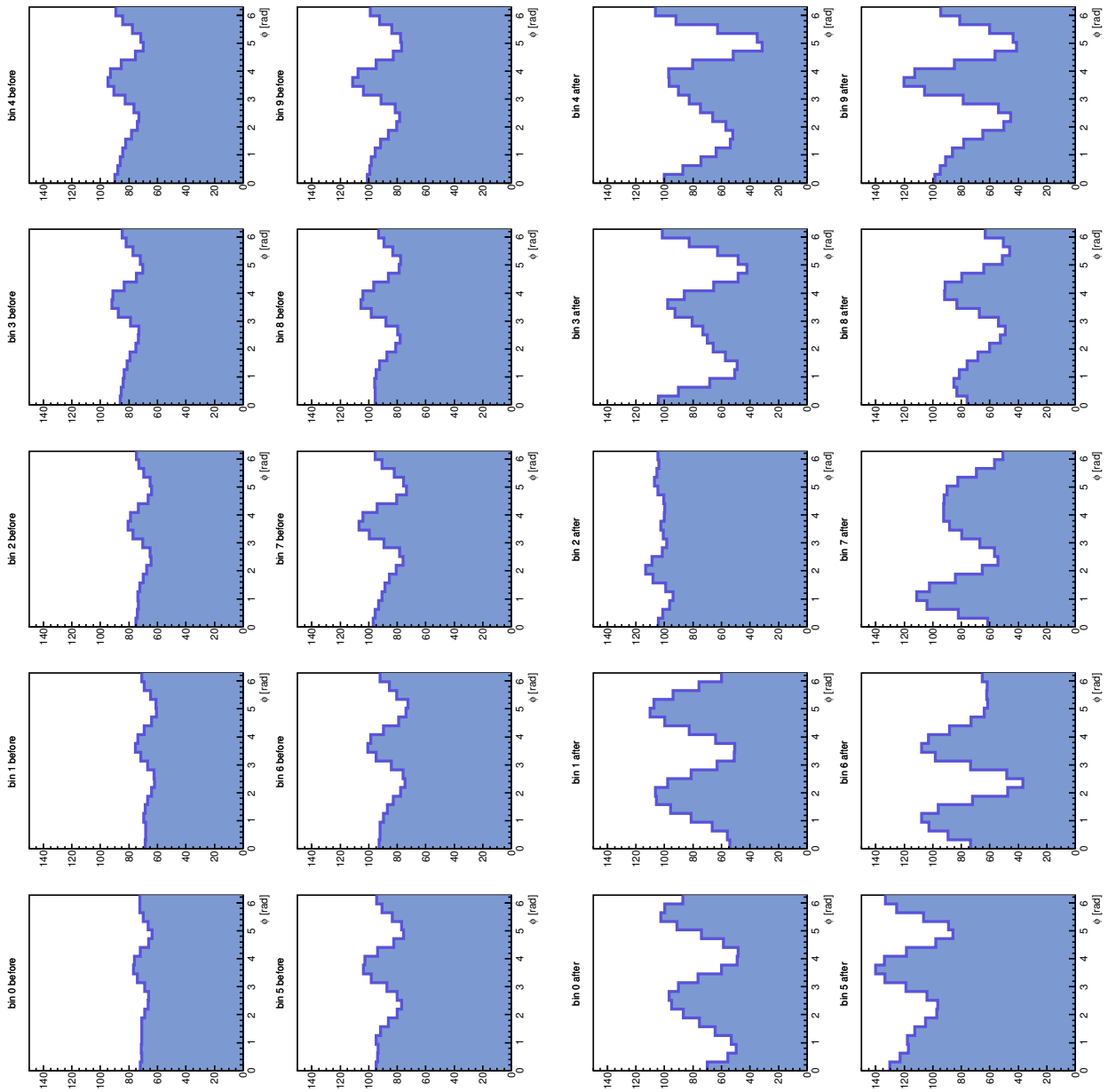

(a) (b)

Figure 107: Average histograms results for initial arrangement according to q_2 and rotation according to Ψ_2 and Ψ_3. The y-axis are missing label for the sake of viewers comfort, the y-axis depicts number of particles in the bin. (a) Average angle distribution *before* the algorithm had been used. (b) Average angle distribution *after* the algorithm had been used.

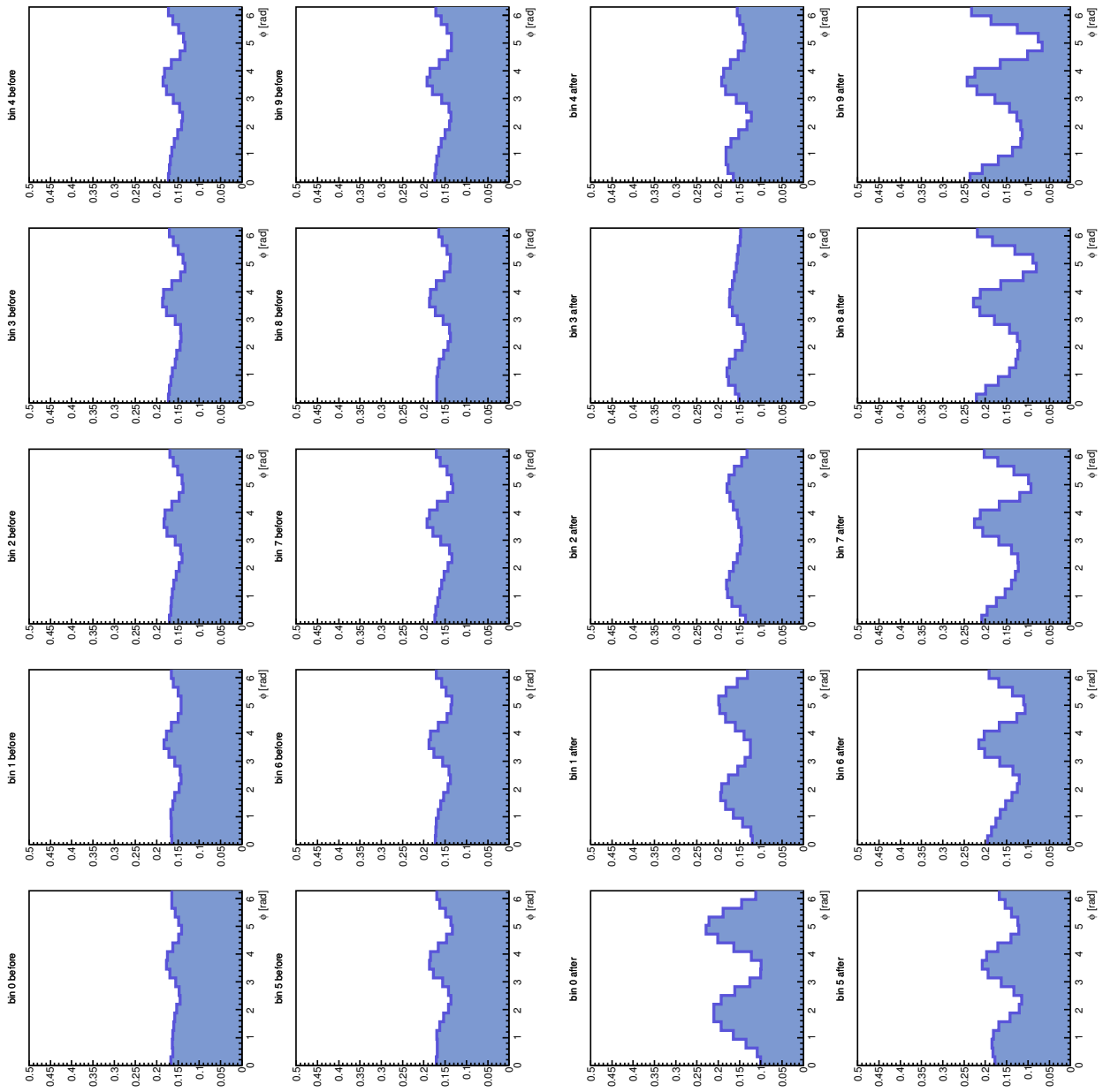

(a) (b)

Figure 108: Average normalized histograms results for initial arrangement according to q_2 and rotation according to Ψ_2 and Ψ_3. The y-axis are missing label for the sake of viewers comfort, the y-axis depicts number of particles in the bin. (a) Average angle distribution *before* the algorithm had been used. (b) Average angle distribution *after* the algorithm had been used.

E DRAGON

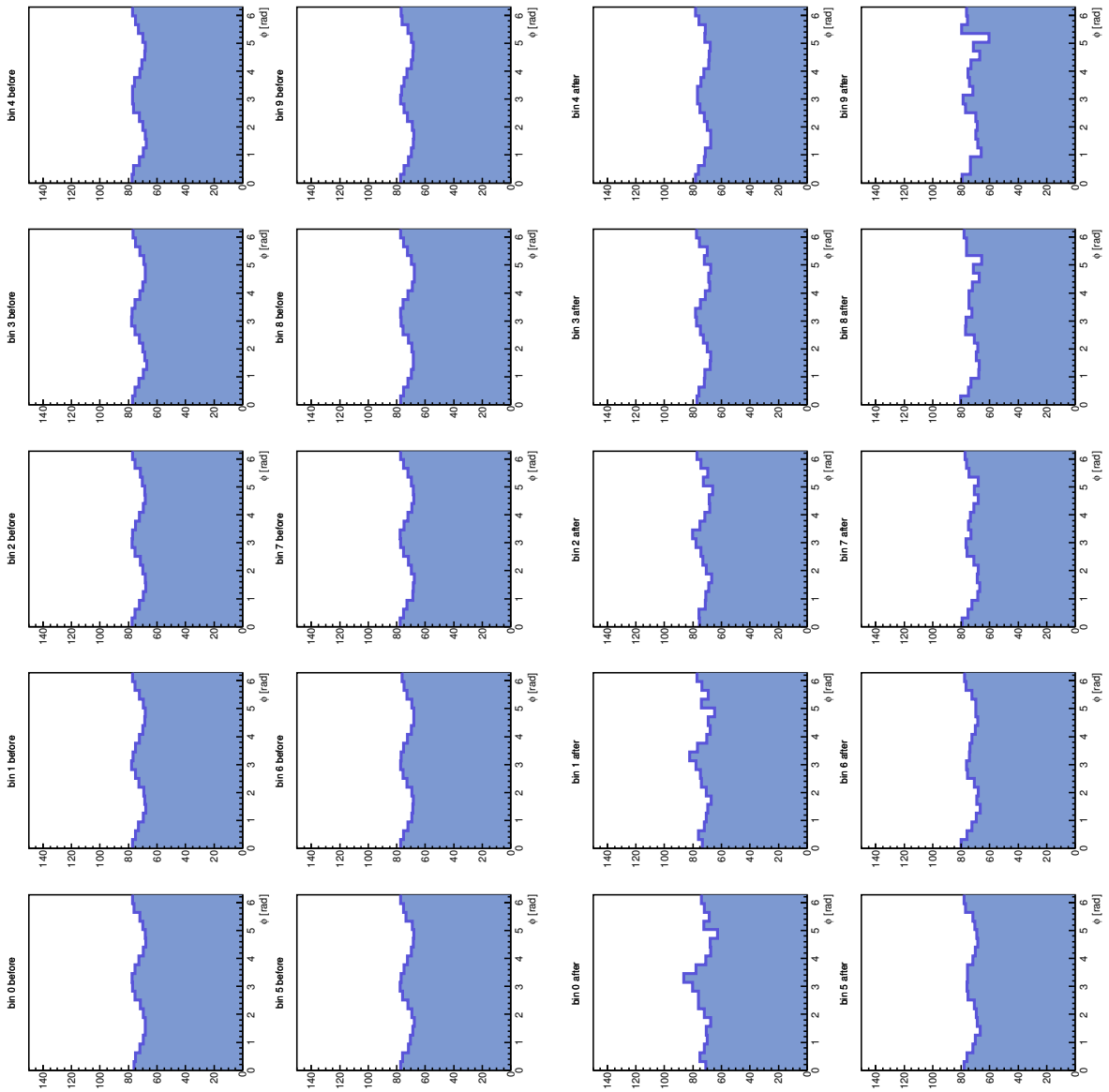

(a) (b)

Figure 109: Average histograms results for initially random arrangement. The y-axis are missing label for the sake of viewers comfort, the y-axis depicts number of particles in the bin. (a) Average angle distribution *before* the algorithm had been used. (b) Average angle distribution *after* the algorithm had been used.

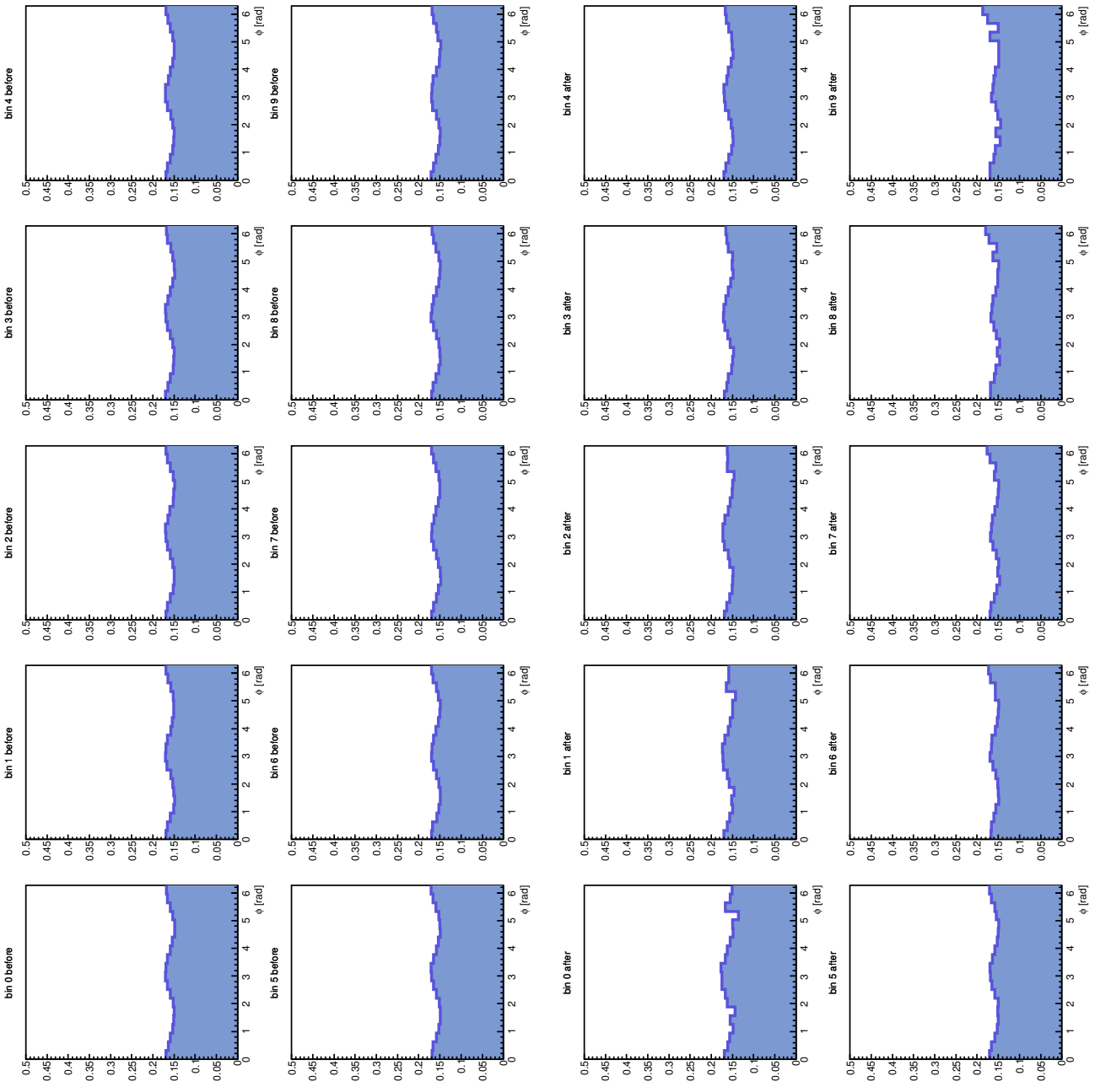

Figure 110: Average histograms results for initially random arrangement and normalized events. The y-axis are missing label for the sake of viewers comfort, the y-axis depicts normalized number of particles in the bin. (a) Average angle distribution *before* the algorithm had been used. (b) Average angle distribution *after* the algorithm had been used.

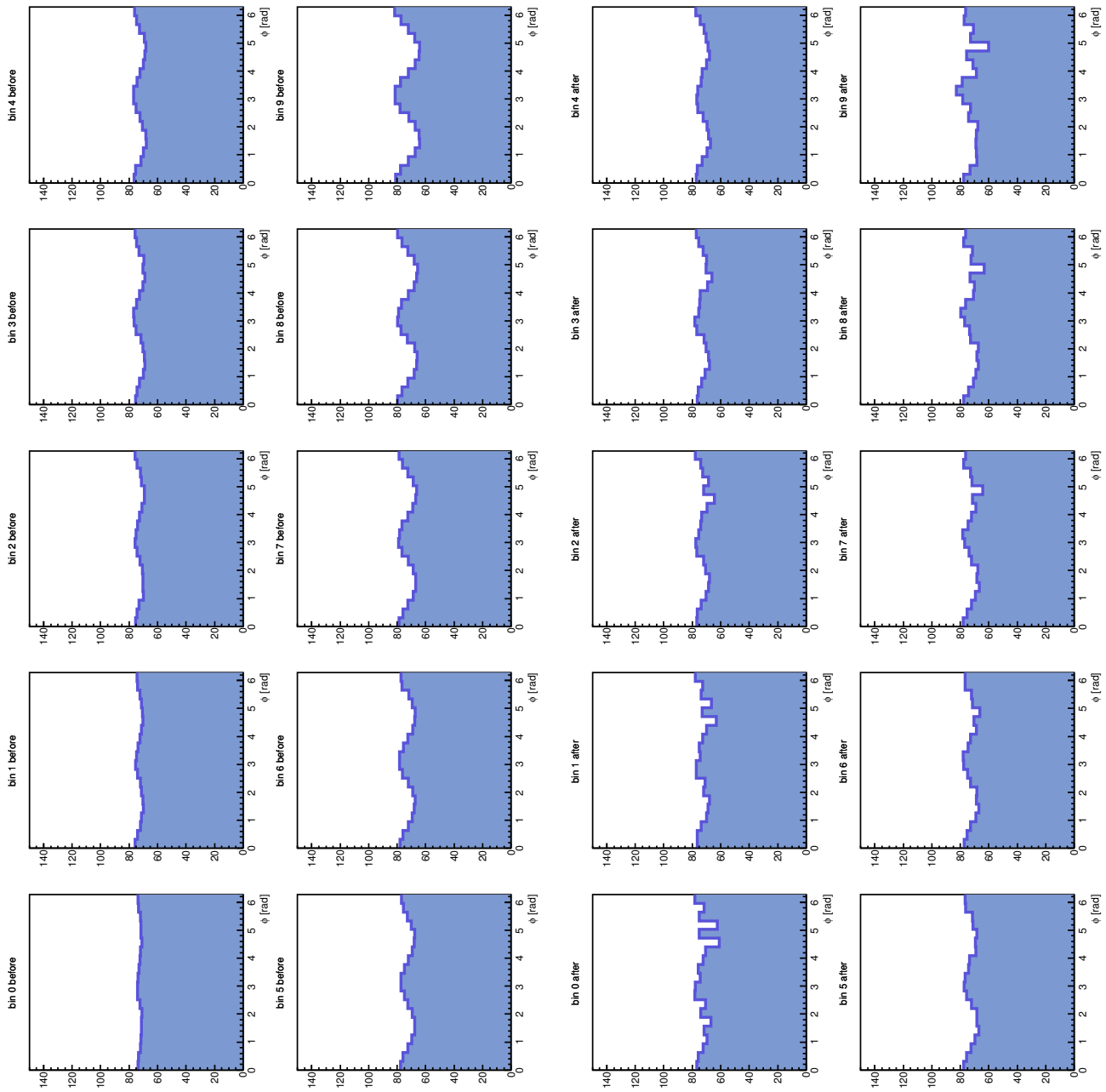

(a) (b)

Figure 111: Average histograms results for initial arrangement according to q_2. The y-axis are missing label for the sake of viewers comfort, the y-axis depicts number of particles in the bin. (a) Average angle distribution *before* the algorithm had been used. (b) Average angle distribution *after* the algorithm had been used.

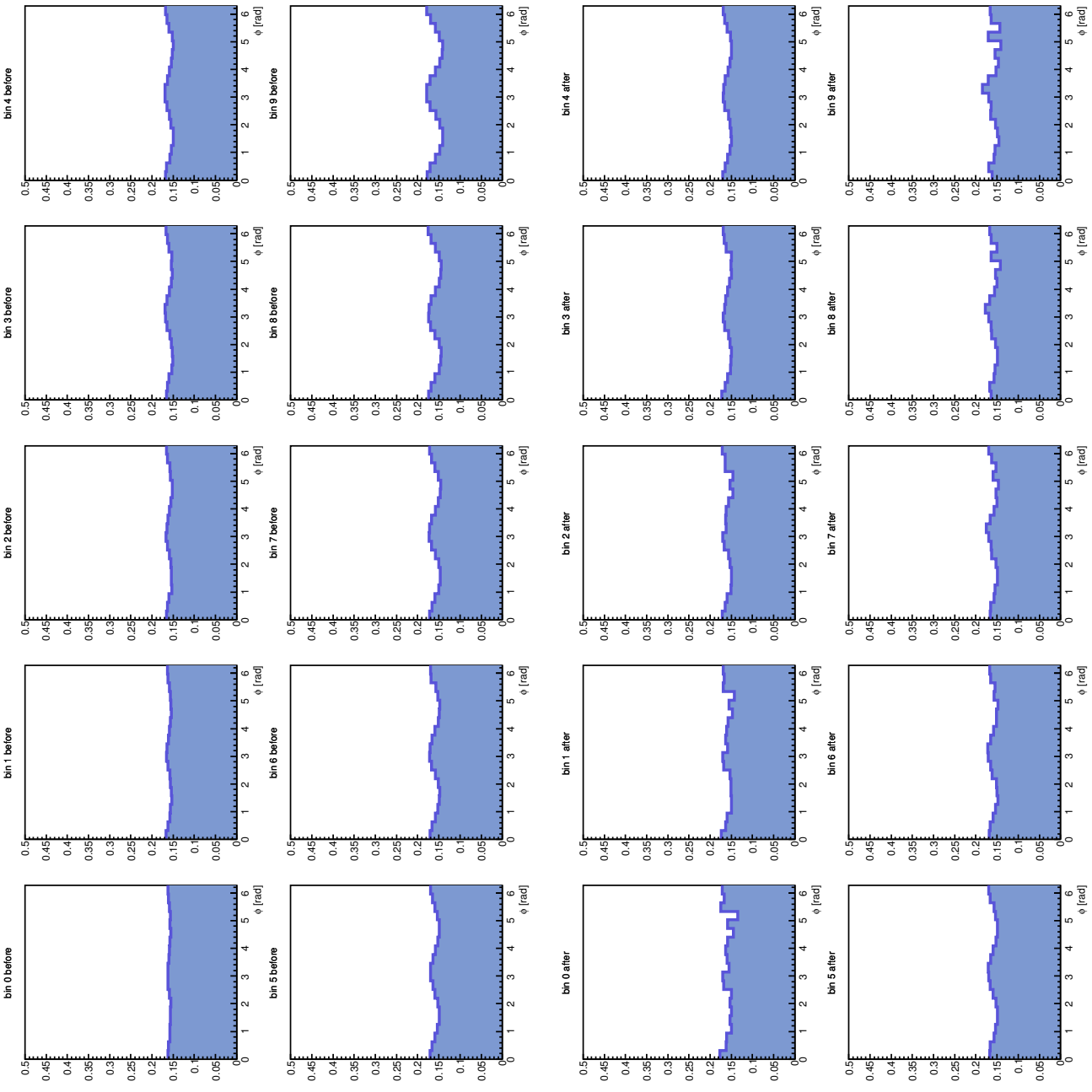

(a) (b)

Figure 112: Average histograms results for normalized events and initial arrangement according to q_2. The y-axis are missing label for the sake of viewers comfort, the y-axis depicts number of particles in the bin. (a) Average angle distribution *before* the algorithm had been used. (b) Average angle distribution *after* the algorithm had been used.

References

[1] J. Schukraft, A. Timmins, S. Voloshin: Ultrarelativistic nuclear collisions: event. shape engineering, Phys. Lett. B 719 (2013) 394-398

[2] S. Lehmann, A.D.Jackson, B. Lautrup: Measures and Mismeasures of Scientific Quality, arXiv: physics/0512238

[3] S. Lehmann, A.D.Jackson, B. Lautrup: Measures for Measures, Nature 444 (2006) 1003-1004

[4] B. Tomášik: DRAGON: Monte Carlo generator of particle production from a fragmented fireball in ultrarelativistic nuclear collisions, Comp. Phys. Commun. 180 (2009) 1642-1653

[5] Sergei A. Voloshin and Arthur M. Poskanzer and Raimond Snellings. Collective phenomena in non-central nuclear collisions. 2008. arxiv:0809.2949 *Relativistic Heavy Ion Physics*, 23:293–333, 2010. `http://dx.doi.org/10.1007/978-3-642-01539-7_10`.

[6] G. Aad et al. (ATLAS collaboration): Measurement of the azimuthal anisotropy for charged particle production in $\sqrt{s_{NN}}$=2.76 TeV lead-lead collisions with the ATLAS detector, Phys.Rev.C 86 (2012) 014907

[7] S.James Press: Subjective and Objective Bayesian Statistics: Principles, Models, and Applications, ISBN 9780470317945, Wiley 2009

[8] William H. Press, Saul A. Teukolsky, William T. Vetterling and Brian P. Flannery, *Numerical Recipes 3rd Edition: The Art of Scientific Computing*. Cambridge University Press, New York, NY, USA, 3 edition, 2007.

[9] G. Aad et al. (ATLAS collaboration): Measurement of the azimuthal anisotropy for charged particle production in at $\sqrt{s_{NN}}$ = 2.76 TeV lead-lead collisions with the ATLAS detector, Phys. Rev. C 86 (2012) 014907

[10] G. Eyyubova: Charged particle directed flow in Pb-Pb collisions at $\sqrt{s_{NN}} = 2.76$ TeV measured with ALICE at the LHC, EPJ Web of Conferences 70 00075 (2014), DOI: 10.1051/epjconf/20147000075

[11] ROOT |A Data Analysis Framework, `http://root.cern.ch`,
citation date: June 23, 2015

[12] LAPACK – Linear Algebra PACKage, `http://www.netlib.org/lapack/`,
citation date: June 23, 2015

[13] K. Aamodt et al. (ALICE collaboration): Elliptic Flow of Charged Particles in Pb+Pb collisions at $\sqrt{s_{NN}} = 2.76$ TeV, Phys. Rev. Lett. 105 (2010) 252302

[14] G. Aad et al. (ATLAS collaboration): Measurement of the distributions of event-by-event flow harmonics in lead-lead collisions at $\sqrt{s_{NN}} = 2.76$ TeV with the ATLAS detector at the LHC, JHEP 1311 (2013) 183, arXiv:1305.2942

[15] S. Chatrchyan et al. (CMS collaboration): Measurement of higher-order harmonic azimuthal anisotropy in PbPb collisions at $\sqrt{s_{NN}} = 2.76$ TeV, Phys. Rev. C 89 (2014) 044906